# Characterisation of a novel non-coding RNA and its involvement in polysaccharide intercellular adhesin (PIA)-mediated biofilm formation of *Staphylococcus epidermidis*

Charakterisierung einer neuen nicht-kodierenden RNA und deren Beteiligung an der PIA-vermittelten Biofilmbildung von *Staphylococcus epidermidis*

Doctoral thesis for a doctoral degree (Dr. rer. nat.)

at the Graduate School of Life Sciences (GSLS),

Julius-Maximilians-Universität Würzburg

Section: Infection and Immunity

Submitted by

Maike Franziska Lerch, Diplom-Biologin Univ.

from Hildesheim, Germany

Celle, October 2017

Submitted on: 11.10.2017

Members of the Supervisory Committee:

Chairperson: Prof Dr Thomas Dandekar

Primary Supervisor: PD Dr Wilma Ziebuhr

Supervisor (Second): PD Dr Knut Ohlsen

Supervisor (Third): Dr Martin Fraunholz

Supervisor (Fourth): Prof Dr Cynthia Sharma

Date of Public Defence:

Date of Receipt of Certificates:

Eingereicht am: 11.10.2017

Mitglieder des Promotionskomitees:

Vorsitzende/r: Prof. Dr. Thomas Dandekar

1. Betreuer: PD Dr. Wilma Ziebuhr

2. Betreuer: PD Dr. Knut Ohlsen

3. Betreuer: Dr. Martin Fraunholz

4. Betreuer: Prof. Dr. Cynthia Sharma

Tag des Promotionskolloquiums:

Doktorurkunden ausgehändigt am:

Affidavit

I hereby confirm that my thesis entitled 'Characterisation of a novel non-coding RNA and its involvement in polysaccharide intercellular adhesin (PIA)-mediated biofilm formation of *Staphylococcus epidermidis*' is the result of my own work. I did not receive any help or support from commercial consultants. All sources and / or materials applied are listed and specified in the thesis.

Furthermore, I confirm that this thesis has not yet been submitted as part of another examination process neither in identical nor in similar form.

Celle,

Eidesstattliche Erklärung

Hiermit erkläre ich an Eides statt, die Dissertation „Charakterisierung einer neuen nicht-kodierenden RNA und deren Beteiligung an der PIA-vermittelten Biofilmbildung von *Staphylococcus epidermidis*" eigenständig, d.h. insbesondere selbständig und ohne Hilfe eines kommerziellen Promotionsberaters, angefertigt und keine anderen als die von mir angegebenen Quellen und Hilfsmittel verwendet zu haben.

Ich erkläre außerdem, dass die Dissertation weder in gleicher noch in ähnlicher Form bereits in einem anderen Prüfungsverfahren vorgelegen hat.

Celle,

Acknowledgement

Thank you!

Contributions by others

The work described in this thesis was done under supervision of PD Dr Wilma Ziebuhr in the Nosocomial Infections group at the Institute for Molecular Infection Biology (IMIB, Würzburg, Germany) and financially supported by Deutsche Forschungsgemeinschaft (DFG)-SFB/Transregio 34 'Pathophysiologie von Staphylokokken in der Post-Genom-Ära' (TRR 34).

The experiments described here were carried out between January 2012 and July 2016. Parts of this work which have been conducted in collaboration with others or were carried out by students under supervision by the author are indicated below:

Chapter III: Characterisation of IcaZ, a long ncRNA specific for *S. epidermidis*

- The additional search for ORFs within ncRNA IGR*ica*-RNA was carried out by Lena Müller during conduction of her bachelor's thesis under supervision of the author (Müller, 2012; Nosocomial Infections, IMIB, Würzburg).

Chapter IV: Functional analysis of IcaZ by classical methods and global approaches

- Cloning of plasmids and strains were partly carried out by students during student internships or while preparation of bachelor's theses (Schreier, 2014; Wicke, 2015) under supervision of the author (Nosocomial Infections, IMIB, Würzburg).
- SEM analysis was conducted with technical assistance of Dr Karen Wolf (Pathogenic Enterobacteria, IMIB, Würzburg) at the biocentre of the University of Würzburg.
- *In vivo* biofilm formation assays were conducted with Dr Sonja Schoenfelder (Nosocomial Infections, IMIB, Würzburg). Prof Dr Kai Thormann (Justus Liebig University, Giessen) supervised the initial experiments and kindly provided parts of the equipment (*e.g.* the peristaltic pump).
- Bioinformatical data analysis was carried out in collaboration with Dr Konrad Förstner (Bioinformatics, IMIB, Würzburg).

Chapter V: Establishing and challenging a hypothetical biofilm regulation model involving ncRNA IcaZ

- Northern blot and CLSM analysis were carried out with technical assistance by Dr Sonja Schoenfelder.

Data that were referred to or analysed here, but experimentally conducted by others prior to this work are listed below:

- IGR*ica*-RNA was identified and initially characterised by Dr Martin Eckart, during his doctoral work under supervision of PD Dr Wilma Ziebuhr (Eckart, 2006; Nosocomial Infections, IMIB, Würzburg), who also generated *S. epidermidis* 307ΔIGR*ica*-sRNA (strain collection code ME19).

- IcaZ mutants *S. epidermidis* O-47Δ*tRNA*$^{Thr-4}$Δ*icaZ*Δ*icaR*-3′ UTR (O-47ΔΔΔ; strain collection code FL1Δ2) and *S. epidermidis* O-47ΔP$_{tRNA}$$^{Thr-4}$Δ*tRNA*$^{Thr-4}$Δ*icaZ* Δ*icaR*-3′ UTR (O-47ΔΔΔΔ; strain collection code FL2Δ1) were created by Franziska Herbst (Nosocomial Infections, IMIB, Würzburg).

- Preparation of RNA from *S. epidermidis* PS2 and PS10 used for RNA-seq (±TEX treatment) was carried out by Svitlana Kosytska. Bioinformatic pre-analysis was done by Dr Konrad Förstner.

- RNA sampling for Microarray analysis and protein sampling for proteome analysis was done by Dr Sonja Schoenfelder. Prof Jacques Schrenzel and Dr Patrice Francois (Geneva, Switzerland) conducted the Microarray analysis. Pre-analysed data were obtained from PD Dr Wilma Ziebuhr. Proteome analysis was done in collaboration with Prof Dr Susanne Engelmann and Swantje Reiss, who carried out the 2D gel analysis (Ernst Moritz Arndt University, Greifswald).

The plasmids provided by collaborators are listed in Tab. II-7.

Summary

Coagulase-negative staphylococci, particularly *Staphylococcus epidermidis*, have been recognised as an important cause of health care-associated infections due to catheterisation, and livestock-associated infections. The colonisation of indwelling medical devices is achieved by the formation of biofilms, which are large cell-clusters surrounded by an extracellular matrix. This extracellular matrix consists mainly of PIA (polysaccharide intercellular adhesin), which is encoded by the *icaADBC*-operon. The importance of *icaADBC* in clinical strains provoking severe infections initiated numerous investigations of this operon and its regulation within the last two decades. The discovery of a long transcript being located next to *icaADBC*, downstream of the regulator gene *icaR*, led to the hypothesis of a possible involvement of this transcript in the regulation of biofilm formation (Eckart, 2006). Goal of this work was to characterise this transcript, named ncRNA IcaZ, in molecular detail and to uncover its functional role in *S. epidermidis*.

The ~400 nt long IcaZ is specific for *ica*-positive *S. epidermidis* and is transcribed in early- and mid-exponential growth phase as primary transcript. The promotor sequence and the first nucleotides of *icaZ* overlap with the 3′ UTR of the preceding *icaR* gene, whereas the terminator sequence is shared by $tRNA^{Thr-4}$, being located convergently to *icaZ*. Deletion of *icaZ* resulted in a macroscopic biofilm-negative phenotype with highly diminished PIA-biofilm. Biofilm composition was analysed *in vitro* by classical crystal violet assays and *in vivo* by confocal laser scanning microscopy under flow conditions to display biofilm formation in real-time. The mutant showed clear defects in initial adherence and decreased cell-cell adherence, and was therefore not able to form a proper biofilm under flow in contrast to the wildtype. Restoration of PIA upon providing *icaZ* complementation from plasmids revealed inconsistent results in the various mutant backgrounds.

To uncover the functional role of IcaZ, transcriptomic and proteomic analysis was carried out, providing some hints on candidate targets, but the varying biofilm phenotypes of wildtype and *icaZ* mutants made it difficult to identify direct IcaZ mRNA targets. Pulse expression of *icaZ* was then used as direct fishing method and computational target predictions were executed with candidate mRNAs from aforesaid approaches. The combined data of these analyses suggested an involvement of *icaR* in IcaZ-mediated

biofilm control. Therefore, RNA binding assays were established for IcaZ and *icaR* mRNA. A positive gel shift was maintained with *icaR* 3′ UTR and with 5'/3' *icaR* mRNA fusion product, whereas no gel shift was obtained with *icaA* mRNA. From these assays, it was assumed that IcaZ regulates *icaR* mRNA expression in *S. epidermidis*. *S. aureus* instead lacks ncRNA IcaZ and its *icaR* mRNA was shown to undergo autoregulation under so far unknown circumstances by intra- or intermolecular binding of 5′ UTR and 3′ UTR (Ruiz de los Mozos *et al.*, 2013). Here, the Shine-Dalgarno sequence is blocked through 5'/3' UTR base pairing and RNase III, an endoribonuclease, degrades *icaR* mRNA, leading to translational blockade. In this work, *icaR* mRNA autoregulation was therefore analysed experimentally in *S. epidermidis* and results showed that this specific autoregulation does not take place in this organism. An involvement of RNase III in the degradation process could not be verified here. GFP-reporter plasmids were generated to visualise the interaction, but have to be improved for further investigations.

In conclusion, IcaZ was found to interact with *icaR* mRNA, thereby conceivably interfering with translation initiation of repressor IcaR, and thus to promote PIA synthesis and biofilm formation. In addition, the environmental factor ethanol was found to induce *icaZ* expression, while only weak or no effects were obtained with NaCl and glucose. Ethanol, actually is an ingredient of disinfectants in hospital settings and known as efficient effector for biofilm induction. As biofilm formation on medical devices is a critical factor hampering treatment of *S. epidermidis* infections in clinical care, the results of this thesis do not only contribute to better understanding of the complex network of biofilm regulation in staphylococci, but may also have practical relevance in the future.

Zusammenfassung

Koagulase-negative Staphylokokken besiedeln die menschliche und tierische Haut, sowie die Schleimhäute. Durch Läsionen oder das Einbringen von medizinischen Instrumenten wie Kathetern gelangen sie in tiefere Hautschichten oder die Blutbahn und können dort schwerwiegende Infektionen auslösen, vor Allem bei Risikopersonen. Besonders *Staphylococcus epidermidis* hat sich als Verursacher von nosokomialen Infektionen, aber auch als Pathogen in der Tierhaltung etabliert. Die Bakterien bilden bei der Besiedlung sogenannte Biofilme aus (d.h. eine Akkumulation der Keime, die von einer extrazellulären Matrix umgeben sind). Diese Matrix besteht neben Proteinen und eDNA hauptsächlich aus einem Polysaccharid, dem interzellulären Adhäsin PIA (*engl.: polysaccharide intercellular adhesin*). Dieses wird durch die Ica-Proteine synthetisiert, die im *icaADBC*-Operon (*engl.: intercellular adhesin operon*) kodiert sind. Das Operon hat große Bedeutung in klinischen Stämmen und wurde daher innerhalb der letzten beiden Jahrzehnte eingehend untersucht, auch im Hinblick auf seine Regulation. In der unmittelbaren Umgebung des *icaADBC*-Operons, stromabwärts des *icaR* Gens, das für den Repressor des *ica*-Operons (IcaR) kodiert, wurde ein großes Transkript identifiziert, von dem vermutet wird, dass es möglicherweise an der Regulation der Biofilmbildung beteiligt ist (Eckart, 2006). Ziel dieser Arbeit war es, dieses Transkript zu charakterisieren und seine Funktion in *S. epidermidis* aufzudecken.

Die nicht-kodierende RNA, genannt IcaZ, hat eine Länge von ~400 nt und ist spezifisch für *ica*-positive *S. epidermidis*. Sie wird in der frühen bis mittleren exponentiellen Phase temperaturabhängig exprimiert. Stromaufwärts überlappt das *icaZ*-Gen und dessen Promotor mit der 3' UTR vom *icaR*-Gen. Stromabwärts wird das *icaZ*-Gen vom einem Transkriptionsterminator begrenzt, der auch für das $tRNA^{Thr-4}$-Gen benutzt wird, das auf dem gegenüberliegenden Strang in Richtung des *icaZ*-Gens lokalisiert ist. Die Deletion der RNA führte zu einem makroskopisch sichtbaren Biofilm-negativen Phänotyp mit deutlich verminderter PIA Bildung. Die Biofilmzusammensetzung wurde *in vitro* mittels eines klassischen Kristallviolett-Assays gemessen und die Biofilmbildung *in vivo* in Echtzeit mittels konfokaler Mikroskopie (CLSM) betrachtet. Dabei wurde mit einer peristaltischen Pumpe ein Mediumfluss appliziert. Die Mutante zeigte klare Defekte in der initialen

Adhärenz und in der Zell-Zell Adhäsion. Sie bildete im Gegensatz zum Wildtyp keinen strukturierten Biofilm aus. Zur Komplementierung des Biofilms wurde die IcaZ von einem Plasmid exprimiert und die Biofilmzusammensetzung nach 18-20 Stunden Wachstum gemessen. Die Ergebnisse dieser Untersuchungen in den verschiedenen Mutanten waren nicht eindeutig.

Um die Funktion von IcaZ aufzudecken, wurden Transkriptom- und Proteomvergleiche zwischen Wildtyp und Mutante gemacht. Diese lieferten einige Hinweise, aber da der metabolische Unterschied eines Biofilmbildners zu einem Nicht-Biofilmbildner zu groß war, wurde eine direktere Methode angewandt, die induzierte Expression (Pulsexpression). Zudem wurden potentielle Interaktionspartner der IcaZ mittels computer-basierter Bindungsvorhersagen analysiert. Die *icaR* mRNA kristallisierte sich dabei als Target heraus und die Interaktion zwischen IcaZ und *icaR* mRNA wurde mit Gelshift-Assays (EMSA) untersucht. Eine Bandenverschiebung wurde mit *icaR* 3' UTR und mit dem *icaR*-5'-3' UTR-Fusionsprodukt detektiert, wohingegen keine Interaktion zwischen IcaZ und *icaA* mRNA stattfand. Aufgrund dieser Assays wurde vermutet, dass IcaZ die Translation von *icaR* in *S. epidermidis* reguliert. In *S. aureus* fehlt die nicht-kodierende RNA IcaZ und für *icaR* mRNA wurde eine Autoregulation gezeigt, bei der die *icaR* 5' UTR mit der *icaR* 3' UTR intramolekular oder intermolekular durch Basenpaarung interagiert, wodurch die Shine-Dalgarno Sequenz blockiert wird und es aufgrund dessen zu einer Hemmung der Translation kommt. Die Umweltfaktoren, die dazu führen sind bisher unbekannt. Der Komplex wird durch eine Endoribonuklease, RNase III, abgebaut (Ruiz de los Mozos et al., 2013). In *S. epidermidis* wurde eine solche Interaktion theoretisch ausgeschlossen. Experimentelle Analysen dieser Arbeit haben gezeigt, dass diese Autoregulation in *S. epidermidis* nicht stattfinden kann und es wird angenommen, dass IcaZ diese Regulation übernimmt. Um die Interaktion zu visualisieren wurden GFP-Reporter Plasmide generiert, die aber für weitere Experimente noch zu verbessern sind.

Zusammenfassend lässt sich sagen, dass IcaZ mit der *icaR* mRNA interagiert, was höchstwahrscheinlich zu einer Hemmung der Translation des Repressors IcaR führt und damit letztlich PIA-Synthese und Biofilmbildung positiv reguliert. Zusätzlich wurde gefunden, dass Ethanol die Expression der IcaZ-RNA induziert, während NaCl nur schwache Effekte zeigte und Glucose keinen Einfluss auf die Expression von *icaZ* hatte. Ethanol ist ein Bestandteil von Desinfektionsmitteln, die in Krankenhäusern verwendet werden und ist bekannt dafür Biofilmbildung auszulösen. Da die Bildung von Biofilmen auf medizinischen Geräten kritisch ist und diese die Behandlung von *S. epidermidis* Infektionen erschweren, tragen die Ergebnisse dieser Arbeit nicht nur zu einem besseren Verständnis des komplexen Netzwerks der Biofilmregulation bei, sondern haben möglicherweise auch praktischen Nutzen in der Zukunft.

Table of Contents

List of Figures and Tables

Figures

Annexe

Tables

Annexe

Abbreviations

(v/v)	(volume/ volume)
(w/v)	(weight/ volume in g/ml)
Aa	amino acid
AMP	ampicillin
approx.	approximately
APS	ammonium persulfate
agr	accessory gene regulator
BHI	brain heart infusion
BLAST	Basic Local Alignment Search Tool
bp	base pair(s)
Cat.-No.	catalogue number
CDM	chemically defined medium
cDNA	complementary DNA
CFU	colony forming unit
CLSM	confocal laser scanning microscopy
CM	chloramphenicol
CoNS	coagulase-negative staphylococci
CRA	Congo red agar
ddH$_2$O	double deionised water
DEPC	diethylpyrocarbonate
DMSO	dimethyl sulfoxide
DNA	deoxyribonucleic acid
DNase	deoxyribonuclease
ECL	enhanced chemiluminescence
E. coli	*Escherichia coli*
EDTA	ethylenediaminetetraacetic acid
EM	erythromycin
e.g.	for example [lat. *exempli gratia*]
end conc.	end concentration
et al.	and others [lat. *et alii*]

EtOH	ethanol
Fig.	figure
g	gravitational acceleration (9.81 m/s^2)
GER	Germany
GFP	green fluorescent protein
GMO	genetically modified organism
HPSF	high purity salt free
ica	intercellular adhesion
i.e.	that is [lat. *it est*]
IGR	intergenic region
IVT	*in vitro* transcription
LB	Luria-Bertani
MCS	multiple cloning site
MOPS	3-morpholinopropane-1-sulfonic acid
mRNA	messenger RNA
MRSA	methicillin resistant *S. aureus*
MRSE	methicillin resistant *S. epidermidis*
MS	Microsoft
NaAc	sodium acetate
NCBI	National Center for Biotechnology Information
ncRNA	non-coding RNA
nt	nucleotide(s)
OD	optical density
o/n	overnight
ONC	overnight culture
ORF	open reading frame
ori	origin of replication
P$_{(x)}$	promoter of x
PAA	polyacrylamide
PAGE	polyacrylamide gel electrophoresis
PBS	phosphate buffered saline
P:C:I	phenol/chloroform/isoamyl alcohol
PCR	polymerase chain reaction
PFU/ml	plaque forming units per millilitre
PIA	polysaccharide intercellular adhesion
PLG	phase lock gel
RACE	rapid amplification of cDNA ends
RBS	ribosome binding site

RNA	ribonucleic acid
RNA-seq	RNA sequencing
RNase	ribonuclease
rNTP	ribonucleotide triphosphate
rRNA	ribosomal RNA
RT	room temperature
SCC	staphylococcal cassette chromosome
SD	Shine-Dalgarno
SDS	sodiumdodecylsulfate
snp	single nucleotide polymorphisms
spp.	Species
sRNA	small RNA
T_A	annealing temperature
Tab.	Table
T_E	elongation temperature
TBE	Tris/Borate/EDTA
TEMED	tetramethylethylenediamine
TIR	translation initiation region
T_M	melting temperature
TT	transcription terminator
TRIS	tris-(hydroxymethyl)-aminomethane
tRNA	transfer RNA
TSB	tryptone soya broth
TSS	transcription start site
$t_{1/2}$	half-live
U	unit
UK	United Kingdom
USA	United States of America
UTP	uridine triphosphate
UTR	untranslated region
UV	ultraviolet
Vol.	volume
Wt	wildtype

Units and Multiples

%	per cent
°C	degree Celsius
A	ampere
Ci	Curie
Da	Dalton
g	gram
h	hour(s)
J	Joule
kb	kilo bases
l	litre(s)
m	milli-
M	molar
min	minute(s)
rpm	revolutions per minute
sec	second(s)
V	Volt
W	Watt

k	kilo (10^3)
m	milli (10^{-3})
μ	micro (10^{-6})
n	nano (10^{-9})
p	pico (10^{-12})

I. Introduction

1. The genus *Staphylococcus*

1.1 General features and clinical relevance

Staphylococci are coloniser of the human and animal skin and mucosa. Humans are preferentially colonised on arms and legs, axillary and upon the head (Kloos and Musselwhite, 1975). Microbiome analysis revealed moist regions to be preferred during colonisation (Grice and Segre, 2011). Within CoNS, *S. epidermidis* is the dominant species on axillae, groin and knee body sites, followed by *S. hominis*. *S. capitis* is frequently found in the samples from the groin and the knee pit (Cavanagh *et al.*, 2016).

The phenotype of these gram-positive bacteria is a non-motile and non-sporulating coccus with a diameter of about 1 µm. The bacterial cells appear as clusters (**Fig. I-1 A+B**), as the Scottish surgeon Sir Alexander Ogsten had described it before (Ogston, 1882). **Fig. I-1 C** shows *E. coli* cells for size comparison to staphylococci by same scale. Species of this genus have a low GC-content (30-40 mol%), are facultative anaerobe, produce catalase and grow on bile salts.

As gram-positive bacteria in general, they are surrounded by a thick layered cell wall, that contains 50% peptidoglycan by weight, which is made of alternating saccharide subunits of β-1,4 linked N-acetylglucosamin and N-acetylmuramic acid. The polysaccharides are cross-linked by tetrapeptide chains bound to N-acetylmuramic acid and by a pentaglycine bridge that is specific for *S. aureus*. Additional, ribitol teichoic acids are covalently bound to the peptidoglycan (Lowy, 1998). The pentaglycine bridge can be digested by lysostaphin (Schindler and Schuhardt, 1964), an endopeptidase, which results in a destabilised cell wall.

Staphylococci are divided into coagulase-positive staphylococci (CoPS) that produce coagulase, an enzyme causing blood clotting by catalysing the reaction from fibrinogen into fibrin, and coagulase-negative staphylococci (CoNS) that lack coagulase. Based on this characteristic and the presumed importance of coagulase production in virulence, coagulase-negative staphylococci were often referred to as apathogenic bacteria (Huebner and Goldmann, 1999).
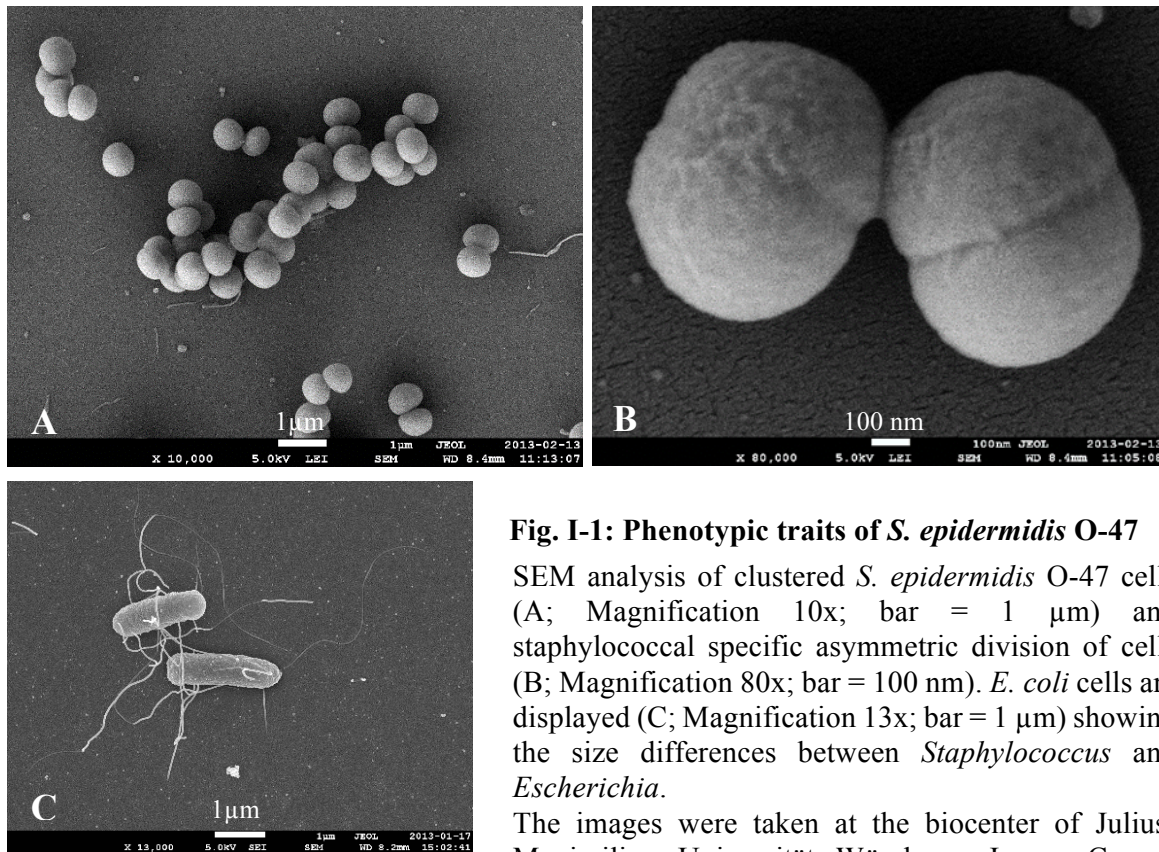
Fig. I-1: Phenotypic traits of *S. epidermidis* O-47

SEM analysis of clustered *S. epidermidis* O-47 cells (A; Magnification 10x; bar = 1 µm) and staphylococcal specific asymmetric division of cells (B; Magnification 80x; bar = 100 nm). *E. coli* cells are displayed (C; Magnification 13x; bar = 1 µm) showing the size differences between *Staphylococcus* and *Escherichia*.

The images were taken at the biocenter of Julius-Maximilians-Universität Würzburg. Image C was kindly provided by Dr Karen Wolf.

In the 1990s, CoNS and particularly *S. epidermidis* emerged as opportunistic pathogens and elicitors of nosocomial infections, mostly in immunocompromised persons (NNIS, 1999). The healthcare associated infections range from catheter-related bloodstream infections and prosthetic joint infections to early-onset neonatal sepsis, prosthetic valve endocarditis and other biomedical device-related infections (Asaad *et al.*, 2016; Huebner and Goldmann, 1999; Schoenfelder *et al.*, 2010; Uckay *et al.*, 2009; von Eiff *et al.*, 2002; Weisser *et al.*, 2010; Ziebuhr *et al.*, 2006). In recent years, it became clear that they are also a cause of livestock-associated infections (Cuny et al., 2016; Schoenfelder et al., 2016).

The main virulence factor of these bacteria is the formation of biofilms on indwelling biomaterials (*i.e.* medical devices, prostheses and catheters) that are hard to eradicate. CoNS therefore became more and more important (Meric *et al.*, 2015; Otto, 2009; Schoenfelder *et al.*, 2010; Ziebuhr, 2001). As they are part of the skin flora, pathogenic CoNS are often misidentified as harmless wound contaminants and misjudged by clinicians. Moreover, they still represent a diagnostic challenge to the health system (Rogers *et al.*, 2009; Widerstrom, 2016). For these reasons and to wake up the medical and scientific communities, Micael Widerström announced a 'Wake-Up Call' in the Journal of Clinical Microbiology last year, in which he emphasised again the importance of these bacteria (Widerstrom, 2016).

1.2 Virulence factors of CoPS and CoNS

Staphylococcus aureus was identified, already in 1884 by Rosenbach, as the causative agent for wound infections (Rosenbach, 1884) and was counted for a long time as the leading cause of nosocomial infections. Beside the production of coagulase, *S. aureus* as CoPS possesses a variety of other virulence factors that range from surface proteins to secreted toxins.

Surface proteins, called 'microbial surface components recognising adhesive matrix molecules' (MSCRAMMs), mediate adherence to host tissues and medical devices by binding collagen, fibronectin and fibrinogen. *S. aureus* produces biofilm matrix to evade the immune system and to protect themselves from antimicrobials (Gordon and Lowy, 2008). Since 1985, this microbe is also regarded as an intracellular pathogen and the molecular mechanism of invasion as well as post-invasion events were subject for many discussions (Flannagan *et al.*, 2016; Garzoni and Kelley, 2009; Hamill *et al.*, 1986; Ogawa *et al.*, 1985; Sinha and Fraunholz, 2010). A survival strategy of these bacteria is also the formation of small colony variants (Kahl, 2014). They furthermore express a toxin export system to release phenol soluble modulins (PSMs) (Chatterjee *et al.*, 2013) and toxin-antitoxin systems (Schuster and Bertram, 2016) beside other toxins. Nowadays, *S. aureus* is overtaken by *S. epidermidis*, the predominant CoNS, and is only the second leading cause of nosocomial infections.

CoNS include all staphylococcal species that lack the synthesis of coagulase. In comparison to *S. aureus*, they contain less virulence factors and are therefore less virulent, except for persons at risk (*i.e.* elderly persons, children and immunocompromised persons at most). Not only the ability to produce tenacious biofilms makes these commensals serious pathogens, but most of the virulence factors relate to biofilm formation (**Tab. I-1**).

Due to the increased research on *S. aureus* within the last years and the technical possibilities for DNA sequencing, the genome sequences for various *S. aureus* strains are available to date and can be extracted from NCBI database. Among *S. epidermidis*, only two fully assembled genomes are available and various shot gun sequences that are unassembled to full genomes. The available genomes are the genome of *S. epidermidis* RP62A, a strong biofilm former, and the genome of *S. epidermidis* ATCC 12228, a non-biofilm former (Gill *et al.*, 2005; Zhang *et al.*, 2003).

Tab. I-1: Virulence factors of *S. epidermidis*

The table was taken from Otto, 2012. The major virulence factor, the biofilm formation, beside toxins, exoenzymes and others are listed.

Virulence factor	Gene	Function
Biofilm formation		
<u>Primary attachment</u>		
AtlE	*atlE*	Bifunctional autolysin/adhesin
Aae	*aae*	Bifunctional autolysin/adhesin
Teichoic acids	(multiple biosynthetic genes)	Attachment (shown in *S. aureus*)
SdrF	*sdrF*	Binds to collagen
SdrG (Fbe)	*sdrG*	Binds to fibrinogen
SdrH	*sdrH*	Putative binding function only
Ebp	*ebp*	Binds to elastin
Embp	*embp*	Binds to fibronectin
AtlE/Aae	*atlE/aae*	Bind to multiple matrix proteins
Aap	*aap*	Binds to corneocytes
<u>Intercellular aggregation</u>		
PNAG/PIA	*icaADBC*	Intercellular polysaccharide adhesin
Bap	*bap*	Intercellular protein adhesin
Aap	*aap*	Intercellular protein adhesin precursor (requires proteolytic processing for activity)
Embp	*embp*	Intercellular protein adhesin
Teichoic acids		Component of biofilm matrix
Protective exopolymers		
PNAG/PIA	*icaADBC*	Protects from IgG, AMPs, phagocytosis, complement
PGA	*capABCD*	Protects from AMPs, phagocytosis
Resistance to AMPs		
SepA protease	*sepA*	AMP degradation
Dlt, MprF, VraFG	*dltABCD* *mprF* *vraFG*	In analogy to *S. aureus*: D-alanylation of teichoic acids (Dlt), lysylation of phospholipids (MprF), putative AMP export (VraFG)
Aps system	*apsR (graR), apsS (graS), apsX*	AMP sensor, regulator of AMP resistance mechanisms
Toxins		
Enterotoxins		
SEC3, SE1L	*sec3, selL*	Pathogenicity island-located enterotoxins
Phenol-soluble modulins (PSMs)		
PSMα	*psm α*	Cytolysin (moderate activity), pro-inflammatory
PSMβ1, PSMβ2	*psmβ1, psmβ2*	Biofilm-structuring surfactants, pro-inflammatory
PSMδ	*psm δ*	Cytolysin (strong activity), pro-inflammatory
PSMε	*psm ε*	Cytolysin (moderate activity), pro-inflammatory
δ-toxin	*hld*	Cytolysin (moderate activity), pro-inflammatory
PSM-mec	*psm-mec*	Cytolysin (moderate activity), pro-inflammatory
Exoenzymes		
Proteases		
Cysteine protease (SspB, Ecp)	*sspB*	Unknown, tissue damage?
Metalloprotease/elastase (SepA)	*sepA*	Tissue damage?, AMP resistance
Glutamylendopeptidase (GluSE, SspA, Esp)	*sspA*	Degradation of fibrinogen and complement factor C5, competition with *S. aureus* (by proteolysis of biofilm matrix proteins?)
Lipases GehC, GehD	*gehC, gehD*	unknown
Others		
Fatty acid modifying enzyme unidentified (FAME)		Detoxification of bactericidal fatty acids

2. Biofilm formation of staphylococci and regulation

2.1 Definition of a biofilm

Although Ogston and Rosenbach identified staphylococci as elicitors of an infection in 1884, the first publications reporting the slime production of bacteria were in 1958 by Wilkinson, and Catlin and Cunningham (Arciola *et al.*, 2015). In 1978, Costerton asserted that bacteria stick on available surfaces in glycocalyx-enclosed biofilms and that the sessile bacterial population becomes predominant particularly in medical ecosystems (Costerton *et al.*, 1978). Biofilm formation was later defined by him as the aggregation of bacteria of the same or different species embedded in an extracellular matrix. He also mentioned, that the formation of these sessile communities and their inherent resistance to antimicrobial agents are at the root of many persistent and chronic bacterial infections and that biofilms contain differentiated, structured groups of cells with community properties (Costerton *et al.*, 1999). This definition of a biofilm is still valid and within the last eighteen years more and more details concerning the biofilm composition and regulation were uncovered.

2.2 Biofilm types and development process

The biofilm development includes three phases, the initial attachment, the accumulation/maturation phase and the final detachment/dispersal phase (Otto, 2013; **Fig. I-2**). In addition, Moormeier *et al.* identified a fourth phase in *S. aureus* that is timed between multiplication and maturation phase. Prior to tower formation, a subpopulation of cells expresses in Sae-dependent manner the secreted staphylococcal nuclease (*nuc*), which leads to the degradation of the previously formed nucleoprotein matrix and thus to the release of bacterial cells from the biofilm. Because of this, the phase is called "exodus". These findings are consistent with a model in which biofilms exhibit multicellular characteristics including the presence of specialized cells and a division of labour that imparts functional consequences to the remainder of the population. The exodus phase is distinct from *agr*-mediated dispersal events of the detachment phase (Moormeier *et al.*, 2014).

The amount, composition and stickiness of the matrix can vary from species to species (*e.g.* among CoNS and compared to *S. aureus*) and within a species (*e.g. S. epidermidis* O-47 compared to RP62A). The biofilm matrix can be formed *icaADBC*-operon dependent, *icaADBC*-operon independent or by both mechanisms at the same time (**Fig. I-3**). The biofilm formation of strain RP62A, for example, is mainly *ica*-dependent, whereas strain O-47 forms a mixed biofilm *ica*-dependently and *ica*-independently.
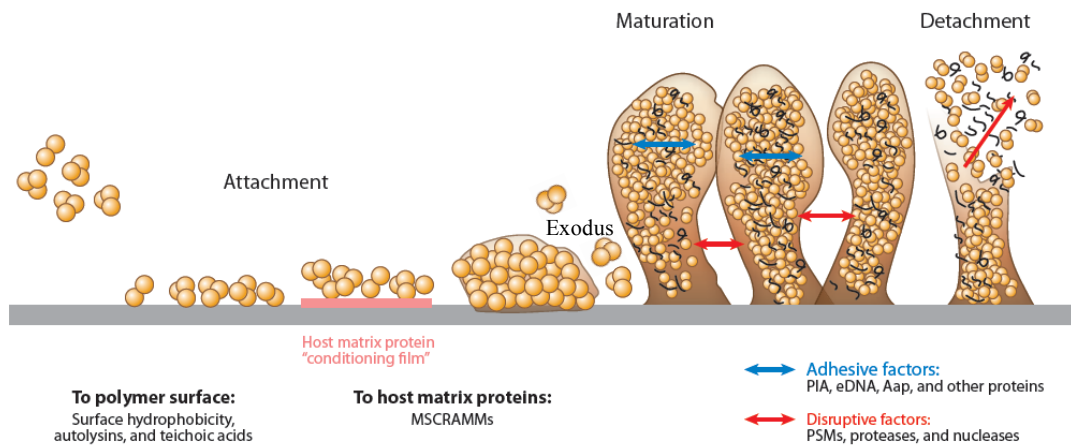
Fig. I-2: Phases of biofilm development

> Figure modified from Otto, 2013 (Figure 1). Shown are the phases of biofilm development including attachment, maturation and detachment phase. Main factors contributing to biofilm formation and dissemination are mentioned below. The original figure was extended by the exodus phase.

Moreover, it was shown that the composition of the extracellular matrix is dynamic and adjustable during an infection, *e.g.* a switch from protein- to polysaccharide intercellular adhesin/poly-N-acetylglucosamine (PIA/PNAG)-mediated-biofilm production (Weisser *et al.*, 2010). Other biofilms contain a combination of proteins and eDNA (**Fig. I-3 B**) or amyloid fibers (**Fig. I-3 D**). An extra biofilm type, formed only by *S. aureus* due to its ability to produce coagulase (Coa), is the fibrin-biofilm (**Fig. I-3 C**) that enables *S. aureus* to survive in human blood (Zapotoczna *et al.*, 2016).
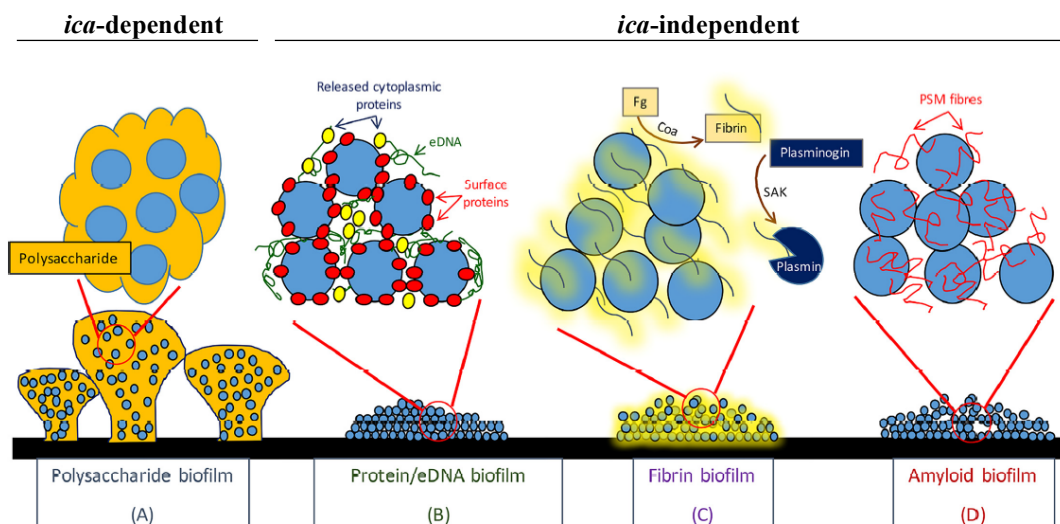
Fig. I-3: Biofilm types of Staphylococci

> Figure was modified from Zapotoczna *et al.*, 2016. **A-D** depict different biofilm types. Type C is only formed by *S. aureus*. Type A, B and D are formed by *S. aureus* and *S. epidermidis*. To emphasise the regulation of the different types in matters of *ica*-dependence and *ica*-independence, the original figure was modified.

2.3 Polysaccharide mediated biofilm

2.3.1 *Genetic requirements for PIA synthesis*

Polysaccharide intercellular adhesion or poly N-acetylglucosamine (PIA/PNAG) is the major component of *S. epidermidis* biofilm matrix (Vuong *et al.*, 2004b). It consists of poly-β(1-6)-N-acetylglucosamine, a linear glucosaminylglycan that has a fundamental function in mediating intercellular adhesion of bacterial cells (Mack *et al.*, 1996a; Mack *et al.*, 1996b; McKenney *et al.*, 1998). Approximately 20% of the molecule is de-acetylated. The de-acetylation creates free amino groups, which at neutral or acidic pH give the molecule a cationic character (marked with a circle in **Fig. I-4**; Joo and Otto, 2012).

E

PIA (PNAG)

β-D-GlcNAc-(1->6)-2-amino-2-deoxy-β-D-Glc*p*-
(1->6)-β-D-GlcNAc-(1->6)-β-D-GlcNAc
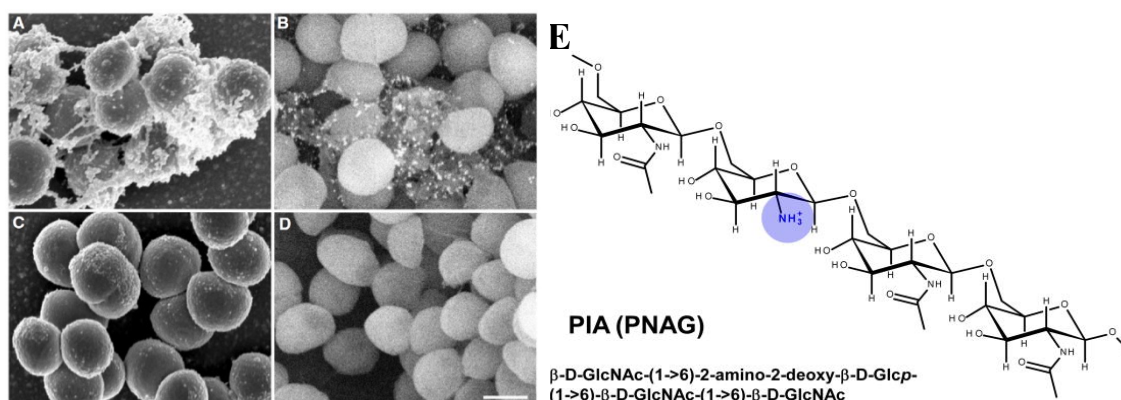
Fig. I-4: Molecular structure of PIA/PNAG in chair form

A-D: Figure taken from Vuong *et al.*, 2004b, showing an ultrastructural analysis of *S. epidermidis*. Scanning electron and immunoelectron microscopy images of the wildtype (A and B) and *ica*-negative mutant (C and D). PIA was immunogold labelled using αPIA-antisera (B and C). Magnification 25000x. The scale bar represents 0.6 μm. **E**: Figure modified from Joo and Otto, 2012. The molecular structure of PIA/PNAG is depicted in chair form.

PIA is synthesized, exported and modified by the gene products of the *icaADBC*-operon, which is depicted in **Fig. I-5** (Heilmann *et al.*, 1996b; Mack *et al.*, 1996a; Mack *et al.*, 1996b; McKenney *et al.*, 1998). This operon was initially described in *S. epidermidis* and shortly after also found in other CoNS and in *S. aureus* (Cramton *et al.*, 1999). In 2002, IcaR protein was identified as the negative regulator of *icaADBC* (Conlon *et al.*, 2002a). The genomic sequence of *icaR* gene is located divergent to the nucleotide sequence of *icaADBC*-operon (**Fig. I-5**).
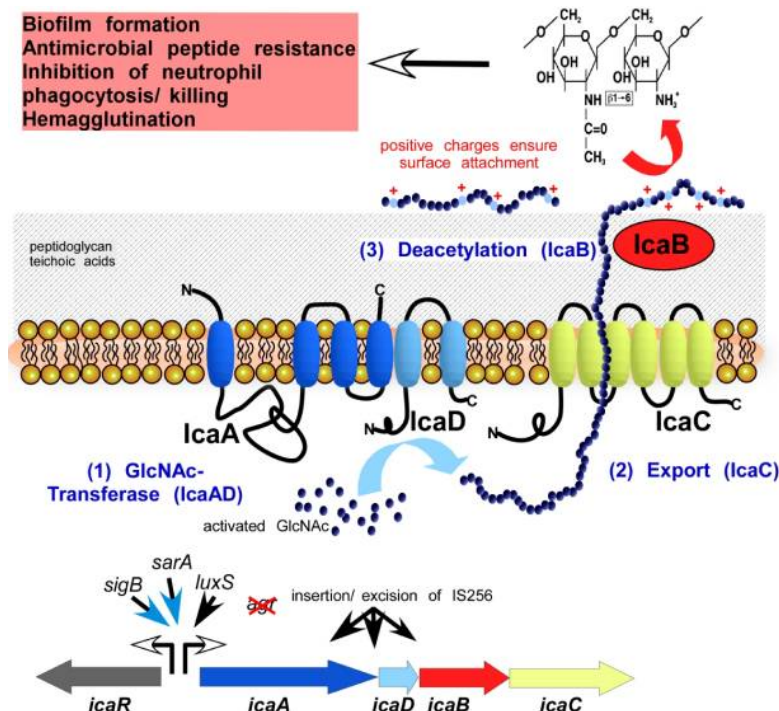
Fig. I-5: The exopolysaccharide PIA/PNAG synthesis

Figure taken from Otto, 2012 (Figure 1). **Bottom**: Schematic overview of the *ica*-operon and its regulator IcaR. The big arrows indicate the genomic direction for transcription. The small arrows indicate the position of the promotors of *icaA* and *icaR*. **Middle**: Three steps of PIA/PNAG synthesis carried out by Ica-proteins. In step 1, the transmembrane proteins IcaA and IcaD function together as IcaAD to connect the N-acetylglucosamine residues. In step 2, IcaC exports the molecule from the cytoplasm through the cytoplasmic membrane to the extracellular surface. In step 3, IcaB deacetylates parts of the PIA/PNAG. **Top**: PIA/PNAG molecular structure in Haworth projection.

The proteins IcaA and IcaD are located in the cytoplasmic membrane and together as IcaAD produce N-acetylglucosamine oligomers of 20 residues maximal length by connecting GlcNac residues (Gerke *et al.*, 1998). IcaC also has all structural features of an integral membrane protein and a close interaction between IcaA, IcaD and IcaC was proposed by the authors. IcaC was supposed to function as a translocase and be responsible for the export of the oligomers. The surface-attached protein IcaB is responsible for the extracellular deacetylation of the poly-N-acetylglucosamine molecule (Pokrovskaya *et al.*, 2013; Vuong *et al.*, 2004a). De-acetylation is important, as it introduces positive charges that are crucial for the PIA polymer to adhere to the bacterial surface (Otto, 2013).

But, the role of IcaC was questioned again by Atkin and colleagues in 2014. They compared the IcaADBC system of staphylococci with the PgaABCD system of *E. coli* and claimed a different function for IcaC (**Fig. I-6**). In their model, IcaC is a O-succinyltransferase that adds succinyl groups to the PNAG polysaccharide as it emerges from the outer leaflet of the cytoplasmic membrane. IcaC is not a conserved component of synthase-type polysaccharide biosynthesis systems and is not even widely found in *ica*-operons in other

Gram-positive bacteria, but in *S. epidermidis* and in *S. aureus*, which also have O-succinylated PNAG. It appeared to the authors that IcaC has a function specific for selected Staphylococcal species (Atkin *et al.*, 2014).
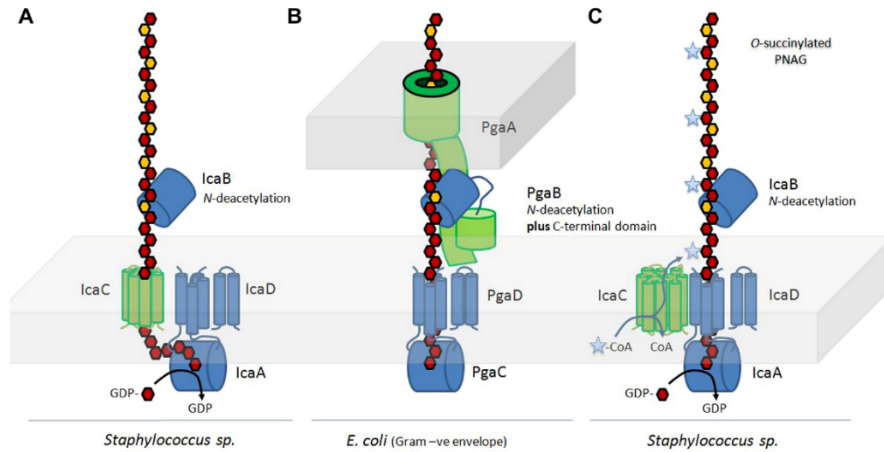
Fig. I-6: Schematic comparison of the models for Ica and Pga gene functions in the biosynthesis of PNAG

> Figure was taken from Atkin *et al.*, 2014. (**A**) Current model in Gram-positive bacteria. (**B**) Pga system from Gram-negative *E. coli*. (**C**) Refined model of the authors, that has a different route for PNAG export through IcaAD and the added O-succinylation of the PNAG which they propose is catalysed by IcaC. In each system, shared components are coloured blue and unique components are coloured green. The indicated degree of deacetylation and O-succinylation are not stoichiometrically accurate and are for illustrative purposes only.

In *ica*-positive *S. epidermidis*, the *icaADBC*-operon is located next to a threonyl-tRNA, a multidrug resistance transporter and some hypothetical proteins on the one side and to lipase *geh-1* on the other side. *ica*-negative *S. epidermidis* lack the *ica*-operon sequence and the genomic region downstream of the threonyl-tRNA is different (Eckart, 2006).

Several studies identified the ability to form biofilms and to synthesise PIA as an important factor for pathogenicity, so that the *icaADBC*-operon became a relevant marker (Fowler *et al.*, 2001; Galdbart *et al.*, 2000; Rupp *et al.*, 1999a; Rupp *et al.*, 1999b; Rupp *et al.*, 2001; Ziebuhr *et al.*, 1997). The importance of this locus was confirmed by expressing the whole operon from a plasmid in *ica*-negative strains (*i.a.* Tü3298 and ATCC 12228), which produced biofilms afterwards (Li *et al.*, 2005). Moreover, PIA was reported to directly protect against the innate immune system (Vuong *et al.*, 2004b). For skin colonisation, though, the commensal lifestyle, the carriage of *ica* seems to be a fitness cost, because *ica*-negative strains have the ability to outcompete isolates producing PIA (Rogers *et al.*, 2008). Under high shear stress environments, *icaADBC* transcription was found to be upregulated in *S. epidermidis* and only PIA producer and strong biofilm forming strains, but no *ica*-negative strain, were isolated (Schaeffer *et al.*, 2016), underlining the importance of PIA for colonisation of catheters.

2.3.2   *Regulation of the icaADBC-operon*

Biofilm formation, *ica*-dependent and -independent, is regulated by a complex regulatory network. Ica-dependent biofilm formation involves regulators, like for instance transcription factors, two-component systems and also an alternative sigma factor of RNA polymerase. They regulate *icaADBC* expression either directly or indirectly.

IcaR, the most prominent regulator of them, directly binds to P*icaA* and represses the transcription of the operon. The repressor, first described in 2002 (Conlon *et al.*, 2002a), is encoded by the gene *icaR* that is located upstream of the *icaADBC*-operon and transcribed divergently to *icaA* (**Fig. I-7**). An *icaR*::Em^r insertion mutation in *S. epidermidis* CSF41498 resulted in an at least 5.8-fold increase in *ica*-operon expression, but did not significantly alter transcription of the gene itself. IcaR, thus, was identified as repressor of *ica*-operon transcription in *S. epidermidis* (Conlon *et al.*, 2002a). This was also verified for *S. aureus* (Jefferson *et al.*, 2003). The crystal structure of IcaR from *S. epidermidis* revealed a homodimer comprising entirely α-helices, which is typical for the tetracycline repressor protein family (TetR family) (Jeng *et al.*, 2008). The N-terminal domain of the protein contains a conserved helix-turn-helix DNA binding motif and the C-terminal domain shows characteristics ideal for efficient and specific dimer formation. Two IcaR dimers specifically bind to the *ica*-operator and engulf 28 bp of core segment, thereby repressing the transcription of *icaA* (Conlon *et al.*, 2002a; Jeng *et al.*, 2008; **Fig. I-7; Fig. V-10**).
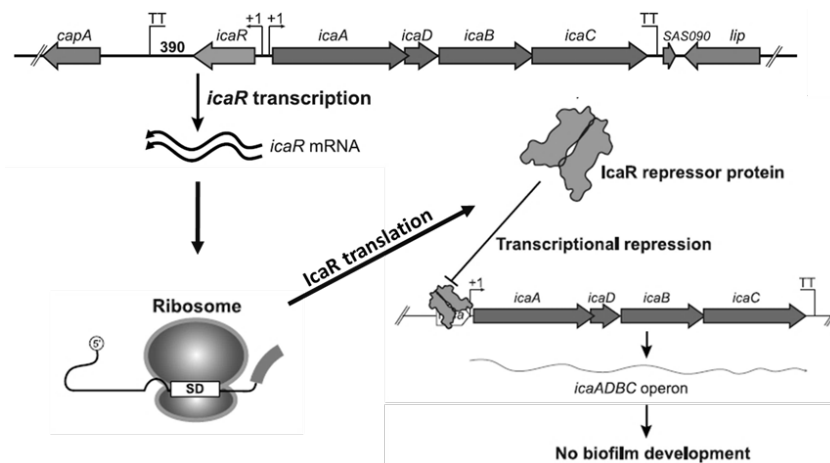
Fig. I-7: Ica-operon regulation mediated through IcaR repressor protein

The figure was modified from Ruiz de los Mozos *et al.*, 2013. Transcription of *icaR* and translation of *icaR* mRNA into the functional IcaR protein leads to the transcriptional repression of the *icaADBC* operon and in consequence to the repression of biofilm formation.

Since PIA production is a metabolically costly process, its production is influenced by external (environmental) signals and the internal (metabolic) status. Various regulators respond to these stimuli and regulate *ica*-operon expression either directly or indirectly

through the regulation of *icaR*. Thereby, regulation is carried out by yet unknown σ^B-dependent and σ^B-independent regulators. Ethanol, for example, represses *icaR* transcription σ^B-independently (Conlon *et al.*, 2002a), but so far requires an unknown additional factor (Knobloch *et al.*, 2004). Another environmental stress, NaCl, regulates *icaR* σ^B-dependent through RsbU, a positive regulator of σ^B (Knobloch *et al.*, 2001; Knobloch *et al.*, 2004), but not on transcriptional level (Conlon *et al.*, 2002a).

Moreover, *icaR* mRNA of *S. aureus* represses under yet unknown circumstances its own translation (autoregulation). Thereby, 5′UTR and 3′UTR of *icaR* mRNA bind to each other and block the ribosome binding site. The formed complex is degraded subsequently by RNase III. In consequence, *icaR* is not translated into IcaR protein and thus *ica*-operon regulation by IcaR is inhibited (Ruiz de los Mozos *et al.*, 2013), leading to PIA synthesis. The factor leading to *icaR* autoregulation is still unknown and a RNA regulator was speculated by the authors to be involved. The authors excluded such a regulation for *S. epidermidis*.

The following table (**Tab. I-2**) lists the known *icaADBC*-regulators of *S. epidermidis* and *S. aureus* and shows that there are a lot of differences in the regulation of this operon between these two staphylococcal species.

Tab. I-2: Regulatory factors affecting *icaADBC* expression in staphylococci

The table was extended from Cue *et al.*, 2012. Regulatory factors are listed with the overall effect on *icaADBC* transcription, the probable mechanism and the references. Abbreviations: Sa = *S. aureus*, Se = *S. epidermidis*. *[1] The authors identified DNA binding protein II and topoisomerase IV beside SarA and TcaR to bind to *ica* promoter.

Regulatory factor	Effect on *icaADBC* transcription	Probable mechanism	Reference
Se IcaR	Negative	Two dimers bind *ica*-operator; inhibition of *icaA* transcription; IcaR is dominant over the Rbf-SarR-SarX axis	Conlon *et al.*, 2002a; Jeng *et al.*, 2008 Rowe *et al.*, 2016
Sa IcaR	Negative	Two dimers bind *ica*-operator; inhibition of *icaA* transcription	Jefferson *et al.*, 2003; Jefferson *et al.*, 2004*[1]
Se SarA	Positive	Direct binding to *icaA* promoter region	Tormo *et al.*, 2005
Sa SarA	Positive	Direct binding to *icaA* promoter region	Valle *et al.*, 2003
Se SarZ	Positive	SarA paralog; unknown	Wang *et al.*, 2008
Se SarX	Positive	Binding to *ica* operon promoter and to *agr* P3 promoter (RNAIII transcription activation)	Rowe *et al.*, 2011
Sa SarX	-	Expressed in stat. phase; binds to *agr* promoter;	Manna and Cheung, 2006
	Positive	Binding of *ica* promotor region and within *icaR* DNA; Activation of *icaADBC* via	Cue *et al.*, 2013

		inhibition of IcaR at low levels of SarX and by stabilizing RNA polymerase binding at high levels; regulated by Rbf	
Se Spx	Negative	*icaR*-independent	Wang *et al.*, 2010
Sa Spx	Negative	Upregulation of *icaR*	Pamp *et al.*, 2006
Se σ^B	Positive	Repression of *icaR*	Knobloch *et al.*, 2004
Sa σ^B	Positive	-	Rachid *et al.*, 2000
Sa TcaR	Negative	Binding to *ica* promoter sequence; Weak repressor in comparison to IcaR	Jefferson *et al.*, 2004*[1]
Se TcaR	Negative	Repressor; Six TcaR dimers bind specifically to three approx. 33 bp segments close to the IcaR binding region with varying affinities; preferentially ssDNA over dsDNA unlike other MarR family proteins or TetR family proteins	Chang *et al.*, 2010; Chang *et al.*, 2012; Chang *et al.*, 2014
Se CcpA	Positive	Unknown	Sadykov *et al.*, 2011
Sa CcpA	Positive	Indirect; presumably via down-regulation of TCA cycle genes *citB* and *citZ*	Seidl *et al.*, 2008
Se Ygs	Positive	Unknown	Wang *et al.*, 2011
Se LuxS	Negative	Unknown	Xu *et al.*, 2006
Se GdpS	Positive	Increasing *icaADBC* mRNA levels; unknown mechanism; σ^B independent; no effect on transcription of IcaR, SarA, TcaR	Holland *et al.*, 2008
Sa GdpS	Positive	Unknown	Tu Quoc *et al.*, 2007
Se ArlRS	Positive	Direct binding to *ica* promoter region; *icaADBC*, *sigB*, and *sarA*, were decreased and *icaR* increased in 1457ΔArlRS	Wu *et al.*, 2012
Sa ArlRS	-	- (modifies extracellular proteolytic activity)	Fournier and Hooper, 2000; Fournier *et al.*, 2001; Fournier and Klier, 2004
Sa Rob	Positive	Repressor activity, but binding of TATTT motif within the *icaR-icaA* intergenic region leads to increased *icaADBC*-operon expression (no TATTT motif in Se and also no *rob*)	Yu *et al.*, 2017
Se Rbf	Positive	No direct binding to *ica* operon promoter region; binds to SarR promoter	Rowe *et al.*, 2016
Sa Rbf	Positive	Repression of *icaR* through a hypothetical regulator (SarX identified by Cue *et al.*, 2013)	Cue *et al.*, 2009
Se SrrAB	Positive	binds to promoter regions of *icaR*, *icaA*, *qoxB*, *pflBA*; *icaA* downregulated in 1457ΔSrrAB whereas *icaR* was upregulated (oxic conditions) and downregulated (anoxic conditions)	Wu *et al.*, 2015
Sa SrrAB	Positive	Direct binding to region 100 bp upstream of *icaA*	Ulrich et al., 2007
Sa GbaB	Positive	Unknown	You *et al.*, 2014
Se YycFG	Positive	Repression of *icaR* by binding of YycF to P$_{icaR}$	Xu *et al.*, 2017

3. RNA-mediated regulation of gene expression

A bacterial infection requires the bacteria to adapt to the host environment. The adaptation process requires detection, integration and response to different external and intracellular conditions. In response to specific signals, regulatory proteins and riboregulators of the pathogens change the gene expression of metabolic genes and facilitate virulence factor expression, thereby directly supporting the infection process. Gene expression can be regulated by transcriptional and post-transcriptional control; the latter includes the regulation of mRNA translation, mRNA stability and processing (Svensson and Sharma, 2016). Riboregulators are encoded on the bacterial chromosome or on mobile genetic elements (Brantl, 2007).

3.1 Regulatory mechanisms

3.1.1 *Cis-and trans-acting sRNAs*

RNA-based regulation by sRNAs controls posttranscriptional events by using two general mechanisms: (i) sRNAs act by base-pairing with other RNAs (antisense mechanism) or (ii) by binding proteins.

Protein binding sRNAs mimic the protein binding sequences found in mRNAs (Chambers and Sauer, 2013). They modulate the activity of the protein leading the protein to bind its target RNA with induced or lowered affinity, meaning the sRNA can titrate the affinity of the protein and even sequester the protein regulator from target mRNAs. The Csr/Rsm regulatory network and the 6S rRNA are known examples for such a regulatory mechanism (for detailed information see the review of Svensson and Sharma, 2016).

Base-pairing sRNAs are categorized as *cis* or *trans* based on their location within the bacterial genome relative to their mRNA target. *Cis*-encoded sRNAs are transcribed from the opposite DNA strand and are in parts complementary to their mRNA targets (> 75 nt; **Fig. I-8 A**). *Trans*-encoded sRNAs are transcribed from different genomic locations than their targets and interact with imperfect base-pairing. They are often encoded in intergenic regions, but can also derive from untranslated regions (5′ and 3′ UTRs) and coding regions (ORFs) (**Fig. I-8 B**). Some of the sRNAs require the RNA chaperone Hfq for stability and function. These RNAs contain a 'seed region' that interacts with mRNAs, an AU-rich Hfq-binding region and a structured terminal loop for Rho-independent transcription termination. The unpaired sequences in hairpin loops of a folded RNA are also interaction sites and pair with a target (*e.g.* mRNAs). Many C- or C/U-rich loops have been reported to bind to the G-rich SD sequence of mRNAs. The base-pairing leads to activation or repression of target gene expression (see review of Svensson and Sharma, 2016; **Fig. I-9 A**).
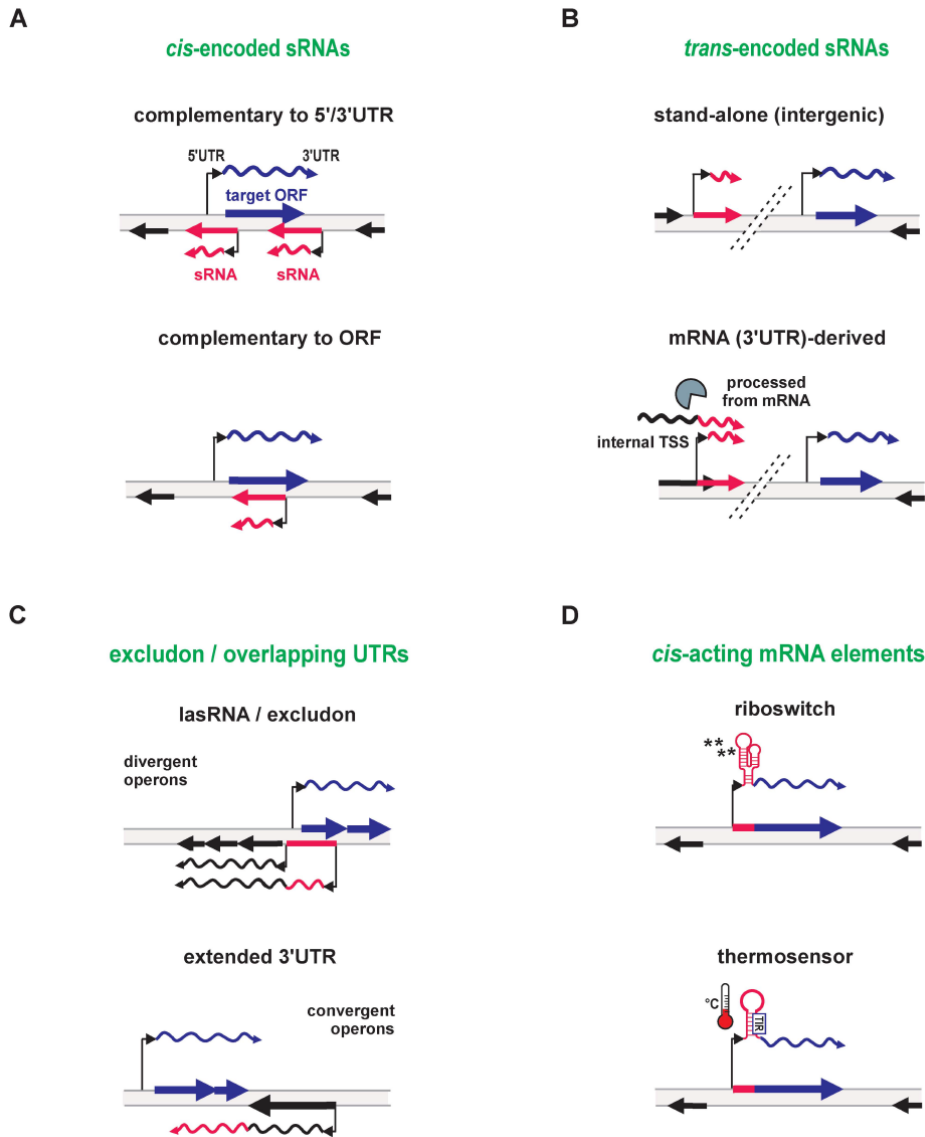
Fig. I-8: Genomic location and regulatory relationships between bacterial riroregulators and their mRNA targets

Figure was taken from Svensson and Sharma, 2016 (Figure 1). Riboregulators are depicted in red; target mRNAs are shown in blue. Flanking open reading frames (ORFs) are shown in black. Arrows indicate transcriptional start sites. (**A**) *Cis*-encoded antisense RNAs are transcribed from the opposite strand to their target mRNAs and can overlap with target 5′/3′ untranslated regions (UTRs) (top panel) and/or the mRNA ORF (bottom panel). (**B**) *Trans*-encoded sRNAs can be expressed from distinct regions of the chromosome from their target genes: either from stand-alone genes encoded intergenically (top panel) or from ORFs/3′UTRs via either processing or internal transcriptional start sites (bottom panel). (**C**) Extended UTR elements of adjacent operons can allow for co-regulation of related genes at the posttranscriptional level. The long-antisense RNA (lasRNA) of the excludon paradigm arises from transcription of an extended 5′UTR that has complementarity to a divergently transcribed operon (top panel). Also, extended 3′UTR elements can potentially base-pair with transcripts expressed from convergently transcribed operons (bottom panel). (**D**) *Cis*-elements within mRNAs themselves can regulate expression of their associated transcripts. These include ligand-binding riboswitches (top panel) and temperature-responsive RNA thermosensors (bottom panel).
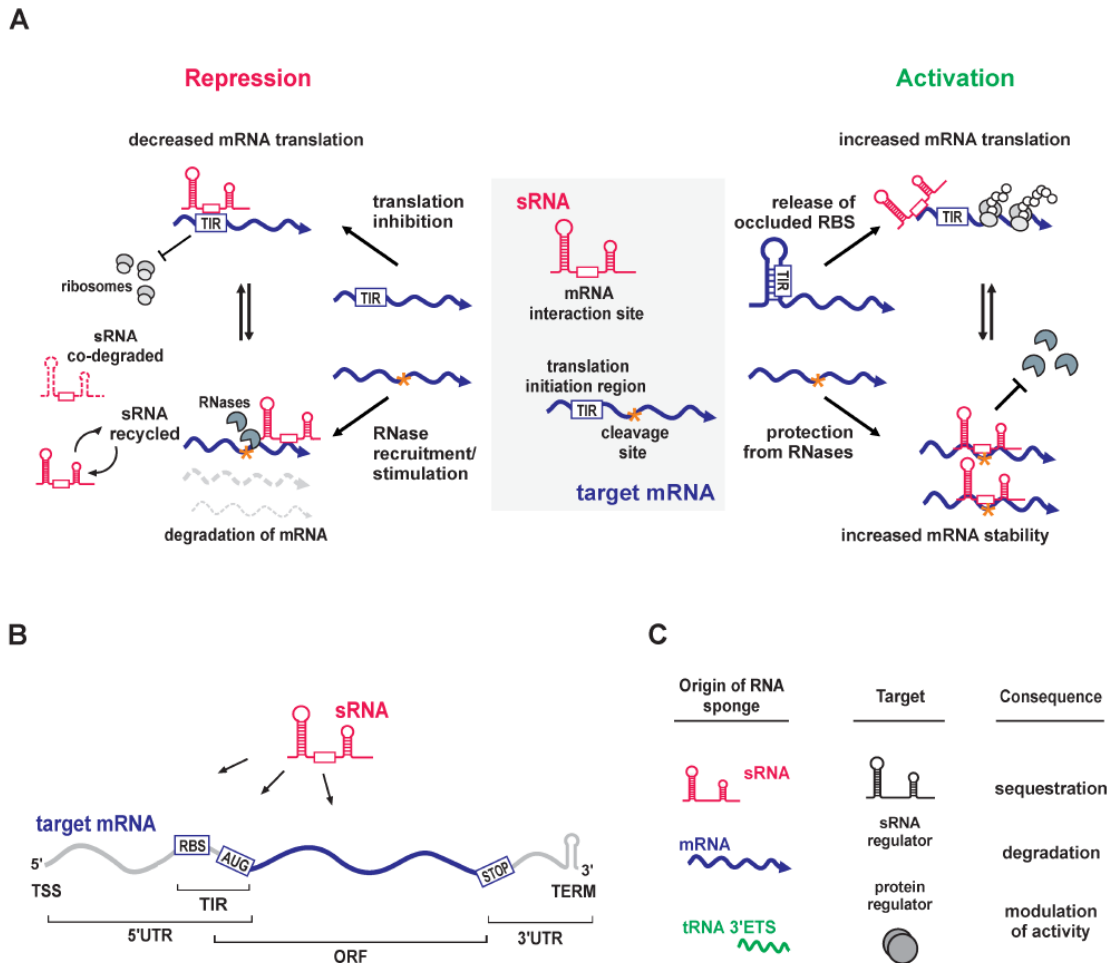
Fig. I-9: Mechanisms of posttranscriptional control by regulatory RNAs

Figure taken from Svensson and Sharma, 2016 (Figure 2). (**A**) Gene repression (left) and activation (right) mechanisms used by base-pairing sRNAs (depicted in red) for direct regulation of target mRNAs (shown in blue) at the level of translation or stability. Base-pairing interaction sites in mRNAs and sRNAs are shown with blue- and red-lined boxes, respectively. Potential RNase cleavage sites are indicated with an orange asterisk. TIR, translation initiation region, including RBS and start codon. (**B**) Potential sRNA interaction sites in regulated target mRNAs, starting from the TSS (transcriptional start site) to the transcriptional terminator (TERM). (**C**) Targeting/titration of other regulatory molecules by riboregulators acting as so-called sponges to affect gene expression. RNA sponges can be stand-alone sRNAs, regions of mRNAs themselves (either intact or processed), or those derived from housekeeping RNAs such as the 3′ external transcribed spacer (3′ ETS) of tRNAs. They can target either sRNA or protein regulators and have been shown to sequester them from their targets, trigger their degradation, and/or modulate their regulatory activity.

3.1.2 *Cis-acting endogenous mRNA elements*

In addition to regulatory sRNAs, endogenous highly conserved and structured regions within mRNAs also control mRNA expression (Svensson and Sharma, 2016; **Fig. I-8 D**). These c*is*-acting regulatory elements, such as riboswitches and thermosensors, are part of long bacterial 5′-UTRs, that exceed the average 5′-UTR-length of 20-40 nt. Furthermore, the translation initiation region that includes the ribosome binding site and the start codon, as well as upstream or downstream regions are important for the binding by ribosomes and therefore can influence the translation frequency. This is the case especially for weaker start codons like TTG. CDS with strong start codons like ATG are more easily accessible and the genes often lack these structural elements (Duval *et al.*, 2015).

Riboswitches detect intermediate metabolites or end products of the pathway they regulate. Such metabolites are *e.g.* thiamine pyrophosphate, Mg^{2+} purines, amino acids, charged tRNAs or phosphosugars (Svensson and Sharma, 2016). The metabolite is sensed within the aptamer region, causing a conformational change in a second region, the expression platform, leading to transcriptional or translational inhibition. Riboswitches of Gram-positive bacteria usually affect transcriptional attenuation, whereas Gram-negative riboswitches more frequently inhibit translation (Waters and Storz, 2009).

Thermosensors, also called 'RNA thermometers', regulate gene expression in response to temperature changes by base pairing with the RBS of the mRNA at low temperatures. When the temperature increases, the base pairing loosens and the RBS becomes accessible for ribosomes leading to translation of the downstream genes. Known thermosensors are the FourU element and the ROSE element. They are found in heat shock genes or virulence genes necessary for survival during inflammation (Grosso-Becera *et al.*, 2015; Kortmann and Narberhaus, 2012).

The role of bacterial 3′-UTRs in gene regulation is less explored than in eukaryotes. However, they recently emerged as a new class of post-transcriptional regulatory elements that for example contain small regulatory RNAs and regulate target gene expression, are a target of regulatory RNAs themselves or regulate translation initiation and decay in their own mRNAs (Ren *et al.*, 2017). The latter was found for *S. aureus icaR* mRNA. An intrinsic interaction between the 3′-UTR and the 5′-UTR of *icaR* mRNA results in translational inhibition (Ruiz de los Mozos *et al.*, 2013; see chapter I-4.3.2). Unfortunately, the environmental signal leading to this autoregulation is still unknown.

3.1.3 *Cis-encoded antisense sRNAs acting in trans*

S. aureus SprA1/A1$_{AS}$ toxin-antitoxin module represents an example for a *cis*-encoded antisense sRNA that acts in *trans* (**Fig. I-10**). SprA1$_{AS}$ is located on the opposite strand to SprA1 with overlapping 3′-UTRs. Unlike *cis*-acting RNAs, the overlapping region is not involved in regulation, but the non-overlapping 5′-UTR of SprA1$_{AS}$. Therefore, this RNA acts in *trans*.
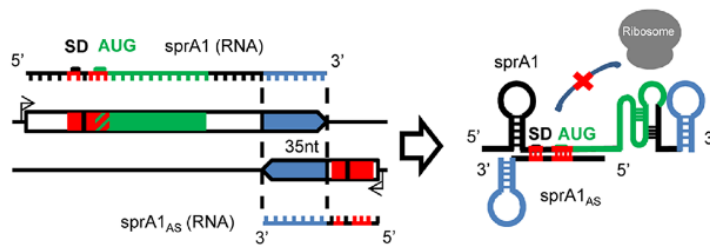
Fig. I-10: Regulatory mechanism of *cis*-encoded antisense sRNAs acting in *trans* Figure modified from Guillet *et al.*, 2013 (Figure 1).

3.2 Regulatory RNA elements in staphylococci

3.2.1 *Dual-function RNAs and their impact in virulence*

Two well-studied dual-function RNAs in *S. aureus* are RNAIII, the effector molecule of the quorum sensing *agr* system, and the Psm-mec RNA of MRSA.

RNAIII of *S. aureus* was the first sRNA shown to directly affect virulence (Svensson and Sharma, 2016; Vanderpool *et al.*, 2011). It is expressed by the P3 promoter of the *agr*-system, one of the quorum sensing (QS) systems in staphylococci (**Fig. I-11 top**). This dual-function RNA is a key virulence regulator with a length of 514 nt (Balaban and Novick, 1995; Morfeldt *et al.*, 1995; Novick *et al.*, 1993). It is a multifunctional RNA that encodes a small peptide (δ-haemolysin), and its noncoding parts act as antisense RNAs to regulate the translation and/or the stability of mRNAs encoding transcriptional regulators, major virulence factors, and cell wall metabolism enzymes (Bronesky *et al.*, 2016).

RNAIII contains various C-rich sequence motifs as seed regions that bind to the Shine-Dalgarno (SD) sequence of mRNA targets. Binding of RNAIII to several mRNAs (*spa*, *coa*, *rot*, *sbi*) can prevent binding of the 30S small ribosomal subunit, and in several cases this step is followed by rapid degradation initiated by the double strand–specific endoribonuclease III (RNase III). Binding of RNAIII to target mRNAs can also activate synthesis of exotoxins. For *hla* mRNA, interaction with RNAIII prevents the formation of an inhibitory structure sequestering the SD, whereas for *mgrA* mRNA, binding of RNAIII stabilizes the mRNA against an RNase attack (Bronesky *et al.*, 2016). More regulatory activities are depicted in **Fig. I-12 A**.
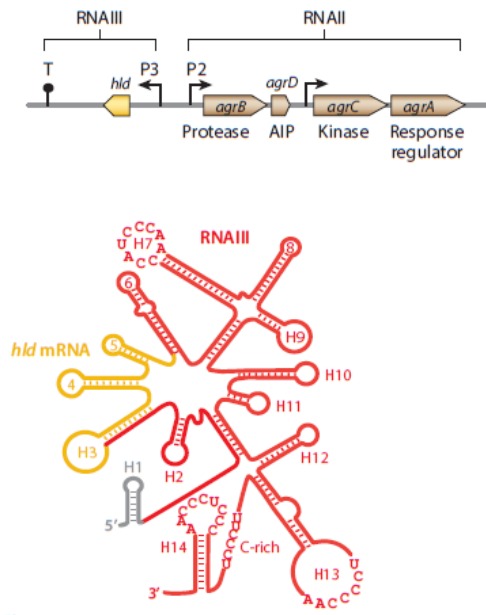
Fig. I-11: Quorum sensing *agr* system and RNAIII secondary structure

Figure modified from Bronesky *et al.*, 2016 (Figure 1). Genomic organization of the quorum-sensing *agr* system is given at top. The schematic secondary structure of RNAIII (red) is from Benito *et al.* (Benito *et al.*, 2000). The *hld* gene encoding δ-haemolysin is yellow. Abbreviation: AIP, autoinducing thiolactone peptide.
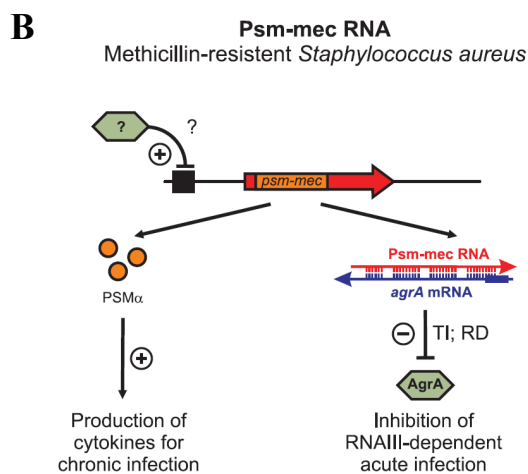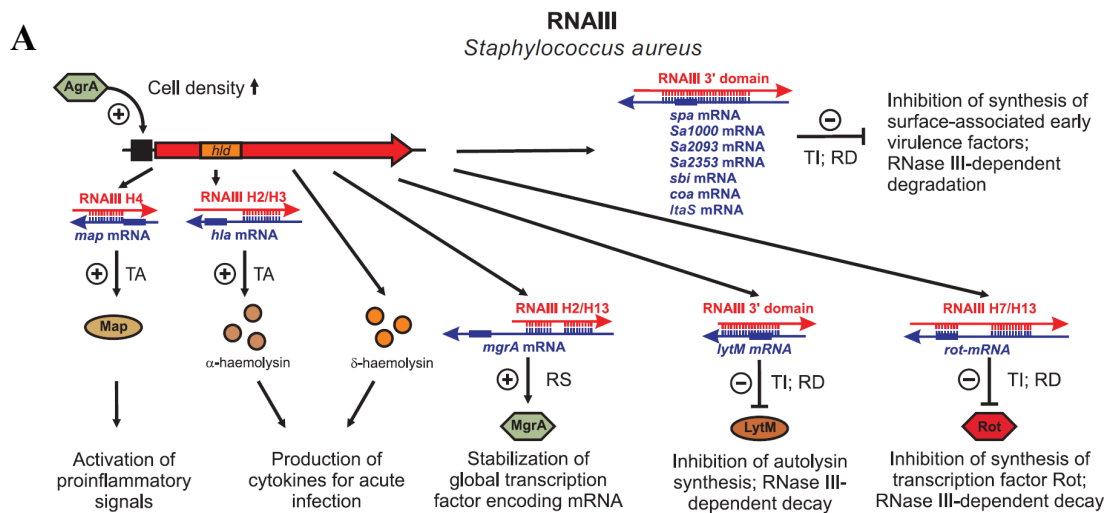
Fig. I-12: Regulatory activities of the dual-function RNAs of staphylococci: RNAIII and Psm-mec RNA

Figure was taken from Gimpel and Brantl, 2017 (Figure 2 in parts). RNAIII (**A**) and Psm-mec RNA (**B**) are displayed with interaction targets and regulatory effect.

The second dual-function RNA mentioned here is Psm-mec RNA of MRSA (**Fig. I-12 B**). The regulatory RNA base pairs with *agrA* mRNA, thus prevents AgrA synthesis and leads in consequence to the downregulation of RNAIII synthesis. The coding region encodes a phenol soluble modulin (PSMα), which is an alpha-helical peptide toxin. Psm-mec is an exception within PSMs, due to the localisation on SCC*mec* methicillin resistance mobile genetic elements of MRSA and CoNS (Kaito *et al.*, 2011; Kaito *et al.*, 2013; Qin *et al.*, 2016).

3.2.2   *Autoregulation of icaR mRNA in S. aureus by 3'-UTR repression*

The gene product of *icaR*, protein IcaR, acts as a repressor of the *ica*-operon (Conlon et al., 2002a; b; chapter I-2.3.2). The 3′ UTR of *S. aureus icaR* mRNA was found to exhibit an unusual long nucleotide sequence of 390 nt (**Fig. I-13 A+B**) and because of that a regulatory role of the 3′-UTR was speculated. Indeed, *icaR* mRNA was found to perform autoregulation by base pairing of the 3′ UTR with the 5′ UTR of one RNA molecule or by binding of two mRNAs (**Fig. I-13 C**). This interaction blocks the SD sequence and ribosomes are inhibited to bind to this region. The translation is thereby repressed. Because the mRNA is not functional anymore, this results in mRNA decay by RNase III, an RNA double-strand binding endonuclease that degrades the complex. Consequently, biofilm formation is not repressed by IcaR and PIA is synthesised (Ruiz de los Mozos *et al.*, 2013).
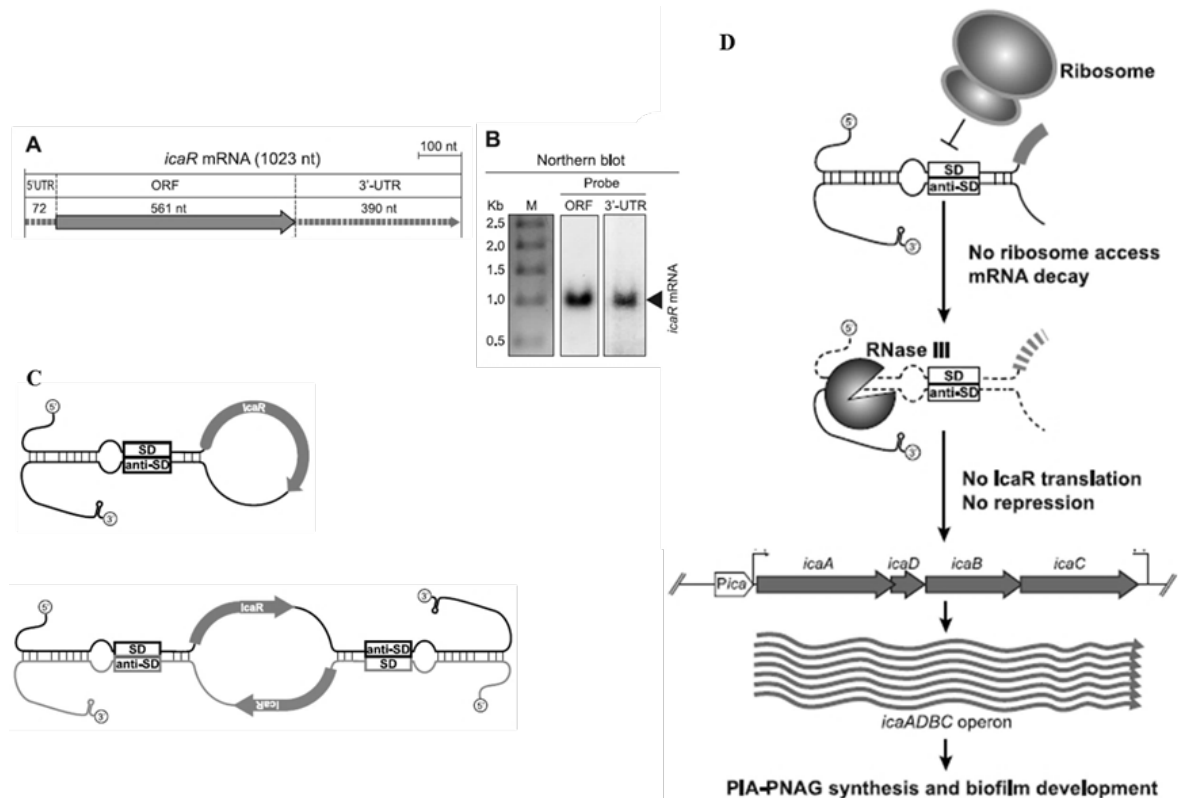
Fig. I-13: Base pairing interaction between 5′- and 3′-UTRs of *S. aureus icaR*-mRNA

Modified from Ruiz de los Mozos *et al.*, 2013. (**A**) Schematic overview of *icaR* mRNA length. (**B**) Northern blot detection of *icaR* mRNA with specific probes for the ORF and the 3′ UTR. (**C**) Depicted is the base-pairing of 5′ and 3′ UTR of one mRNA molecule (top) or the interaction of two mRNA molecules (bottom). (**D**) The interaction leads to the inaccessibility of the RBS. Ribosomes cannot bind and translate the mRNA. RNase III degrades the RNA complex. Biofilm formation is not repressed by IcaR and PIA synthesis is not inhibited.

4. Putative staphylococcal regulatory RNA: IcaZ

The transcript IGR*ica*-RNA, later renamed as IcaZ, was identified in our group in *ica*-positive staphylococci and supposed to be a regulatory (non-coding) RNA (Eckart, 2006: chapter 4.3). The ncRNA was determined to be located within IGR*ica* (the intergenic region between the genes SERP2289 and *icaR*) in *S. epidermidis* RP62A (position 2.333.155 to 2.332.670) and was named hereafter. The transcript sequence was identified to have a length of 486 nt (487 nt in *S. epidermidis* O-47) and was not supposed to genetically overlap on the same strand with the preceding *icaR* gene, but with the downstream located antisense sequence of $tRNA^{Thr-4}$ (**Fig. I-14**). For functional analysis, a deletion mutant with wide-ranging deletion of this RNA was generated in *S. epidermidis* 307 (*S. epidermidis* 307ΔIGR*ica*-sRNA). The IGR*ica*-RNA::*ermC* exchange let to diminished biofilm formation in standard *in vitro* plate assays. Microarray and RT-PCR analysis, however, revealed the formation of an unwanted antisense transcript influencing *icaADBC* expression (Eckart, unpublished data). To continue functional analysis, a markerless deletion mutant was generated in *S. epidermidis* O-47 (Herbst, unpublished data, characterised in chapter IV-1.1).
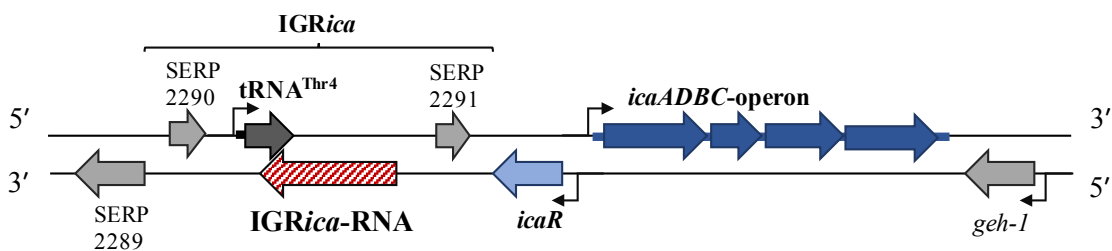
Fig. I-14: Genomic localisation of IGR*ica*-RNA in *S. epidermidis* RP62A

Schematic depiction of the genomic localisation and the length of IGR*ica*-RNA as described by Eckart, 2006.

5. Scientific relevance and objectives of this study

This doctoral study aimed to investigate the RNA, named IcaZ, in more detail. The assumed non-coding RNA is genomically located next to the *icaADBC*-operon, which codes for the enzymes needed for PIA synthesis. PIA is the main component of biofilms produced by *S. epidermidis*. The established nosocomial pathogen is known for its formation of sticky biofilms on indwelling materials and is therefore a high health risk for persons at risk, *i.e.* children, elderly or immunocompromised persons. The genomic localisation of IcaZ suggested a regulatory role of this RNA for biofilm formation, so this doctoral study furthermore aimed to decipher its functional role in the complex regulatory network of biofilm formation.

II. Laboratory Safety, Materials and Methods

1. Laboratory safety

1.1 General laboratory safety in S2-areas and the radioactivity laboratory

All experiments were carried out according to the safety regulations of the Institute for Molecular Infection Biology, belonging to Julius-Maximilians-Universität Würzburg. Safety briefings were carried out annually by the safety officers of the institute. During work with radioactive substances a radiation dosimeter badge was worn in front of the body to monitor the radiation dose the person was exposed to.

1.2 Sterilisation

Any bacterial contaminated solution, glass and plastic ware was sterilised by autoclaving for 20 min at 121°C. Heat labile plastic ware (*e.g.* prepared bubble traps used for CLSM analysis) was sterilised by autoclaving for 10 min at 80°C. Heat labile solutions were sterilised by passage through a 0.2 µm filter membrane. This sterilisation process was carried out in a class II microbiological safety cabinet.

1.3 Waste disposal

Glassware or reusable plastic ware contaminated with bacteria was autoclaved prior to washing. Disposable contaminated plastic ware was autoclaved prior to disposal and incineration process. Solutions containing bacteria were autoclaved prior to disposal down the sink with copious amounts of water. Aqueous solutions containing ethidium bromide were collected in containers and disposed as special waste. Solutions containing phenol and chloroform were collected in a bottle and then discarded as special waste for organic solvents. Plastic ware having been in contact with aforesaid was stored under the fume hood until harmful gases evaporated and then were disposed by incineration. Acidic or alkaline solutions were neutralised by pH adjustment and then disposed down the sink with copious amounts of water. Scalpels and needles were collected in a designated sharp container. Radioactive waste was collected in a shielded box and disposed as special waste.

2. Materials

2.1 Equipment and plastic ware

The utilised hardware equipment is listed in **Annexe Tab. VIII-8**. **Annexe Tab. VIII-9** lists glass and plastic ware.

2.2 Chemicals

Chemicals and nucleotides used in this work are listed in **Annexe Tab. VIII-10**. The molecular weight is given, when relevant for calculation of solutions. Chemicals in the table marked with an asterisk were used specifically for work with RNA.

2.3 Enzymes and kits

Restriction enzymes and enzymes for cloning were purchased from New England Biolabs® Inc., UK: Antarctic Phosphatase (#M0289S; 5 U/µl), BamHI-HF (#R3136S; 20 U/µl), BglII (#R0144S; 10U/µl), DpnI (#R0176S; 20 U/µl), EcoRI-HF (#R3101S; 20 U/µl), EcoRV-HF (#R3195S; 20 U/µl), KpnI-HF (#R3142S; 20 U/µl), PstI-HF (#R3140S; 20 U/µl), XmaI (#R0180S; 10 U/µl). Enzymes used for PCR: DreamTaq DNA Polymerase (Thermo Fisher Scientific Inc.; #EP0713; 5 U/µL), Phusion Green High-Fidelity DNA Polymerase (Biozym Scientific GmbH; #F-534S; 1 U/µL). **Tab. II-1** lists further enzymes and the purpose. **Tab. II-2** lists the kits that were used in this work.

Tab. II-1: List of enzymes for degradation or transformation reactions

Enzyme	Distributor	Cat.no. and conc.	Purpose
Alkaline Phosphatase, Calf Intestinal (CIP)	New England Biolabs GmbH	M0290S	dephosphorylation of DNA prior to end-labelling using T4 PNK
Proteinase K	Merck Millipore	1245680500 30 mAnson-U/mg	degradation of proteins
Lysostaphin	Genmedics GmbH, GER	2.5 mg per glass vial → endconc.: 2 mg/ml	cleavage of pentaglycin bridges
rDNaseI	Thermo Fisher Scientific Inc. (Ambion), USA	AM2235 2 U/µl	degradation of DNA
Superase-in	Thermo Fisher Scientific Inc. (Ambion), USA	AM2694 20 U/µl	inhibits RNases
T4 Polynucleotid Kinase (T4 PNK)	Thermo Fisher Scientific Inc., USA	EK0031 10 U/µl	radioactive labelling of RNA

Tobacco Acid Pyrophosphatase (TAP)	Epicentre Biotechnologies	T19050 10 U/µl	converts 5′-triphosphate RNA into 5′-monophosphate RNA
Terminator™ 5′-Phosphate-Dependent Exonuclease (TEX)	Epicentre Biotechnologies	TER51020 1 U/µl	digestion of 5′-monophosphate RNA for primary transcript enrichment
RevertAid Premium Reverse Transcriptase	Thermo Fisher Scientific Inc., USA	EP0441 200 U/µL	cDNA synthase
RiboLock RNase Inhibitor	Thermo Fisher Scientific Inc., USA	EO0381 40 U/µL	inhibits RNases
RNase A	Thermo Fisher Scientific Inc., USA	EN0531 10 mg/ml	degradation of RNA
T4 RNA ligase	Thermo Fisher Scientific Inc., USA	EL0021 10 U/µL	RNA ligation reactions

Tab. II-2: Kits used in this work

Kit	Manufacturer	Purpose
NucleoSpin® Gel and PCR Clean-up kit	MACHEREY-NAGEL GmbH & Co. KG REF 740609.250	clean-up of PCR products
NucleoSpin® Plasmid	MACHEREY-NAGEL GmbH & Co. KG REF 740588.250	plasmid isolation
API®Staph kit	bioMérieux	species identification
Bacteria Live/Dead Staining Kit	PromoCell GmbH, GER (PromoKine; Cat. No. PK-CA707-30027)	differential staining of live or dead bacterial cells
Agilent RNA 6000 Nano Kit	Agilent Technologies	quality control for RNA
MEGAscript® T7	Thermo Fisher Scientific Inc. (Ambion; AM1333), USA	*in-vitro* transcription of RNA
pGEM®-T Easy Vector System I	Promega, USA (#A1360)	cloning of PCR products
Amersham Megaprime DNA Labeling System	Amersham, GE Healthcare, UK (RPN1606)	radioactive labelling of DNA
QIAquick® PCR Purification Kit	Qiagen (Cat. No. 28106)	clean-up of PCR products

2.4 Solid and liquid growth media

Growth media were set up as listed in **Tab. II-3**. Solid growth media contained 1.5% (w/v) agar additionally and were poured into sterile petri dishes. Antibiotics were added before pouring, when necessary. Liquid media were stored at RT; solid media at 4°C for several months. Media containing up to three individual mixes like CRA were merged right after being autoclaved and then poured into sterile petri dishes. The media ingredients and manufacturers are listed in **Annexe Tab. VIII-11**. For milk agar, milk was prepared separately and autoclaved for 10 min at 115°C prior to mixing with the other preheated components.

Tab. II-3: Components of solid and liquid growth media

Growth media are listed below. For pouring LB-, BHI-, B- and TSB-agar plates 1.5% (w/v) agar was added to the particular components and the volume adjusted to 1l with ddH$_2$O. BM-soft agar was prepared in a total volume of 40 ml ddH$_2$O and contained 0.6% (w/v) agar. This soft agar was stored solidified at RT and boiled for 2 min before it was used.

Media	Components	Amount
Luria-Bertani (LB) broth	Tryptone/Peptone ex casein	1% (w/v)
	Yeast Extract, micro-granulated	0.5% (w/v)
	NaCl	0.5% (w/v)
Brain Heart Infusion (BHI) broth	Brain Heart Infusion	3.7% (w/v)
Trypticase™ Soy Broth (TSB)	Trypticase™ Soy Broth	3% (w/v)
Congo red agar (CRA)	Brain Heart Infusion	3.7% (w/v)
	Agar-Agar, Kobe I	1.5% (w/v)
	ddH$_2$O	ad 800 ml
	Congo red dye	0.08% (w/v)
	ddH$_2$O	ad 100 ml
	sucrose	3.6% (w/v)
	ddH$_2$O	ad 100 ml
Mannitol Salt Agar (MSA)	Mannitol Salt Agar	11,1% (w/v)
	Agar-Agar, Kobe I	1.5% (w/v)
Milk agar	Skim milk powder	1.0% (w/v)
	ddH$_2$O	ad 500 ml
	Tryptone/Peptone ex casein	1% (w/v)
	Yeast Extract, micro-granulated	0.5% (w/v)
	NaCl	0.5% (w/v)
	Agar-Agar, Kobe I	1.5% (w/v)

	ddH$_2$O	ad 500 ml
BM (B-media)	Tryptone/Peptone ex casein	1% (w/v)
	Yeast Extract, micro-granulated	0.5% (w/v)
	NaCl	0.5% (w/v)
	K$_2$HPO$_4$	0.1% (w/v)
	Glucose	0.1% (w/v)
Tryptone/Peptone ex casein	Carl Roth GmbH + Co. KG, GER	8952
Yeast Extract, micro-granulated	Carl Roth GmbH + Co. KG, GER	2904

Chemically defined medium (CDM) was kindly provided by Freya Wencker and consisted of 25 mM Na$_2$HPO$_4$, 20 mM KH$_2$PO$_4$, 3.3 mM MgSO$_4$, 18.5 mM NH$_4$Cl, 17 mM NaCl, 0.142 mM sodium citrate tribasic dihydrate, 75 mM α-D(+) glucose, 1 mM of each L-amino acid [alanine (A), valine (V), leucine (L), isoleucine (I), aspartate (D), glutamate (E), serine (S), threonine (T), methionine (M), cysteine (C), arginine (R), lysine (K), proline (P), phenylalanine (F), tryptophan (W), histidine (H), asparagine (N), glutamine (Q), glycine (G)] and 0.1 mM of L-amino acid tyrosine (Y). Furthermore, vitamins were added [0.87 μM 4-aminobenzoic acid (B10), 0.87 μM thiamine hydrochloride (B1), 0.63 μM Ca-D-panthothenic acid (B5), 0.108 μM cyanocobalamin (B12), 0.12 μM D-biotine (B7), 2.43 μM nicotinamid (B3), 1.86 μM pyridoxine hydrochloride (B6) and 0.6 μM riboflavine (B2)] and trace elements (0.51 μM ZnCl$_2$, 0.5 μM MnCl$_2$*4H$_2$O, 0.097 μM H$_3$BO$_3$, 1.46 μM CoCl$_2$*6H$_2$O, 0.015 μM CuCl$_2$, 0.1 μM NiCl$_2$*6H$_2$O, 0.148 μM Na$_2$MoO$_4$*2H$_2$O, 1.5 μM FeCl$_3$ in 1N HCL).

2.5 Buffers and solutions

Buffers and solutions were prepared in ddH$_2$O and adjusted to pH, when indicated. Heat labile ingredients were filtered and mixed with autoclaved solutions. Unless stated otherwise, storage was at RT. See detailed information about components of buffers and solutions in the individual chapters.

2.6 Antibiotics and antibiotic analogues

Media additives were prepared as stock solutions in the appropriate solvent and then diluted to the working solution. The solvents for stock or working solutions are listed in **Tab. II-4**.

Tab. II-4: List of stocks and working solutions of antibiotics and ATc

 The listed antibiotics and the antibiotic analogue ATc were solved in the given concentration as stock solutions and further used to obtain the working end concentration.

Antibiotic (abbreviation, manufacturer, Cat.-No.)	Solvent	Stock conc. [mg/ml]	Working conc. [µg/ml]
Ampicillin (Amp; Carl Roth GmbH + Co. KG, K029.2)	ddH$_2$O	100	100
Chloramphenicol (CM; Carl Roth GmbH + Co. KG, 3886.2)	70% EtOH	30	30
Erythromycin (Erm; AppliChem GmbH, A2275.0005)	70% EtOH	10-25	10-25
Rifampicin (Rif; Sigma-Aldrich Co. LLC, R3501-1G)	DMSO	100	100

Antibiotic analogue (abbreviation, manufacturer, Cat.-No.)	Solvent	Stock conc.	Working conc. [ng/ml]
Anhydro-tetracycline (ATc; Sigma-Aldrich Co. LLC, 37919-100MG-R)	70% EtOH	1 [mg/ml]	-
	1X PBS	100 [µg/ml]	100

2.7 Bacterial strains

The bacterial strains used in this work are subdivided into different lists. General strains either used as controls for the experiments or to generate genetically modified organisms are listed in **Tab. II-5**. The genetically modified organisms themselves are listed in the specific sections.

Tab. II-5: List of bacterial strains used as controls or for cloning

 The listed strains were obtained from the strain collection of Ziebuhr group. Each strain is given with the individual code, the properties and the reference.

Strain	Properties	Reference	Strain collection code
E. coli DC10B	*E. coli* DH10B Δ*dcm* (cytosine methylase deficient) for direct cloning	Monk and Foster, 2012; Monk *et al.*, 2012	H47
S. aureus Newman	methicillin-sensitive isolate, NCTC 8178	Baba *et al.*, 2008; Duthie and Lorenz, 1952	H29
S. aureus Newman 107	RNase III mutant *rnc*::pMUTIN, Erm(5)	Schoenfelder *et al.*, 2013	H36

S. aureus PS187	wildtype; clinical ST395 isolate	Winstel *et al.*, 2013; Winstel *et al.*, 2015	H52
S. aureus PS187Δ*hsdR*Δ*sauUSI*	deficient in restriction system type IV and I; marker less mutant	Winstel *et al.*, 2013; Winstel *et al.*, 2015	H53
S. aureus RN4220	restriction-deficient derivative of *S. aureus* 8325-4, cloning host	Nair *et al.*, 2011	H1
S. carnosus TM300	biofilm-negative control strain, IS negative	Gotz, 1990; Rosenstein *et al.*, 2009	H15
S. epidermidis 567	inducible biofilm-former, UTI, *ica*-positive, IS*256*-positive	Batzilla *et al.*, 2006	H12
S. epidermidis 567-1	Isogenic *agr*-mutant of *S. epidermidis* 567	Batzilla *et al.*, 2006	H25
S. epidermidis ATCC 12228	biofilm-negative, *ica*-negative,	Zhang *et al.*, 2003	H13
S. epidermidis O-47	biofilm-positive, *ica*-positive, IS*256*-negative	Heilmann *et al.*, 1996a	H43
S. epidermidis PS2	biofilm-positive (protein), *ica*-positive, IS*256*-positive, blood culture isolate	U. Flückiger, UH Basel; Weisser *et al.*, 2010	PS2
S. epidermidis PS10	biofilm-positive (PIA), *ica*-positive, IS*256*-positive, blood culture isolate	U. Flückiger, UH Basel; Weisser *et al.*, 2010	PS10
S. epidermidis RP62A	catheter sepsis isolate, biofilm-positive control strain, *ica*-positive, IS*256*-positive	Gill *et al.*, 2005	H10
S. epidermidis Tü3298	Biofilm-negative, *ica*-negative	Augustin and Gotz, 1990; Moran and Horsburgh, 2016	H21

2.8 Oligonucleotides

Oligonucleotides were used as primers for PCR or manipulation of various plasmids (see **Annexe Tab. VIII-12**). They were purchased from Eurofins Genomics (www.eurofins genomics.eu, Ebersberg, GER) with HPSF pureness as unmodified or modified DNA oligonucleotides. The lyophilised oligonucleotides were adjusted with ddH$_2$O, according to manufacturer's instructions, to get the stock concentration of 100 pmol/µl. The stock solution was then diluted to 10 pmol/µl to obtain the working solution.

2.9 Radioactive nucleotides

Radioactive nucleotides were purchased from HARTMANN ANALYTIC GmbH (Brunswick, GER).

Tab. II-6: List of radioactive nucleotides and the designated use
Radioactive nucleotides are listed with the specific activity and concentration as well as the experimental purpose.

Radioactive nucleotide	Activity	Concentration	Purpose
$[\gamma^{32}P]$-ATP (cat. no. SRP-501)	6000 Ci/mmol	10 µCi/µl	end labelling of oligonucleotides
$[\alpha^{32}P]$-dCTP (cat. no. SRP-205)	3000 Ci/mmol	10 µCi/µl	radioactive labelling of PCR products
$[\alpha^{32}P]$-UTP (cat. no. SRP-810)	800 Ci/mmol	20 µCi/µl	control reaction in EMSA

2.10 Plasmids

The general plasmids used in this work are listed in **Tab. II-7**. Corresponding vector maps are depicted in Annexe - CLC vector maps of the plasmids. The constructs made during this work and the strains carrying these constructs are listed in the corresponding sections.

Tab. II-7: List of shuttle vectors used for cloning

Plasmid	Properties	Size (bp)	Selection	Reference
pBASE6	ori ColE1, antisense *secY* under $P_{xyl/tet}$ for counter selection	6600	Gram (-): Amp^R Gram (+): Cm^R	Bae and Schneewind, 2006
pCG248	ori ColE1, ori pT181, $P_{xyl/tet}$ inducible gene expression	6443	Gram (-): Amp^R Gram (+): Cm^R	PD Dr Ralph Bertram; Helle *et al.*, 2011
pCN33	ori ColE1, ori pT181, pUC19 MCS,	5691	Gram (-): Amp^R Gram (+): Erm^R	Prof Dr Brice Felden (Université de Rennes)
pCerulean	pALC2084 expressing codon-improved Cerulean	7200	Gram (-): Amp^R Gram (+): Cm^R	Dr Martin Fraunholz; Paprotka *et al.*, 2010
pGEM®-T Easy Vector System I	ori pBR322, 3´-T overhang, system for the cloning of PCR products, blue/white screening	3015	Gram (-): Amp^R	Promega

2.11   Software for *in silico* predictions and data analysis

The following table lists the software used in this work (**Tab. II-8**).

Tab. II-8: Software list

Software	Manufacturer
Blastn, Blastx	NCBI (https://blast.ncbi.nlm.nih.gov/Blast.cgi)
CLC Main Workbench, vers. 6.8.4	CLC bio (http://www.clcbio.com/)
GIMP, version 2.8	The GIMP team (www.gimp.org)
GraphPad Prism, vers. 6.0.4.0	GraphPad Software, Inc. (www.graphpad.com)
IGB-Integrated Genome Browser, version 8.4.3	Freese *et al.*, 2016a (www.bioviz.org)
IGV-Integrated Genomics Viewer	Robinson *et al.*, 2011; Thorvaldsdottir *et al.*, 2013 (http://software.broadinstitute.org/software/igv/home)
ImageJ ver. 1.46r	National Institute of Health (https://imagej.nih.gov/ij/index.html)
Imaris	Bitplane AG (http://www.bitplane.com/)
IntaRNA	Busch *et al.*, 2008; Mann *et al.*, 2017; Wright *et al.*, 2014 (http://rna.informatik.uni-freiburg.de/IntaRNA/Input.jsp)
LAS AF Lite, version 2.5.2	Leica Microsystems
MS Office	Microsoft
RNAPredator	Eggenhofer *et al.*, 2011 (http://rna.tbi.univie.ac.at/cgi-bin/RNApredator/target_search.cgi)
TargetRNA2	Kery *et al.*, 2014 (http://cs.wellesley.edu/~btjaden/TargetRNA2/)
Typhoon FLA 7000, vers. 1.2	GE Healthcare

GIMP 2 software was used for Northern Blot data analysis. The size for all layers was set based on one blot. Then, every probe signal was adjusted using the tool 'curves' and exported to .jpg file. *MS Office 2016* was used for display of the results.

Image J software was used for quantification of Northern blot bands. Probe signals were displayed in jpg-files exported from *GIMP 2*. These files were opened in Image J and the region of interest was set by using the rectangle tool covering the band of interest. After measuring the last band, the signals were plotted and the background noise was removed by closing the area under the curve. The enclosed areas under the curves were measured by the programme. The data were exported from the results table into MS Excel and further calculated to get the relative amount of RNA for each band depending on the reference 5S

rRNA signal. The results were displayed as graphs containing the time and the relative amount of RNA (RNA_{rel}). The RNA half-life was given at $RNA_{rel} = 0.5$.

Leica Microsystems *LAS AF* software was used for the experimental setup for biofilm formation analysis with CLSM and subsequent data analysis, as well as the 'lite' version of the programme and the software *Imaris*.

3. Bacterial culture and storage

All work with bacterial strains was carried out under sterile conditions in a class II microbiological safety cabinet to avoid any cross-contaminations.

3.1 Long term storage of bacteria

For long term storage, bacterial colonies were grown overnight in TSB medium (± antibiotic) and then mixed with sterile 86% glycerol solution to obtain a 30-35% glycerol stock, which was stored in a cryogenic tube at -80°C.

3.2 Cultivation of bacteria

Bacterial cells were streaked out from glycerol stock with a sterile inoculation loop onto agar plates, containing antibiotics when required. Agar plates were then incubated overnight at 37°C and stored at 4°C for up to 6 weeks.

For the preparation of liquid bacterial cultures, bacteria were scratched from agar plate with a sterile inoculation loop or a sterile pipetting tip and used to inoculate 4 ml of sterile medium, containing antibiotics when required, in an autoclaved glass tube. The glass tube was closed with a lid and incubated overnight in a circulatory shaker with 175-220 rpm at 30°C or 37°C.

3.3 Growth curves and CFU determination

Bacterial growth curves were analysed for fitness control of the strains and to observe changes in growth behaviour between wildtype and genetically changed organisms. The growth curves were measured spectrophotometrically either with the standard method in an Erlenmeyer flask or with a minimal volume approach in an automatized microplate reader (TECAN system).

For the standard method, a liquid overnight culture was prepared and used for inoculation of fresh medium with a starting OD_{600} of 0.05 and a liquid to air ratio of about 1:5. The culture was incubated for 24 h at 30°C or 37°C and the OD was measured at different time points. The automatized growth measurement also started with a bacterial culture at OD_{600}

of 0.05 in 200 µl medium per well. Each strain was set up in duplicate or triplicate. The microplate reader measured every half an hour and gave the result tabular (a number for each well and each time point). The data were analysed with the software *Microsoft Excel* and displayed as graphs.

In both methods, the growth was determined by measurement of the optical density of the bacterial culture. To examine the actual number of live bacterial cells, colony forming units per ml (CFU/ ml) were determined. For that, a serial dilution of the culture was plated out, grown o/n to single colonies, which were then counted. The colony number was multiplied with the dilution factor to get the initial number of cells.

3.4 Species identification and verification

API®Staph kit, provided by the company bioMérieux (Marcy-l'Étoile, France), was used for staphylococcal species identification. The test included 20 biochemical reactions that gave a specific bacterial profile, when bacteria were grown overnight in the test slots. For conducting the test, 60 µl of an overnight culture were mixed with the test medium and the bacterial suspension was transferred into the slots of the API®Staph test strip. The test strip was then placed into a wet chamber. The last two slots for adenine dehydrogenase and urease were covered with oil to create anoxic conditions and then the chamber was closed with a lid and incubated overnight at 37°C. After 18-20h, the biochemical reactions were analysed according to manufacturer's instructions.

Mannitol salt agar (MSA) was first described by Chapman in 1945 and used for the isolation of pathogenic staphylococci. MSA, purchased from Carl Roth® (Karlsruhe, GER), contained 5 g/l pancreatic digest of casein, 5 g/l peptone, 1 g/l beef extract, 75 g/l sodium chloride, 10 g/l D-mannitol, 0.025 g/l phenol red, 15 g/l agar and was pre-adjusted to the pH-value of 7.4±0.2. Due to the high content of salt, the medium was selective for staphylococci and inhibited most of the other bacteria. In this work, the specific medium was used for differentiation between *S. aureus* and *S. epidermidis*. Through the degradation of mannitol during growth, the medium was acidified and the colour changed from red/pink towards yellow. After overnight growth at 37°C *S. aureus* colonies were yellow and surrounded by a yellow zone, whereas *S. epidermidis* cells didn't change the colour and were surrounded by a red/pink zone.

B-agar was also used for differentiation between *S. aureus* and *S. epidermidis*, *e.g.* subsequent to phage transduction. Colonies of *S. aureus* appeared yellowish and colonies of *S. epidermidis* whitish on B-agar.

4. Phenotypic characterisation

4.1 Morphology of staphylococci analysed by scanning electron microscopy

Scanning electron microscopy (SEM) was used for the morphological analysis of *S. epidermidis* O-47 Wt and O-47Δ*tRNA*$^{Thr-4}$Δ*icaZ*Δ*icaR*-3' UTR (FL1Δ2). An ONC of each strain was given to the collaboration partner Dr Karen Wolf (Group Ölschläger, IMIB) and further prepared by her for SEM-analysis. Thereby, the bacterial cultures incubated on 0.1% poly-L-lysine (solved in ddH$_2$O) pre-coated cover slips, which were placed beforehand into the wells of a 24-well plate, under static conditions at 37°C for two hours. Then, the fluid culture was exchanged to 500 µl 6.5% glutaraldehyde (solved in 100 mM Sörensen buffer) and the plates were further incubated overnight. The cover slips were uncovered from glutaraldehyde, then covered with Sörensen buffer (12.2% 100 mM N$_2$HPO$_4$ in 100 mM KH$_2$PO$_4$) and dehydrated with successive acetone blends. Afterwards, vapour deposition with gold/palladium was done by the technical assistants from the department of electron microscopy at the biocenter. The cover slips with immobilised bacteria were inserted into SEM and the scanning electron microscopy was conducted together with Karen at the biocenter in Würzburg.

4.2 Differentiation of biofilm and non-biofilm formers on Congo red agar

Congo red agar (CRA) was first published by Freeman in 1989 and was an alternative method to the Christensen method for the detection of slime produced by coagulase negative staphylococci. This new method allowed the bacteria to remain viable on the medium (Freeman *et al.*, 1989). The CRA used in this work composed of 3.7% BHI, 1.5% agar, 3.6% sucrose and 0.08% Congo red. Bacteria were streaked out onto the solid agar and the agar plates were incubated at 37°C for 1-2d with subsequent incubation at RT. The strong biofilm producer *S. epidermidis* RP62A formed black colonies with a wrinkled morphology and a dry, crystalline surface appearance. Non-biofilm forming strains like *S. epidermidis* ATCC 12228 or *S. carnosus* TM300 exhibited pink colonies with a smooth surrounding and a wet/shiny surface. Depending on the biofilm composition, colonies also showed intermediate states when protein to PIA ratio was higher. Every batch of CRA plates required to be tested with the control strains named above, before the first experiments were conducted.

4.3 *In vitro* analysis of biofilm formation with crystal violet assay

The biofilm forming ability of staphylococcal strains was measured *in vitro* by classical crystal violet staining. Three to four microtiter plates were inoculated equally with the strains to be tested. One plate was analysed for total biofilm formation, two for the discrimination of protein and PIA biofilm and one additional plate for the release of eDNA

from biofilm forming cells. The test allowed a quantitative and qualitative analysis of the biofilm amount and composition from bacterial strains.

The strains to be tested for biofilm formation, were set up as an ONC in the medium of choice (mostly TSB) with or without antibiotics. The next day, the optical density of the ONC was measured and the cells were diluted under sterile conditions with fresh media to $OD_{600} = 0.05$. For each strain 10 ml fresh medium were filled in a sterile petri dish and additional ingredients *i.e.* antibiotics or antibiotic analogues or both, were added. The calculated number of cells was added, mixed and then the bacterial cultures were added to three or four microtiter plates, whereby each strain was added into at least four wells per plate (each well with 200 µl). This was done rapidly with a multichannel pipette. The plates were incubated under static conditions at 30°C and 37°C for 18-20h.

The supernatant was discarded from three of the four plates and each well was washed very gently two times with 1X PBS. 10X PBS stock solution contained 1.37 M NaCl, 14.7 mM KH_2PO_4, 26.8 mM KCl, 80 mM Na_2HPO_4, adjusted to pH 7.4. The 1st plate/ control plate, for the measurement of the total biofilm, was placed on a 65°C heating block for up to 45 min to fix the bacterial cells on the surface. The 2nd plate/ proteinase K plate was used for the indirect measurement of the PIA biofilm by enzymatic digestion of proteins within the biofilm through proteinase K. Each well of the plate was filled with 200 µl of 1 mg/ml proteinase K solved in 100 mM Tris pH 7.5. The plate was incubated for 4h at 37°C and then washed and fixated as stated above. The 3rd plate/ NaIO$_4$ plate, gives the indirect amount of proteins within the biofilm due to the degradation of polysaccharides. 200 µl of 40 mM sodium periodate (NaIO$_4$) was added to the wells and the plate was incubated for 24h at 4°C wrapped in aluminium foil. After incubation, the plate was also washed and fixated. For biofilm staining, one drop of saturated crystal violet solution was filled into each well. The crystal violet solution stained the adherent cells for 30 sec, was then removed and the wells were washed gently with water. After drying at RT, the plates were measured with an ELISA-reader at 492 nm wavelength.

The 4th plate/ eDNA plate, was washed like the other plates. 50 µl of "dead stain" solution was filled into each well, the plate was wrapped into aluminium foil to avoid day light and the plate incubated at RT for 30 min. The wells were washed again one time with 1X PBS and the fluorescence was measured with TECAN imager at 535 nm/ 595 nm wavelengths. The 'dead stain' solution contained a mixture of 54.54 µl dead stain (Ethidium Homodimer III, Bacteria Live/Dead Staining Kit) and 245.45 µl 0.85% NaCl with further added 29.7 ml of 0.85% NaCl.

4.4 Adherence assay

Bacterial cells were grown as ONC and diluted with fresh media to $OD_{600} \sim 0.05$ or $OD_{600} \sim 0.1$. 2-4 ml of the culture was poured into one well of a six well plate. The plate was incubated for 1-2 h at 30°C or 37°C before the cells were tipped out and the wells were washed with 1X PBS. Adherent cells were analysed with light microscopy and subsequently heat fixated before staining with crystal violet solution.

4.5 *In vivo* imaging of biofilm formation by confocal laser scanning microscopy

In contrast to the *in vitro* measurement of biofilm amount by crystal violet staining, where only the established biofilm is measured, the *in vivo* confocal laser scanning microscopy (CLSM) measurement allowed to visualise the development and the composition of the biofilm in real-time. Additionally, the confocal laser scanning microscopy enabled the three-dimensional view of a biological sample, because several planes of focus could be scanned. It coupled a laser source to a fluorescent microscope. The specimen was excited with a specific wavelength and the emitted fluorescence was read-out. Different images of one sample were then merged and reconstructed for a 3D image.

During *in vivo* imaging of biofilm formation, different fluorescent dyes were used to stain various components of the biofilm matrix *i.e.* polysaccharides, proteins or eDNA or the bacterial cells themselves. For the analysis, different approaches were conducted that ranged from the analysis of biofilms under static conditions in a 35 mm μ-dish or 4 well μ-slide to biofilm analysis under dynamic conditions with additional application of flow through a peristaltic pump in μ-slide $VI^{0.4}$, a six-chamber slide. All slides were uncoated, hydrophobic and sterile.

The layers of one single location were measured at different time points (z-stacks) to illustrate the developing biofilm in real-time. More realistic conditions a biofilm is exposed to *in vivo*, were created by using a peristaltic pump to simulate medium flow and pressure. The comparison of static biofilm conditions to dynamic conditions gave new insights into biofilm formation, specially between *S. epidermidis* O-47 Wt and the IcaZ mutants. The biological samples were kept at 37°C or 30°C throughout the whole experiments.

The CLSM experiments were conducted in collaboration with group member Dr Sonja Schönfelder at the Institute for Molecular Infection Biology in Würzburg. The peristaltic pump was loaned from Prof Kai Thormann (Institut für Mikrobiologie und Molekularbiologie, Justus-Liebig-Universität Gießen), who also introduced the method to us and helped with the initial experiments.

Tab. II-9: List of staining dyes for biofilm formation analysis with CLSM

Different dyes were used to stain specific components of the biofilm or the bacterial cells themselves. They were purchased from Thermo Fisher Scientific Inc. and were used as ready-to-use solutions or were prepared as listed in the table. The staining dyes from PromoKine were prepared as a 100x dye solution. For DMAO + EtD-III, the 100x dye solution contained a mixture of one volume of DMAO and two volumes of EtD-III plus eight volumes of 0.85% NaCl solution. EtD-III solution contained two volumes of EtD-III plus eight volumes of 0.85% NaCl solution. Furthermore, excitation and emission maxima of the specific staining dyes are given in the table below.

Staining dye	Distributer	Cat.-No.	Preparation	Stained component	Excitation/ emission max. [nm]
Hoechst33342 (NucBlue® Live ReadyProbes® Reagent)	Thermo Fisher Scientific Inc.	R37605	ready to use solution: 2 drops/ ml	nucleic acids (cells)	360/460 (blue)
NucRed® Live 647 ReadyProbes® Reagent		R37106			638/686 (red)
Oregon Green® 488 Conjugate (WGA)		W6748	1 mg/ ml stock solution; 5 µg/ml working solution; both in 1X PBS	sialic acid and N-acetylglucosaminyl residues (poly-saccharides; PIA)	496/524 (green)
Texas Red®-X Conjugate (WGA-TexasRed)		W21405			595/615 (red)
EtD-III (ethidium-homodimer-III)	PromoKine	PK-CA707-30027	0.5x from 100x dye solution	nucleic acids (only dead/leaky cells)	488/575 (red)
DMAO + EtD-III		PK-CA707-30027	1 µl/100 µl from 100x dye solution	nucleic acids (double-staining of viable and dead cells)	488/525+575 (green + red)
SYPRO® Ruby	Thermo Fisher Scientific Inc.	F10318	ready to use	proteins in matrices of biofilms	450/610 (red)
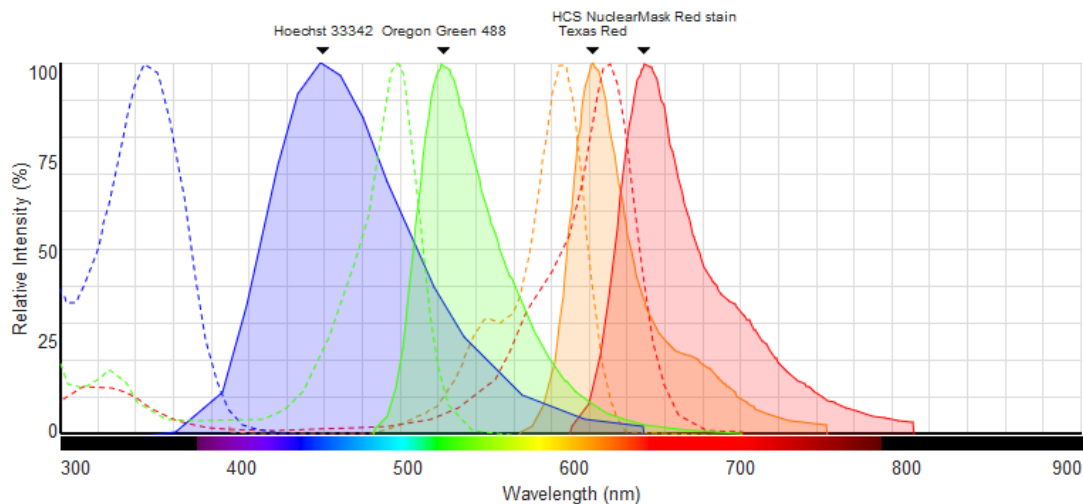
Fig. II-1: Fluorescence spectra of the staining dyes

Fluorescence spectra of the staining dyes are shown. The figure was created by using the Fluorescence SpectraViewer of Thermo Fisher Scientific. Inc. (https://www.thermofisher.com/de/de/home/life-science/cell-analysis/labeling-chemistry/ fluorescence-spectraviewer.html?ICID=svtool&UID =6390p72)

4.5.1 *Experimental setting for static biofilm growth*

Bacteria were setup as ONCs in TSB medium with antibiotic, when required, at 37°C or 30°C, depending on the experiment. The strains were diluted with fresh media to OD_{600} ~ 0.05 and 800 µl of the bacterial culture were filled in 35 mm µ-dish or 4-well µ-slide. After 16-20 h static growth at the desired temperature, the culture medium was pipetted out and the adherent cells surrounded with biofilm matrix were washed very gently with 1X PBS. The biofilm components or cells were then stained with the specific staining dyes and washed again. Microscopic analysis took place shortly after staining to avoid drying out of the liquid.

4.5.2 *General experimental setting for dynamic biofilm growth analysis*

Preparation of equipment and assembly of the flow system (**Fig. IV-11**;**Fig. IV-12**): The silicone tubing was cut into inflow tubing (6x 2 m), outflow tubing (6x 1.5 m) and reservoir tubing (6x 0.45 m). These were rinsed with 70% ethanol by using 0.9 mm needle and 10 ml syringe and subsequently dried by blowing out the liquid. The inflow (6) and the outflow (8) tubing were connected at one end with an elbow Luer connector (6b and 8a) and both ends (a and b) were marked and wrapped in aluminium foil, before they were autoclaved in a beaker. The reservoir tubing (2) was wrapped in foil at both ends (a and b), but without connector, before autoclaving in a beaker. Pump tubes (4), containing the connector for the reservoir tubing (at 4a), were connected to the bubble traps (4b with 5a). The bubble traps (5) were arranged with the high site (5a) towards the pump tubes and the low site (5b)

towards the inflow tubing (6). The short tubing on top of the bubble traps (5c) were closed with a clamp and the pump tubes were inserted into the pump. The bubble traps were rinsed with 20% ethanol and tested for permeability. When the system was not leaky, but allowed flow, the pump tubes were taken out of the pump and the clamps were removed. The bubble trap/ pump tube system was wrapped in aluminium foil and autoclaved at 80°C for 15 min, otherwise plastic materials melted. Medium was calculated (1.5 rpm ~ 15 ml/h; at 0.5 rpm ~ 5 ml/h), prepared in separate bottles ± antibiotics or other additives and autoclaved.

The next day, the individual parts were assembled under sterile conditions. The autoclaved reservoir tubing (2a) were added into the sterile medium (1), with one aluminium foil covered end hanging outside the medium reservoir (2b). The open medium reservoir was covered with aluminium foil to keep the media sterile.

Further assembling was performed on the rolling transport table. Pump tubes were connected to the foil covered end of the reservoir pumps (4a to 2b). For that one drop of 70% ethanol was added to the unwrapped end (2b) to sterilize and to facilitate connection to the connector of the pump tube (4a). After that, the pump tubes were inserted into the pump and the connection to the bubble trap (4b with 5a, assembled before autoclaving) was checked again. The bubble trap was then connected to the foil wrapped ends of the inflow tubing (5b with 6a), not containing the elbow Luer. The ends containing the elbow Luer (6b) were connected to the six-chamber slide and the chamber slide was connected on the other side to the outflow tubing (8a). The free ends of the outflow tubing (8b) were inserted into the waste bin and fixated with adhesive tape. Additionally, the opening of the bottle was closed with aluminium foil to later avoid any spread of contaminated waste media. The rolling table was moved to the CLSM. The system was checked by starting the pump at 45 rpm, then pressing the button to achieve 90 rpm max. pump speed to fill all tubes and the bubble traps with medium. As soon as the traps were filled, they were closed with a metal clamp (at 5c). When all air bubbles were removed (out of the tubing into the bubble traps), the pump was set to 0.5 rpm overnight to pre-run the system.

Inoculation of the bacteria: The next day, the system was checked again for air bubbles and they were removed gently, if necessary, especially in the inflow tubing and the chamber slide itself. ONCs of the bacterial strains to be analysed, were diluted with fresh media to $OD_{600} \sim 0.05$ in a total volume of 2 ml. Antibiotics were added, when required. The dilution was then carefully drawn up into a sterile 2 ml syringe by using 0.9 mm needle. A smaller needle would have caused more air bubbles and this was strictly to avoid. Before injection of the bacteria into the inflow tubing, the area next to the bubble traps was wiped with 70% ethanol and the pump was shortly stopped. All air bubbles in the needle were removed and the bacteria were injected with a 0.3 mm needle into the inner tube volume of the inflow tubing. Holding the needle first at a 45° angle to punch through the silicon wall and then

changing to a 20° angle to insert the needle further into the inner volume of the tube was the best way to slowly inject 1 ml of the bacteria. Before taking out the needle, a few seconds needed to pass by to allow the pressure built up by the injection to resolve. After taking out the needle the drops leaking out of the tubes were wiped away with a tissue and the insertion hole was sealed with silicone. After inoculation of all six inflow tubing, the six-chamber slide was generously coated with immersion oil underneath and moved to the pre-warmed microscope area, where it was mounted on the microscopic stage, which was initialised before by the Leica *LAS AF* programme. The inflow tubing was laid in several loops next to the stage to allow warming of the media before it was running through the chambers. The loops were fixated to further stay on the microscopic stage even when it was moving during the measurements of the six chambers. The bacteria settled down on the chamber slide bottom for 1h before the flow was started again at 0.5 rpm for the time of the experiment.

Application of the staining dye to the flow system: Before the injection of 1.5 ml staining dye (see table below) to the bubble trap of one chamber, the clamp from the short tubing on top of the bubble trap (5c) was released, the according pump tube was un-clicked and the inflow tubing downstream of the bubble trap was clamped. The media was removed from the bubble trap with a long needle and exchanged to the staining dye. Then the clamp on the inflow tubing downstream was removed, the pump tube was clicked into the pump again and the bubble trap tubing (5c) was clamped. These steps were carried out quickly, so that there was no effect on the developing biofilm in the chamber due to a loss of flow. The staining dye was then slowly transported together with the medium towards the chamber. 1h later, the biofilm could be scanned by using the specific excitation and emission spectrum for each staining dye.

De-assembly of the flow system: After completion of the experiment, the chamber slide was taken away from the microscopic table. The reservoir pumps were moved into 0.5l of 20% ethanol solution and the system was rinsed at 45 rpm with several bursts at 90 rpm. Afterwards, it was rinsed with 0.5l of water. The inflow tubing was unconnected from the bubble traps and the outflow tubing was un-taped from the waste bin. They were discarded into the autoclave waste bag as well as the reservoir tubing. The pump tubes and the bubble traps were rinsed again with 20% ethanol and water, before the syringes were replaced and all was autoclaved again at 80°C for 15 min. For the next experiment the steps for preparing the system were repeated.

Tab. II-10: Equipment list for CLSM experiments

Equipment, marked with an asterisk (*), was loaned from Prof Dr Kai Thormann.

Equipment	Manufacturer	Cat.-No.
µ-Dish 35 mm, low wall (800 µl volume), uncoated, hydrophobic, sterilized	ibidi GmbH, GER	80131
µ-Slide 4 Well (700 µl volume each well), uncoated, hydrophobic, sterilized	ibidi GmbH, GER	80421
Bubble traps*	-	-
Chamber slide (µ-slide VI$^{0.4}$)	ibidi GmbH, GER	80601
Clamps*	-	-
Erlenmeyer flask, DURAN® 500ml	A. Hartenstein GmbH, GER	EK08
Ethanol (70%, 20%)	Carl Roth GmbH + Co. KG, GER	5054
Laboratory bottles DURAN® 100ml-1l	A. Hartenstein GmbH, GER	FL02-05
Luer connector (elbow)	ibidi GmbH, GER	10802
Luer connector (male + female)	ibidi GmbH, GER	10826 + 10825
Luer connector (male)	ibidi GmbH, GER	10824
Luer-lock needle, 0.30 x 12mm	megro GmbH & Co. KG, GER	4710003012
Medium reservoir, 500ml	A. Hartenstein GmbH, GER	FL04
Needles short (0.45mm, 0.9mm)	B. Braun Melsungen AG, GER	4657683/ 4657519
Peristaltic pump*	Watson-Marlow Fluid Technology Group, UK	205S/CA
Pump tubes (1.65 mm)*	Watson-Marlow Fluid Technology Group, UK	-
Silicone*	JUWEL Aquarium GmbH & Co. KG, GER	88350
Six chamber slide, µ-slide VI$^{0.4}$	ibidi GmbH, GER	-
Syringes (2ml, 5ml, 10ml)	B. Braun Melsungen AG, GER	4606027V/ 4606051V/ 4606108V
Tubing, inflow (6x 2m)	A. Hartenstein GmbH, GER	S02S
Tubing, outflow (6x 1.5m)	A. Hartenstein GmbH, GER	S02S
Tubing, reservoir (6x 0.45m)	A. Hartenstein GmbH, GER	S02S
Waste reservoir (5l flask in bucket)	A. Hartenstein GmbH, GER	EK12

4.5.3 *Confocal laser scanning microscopy data analysis*

The images taken from the defined spots were analysed with *Imaris* software package (Bitplane AG, Zürich, Switzerland) and Leica Microsystems *LAS AF Lite* (Leica Microsystems GmbH, Wetzlar, Germany). The image stacks were processed using *Imaris*.

4.6 Application of oxidative stress with H_2O_2

Dilutions of *S. epidermidis* O-47 Wt and O-47$\Delta tRNA^{Thr-4}\Delta icaZ\Delta icaR$-3′ UTR (FL1$\Delta$2) ONC, previously prepared in TSB, were plated on TSB agar. A disk was placed in the middle of the agar plate and was basted with 10 µl of 0.23% and 0.46% H_2O_2 solution. The plates were incubated overnight at 37°C or 30°C. Three independent replicates were analysed.

4.7 Milk agar test

S. epidermidis O-47 Wt and O-47$\Delta tRNA^{Thr-4}\Delta icaZ\Delta icaR$-3′ UTR (FL1$\Delta$2) were streaked out onto milk agar plates. The plates were incubated o/n at 37°C or 30°C. The appearance of a clearing zone next to the bacterial colony indicated, that the bacteria secreted proteases, which degraded the proteins in the milk agar. Proteases are under the control of the *agr*-system, so that the milk agar test gave indirect information about the functionality of the *agr*-system.

4.8 Phenotype on $MgCl_2$ agar

Strains were grown on LB standard agar mixed with 100 mM $MgCl_2$. This agar was previously used to analyse the biofilm formation of *S. aureus* strains (personal communication with Lopez group, IMIB, Würzburg). The plates were incubated at 30°C for up to seven days and the morphology of the bacterial single colonies was photographed with the digital camera, which was connected to the binocular microscope.

5. Working with DNA

5.1 Extraction of chromosomal DNA from *Staphylococcus*

4 ml of sterile LB medium containing 1% (w/v) glycine were inoculated with a single colony from agar plate under sterile conditions and grown in a circulatory shaker overnight at 37°C. 2 ml of the ONC were collected in a 2 ml safe lock reaction tube by centrifugation for 1 min at 10 000 rpm. The cell pellet was washed with 1 ml TE-buffer (10 mM Tris-HCl pH 8.0, 1 mM EDTA) and then resuspended in 100 µl TS-buffer (25% saccharose, 10 mM Tris-HCl pH 7.5). After addition of 15 µl 0.5 M EDTA (pH 8.0) and 10 µl lysostaphin (2 mg/ml) the mixture was incubated at 37°C for 20 min until it became slightly viscous because of cell disruptions due to the lysostaphin treatment. EDTA is a chelating agent and sequesters divalent cations. In consequence, DNases are inactivated because of unusable cations and DNA remains intact. 375 µl TE-buffer (10 mM Tris-HCl pH 8.0, 1 mM EDTA), 225 µl 10% SDS and 20 µl proteinase K (10 mg/ml) were added to further disperse cell particles, such as cell wall, membrane and proteins. The reaction tube was mixed by inversion and set to 55°C for 30 min. In order to extract the chromosomal DNA, 150 µl 5 M sodium perchlorate and 450 µl chloroform/isoamyl alcohol (24:1) were added under the fume hood and mixed with the vortex for at least 1.5 h. The sample was centrifuged at 13 000 rpm for 10 min to separate organic and aqueous phases. The upper aqueous phase was transferred into two fresh 1.5 ml reaction tubes and ethanol precipitation was performed by addition of 2X Vol. 99.9% pure ethanol. After inversion of the reaction tube chromosomal DNA was visible as a white, thread-like precipitate and collected with centrifugation at 13 000 rpm for 10 min. The DNA pellet was washed with 70% ethanol and air-dried for 5 min after removing the supernatant carefully and completely. The extracted chromosomal DNA was rehydrated with 50 µl H_2O or 10 mM Tris (pH 8.5) and stored at 4°C in the fridge.

5.2 Mini scale plasmid preparation from *E. coli*

4 ml of sterile LB medium containing the required antibiotic were inoculated with a single colony from agar plate and grown in a circulatory shaker overnight at 37°C. 2 ml of the ONC were collected in a 2 ml safe lock reaction tube by centrifugation at 10 000 rpm for 1 min. The supernatant was discarded and the pellet was resuspended in 200 µl buffer I (50 mM Tris-HCl pH 7.5, 10 mM EDTA pH 8.0, 0.1 mg/ml RNase A) subsequently followed by 200 µl buffer II (200 mM NaOH, 1% SDS) and 2-5x careful inversion of the reaction tube before addition of 200 µl buffer III (3M sodium acetate pH 4.8 or 3M potassium acetate pH 5.2). Mixing of the solution lead to precipitation of cell structures and proteins, which then were collected by centrifugation for 10 min at 13 000 rpm. The supernatant containing the plasmid was transferred into a fresh 1.5 ml reaction tube and centrifuged again to get rid of potential precipitate contamination. The supernatant was

again transferred to a fresh 1.5 ml reaction tube and DNA was precipitated with 0.8X Vol. of isopropanol, followed by centrifugation for 10 min at 13 000 rpm. 500 µl 70% ethanol was used to wash the DNA pellet, which then was air-dried for 5-10 min and rehydrated with 50 µl ddH$_2$O. The solved plasmid DNA was stored at 4°C in the fridge or for long term at -20°C in the freezer.

5.3 Plasmid preparation from *Staphylococcus*

4 ml of sterile LB medium or TSB containing 1% (w/v) glycine were inoculated with a single colony from agar plate under sterile conditions and grown in a circulatory shaker overnight at 37°C. 1.5 ml of the ONC were collected in a 2 ml safe lock reaction tube by centrifugation for 10 min at 7 000 rpm. The supernatant was discarded and the pellet was resuspended in 100 µl buffer P1 (50 mM Tris-HCl pH 7.5, 10 mM EDTA pH 8.0, 0.1 mg/ml RNase A). The solution was mixed with the vortex and 10µl lysostaphin (2 mg/ml) was added. The reaction was set to 37°C for at least 10 min until the sample was very viscous to almost solid. 200 µl buffer P2 (200 mM NaOH, 1% SDS) was added, the tube was inverted and incubated for 5 min on ice. 150 µl buffer P3 (3M sodium acetate pH 4.8 or 3M potassium acetate pH 5.2) was added, vortexed and incubated for 10 min on ice. The solution was centrifuged for 30 min at 4°C and 14 000 rpm. The supernatant (~450 µl) was transferred to a fresh 1.5 ml tube and centrifuged. This step was repeated when necessary to get rid of potential precipitate contamination. The supernatant was again transferred into a fresh 1.5 ml tube and DNA was precipitated with ethanol. For that, 1 ml ice-cold absolute ethanol was added, the sample incubated for 1 h at RT and centrifuged again 30 min at 4°C and 14 000 rpm. The DNA pellet was washed with 500 µl 70% ethanol, centrifuged for 10 min at 14 000 rpm and 4°C and air-dried for 5-10 min. 30 µl ddH$_2$O or 10 mM Tris-HCl (pH 8.5) were added to solve the pellet and plasmid DNA was stored at -20°C in the freezer.

5.4 Measurement of nucleic acid concentration and purity

The quality and quantity of nucleic acids was measured spectrophotometrically. Nucleic acids absorb UV light optimally at a wavelength of 260 nm whereas proteins have their maximum absorption at 280 nm. Measuring A$_{260}$ gave the amount of nucleic acids in solution and the ratio of A$_{260}$/A$_{280}$ indicated the purity of the solution. Ranges from 1.7-2.1 were acceptable. Numbers above indicated a contamination with RNA and numbers below indicate contamination with proteins and aromatic molecules.

The correct formula for calculation of DNA concentration is:

c [µg/ml] = A$_{260}$ x 50 x dilution factor

For calculation of RNA concentration, absorption and dilution factor were multiplied with 40 instead of 50. The measurement was performed with the high-sensitive NanoDrop

system, according to manufacturer's instructions, which required only 1 µl of DNA solution.

5.5 Amplification of specific sequences with PCR

Polymerase chain reaction (PCR) was used to quickly amplify specific regions of any template DNA. In the first step template DNA was heat denatured to un-pair the DNA strands. The next three steps were repeated 34 times and included denaturation for 30s at 95°C, annealing of the primer for 30s at x°C and elongation of the newly synthesised DNA strand for y min at 72°C. The temperature used for binding of the oligonucleotides depended on the pair of primers used. The elongation time depended on the length of the template and on the polymerase. In this step, a heat stable polymerase added deoxynucleotide triphosphates (dNTPs) to the 3′ end of the primers. The new added nucleotides paired with the opposite DNA strand. PCR ended with the final elongation step, in which the polymerase enzyme finished all started reactions. The PCR machine subsequently cooled down the reaction sample to 16°C. PCR products were stored at -20°C or analysed directly by gel electrophoresis.

For routine PCR amplification of DNA, templates with sizes up to 6 kb, DreamTaq DNA Polymerase was the standard polymerase. This polymerase was used in reactions, in which fidelity of amplification was of minor relevance, because DreamTaq DNA Polymerase has no proof reading ability and sometimes causes DNA mispairings. The elongation time for this enzyme was set according to the expected PCR product length, following the rule, that the Taq polymerase adds 1000 nucleotides per minute.

Phusion High-Fidelity DNA Polymerase possesses $3′\rightarrow 5′$ exonuclease activity and was used in PCRs, in which fidelity of amplification was of relevance (*e.g.* subsequent cloning reactions or *in vitro* transcription reactions). This enzyme doubled the speed of amplification in comparison to DreamTaq DNA Polymerase and was also used when longer PCR products had to be generated (*e.g.* amplification of plasmids).

5.5.1 *Standard PCR and clean-up of reactions*

DreamTaq Polymerase: Each PCR reaction volume consisted of 1X reaction buffer, which already included 2 mM $MgCl_2$ and loading dye, 0.2 mM of each of the four dNTPs (dATP, dTTP, dGTP, dCTP), 0.2 µM of forward and reverse primer, 1U of DreamTaq polymerase and 50-250 ng template DNA. The remaining volume was filled up with ddH_2O to the desired end volume.

Phusion High-Fidelity DNA Polymerase: Each PCR reaction volume consisted of 1X reaction buffer, which already included 1.5 mM $MgCl_2$ and loading dye, 0.2 mM of each of the four dNTPs (dATP, dTTP, dGTP, dCTP), 0.5 µM of forward and reverse primer,

0.02 U/µl of Phusion High-Fidelity DNA Polymerase and 50-250 ng template DNA. The remaining volume was filled up with ddH$_2$O to the desired end volume.

PCR reactions were set up on ice. A master mix was prepared for the appropriate number of samples to be amplified. Usually this was the number of samples including control reactions plus one extra sample. Polymerases and buffers were pipetted with low retention filter tips.

Before used in any downstream applications, PCR products were cleaned up from components of the PCR mix with the NucleoSpin® Gel and PCR Clean-up kit from MACHEREY-NAGEL GmbH & Co. KG according to the manufacturer's instructions. The same kit was used for the clean-up of PCR products, that were separated previously by gel electrophoresis and cut out from an agarose gel, but a slightly different protocol was used following manufacturer's instructions. DNA was eluted from the column with 30-50 µl of ddH$_2$O and concentration as well as purity of the DNA was measured with Nano Drop from Thermo Fisher Scientific Inc.

5.5.2   *Preparation of DNA for sequencing reaction*

The DNA was prepared according to the instructions of 'Seqlab - Sequence Laboratories Göttingen GmbH' which was as follows: The total reaction volume of 15 µl included 30 pmol of sequencing primer, DNA template amount and $_{dd}$H$_2$O to fill up the volume. DNA amount was calculated for PCR products: 22.5 ng/100 bp. The 1.5 ml reaction tubes were laminated with the barcode label and registered online at the company's homepage before sending them in. Sequencing results were obtained routinely the next day by downloading the files from the web server. Chromatograms were analysed using the software *CLC Main Workbench*.

5.5.3   *PCR for site directed mutagenesis*

Site directed mutagenesis (SDM) was used for changing single bases in the sequence of ncRNA IcaZ in plasmid pCG248_icaZs. Constructs, resulted from SDM are listed in **Tab. II-11**. The primers used for PCR were complementary outward primers containing the desired nucleotide change and the appropriate length of flanking sequences.

Reactions were set up in 50 µl total reaction volume. Each reaction contained 31.8 µl ddH$_2$O, 10 µl 5X HF-buffer, 2 µl dNTP solution, 25 pmol of each primer, 250 ng template DNA and 0.5 µl Phusion High-Fidelity DNA Polymerase. PCR was run at 98°C for 3 min, then 5 cycles with 40s at 98°C for denaturation, 45s at 65°C for primer annealing (each cycle – 0.5°C) and 3 min 40s at 72°C for elongation. Followed by 12 cycles of 98°C for 40s, 62°C for 45s and 72°C for 3 min 40s. Final elongation was carried out for further 10 min at 72°C.

Tab. II-11: Constructs generated with site directed mutagenesis and mutations caused

> List for primers used for each construct in site directed mutagenesis PCR. Given is the original and the mutated nucleotide sequence. * Constructs used for IcaZ overexpression in *S. epidermidis* O-47 Wt.

Constructs	Primer name	Primer sequence	Mutation
Template: pCG248_icaZs			
pCG248_icaZs_G167T*	O47icaZ_G167T_r	tgaaaaagTagtgaaatgaggtacagcg	pos. 167 G→T
	O47icaZ_G167T_f	ttcactActttttcacgtaaaagtaatagtcac	
pCG248_icaZs_d251*	O47icaZ_d251_f	ccactctttttttatttaatcgaacttcaacg	pos. 251 deleted
	O47icaZ_d251_r	gattaaataaaaaaaagagtggaaccaaatttcattg	
Template: pCG248_icaZs_G167T			
pCG248_icaZs_G167T+G195C*	O47icaZ_G195C_f	atttgtGtaacactacgctgtacctc	pos. 167 G→T pos. 195 G→C
	O47icaZ_G195C_r	tgttaCacaaataacataatgaagaagaaatgt	
pCG248_icaZs_G167T+d251	O47icaZ_d251_f	ccactctttttttatttaatcgaacttcaacg	pos. 167 G→T pos. 251 deleted
	O47icaZ_d251_r	gattaaataaaaaaaagagtggaaccaaatttcattg	
pCG248_icaZs_G167T+A323G*	O47icaZ_A323G_f	ataacattCatttcatttttccttcattttaacta	pos. 167 G→T pos. 323 A→G
	O47icaZ_A323G_r	atgaaatGaatgttatttagattgagatatttaatgc	
Template: pCG248_icaZs_d251			
pCG248_icaZs_d251+A323G*	O47icaZ_A323G_f	ataacattCatttcatttttccttcattttaacta	pos. 251 deleted pos. 323 A→G
	O47icaZ_A323G_r	atgaaatGaatgttatttagattgagatatttaatgc	

5.6 Separation of DNA fragments by gel electrophoresis

Agarose gel electrophoresis was carried out in TAE buffer to separate DNA fragments amplified by PCR or generated by enzymatic digestion. 50X TAE stock solution contained 50 mM EDTA, 1 M acetic acid, 2 M Tris.

Nucleic acids are negatively charged and migrate towards the positively charged anode when electrical current is applied. Small fragments migrate faster than larger ones and thereby separate from each other. Separation also depends on the pore size of the gel, which is determined by the concentration of agarose. For sizing and approximate quantification of the DNA fragments two size markers were used covering different size ranges. GeneRuler 1 kb Plus DNA Ladder was used with 1% TAE gels whereas GeneRuler 100 bp Plus DNA Ladder was used with 2% TAE gels (**Fig. II-4**). Gels were run in 1X TAE buffer for 45 min to 1 h at 120-140V.

To prepare an agarose gel, the agarose was boiled in 1X TAE buffer until agarose was completely solved using a micro wave. The solution cooled down to approx. 50°C while stirring on a magnetic stirrer before Midori Green was added (4 µl/ 100 ml). Midori Green was distributed by stirring for additional 2 min and the mix was poured into a prepared tray with built-in comb. The agarose gel polymerised at least 30 min at RT or 20 min at 4°C prior to usage for electrophoresis. After polymerisation agarose gels could be stored wrapped in foil for up to 4 weeks at 4°C or directly used for electrophoresis. For this, the gel was removed from the tray and put into an electrophoresis chamber filled with 1X TAE. Samples that did not already contain loading dye in the PCR buffer were supplemented with loading dye and 2-5 µl of PCR product was pipetted into a slot. 4-5 µl of DNA size marker run in another slot. The run time was adjusted according to the desired separation of fragments. The result was visualised and documented with a UV imaging system.
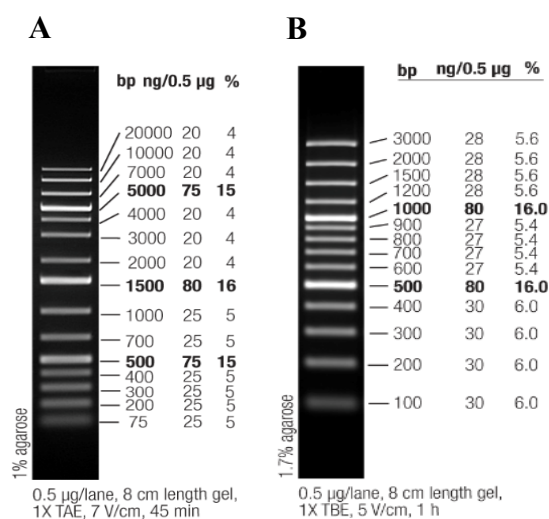
Fig. II-2: DNA size standards used in gel electrophoresis

(**A**) GeneRuler 1 kb Plus DNA Ladder (cat. no. #SM1331) by Thermo Scientific™. (**B**) GeneRuler 100 bp Plus DNA Ladder (cat. no. #SM0321) by Thermo Scientific™.

6. Working with RNA

Prior to working with RNA samples, the place and pipettes were cleaned with 70% ethanol and RNaseZap® solution to avoid contamination of RNA samples with RNases. Additional, gloves were worn when handling samples and RNA was always kept on ice. The utilised water was cleared from RNases by DEPC-treatment or was purchased as RNase-free water. For DEPC-treatment, 0.1% DEPC (v/v) was added to 1l ddH$_2$0, heavily mixed and incubated overnight at 37°C. After subsequent autoclaving for two times DEPC-water was used for RNA experiments. RNA samples were stored in RNase-free reaction tubes at -80°C.

6.1 Extraction of total RNA from bacterial cells

4 ml of sterile TSB containing the required antibiotic was inoculated with a single colony from agar plate and grown in a circulatory shaker overnight at 37°C. The optical density of the bacterial culture was measured spectrophotometrically using a 1:10 dilution and the calculated number of cells for OD$_{600}$ ~ 0.05 was used to inoculate 50 ml fresh medium. The culture was grown to the desired growth phase and a volume of 2 ml was sampled for the extraction of total RNA. This volume was mixed by inversion with 800 µl of -20°C cold ethanol/ phenol stop-mix solution (95% v/v ethanol/ 5% v/v phenol) in a precooled 15 ml tube and centrifuged for 10 min (4 000 g, 4°C). The supernatant was discarded and the tube containing the pelleted bacterial cells was frozen at -80°C until extraction process started.

To extract the total RNA, the pellet was resuspended in 750 µl buffer TE (pH 8.0) and the suspension was transferred into Lysing Matrix E glass bead tubes. The strong gram-positive cell wall was disrupted mechanically in FastPrep®-instrument by applying 2x 30 sec at level 6.5. After homogenisation, the tubes were kept on ice for 2 min and then centrifuged for 30 sec at 13 000 rpm/ 4°C. 600-650 µl of supernatant were transferred to a 2 ml safe lock reaction tube and 60 µl 10% (w/v) SDS were added. The tubes were incubated at 64°C for 1-2 min before 66 µl 1 M sodium acetate (pH 5.5) and 750 µl phenol were added. Hot phenol extraction required the tubes to be incubated for 10 min at 64°C with several times of inversion in between and cooling on ice after the incubation phase. During centrifugation for 15 min (13 000 rpm, 4°C) PLG-tubes were prepared. PLG-tubes were shortly centrifuged for 30 sec (13 000 rpm, RT) and 750 µl chloroform was added. After centrifugation of the hot phenol extracts the aqueous phase was transferred into the prepared PLG-tubes and mixed heavily by shaking for at least 30 sec. For chloroform extraction, the mixture was centrifuged for 12 min (13 000 rpm, 15°C). During centrifugation, the 30:1 precipitation mix (pure ethanol/ 3 M sodium acetate pH 6.5) was prepared in a 50 ml tube. For each sample 2x 1.4 ml of this mix were added to fresh 2 ml reaction tubes. 300 – 350 µl of aqueous phase was transferred to 1.4 ml mix (2x for each sample), mixed by inversion and incubated overnight at -20°C for precipitation reaction.

The next day, tubes were centrifuged for 30 min (13 000 rpm, 4°C) and the supernatant was removed by decantation. The pellet was washed with 500 µl 70% ethanol (13 000 rpm, 4°C, 10 min). The pelleted RNA was air-dried at RT and rehydrated with 25 µl 65°C pre-warmed RNase-free water. The RNA from both tubes of each sample was pooled to have a final volume of 50 µl. The extracted total RNA was stored at -80°C. The measurement of the RNA concentration was carried out as explained in the following section.

6.2 Measurement of RNA concentration and RNA integrity

Before any downstream application, the concentration and quality of the isolated total RNA was determined by using either NanoDrop or Bioanalyzer system.

The Agilent 2100 Bioanalyzer provides the size of the analysed RNA, additional to quantitation and quality. The system is a lab-on-a-chip system, using microfluidics technology. Micro scale amounts of RNA are separated electrophoretically in a gel matrix combined with a fluorescent dye and detected by a laser. The manufacturer's software predicts the RNA integrity number (RIN) for each sample. This number is based on the proportion of the ribosomal bands. In case of degradation by RNases the proportion of ribosomal RNA changes and values are low. A high value of 9-10 is acceptable for downstream applications. Agilent RNA 6000 Nano Kit was used for above described application and analysis was carried out following manufacturer's instructions.

6.3 Preparation of RNA for gel electrophoresis

The amount of RNA in each sample used for Northern blotting was 10 µg. The volume of total RNA for 10 µg was mixed with 2.5X Vol. of ice-cold, pure ethanol and then 3 M sodium acetate (pH 5.5) was added to a final concentration of 0.3 M sodium acetate for precipitation reaction. The precipitation mixture incubated overnight at -20°C. For the clean-up of the RNA, RNA was centrifuged for 30 min at 4°C with 13 000 rpm, washed with 100 µl of 70% ethanol and centrifuged again for 15 min. Ethanol was pipetted out and after a short spin down of the RNA, the remaining ethanol was taken out. RNA air-dried at RT for approx. 10 min and was solved in 10 µl of GLII-buffer (625 µl 2% (w/v) bromophenol blue [end. conc.: 0.025%], 625 µl 2% (w/v) xylene cyanol [end. conc.: 0.025%], 1.8 ml 0.5M EDTA pH 8.0 [end. conc.: 18 mM], 129 µl 10% (w/v) SDS [end. conc.: 0.025%], 46.82 ml formamide [end. conc.: 95 %]) for 5 min at 65°C in the heating block with shaking conditions (~800 rpm). RNA was kept on ice until it was used for gel electrophoresis.

6.4 Gel electrophoresis

On the purpose of the experiment, ribonucleic acids were separated using either denaturing conditions in agarose and polyacrylamide gels or native conditions in non-denaturing polyacrylamide gels. The following size markers were used for RNA electrophoresis.
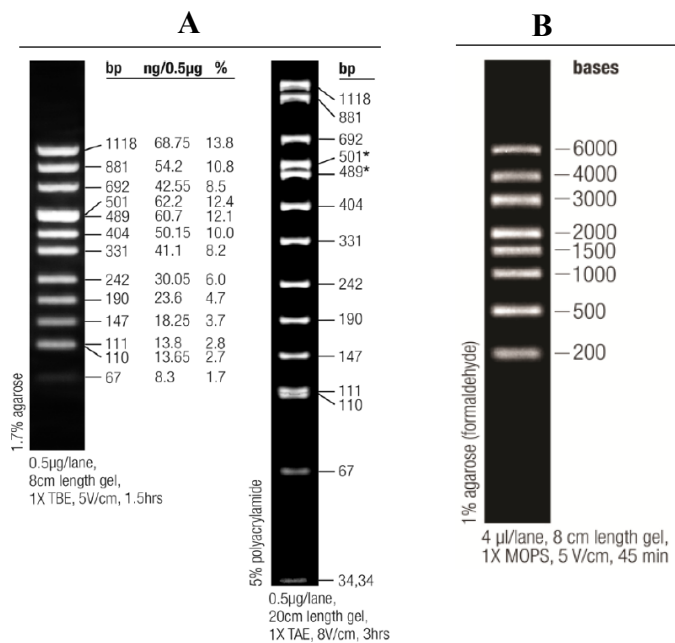
Fig. II-3: Size standards used in RNA electrophoresis

(**A**) DNA marker 'pUC Mix Marker, 8, ready-to-use' from Fermentas (#SM0303). (**B**) RNA marker 'RiboRuler High Range RNA Ladder, ready-to-use' from Thermo Scientific (#SM1823).

6.4.1 *Urea/ polyacrylamide gels*

Polyacrylamide (PAA) gels containing urea denature RNAs and separation from 20 nt up to 1000 nt is conceivable. 6% PAA/ 7 M urea gels were run prior to Northern blotting and subsequent specific detection of RNAs.

The gel plates, spacers and the comb were cleaned properly with soap and water and on one side additionally with 70% ethanol. It was important, that the glassware was free of dust particles or dried acrylamide from former experiments. The glass plates were clamped together with brackets having the cleaned surface towards the inside and spacers on the edges separated the plates. The gel plates were laid down on a holder.

500 ml PAA premix solution was prepared by mixing of 75 ml 40% acrylamide/ bis-acrylamide (19:1) with 210 g urea and 50 ml 10X TBE (0.9 M Tris-HCl pH 8.0, 0.9 M boric acid, 20 mM EDTA). The volume was adjusted with milliQ-water to 445 ml. The remaining 10% (v/v) of 10% APS and 1% (v/v) TEMED were added just before pouring the gel, as follows: 60 ml of this PAA premix solution were mixed with 600 µl 10% APS and 60 µl TEMED and poured carefully between two glass plates clamped together and separated by spacers. The comb was plugged in and the gel polymerised for at least 15 min.

When the gel was polymerised, the comb was removed and the glass plates were plugged into a chamber. Both, chamber and gel was filled with 1X TBE (0.09 M Tris-HCl pH 8.0, 0.09 M boric acid, 2 mM EDTA) and the slots of the PAA gel were rinsed thoroughly with buffer to remove residual urea.

The RNA samples containing 10 µg in 10 µl RNA loading buffer (GLII) and the radioactive labelled DNA ladder were denatured for 5 min at 95°C and placed back on ice. RNA samples were loaded as fast as possible and without air bubbles into the gel slots. The marker was loaded behind a shield. The gel was run for 1.5-2 h at 300 V and max. A. After finishing electrophoresis, the gel was demounted behind a shield and prepared for Northern blot analysis (chapter II-6.5.2).

6.4.2   *Agarose/ formaldehyde gels*

Agarose gels were used for separation of large ribonucleic acids and covered a wide range from a few hundred nt to more than 6000 nt. Formaldehyde denatured the strong secondary structure formed by RNAs.

For the preparation of a denaturing agarose gel, the working place (fume hood), the gel tray, the running chamber, the comb and the additional equipment (*e.g.* pipettes) were cleaned with RNaseZap® and rinsed with DEPC-H_2O before assembled under the fume hood. The comb was plugged into the gel tray. Then 1.8 g agarose was boiled in 130.5 ml DEPC-H_2O in an Erlenmeyer flask using the micro wave and the mixture cooled down for several minutes, before 15 ml 10X MOPS buffer (10 mM EDTA, 200 mM MOPS, 50 mM sodium acetate) as well as 4.5 ml of 37% formaldehyde were added. The solution was thoroughly mixed with a glass pipette without introduction of any air bubbles and was poured very fast, because polymerisation occurred rapidly. After approx. 30 min the solidified gel was put inside the running chamber and incubated in 1X MOPS buffer for at least 30 min. The prepared RNA samples and the RNA size marker were denatured for 5 min at 70°C and cooled down on ice. Then, RNA samples and size marker were loaded into the pockets of the gel and electrophoresis was run for approx. 3.5 h at 100 V. After electrophoresis, the gel was incubated in DEPC-H_2O to wash out the formaldehyde and stained with ethidium bromide. The separation and integrity of the nucleic acids was documented by UV imaging. A UV fluorescent ruler lay next to the gel. The RNA fragments separated by denaturing agarose/ formaldehyde gel electrophoresis were blotted onto a nylon membrane (chapter II-6.5.2).

6.4.3   *Non-denaturing polyacrylamide gels*

Separation of RNA with preservation of the strong secondary structure was performed in non-denaturing polyacrylamide gels *e.g.* gels used in electrophoretic mobility shift assays (EMSA). The equipment was prepared as mentioned in chapter II-6.4.1.

For the preparation of a relative solid 6% PAA gel, 9 ml 40% acrylamide/bis-acrylamide solution (19:1), 30 ml 1X TBE buffer (0.09 M Tris-HCl pH 8.0, 0.09 M boric acid, 2 mM EDTA), 21 ml milliQ-water, 600 µl 10% APS and 60 µl TEMED were mixed and poured. The gel polymerised within 30 min. A more labile 4% PAA gel contained only 6 ml 40% acrylamide/bis-acrylamide solution (19:1). The gel running station was built up, filled with 0.5X TBE buffer and the gel cooled down to 4°C before RNA samples were loaded either for classical or advanced EMSA (chapter II-6.7.4).

6.5 Northern blot analysis

6.5.1 *Radioactive-labelling of "pUC Mix Marker 8" for polyacrylamide gels*

1.4 µg of pUC Mix Marker 8 (14 µl of #SM0303, Fermentas) were denatured at 95°C for 5 min and cooled down on ice for 3 min. 2 µl of 10X T4-PNK buffer A and 1 µl T4-PNK were added and mixed. In the radioactivity laboratory, 1.5 µl $[\gamma^{32}P]$-ATP were added and the reaction incubated 1h at 37°C. 30 µl ddH$_2$O were added and the reaction was cleaned up with G-50 column according to manufacturer's instructions. The eluate was diluted with 40 µl GLII-buffer (625 µl 2% (w/v) bromophenol blue, 625 µl 2% (w/v) xylene cyanol, 1.8 ml 0.5M EDTA pH 8.0, 129 µl 10% (w/v) SDS, 46.82 ml formamide) and stored at -80°C until use. Before usage, the ladder was denatured again for 2 min at 70°C and 10 µl were used per lane for the Northern blot.

6.5.2 *Blotting of RNA to nylon membrane*

Blotting of RNA means the transfer of separated RNA transcripts to a nylon membrane in order to later detect a specific RNA with a specific radioactively labelled probe.

Transfer of RNA by wet blotting: After gel electrophoresis, one glass plate was carefully taken off of the gel and the first lane of the gel was marked by cutting off the edge. The metal clamp from the blotting system was laid open in a plastic tank with the black side down. One sponge saturated with 1X TBE and 3 wet filter papers the size of the gel were put on top of the black side. The gel was taken off the remaining glass plate with a plastic sheet and was subsequently transferred to a filter paper. The filter paper with the gel on top was laid on the 3 wet filter papers in the tank. The prepared nylon membrane was labelled on the backside with a pencil and carefully placed on the gel. The edge near the first lane of the gel was also cut from the membrane. Then three additional wet filter papers were added and air bubbles were removed by rolling over the setup with a glass pipette. After a second saturated sponge was placed on top, the clamp was closed and put into the blotting tank which was then filled with approx. 5l of 1X TBE buffer (0.09 M Tris-HCl pH 8.0, 0.09 M boric acid, 2 mM EDTA). The blotting was carried out for 1 h 15 min at 4°C with 50 V.

Transfer of RNA by capillary blot: The capillary blot was set up as a plastic tank filled with 10X SSC buffer (1.5 M NaCl, 150 mM sodium citrate, pH 7.0), in which a box was placed over which a filter paper the width of the gel size saturated with 10X SSC buffer hang into the buffer reservoir in the tank. The ethidium bromide or Midori Green stained gel was placed onto the filter paper upside down. The edge of the gel, near the first pocket, was cut off and also the edge of the nylon membrane, that was placed on top of the gel. The location of the pockets of the gel were marked on the backside of the nylon membrane with a pen. Three filter papers saturated with 10X SSC were placed onto the membrane and air bubbles were removed with a glass pipette by carefully rolling over the filter papers from one side to the other. 10 cm of filter paper were placed on top, only being in contact with the nylon membrane and not with the buffer in the tank. On top of the tissue papers a weight was placed, that pushed the papers down. Overnight, the capillary forces pulled the RNA to the nylon membrane.

Irreversible connection of RNA and nylon membrane: Blots, wet blot or capillary blot, were demounted and the RNA was crosslinked to the nylon membrane by using the crosslinker and applying UV light at 120 mJ. The membrane was directly hybridised, see next chapters, or wrapped in plastic foil and stored in a shielded box in the radioactivity lab.

6.5.3 *Preparation of radioactively-labelled DNA-oligonucleotide probes and hybridisation of the membrane*

The standard reaction mixture of 10 µl total volume contained 0.5 µl 10 µM oligonucleotide, 1 µl 10X PNK buffer A, 0.5 µl PNK, 6.5 µl milliQ-H_2O and 1.5 µl [γ^{32}P]-ATP. Oligonucleotide and milliQ-H_2O were first heated to 95°C for 2 min, then the other components were added. The reaction was incubated for 1 h at 37°C in a heating block under radioactive protection. Then PNK was inactivated at 95°C for 5 min. The radioactive probe was cleared from non-incorporated nucleotides with G-25 columns. The column was prepared by re-suspending the resin in the column with the vortex, then loosening the cap one-quarter turn and twisting off the bottom closure. The column was placed in the supplied collection tube and centrifuged for 1 min at 735 x g. 30 µl milliQ-H_2O was added to the radioactive probe which then was carefully applied to the prepared column that was placed into a fresh 2 ml safe lock reaction tube. The column was centrifuged for 2 min at 735 x g and the eluate was stored at -20°C in a radioactive protection box or directly used for hybridisation. The column was disposed immediately to the radioactivity waste container, because the remaining free nucleotides were highly radioactive.

For hybridisation, the membrane was first incubated for short time in milliQ-H_2O and then put into a glass-tube filled with 20 ml of hybridisation buffer (Roti Hybri Quick) with its RNA side on the inside. Pre-hybridisation was carried out for 1 h at 42°C under constant

rolling. The hybridisation buffer (Roti Hybri Quick) was replaced and the radioactively-labelled probe was added. Hybridisation was carried out o/n at 42°C under constant rolling. The membrane was washed for 20 min with 40 ml of 5X SSC/ 0.1% SDS buffer, then for 15 min with 40 ml of 1X SSC/ 0.1% SDS buffer and for 15 min with 0.5X SSC/ 0.1% SDS buffer. Then, the membrane was air-dried and shrink wrapped in plastic foil. A storage phosphor screen was exposed to the membrane for up to 7 days and then analysed by FLA-7000 phosphor imaging system.

The membrane was reused directly for probing of transcripts whose length did not overlap with the prior detected transcript or the probe had to be stripped off from the membrane before re-hybridisation. For that, the membrane was incubated with RNA side down for 10 min in 0.5 l boiled ddH$_2$O with 5 ml 10% SDS. Afterwards membrane was washed in cold water and then was ready for (p)re-hybridisation.

6.5.4 *Preparation of radioactively-labelled ds-DNA probes and hybridisation of the membrane*

Labelling of PCR products was done with the Amersham Megaprime DNA Labeling System. The reaction volume given by the manufacturer's instruction for one probe was halved. 25 ng PCR products were mixed with 2.5 µl Random Primer, heat denatured for 2 min at 95°C and chilled on ice. 5 µl of 3X labelling buffer and 1 µl of Klenow fragment were added and the volume adjusted to 15 µl with milliQ-H$_2$O. Under radioactive protection 2.5 µl [α^{32}P]-dCTP were added and the reaction was incubated for 30 min up to 1 h at 37°C. Clean-up from unincorporated nucleotides was carried out with G-25 columns after volume adjustment to 40 µl with milliQ-H$_2$O.

Nylon membranes were pre-hybridised in hybridisation buffer (Roti Hybri Quick) for 1 h at 65°C in the hybridisation oven. Hybridisation of the membranes with the radioactive ds-DNA probe was done overnight at 65°C. The membranes were washed 3x with 40 ml 2X SSC/0.1% SDS buffer and 3x 10 min with 40 ml 0.5X SSC/0.1% SDS buffer. The washing buffer was disposed as liquid radioactive waste in the labelled container. The membranes were shortly air-dried, shrink-wrapped in plastic foil and a storage phosphor screen was exposed overnight. Read-out was done with FLA-7000 phosphor imaging system and *ImageJ* was used for quantification of the specifically detected bands on the Northern blot.

6.6 Pulse-expression of RNA

6.6.1 *pCG248 vector system*

The vector pCG248 (Helle *et al.*, 2011; **Fig. II-4**), contained the P$_{xyl/tet}$ promoter system, which was used for the controlled induction of gene expression by dose-dependent addition

of anhydrotetracycline (ATc). ATc is a derivative of tetracycline, but without antibiotic effect (antibiotic analogue). It leads to the release of TetR repressor that binds to two *tetO* binding sites within P$_{xyl/tet}$ promoter. The binding of the repressor blocks the transcription, whereas the release of the repressor, through ATc, induces the transcription of the downstream gene.
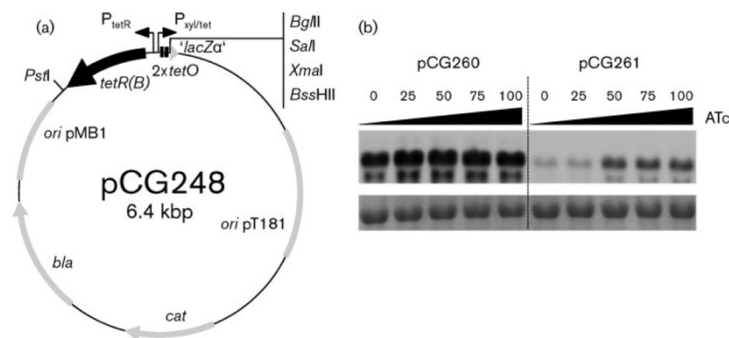
Fig. II-4: pCG248 vector map

(**a**) Figure 3 from Helle *et al.*, 2011 showing the vector map of pCG248. (**b**) dose-dependent induction of *rny* in strain NewmanHG-217 carrying pCG260 (left) or pCG261 (right) together with 16S rRNA as loading control. Vector pCG261 is based on pCG248.

In this work, the nucleotide sequence of IcaZ was cloned downstream of the P$_{xyl/tet}$ promoter in vector pCG248 leading to strain *S. epidermidis* O-47Δ*tRNA*$^{Thr-4}$Δ*icaZ*Δ*icaR*-3′ UTR+pCG248_*icaZ*/tRNA (strain collection code JE13). The induction of IcaZ expression was initiated through the addition of ATc and detected by Northern blot analysis. The experimental setup for the pulse-expression of IcaZ and the subsequent RNA-sequencing analysis is explained in the following chapter.

The TSS of IcaZ on the over-expression plasmids was determined later. Thereby, it was noticed, that the expressed RNA included additional nucleotides deriving from the vector. These nucleotides did not have an influence on the RNA structure, as bioinformatical structure predictions had shown (**Annexe Fig. VIII-9**).

6.6.2   *In-vivo pulse expression of ncRNA IcaZ*

Pre-experiment: Determination of the time frame for the exponential growth phase under static conditions. The bacteria of interest were inoculated ± antibiotics to a defined OD in 30 ml TSB medium in a cell culture flask with a filter screw cap. Bacteria grew at 30°C under static conditions and the OD was measured in between. The data were used to determine the time frame of the exponential growth phase. The early exponential growth phase was reached after approximately six hours and this time point was used for further experiments.

Pulse-expression experiment: *S. epidermidis* O-47$\Delta tRNA^{Thr-4}\Delta icaZ\Delta icaR$-3′ UTR+ pCG248_icaZ/tRNA (strain collection code JE13) was grown in an ONC in TSB medium at 37°C under shaking conditions. The optical density of the bacterial culture was measured spectrophotometrically at 600 nm wavelength. 90 ml fresh TSB medium were inoculated with bacteria to $OD_{600} = 0.06$ and chloramphenicol was added to an end concentration of 20 µg/ml. Then, the bacterial culture was mixed and divided into three flasks (30 ml bacterial culture for each flask). The flasks were incubated statically at 30°C for 6.5-7.25h. Flask 1 was used for growth control measurement. Flask 2 was used for the sampling of bacterial culture without induction of RNA expression (un-induced sample as reference). Flask 3 was filled with 100 ng/ml of ATc to induce the expression of IcaZ 10 min before sampling of the bacterial culture (induced sample). For sampling, flask number two and three were taken under the fume cupboard and filled with the appropriate amount of -20°C cold ethanol/ phenol stop-mix solution.

The RNA was isolated (chapter II-6.1) and DNase treated until the RNA was free of remaining DNA. The RNA samples were controlled by PCR with primers tRNA_x_as and IGRica_rev294 (T_A: 55°C; t_E: 30 sec) for the amplification of IcaZ nucleotide sequence and with primers gyrB_F and gyrB_R (same PCR protocol) for the amplification of the house keeping gene *gyrB*. The quality of RNA was checked with Agilent 2100 Bioanalyzer from Agilent Technologies and samples with high RIN number (RIN 9-10) were sent for RNA-sequencing analysis.

Three individual sets of RNA (un-induced and induced sample) were prepared and stored at -80°C. Set 1 was prepared for sequencing: sample ML1 (un-induced sample) and sample ML2 (induced sample) had each a total volume of 10 µl and a concentration of 250 ng/µl DNA free RNA. The samples were sent in for RNA sequencing and Dr Konrad Förstner normalised the data and did bioinformatics analysis. Reads were mapped to *S. epidermidis* RP62A genome (NCBI reference number NC_002976.3).

6.6.3   *RNA-sequencing data analysis with IGB and IGV*

RNA-sequencing data files (.wig-files) were loaded into '*Integrated genome browser*' (IGB; Freese *et al.*, 2016b) and mapped to the reference sequence file NC_002976.gff. A second data analysis was carried out by Dr Konrad Förstner, leading to very large data files that were opened with 'Integrative Genomics Viewer' (IGV; Robinson *et al.*, 2011; Thorvaldsdottir *et al.*, 2013), which is a high-performance visualisation tool for the exploration of large, integrated genomic datasets (http://software.broadinstitute. org/software/igv/).

6.7 Electrophoretic mobility shift assay (EMSA)

6.7.1   *In-vitro transcription of RNA*

Specific DNA templates were amplified by PCR from chromosomal DNA with Phusion High-Fidelity DNA Polymerase. Cleaned up PCR products were then used for *in-vitro* transcription of the specific RNA.

RNA was transcribed *in-vitro* with MEGAscript® kit from Ambion. The transcription reaction was assembled at RT to avoid a co-precipitation of the reaction buffer with the template DNA. The total reaction volume of 20 µl contained 250 ng DNA template in RNase-free water, which was the specific PCR product including T7 RNA polymerase promoter sequence upstream of the sequence to be transcribed, 8 µl of rNTP solution mixture (2 µl from each ribonucleotide; ATP, CTP, GTP, UTP), 2 µl 10X reaction buffer and 2 µl of enzyme mix. The tube was flicked gently for mixing the components and incubated at 37°C for 6h. 1 µl TURBO DNase was added to degrade the DNA template and further incubated at 37°C for 15 min. 65 µl of RNase-free water and 15 µl Ammonium Acetate Stop Solution (5 M ammonium acetate, 100 mM EDTA) were added to stop the reaction and to adjust the total volume to 100 µl.

RNA was purified by phenol:chloroform:isoamyl alcohol extraction using P:C:I (25:24:1). The reaction volume and the same volume P:C:I (25:24:1) were mixed in a prepared PLG-tube and centrifuged (13 000 rpm, 12 min, 15°C). A MicroSpin G-25 column was prepared during centrifugation time according to manufacturer's instructions. The upper aqueous phase in the PLG tube was transferred to the prepared column and centrifuged at 735 x g for 1 min. The eluate was precipitated with 300 µl of 30:1 precipitation mix (pure ethanol/ 3 M sodium acetate pH 6.5) for 2h at -80°C or overnight at -20°C. Tubes were centrifuged for 30 min (13 000 rpm, 4°C), the supernatant was removed by decantation and the pellet was washed with 100 µl 70% ethanol (13 000 rpm, 4°C, 10 min). The pelleted RNA was air-dried at RT and rehydrated with 33 µl 65°C pre-warmed RNase-free water.

The concentration of the *in-vitro* transcribed RNA was measured and with consideration of the molecular weight diluted to obtain 10 µM stock solutions to be stored at -80°C. RNA quality was controlled (chapter II-6.2).

6.7.2   *Dephosphorylation and end-labelling of RNA*

20 pmol *in-vitro* transcribed RNA (2 µl RNA from 10 µM stock) were mixed with 15 µl RNase-free water and denatured at 95°C for 1 min. The RNA cooled down on ice, while 2 µl 10X NEB reaction buffer (NEB #B7003S) and 1 µl Alkaline Phosphatase were added. The dephosphorylation reaction incubated at 37°C for 1h. 90 µl RNase-free water were added and the whole reaction approach was cleaned up with 110 µl P:C:I (25:24:1) by using a PLG-tube. After centrifugation, the upper aqueous phase was transferred to a fresh

reaction tube. To this tube 1.1 μl GlycoBlue, 5 μl 3 M sodium acetate and 100 μl pure ethanol were added. Precipitation was conducted overnight at -20°C. The dephosphorylated RNA was cleaned up and rehydrated in 16 μl RNase-free water. 1 μl of the RNA was used for determination of RNA concentration.

15 μl dephosphorylated RNA were end labelled with [γ^{32}P]-ATP. To this end, RNA was denatured at 95°C for 1 min and cooled down on ice for 5 min, before 2 μl 10X PNK buffer and 1 μl T4-PNK were added. Additional 2 μl of [γ^{32}P]-ATP were added under radioactive protection in the radioactive laboratory. The labelling reaction incubated at 37°C for 30 min. Radioactive labelled RNA was cleaned up with MicroSpin G-25 column and stored in a shielded box in -20°C freezer until RNA was furthermore cleaned up from PAA-gel.

6.7.3 *Extraction of radioactively-labelled RNA from denaturing polyacrylamide gel*

[γ^{32}P]-ATP end labelled RNA was mixed with the same volume GLII-buffer (20 μl of [625 μl 2% (w/v) bromophenol blue, 625 μl 2% (w/v) xylene cyanol, 1.8 ml 0.5M EDTA pH 8.0, 129 μl 10% (w/v) SDS, 46.82 ml formamide]) and denatured at 95°C for 1 min. Radioactive end labelled pUC Mix Marker 8 (chapter II-6.5.1) was also denatured the same way. Both were separated on a denaturing 6% PAA/7M urea gel at 300V for approx. 1.5h. The gel was wrapped in foil and exposed to a storage phosphor screen. After approx. 1h, the screen was read-out with FLA-7000 phosphor imaging system. A100% print out was positioned behind the gel and marked the right localisation of the labelled RNA band. The exact RNA band was then cut out of the gel and transferred to a 2 ml safe lock reaction tube. 750 μl RNA elution buffer (0.1 M sodium acetate pH 5.5, 0.1% SDS, 10 mM EDTA pH 8.0) were added and the reaction tube was tightly wrapped with parafilm. The gel slices incubated within the elution buffer overnight for up to 16h at 8°C under vigorous shaking (1000 rpm). Gel slices were collected through application of a short spin down. The elution buffer, now containing the labelled RNA, was transferred to the same volume of P:C:I (25:24:1) within a prepared PLG-tube. After mixing and centrifugation (12 min, 13 000 rpm, 15°C), the upper aqueous phase was divided (each 350 μl) and transferred to a fresh 2 ml safe lock reaction tube, that was previously filled with 1 ml of pure ethanol. RNA precipitated for 3h at -20°C. The reaction tubes were centrifuged for 30 min (13 000 rpm, 4°C), then the supernatant was removed by decantation into fluid radioactive waste container. The eluted RNA air-dried at RT and the previously divided samples were pooled and rehydrated in 25-50 μl RNase-free water. RNA was stored at -20°C.

6.7.4 *Measurement of radioactively labelled RNA*

The concentration of radioactively labelled RNA was measured with Nano Drop system against RNase-free water reference in the radioactivity laboratory.

6.7.5 *Experimental setup variants for EMSA*

Electrophoretic mobility shift assays were carried out in two variants. The classical variant, in which the interacting partners have been *in vitro* transcribed before (one of them was then radioactively labelled) and were denatured prior to the interaction reaction. During interaction reaction, both RNAs folded. The second variant included a "live" *in vitro* transcription, meaning that one interaction partner was transcribed *in vitro* at the same time as the other interaction partner refolded.

6.7.5.1 *Classical EMSA*

The following protocol was used as control assay for EMSA experiments, thereby verifying *icaR* mRNA auto-regulation in *S. aureus* and to analyse the binding ability of *icaR* 5′ UTR and *icaR* 3′ UTR in *S. epidermidis*. The primers used for the amplification of the UTR-fragments are listed in Appendix. PCR products were then transcribed *in vitro*. 5′ UTR fragments, IVT_{18} (for *S. epidermidis* O-47) and IVT_{23} (for *S. aureus*), were radioactively labelled; 3′ UTR fragments, IVT_{20} (for *S. epidermidis* O-47) and IVT_{24} (for *S. aureus*) were adjusted to get 10 µM stock and stored at -20°C.

For the assay, 6400 nM target IVT_{20} or IVT_{24} were mixed with RNase-free ddH₂O to a total volume of 5 µl and a dilution series was prepared (**Tab. II-12**). In a separate reaction tube, 16 pmol of radioactively labelled RNA (IVT_{18} and IVT_{23}) were mixed with water to an end volume of 20 µl, then denatured for 1 min at 95°C and chilled on ice for 5 min. The denaturation step and subsequent cooling down was also carried out for the target RNA. 2X TMN-buffer (40 mM Tris/Cl pH 7.5, 20 mM $MgCl_2$, 300 mM NaCl) was mixed with the RNAs to obtain 1X buffer. That means, 2.5 µl of 2X TMN-buffer were added to each target reaction tube and 20 µl of 2X TMN-buffer were added to the radioactively labelled RNA. For interaction reaction, 5 µl of radioactively labelled RNA were given to each target RNA and then the tubes were incubated at RT. After 10 min at RT, the reaction tubes were incubated for further 15 min at 37°C. Each reaction was mixed with 2.5 µl of 5X native loading buffer (50% glycerol, 0,2% bromophenol blue, 0,5X TBE, 0,2% xylene cyanol, filled up to the desired volume with RNase-free water) and separated on 6% native PAA gel for 4h (300 V, 4°C). The gel was then put on a Whatman® paper, labelled and covered with a plastic foil. It was vacuum-dried at 80°C for 1.25 h. The dried gel was put into an X-ray box, together with a storage phosphor screen, and the read-out was done the next day with FLA-7000 phosphor imaging system.

Tab. II-12: Preparation of target mix

Reaction tube	1	2	3	4	5	6	7
target	5 µl	2.5 µl	2.5 µl	2.5 µl	2.5 µl	2.5 µl	-
+ ddH₂O	-	2.5 µl	2.5 µl	2.5 µl	2.5 µl	2.5 µl	2.5 µl

6.7.5.2   *Advanced EMSA*

Protocol for IcaZ (IVT$_{16}$)/5′ 3′ UTR fusion product (IVT$_{19}$)-interaction (**Fig. V-5 E**). The calculated reaction volume of 10 µl contained 2 µl dNTPs (from 10mM stock), 2 µl 5x buffer, 0.25 µl Ribolock, 0.37 µl T7-polymerase, 3.33 µl RNase-free H$_2$O, 1.44 µl IVT$_{16}$-PCR product (0.5 pmol) and 0.64 µl (0.5 pmol) radioactively labelled IVT$_{19}$.

The master mix for *in vitro* transcription (17 reactions) therefore contained 34 µl dNTPs (from 10mM stock), 34 µl 5x buffer, 4.25 µl Ribolock, 6.29 µl T7-polymerase and 56.1 µl RNase-free H$_2$O, because the PCR product and the radioactively labelled RNA were added to a later time point. 16 reaction tubes (PCR stripes) were prepared. 7.92 µl of that mixture were transferred into tube 15 and 16, then 9.64 µl IVT$_{19}$ were added to the master mix (15x 0.64 µl). 5.04 µl of IVT$_{16}$-PCR product were transferred into a fresh tube. From this tube, 1.44 µl each were put into tube 1, 2 and 16. 0.72 µl were transferred into tube 15. 1.44 µl RNase-free H$_2$0 were filled into tubes 2-14; 0.72 µl RNase-free H$_2$0 were filled into tube 15. The PCR product in tube 2 was diluted to tube 11, the residue volume of 1.44 µl was discarded. For tRNA controls, 0.15 µl of tRNA stock solution (20 mg/ml) were filled into tube 13 and 0.3 µl of tRNA stock solution (20 mg/ml) were filled into tube 14. 8.56 µl of the master mix, containing the radioactively labelled IVT$_{19}$, were transferred into tubes 1-14. 0.2 µl of [α^{32}P]-UTP were filled into tube 15. The reaction tubes were closed with a lid and incubated for 2h 10 min at 37°C in the PCR-cycler. The reason, why the PCR-cycler was used, was that the lid was also heated and the small volume inside was held back at the bottom. Hence, constant reaction conditions could be applied. The amount of *in vitro* transcribed RNA was calculated from pre-experiments.

6.7.5.3   *Calculation of in vitro transcribed RNA*

The amount of *in vitro* transcribed RNA, concerning the results displayed in **Fig. V-5 C+D**, was measured in an additional reaction tube. This reaction tube contained 1X IVT-buffer, 0.5 pmol of PCR product and 0.2 µl of [α^{32}P]-UTP in 10 µl total volume. After 2h 10 min, the reaction was cleaned-up by using the standard protocol for G-25 columns. The RNA concentration and quality was measured with the NanoDrop, then the DNA (from PCR-product) was digested with DNaseI (Turbo DNaseI) for 15 min at 37°C. RNA was cleaned-up again using a Kit from Qiagen. RNA was resolved in 30 µl RNase-free H$_2$O and the concentration and quality was measured again with NanoDrop. The concentration was used to calculate the amount of produced RNA.

6.8 Determination of transcript lengths by cRACE

Rapid amplification of cDNA ends (RACE) was used for the determination of transcript length. In this work, circular RACE (cRACE) was performed. DNA-free total RNA was treated with Tobacco Acid Pyrophosphatase (TAP) to convert 5′ triphosphate RNA into 5′ monophosphate RNA, to allow subsequent ligation of 5′ and 3′ ends of the transcripts

(T4 RNA ligase). The transcripts become circularised. Reverse transcriptase generates cDNA from the circularised RNA with specific primers followed by PCR. Each primer is orientated towards the 5′ 3′ ends of the transcripts, so that a PCR product is amplified containing the region of interest, the ends of the specific transcript. Afterwards, the PCR product was ligated into pGEM®-T Easy Vector System I and cloned into *E. coli* DC10B. *E. coli* clones were tested by colony PCR with M13-primers and the longest PCR products were cleaned-up and sequenced by Seqlab - Sequence Laboratories Göttingen GmbH. The sequencing data were analysed with *CLC Main Workbench* and aligned against *S. epidermidis* O-47 Wt reference sequence. Transcription start sites and endings of RNA transcripts (IcaZ, *icaR* mRNA) were identified with this method. The protocol was adapted from Brenneis *et al.*, 2007 (**Fig. II-5**) and was carried out as follows:
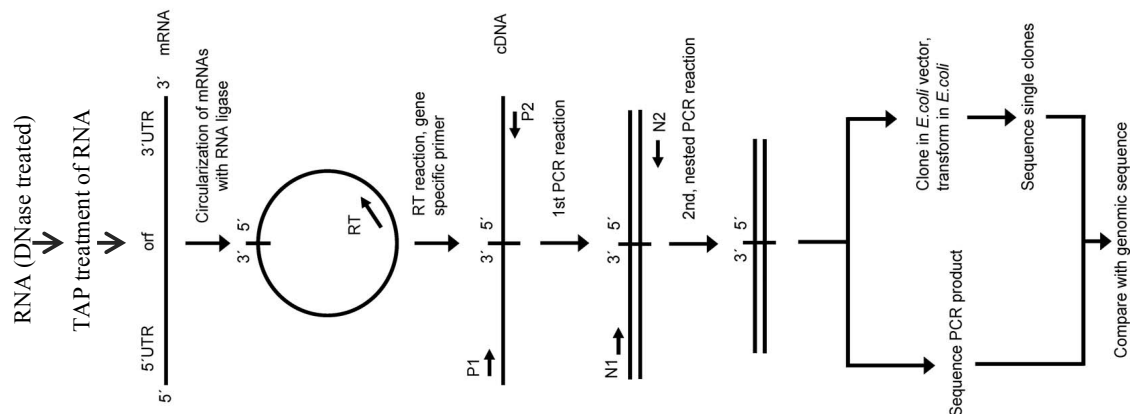
Fig. II-5: Flow scheme for cRACE

The protocol for the rapid amplification of cDNA ends for transcript length determination was modified from Brenneis *et al.*, 2007.

Removal of DNA from RNA samples with DNase digestion: 10-15 µg of RNA were mixed with ddH$_2$0 to receive a total volume of 38 µl. RNA denatured at 65°C for 5 min and subsequently cooled down on ice. 5 µl 10X rDNaseI buffer, 5 µl rDNaseI and 2 µl Superase-in were added and mixed gently. The reaction incubated at 37°C for 45 min. During this incubation time, PLG-tubes were prepared by centrifugation at 13 000 g for 30 sec, labelled and filled with 100 µl P:C:I. (25:24:1). 50 µl ddH$_2$0 were added to the reaction mix after incubation, mixed gently and filled to the provided P:C:I (25:24:1). After mixing, the reaction tube was centrifuged for 12 min (13 000 rpm, 15°C). The upper aqueous phase was transferred into a fresh 2 ml reaction tube and mixed with 2.5 Vol. (~250 µl) of 30:1 precipitation mix (pure ethanol/ 3 M sodium acetate pH 6.5). The precipitation reaction incubated for 2h at -80°C and subsequently for 20-30 min on ice. Tubes were centrifuged for 40 min (13 000 rpm, 4°C), the supernatant was removed by decantation and the pellet was washed with 250 µl 70% ethanol (13 000 rpm, 4°C, 10 min). The pelleted RNA was air-dried at RT and rehydrated with 25 µl 65°C pre-warmed RNase-

free water. The concentration of the extracted total RNA was measured and the success of DNase treatment was controlled by PCR. Remaining DNA would have led to a PCR product. The DNase digestion was repeated, when necessary.

Control PCRs for DNase digestion were carried out as follows: Primers tRNA_x_as and IGRtr_1_RT_rev were used for the amplification of *icaZ* gene (T_A: 50°C, t_E: 30 sec, 169 bp). For *icaR* gene amplification, primer IcaR-F and IcaR-R were used (T_A: 55°C, t_E: 30 sec). The housekeeping gene *gyrB* was also amplified as an additional control. For this, primer gyrF-HK and gyrR-HK were used (T_A: 55°C, t_E: 30 sec). Due to the small PCR product sizes (< 400 bp), a 2% agarose gel was used for gel electrophoresis. After successful DNase digestion, the RNA quality was checked using the Agilent 2100 Bioanalyzer. Only RNA with high RIN were taken for subsequent analysis.

TAP treatment: Tobacco Acid Pyrophosphatase (TAP) converts 5′ triphosphate RNA into 5′ monophosphate RNA. 3-8 µg RNA, 5 µl 10X TAP reaction buffer, 0.5 µl Ribolock (RNase inhibitor) and 1 µl Tobacco Acid Pyrophosphatase (TAP, 10U/µl) were mixed and RNase-free water was added to receive 50 µl total volume. After incubation at 37°C for 30 min, the TAP treated RNA was chilled on ice for several minutes, adjusted with RNase-free water to 100 µl total volume and then cleaned up with P:C:I (25:24:1) precipitation (see above). The precipitated RNA was rehydrated in 13.5 µl of RNase-free water.

Circularisation of transcripts: 5′ monophosphate RNAs were circularised by T4 RNA ligase reaction. TAP treated RNA was denatured for 2 min at 70°C and then chilled on ice for several minutes. After a short spin-down, 2 µl 10X ligation buffer, 2 µl T4 RNA ligase (10U/µl) and 1 µl Ribolock were added. The reaction incubated overnight at 16°C. RNA was cleaned up with P:C:I (25:24:1) precipitation (see above) and rehydrated in 10 µl of RNase-free water.

Specific synthesis of cDNA from circularised, ligated transcripts: 2-4 µg of circulated, ligated RNA were mixed with 20 pmol of a specific primer (for *icaZ* transcripts: 307_sRNA_ica; for *icaR* transcripts: Se_icaR_for1) and 1 µl 10 mM dNTP mix. The volume was adjusted with RNase-free water to 14.5 µl total reaction volume and the mixture denatured for 5 min at 65°C. After cooling down on ice, 4 µl 5X reverse transcriptase buffer, 0.5 µl Ribolock and 1 µl RevertAid Premium Reverse Transcriptase were added. The mixed reaction incubated for 30 min at 50°C, then for 5 min at 80°C. cDNA was stored at -20°C.

Amplification of specific DNA fragments from cDNA template: Amplification of IcaZ cDNA: Primer 307-sRNAica and 307-sRNAica_rev for the first PCR. PCR product was then used as template for a nested PCR with primer IGRtr-1_RT and IGRtr-1_RT_rev. Amplification of *icaR* cDNA: Primer Se_icaR_for1 and Se_icaR_rev1 for the first PCR.

PCR product was then used as template for a nested PCR with primer Se_icaR_for2 and Se_icaR_rev2.

PCR products were cleaned-up and 5-8 µl were separated on an agarose gel to control the product size. Depending on the quality of the PCR product, the first or the nested cleaned-up PCR product were used for the subsequent reactions. When DreamTaq DNA Polymerase was used for PCR, PCR products were ligated directly after clean-up into pGEM®-T Easy Vector System I (Promega GmbH). The vector contains 3′ poly-T overhangs that pair with the 5′ poly-A overhangs that were added to the PCR product by DreamTaq DNA Polymerase during PCR reaction. When Phusion High-Fidelity DNA Polymerase was used, the cleaned-up PCR products were subsequently poly-A-tailed before they were ligated into pGEM®-T Easy Vector System I. For poly-A-tailing 200 µl of PCR product were set up together with 12.1 µl ddH$_2$O, 2.0 µl 10X DreamTaq DNA Polymerase reaction buffer, 0.5 µl DreamTaq DNA Polymerase and 0.4 µl fresh prepared 10 mM dATP in a 20 µl total reaction volume. The reaction was carried out for 50 min at 70°C and cleaned-up afterwards (NucleoSpin® Gel and PCR Clean-up kit from MACHEREY-NAGEL).

Ligation of PCR products into pGEM®-T Easy Vector System I and transformation into E. coli DC10B cells: Ligation reaction was set up according to the manufacturer's instructions in a 3:1 insert to vector molar ratio. 1 µl pGEM®-T Easy Vector containing 50 ng were mixed with 25 ng insert, 5 µl T4 ligase buffer and 1 µl T4 ligase. Then, the reaction volume was adjusted to 10 µl total volume and the reaction tube was incubated for 1h at 25°C, before the complete reaction mix was transformed into *E. coli* DC10B cells using the standard protocol.

Sequencing of clones and data analysis of RACE: Clones from transformation procedure were analysed by colony PCR using M13_for and M13_rev primer pair (T$_A$: 48°C, t$_E$: 45 sec). The PCR products were separated on 2% agarose gel and large PCR products were selected for clean-up reaction and subsequent sequencing reaction. Sequences were analysed with the software *CLC Main Workbench*. The results described in chapter III-1.1.2 were obtained from two different RNA samplings of strain O-47 at both temperatures and from one sampling of RP62A RNA at 37°C.

6.9 Application of atomic force microscopy (AFM)

Atomic force microscopy (AFM) was conducted by Dr Ingrid Tessmer and students, who were supervised by her. 10 µM stock solutions of *in vitro* transcribed RNA were made and aliquots of the stock solutions were provided to her on ice. Also, the predicted IcaZ secondary structures (created by *Mfold*) that later were used by her student to assign the AFM pictures to the predicted secondary structures (see **Annexe Fig.VIII-4**) were provided.

7. Working with proteins

7.1 Extraction of extra- and intracellular proteins

Intracellular and extracellular proteins were isolated from the same bacterial culture. An ONC was set up in TSB and grown overnight at 37°C or 30°C. 150 ml TSB were inoculated with OD_{600} ~ 0.05 and grown until exponential and stationary phase, respectively. 120 ml bacterial culture were pelleted at 7 000 x g for 10 min at 4°C.

For extraction of extracellular proteins, the supernatant was then divided and put into 50 ml screw caps. 100% TCA were added to an end concentration of 10% and the reaction tubes were incubated overnight at 4°C. After 1h of centrifugation, the supernatant was taken off carefully and discarded. Precipitated proteins were washed three times with 20 ml 100% ice-cold ethanol, then again six times with 10 ml and a last time with 70°C ethanol. The pellet air-dried overnight at room temperature and was then renatured in 8 M urea/2 M thiourea. The solution was centrifuged for 15 min at 21 130 x g at room temperature and the supernatant was filled into fresh reaction tubes.

For isolation of intracellular proteins, the pellet was washed three times with 10 ml of ice-cold TE-buffer and then solved in 2 ml of ice-cold TE-buffer, divided and filled into FastPrep-tubes. Cells were lysed for 30 sec at 6.5 m/s^2, then chilled on ice for 5 min and centrifuged for 45 min at 4°C (21 130 x g). The supernatant was transferred carefully into a fresh tube. The extracted proteins were stored for 2h at -20°C before the concentration of the proteins was measured.

7.2 Dot blot analysis

The dot blot assay was used for the specific detection of PIA. PIA-antibody was previously adsorbed against *S. epidermidis* ATCC 12228 to increase the specificity towards PIA producing *S. epidermidis* and to minimise antibody cross reactions.

1X TBS contained 50 mM Tris-HCl (pH 7.5) and 150 mM NaCl. TBS-T contained 1X TBS with 0.1% Tween-20. 10X PBS stock solution contained 1.37 M NaCl, 14.7 mM KH_2PO_4, 26.8 mM KCl, 80 mM Na_2HPO_4 and was adjusted to pH 7.4.

7.2.1 *Adsorption of PIA-antibody*

S. epidermidis ATCC 12228 was inoculated into 5 ml TSB and grown o/n under shaking conditions at 37°C. Bacterial cells were pelleted by centrifugation for 1 min at 13 000 g. The pellet was washed with 5 ml 1X PBS and resuspended in the same volume of 0.5% formaldehyde/ PBS solution. After 20h of gentle shaking at 4°C, the bacterial cells were pelleted again and washed with 5 ml 1X PBS. The pellet was resuspended in 1 ml serum and the mixture incubated for 1h at 4°C under shaking conditions. The bacteria were

pelleted again and the ATCC 12228 adsorbed serum was pipetted into a fresh tube and stored at -80°C with the label: PIA-AK*.

7.2.2   *Dot blot assay setup*

ONCs of the bacteria were set-up in 5 ml of TSB supplemented with CM^{30} when required and incubated o/n at 30°C under shaking conditions. An OD$_{600}$ of 0.05 was inoculated into TSB supplemented with CM^{30} when required and each well of a six-well plate was filled with 4 ml of bacterial culture. The plate was incubated for 18 h at 30°C and 37°C. The bacterial culture was pipetted out into a fresh tube, then the bacteria were scratched from the bottom of each well and added to the previously removed supernatant. The optical density was measured, calculated for OD$_{600}$ = 2.4 and the bacteria were pelleted. The pellet was then resuspended in 50 µl of 0.5 M EDTA (pH 8.0) and incubated for 5 min at 95°C. After centrifugation for 1 min at 13 000 g, 40 µl of the supernatant were moved into a fresh tube and mixed with 10 µl proteinase K solution (10 mg/ ml). The digestion of proteins was carried out for 1h at 37°C, followed by a heat inactivation of proteinase K for 5 min at 95°C. After a short spin down, the supernatant was used for the dot blot assay. 5 µl of each bacterial culture were dropped onto a nitrocellulose membrane that was divided into quadrates of 1 cm x 1 cm before and air-dried for few minutes. The membrane was incubated in 15-30 ml of 3% skimmed milk/ TBS in a 50 ml canonical tube for 1h at RT under constant rolling. Then, the membrane was washed for three times with 1X TBS-T for 10 min. PIA-antibody was added to 10 ml of 3% skimmed milk/ TBS (1:300) and the membrane was incubated in the diluted PIA-antibody for 1h at RT as above. The membrane was washed again three times and was incubated subsequently in anti-rabbit-antibody solution, also prepared in 3% skimmed milk/ TBS (1:5000) as above. After three last washing steps, the PIA was detected by ECL system.

7.2.3   *Detection of PIA with ECL read-out system*

The detection was carried out in the development-room. 1 ml of solution A [200 ml of 0.1 M Tris-HCL (pH 8.6) and 50 mg luminol; 4°C] was mixed with 0.1 ml of solution B (11 mg para-hydroxycoumaric acid in 10 ml DMSO; wrapped in aluminium foil; RT) and 0.3 µl of 35% H$_2$O$_2$. The membrane was incubated in this developing solution for ~ 1 min. After draining of the membrane, the membrane was put, under avoidance of white light, together with a light sensitive film (both separated by a plastic sheet) in an X-ray film box for 2.5 min and for 10 min. The read-out was carried out automatically with an X-ray film processor.

8. Genetic manipulation of bacteria

The efficiency of genetic manipulation of bacteria depends on the species itself. *E. coli* cells are relatively simple to manipulate, whereas staphylococci, especially *S. epidermidis*, is hardly manipulable. Within the last five years, the possibilities for the generation of genetically modified organisms (GMO) increased enormously, when Monk *et al.* created a type IV deficient *E. coli* strain, named *E. coli* DC10B, that allowed direct transformation from *E. coli* to *S. epidermidis* instead of time consuming cloning via *S. aureus* (Monk and Foster, 2012; Monk *et al.*, 2012). This strain was a huge improvement for researchers working with *S. epidermidis*, but also with this strain not every *S. epidermidis* species was manipulable. Winstel *et al.* revolutionised the scientific field again, when they publicised a bacteriophage (φ187) from *S. aureus* PS187Δ*hsdR*Δ*sauUSI* that can be used to transfer plasmids into CoNS (Winstel *et al.*, 2015). Despite this huge progress, still not every species is transformable or transducible, but many more than five years ago.

The following section includes techniques used for the preparation of bacterial cells previously to genetic manipulation, and different methods that were used in this work for the incorporation of foreign DNA into staphylococcal species.

8.1 Preparation of competent cells

The bacterial strains used for this work were not naturally competent, meaning they did not take up and integrate exogenous DNA spontaneously. Therefore, they had to be treated in special way to facilitate the attachment of exogenous negatively charged DNA to the positively charged bacterial surface. The following sections include methods for the preparation of competent *Escherichia coli* and staphylococcal cells.

8.1.1 *CaCl$_2$-competent E. coli DC10B cells*

300 ml of LB medium were inoculated with an ONC of *E. coli* DC10B cells to a starting OD$_{600}$ of 0.05 and further grown to an OD$_{600}$ of about 0.5-0.7 in a circulatory shaker at 37°C. The culture was divided into 6x 50 ml aliquots and incubated on ice for 10 min, in ice-cold reaction tubes. Cells were harvested by centrifugation at 4°C, 4 000 g for 10 min. The cell pellets were resuspended in 25 ml of ice-cold 0.1 M CaCl$_2$ and kept on ice for further 20 min. They were centrifuged again and the pellets were then resuspended in 7.5 ml of ice-cold 0.1 M CaCl$_2$/ 15% (v/v) glycerol. After incubation on ice for 15 min, 150-200 μl aliquots were frozen immediately and stored in -80°C freezer.

8.1.2 *Electro-competent staphylococcal cells*

100 ml of a staphylococcal ONC (*S. epidermidis* or *S. aureus*) were diluted to a starting OD$_{540}$ of 0.05 and grown to an OD$_{540}$ of 0.2-0.25 at 37°C or 30°C. The bacterial culture was divided into 50 ml aliquots and cells were harvested by centrifugation for 10 min at

6 000 rpm. Each cell pellet was first washed with 50 ml of ice-cold 0.5 M sucrose, then with 25 ml, 10 ml and 5 ml. The pellets were pooled and resuspended in 1 ml of ice-cold 0.5 M sucrose and aliquots of 100 µl were frozen immediately and stored at -80°C. This protocol was obtained by Lopez group (IMIB, Würzburg) and extended for the usage of *S. epidermidis* cells.

8.2 Methods for transformation of DNA

E. coli cells were transformed by applying heat shock transformation. The heat shock leads to shortly switching off the restriction-modification systems. Staphylococcal cells have a thick gram-positive cell wall that represents the first barrier for incorporation of exogenous DNA. To weaken the bacterial cell membrane a short but high voltage electrical shock must be applied. This leads to the introduction of pores. The foreign DNA can be taken up by the cell and during subsequent cell growth the pores are restored so that the bacterial cells remain intact afterwards.

8.2.1 *Heat shock transformation*

An aliquot of $CaCl_2$-competent *E. coli* DC10B cells was thawed on ice for 5 min, then mixed with 50-500 ng of plasmid DNA and further incubated on ice for 15 min. The cells were heat-shocked in a heating block for 90 sec at 42°C and cooled down for 2 min on ice before they were mixed with 1 ml of LB medium and incubated under shaking condition for 30 min at 37°C. 100 µl of the transformed cells were plated out onto LB solid agar containing required antibiotics (Amp[100]). The remaining cells were harvested at 10 000 rpm in a benchtop centrifuge and resuspended in 100 µl culture medium. The resuspension was also plated out onto solid media. The plates were incubated overnight at 37°C and could be stored at 4°C for a few weeks until transformed cells have been checked and stored in the strain collection.

8.2.2 *Electroporation method*

An aliquot of electro-competent staphylococcal cells was thawed on ice for 5 min, then mixed with 3-4 µg of plasmid DNA and filled in an electroporation cuvette (1 mm ø). After incubation at RT for 15-20 min, the cells were shocked due to the application of an electrical pulse at 1800 V by using the electroporation machine. 150 µl of TSB were given very gently to the electro-shocked cells and they were incubated under shaking conditions at 37°C for 1.5h, before the suspension was divided and plated out onto selective solid agar. The plates incubated at 37°C for 2-4 days, until genetically manipulated cells could be further analysed. The cells treated by electroporation needed more time for recovery, especially *S. epidermidis* cells.

8.3 Transduction of DNA from *S. aureus* to *S. epidermidis* via Phage φ187

Phages were used as shuttle for the exchange of plasmids between same or different bacterial species. In this work, plasmids were transferred from *S. aureus* to *S. epidermidis* with Phage φ187. **Fig. II-6** displays the workflow for phage transduction (Winstel *et al.*, 2016). The transduction process contains three major steps. In the first step, the DNA of interest is transformed into the donor strain (Fig. II-6; Steps 1-19). In the second step, the donor strain is infected with the phage, who takes up the plasmid of interest from the donor strain during the infection process (Fig. II-6; Steps 26-31). In the last step, the incorporated DNA is released from the phage into the recipient strain, also by an infection process (Fig. II-6; Steps 32-37).
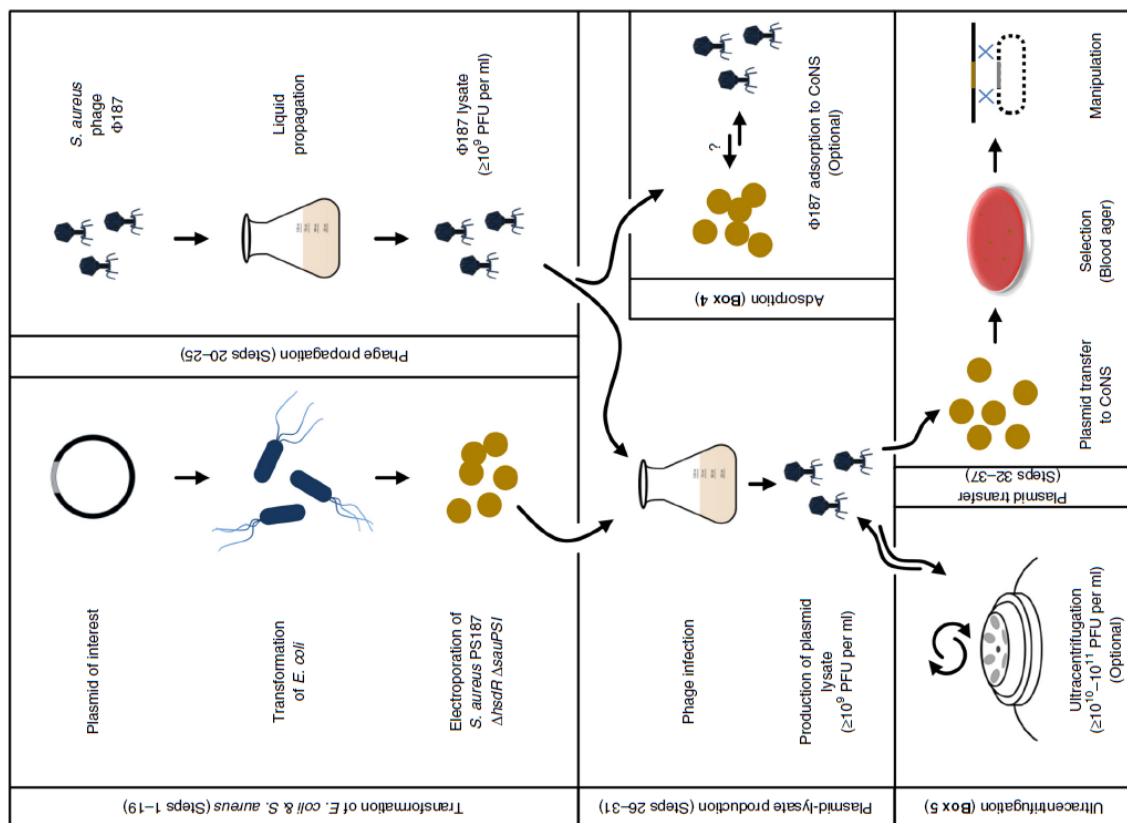
Fig. II-6: Workflow of bacteriophage φ187–mediated plasmid transfer to coagulase-negative staphylococcal (CoNS) pathogens.

Figure was taken from Winstel *et al.*, 2016 (Figure 1). Plasmid construction, transformation of *E. coli* and electroporation of plasmid donor strain *S. aureus* PS187Δ*hsdR*Δ*sauPSI* (formerly named *S. aureus* PS187Δ*hsdR*Δ*sauUSI*) (Steps 1–19), generation of phage and plasmid-containing phage lysates (Steps 20–31) and plasmid transfer to CoNS (Steps 32–37). Optional steps related to this protocol include the analysis of the φ187 adsorption capacity to CoNS (Box 4), and the ultracentrifugation of plasmid-containing phage lysates to increase phage titers (Box 5).

8.3.1   *Preparation of plasmid bearing phage particles (PBPP) from donor strain*

An ONC of the donor strain, a plasmid carrying *S. aureus* PS187Δ*hsdR*Δ*sauUSI*, was set up in 4 ml BM together with the required antibiotic. After overnight incubation at 37°C in a circulatory shaker, 2.5 ml of ONC were mixed with the same volume of fresh media and further incubated for additional 3h. During the last hour of the incubation time, the soft agar was boiled to become liquid and cooled down to 55°C in a pre-warmed water bath. 20 µl of 1 M CaCl$_2$ were added to receive the end concentration of 4 mM CaCl$_2$. After mixing, 200 µl were transferred to a 15 ml reaction tube and mixed with the same amount of phage lysate. Hereby, the phage lysate from Laura Wicke (experiment 1/9th approach, sterile filtered) was used. The mixture containing donor strain and phage incubated at RT for 15 min, then 3.5 ml of soft agar were added, rapidly mixed and poured onto BM-agar plates. The soft agar solidified within a few minutes and the plates were incubated overnight at 30°C. 2 ml of phage buffer I (BM + 4 mM CaCl$_2$) were used to scratch off the soft agar from the BM-agar. The detached soft agar was decanted into a 50 ml reaction tube and the solid fragments were collected at the bottom of the tube by centrifugation at 5000 rpm (4985 x g) for 20 min. The supernatant was filtered twice, first with 0.45 µm filter and second with 0.2 µm filter. The total volume of phage lysate was approx. 500 µl. The phage lysate was used directly for transduction or stored at 4°C for several months. A phage titre was not determined, unless it was necessary.

8.3.2   *Transduction of PBPP into the recipient strain*

An ONC of the recipient strain was set up in 4 ml BM and incubated overnight at 37°C under shaking conditions. The optical density of the culture was measured at 600 nm, the bacteria were diluted with fresh media to an OD$_{600}$ of 0.05 and further grown to an OD$_{600}$ of 0.875. Cells of 1 ml culture were harvested by centrifugation. The cell pellet was resuspended in 200 µl of phage buffer II (50 mM Tris-HCl pH 7.8, 4 mM CaCl$_2$, 1 mM MgSO$_4$, 100 mM NaCl, 0.1% gelatine), then 400 µl PBPP (at best 1x 10^9 PFU/ ml) were added. After 15 min of incubation at 37°C in a rotating heating block (~ 500 rpm), each 200 µl were plated onto pre-warmed selective agar plates (three plates per approach) and then incubated overnight at 37°C. The resulting transduced bacteria were checked by PCR and sequencing and stored within the strain collection at -80°C, before they were used for subsequent experiments.

8.4 Cloning and mutagenesis

The applied cloning techniques ranged from standard cloning techniques, like the classical cut and paste method by application of specific restriction enzymes to site-directed mutagenesis in plasmids or other plasmid modifications, *e.g.* the usage of phosphorylated primers.

8.4.1   *Restriction enzymes and ligation*

Restriction enzymes were used following manufacturer's instructions. Reactions were cleaned up with NucleoSpin® Gel and PCR Clean-up kit from MACHEREY-NAGEL GmbH & Co. KG. T4-ligase was used at 16°C in an overnight reaction, also according to manufacturer's instructions.

8.4.2   *Site-directed mutagenesis*

PCR products (chapter II-5.5.3) were digested by DpnI to degrade template DNA. 1 µl of DpnI was given into the PCR reaction and further incubated for 1h at 37°C. Afterwards, DpnI was heat inactivated at 80°C for 20 min. Then, the reaction was directly transformed into *E. coli* DC10B, the circularised plasmid re-isolated and further transformed into *S. epidermidis* O-47 Wt. Clones were tested by PCR with primers pCG248_MCS_rev and pRAB11_MCS_for (T_A: 56°C, t_E: 1 min 20 sec). After clean-up and sequencing of the PCR product, the confirmed strains were stored within the strain collection at -80°C.

8.4.3   *Generation of mutants by homologous recombination of DNA*

The plasmid pBASE6 carrying the insert of interest was successfully transformed into *S. epidermidis* O-47 Wt before (strain collection codes MF61 and HS02). The insert contained flanking regions (up to 1 kb in size) of the gene that was going to be deleted in *S. epidermidis* O-47 Wt. The deletion of the gene of interest was the result of the homologous recombination of the flanking regions with the same regions on the chromosomal DNA. For the procedure of the double crossover, the protocol from Bae *et al.* (Bae and Schneewind, 2006, Figure 2) was adapted.

Strains MF61 and HS02 from the strain collection were used to inoculate 10 ml TSB containing 30 µg/ml chloramphenicol in a 250 ml flask and incubated with vigorous shaking overnight at 37°C. The cultures were streaked out onto pre-warmed TSB agar plates containing 10 µg/ml chloramphenicol and the plates were incubated at 44°C overnight and then additionally at 43°C overnight. Some colonies were picked to inoculate 5 ml of plain TSB and incubated under shaking conditions at 30°C. After 8.5h 50 ng/ml ATc was added and further incubated at 30°C overnight. The resulting cultures were diluted with sterile 1X PBS (to 10^{-5} and 10^{-6}) and plated out onto TSB agar plates containing 50 ng/ml ATc. Plates were incubated overnight at 37°C. Clones were chosen and streaked out onto plain TSB agar and TSB agar with 20 µg/ml chloramphenicol. The plates incubated overnight at 37°C. Clones only growing on plain TSB and not chloramphenicol plates were directly tested in a colony PCR with primers binding in the chromosomal region outside of the flanking regions to avoid false positive results from residual plasmid DNA. For clones deriving from strain MF61, primers IGRica1 and IGRica2 (T_A: 56°C, t_E: 2 min) were used. For clones deriving from strain HS02, primers O47rnc_seq_for and

O47rnc_seq_rev (T_A: 55°C, t_E: 2.5 min) were used. The PCR products of potential clones were cleaned up and send away for sequencing with primer O47_R2_seq additional to the PCR primers (HS02 derived clones) and with primer 5'BamHI_for additional to the PCR primers (MF61 derived clones). Sequencing results verified clones.

The generated *S. epidermidis* O-47 IcaZ mutant strains, *S. epidermidis* O-47Δ*icaZ*, were stored in the strain collection with code ML38, ML39 and ML2. The three strains derived independently from the homologous recombination procedure. The homologous recombination, leading to ML2 was carried out by Heike Schreier under supervision of the author. ML38 and ML39 were generated directly by the author of this work.

The generated *S. epidermidis* O-47 *rnc* mutant (strain collection code: ML40) was generated in this work by homologous recombination of strain HS02. Strain HS02 was generated by Heike Schreier under supervision of the author.

8.4.4   *Cloning of cerulean reporter system for in vivo measurement of P$_{icaZ}$ activity*

P$_{icaZ}$ activity was analysed with cerulean reporter system, which was generated in this work by classical cut and paste method. Restriction enzymes were used to insert the promoter sequence of *icaZ* upstream of the cerulean gene *cfp* within pCerulean vector.

The fragment containing 138 bp upstream of *icaZ*, whose TSS was determined by cRACE, was amplified with Phusion High-Fidelity DNA Polymerase from *S. epidermidis* O-47 genomic DNA. The PCR reaction was carried out in 50 µl standard reaction volume with primers icaZprom_BamHI and icaZprom_BglII, which included the nucleotide sequences for restriction sites BamHI and BglII. The same restriction sites were integrated into pCerulean vector with primer cerul_BglII_sd and cerul_BamHI by PCR. Both PCR products were cleaned-up and digested with fast digest enzymes BamHI and BglII. The vector was then dephosphorylated with Antarctic Phosphatase.

The digested PCR products were again cleaned-up after separation by gel electrophoresis on a 1% agarose gel in fresh 1X TAE buffer (50 min/ 100V). The bands were cut out and cleaned-up. Ligation reaction was carried out with a vector to insert molar ratio of 1:3 and 1:5. Both ligation reactions were incubated for 15 min at 16°C and then for another 15 min at 25°C. They were transferred into *E. coli* DC10B by transformation. The obtained clones were verified by sequencing of the isolated plasmid and clone number 21 was stored in the strain collection with code ML1. The plasmid of strain ML1, *E. coli* DC10B +pCerulean_icaZprom, was transferred into *S. epidermidis* O-47 by electroporation and the newly generated strain *S. epidermidis* O-47+pCerulean_icaZprom was named ML13.

III. Results – Part A 'Characterisation of IcaZ, a long ncRNA specific for *S. epidermidis*'

1. Characterisation of a long ncRNA in *S. epidermidis*: IcaZ

The first chapter of the results section characterises the ncRNA IcaZ, previously named IGR*ica*-RNA, which is located in the vicinity of the *icaADBC*-operon that codes for the enzymes needed for PIA-biofilm formation in *S. epidermidis* (see chapter I-4 for the description of the locus).

1.1 Analysis of IcaZ transcript

1.1.1 *Temperature and strain dependent expression*

The expression of ncRNA IcaZ was analysed in various *S. epidermidis* strains such as O-47, RP62A and the patient isolates PS2 and PS10. Experiments with strain O-47 were carried out under shaking conditions at two temperatures and the results obtained were compared to results from experiments under static conditions.

Thus, for analysis of *S. epidermidis* O-47, the bacterial cultures were grown under shaking conditions at 30°C and 37°C, respectively. Total RNA from different time points of growth was isolated and Northern blots were carried out, as described in chapter II-6.5. IcaZ transcript was detected with two specific ss-DNA oligonucleotide probes (IcaZ_NB and IcaZ_NB2) and one ds-DNA probe, which were radioactively labelled. The ds-DNA probe was a PCR product of primers tRNA-x-as and IGRica_rev294. The two ss-oligonucleotide probes were chosen based on the predicted IcaZ length of 487 nt by Dr Eckart. They were supposed to detect the 5′ end (IcaZ-NB probe) and the 3′ end (IcaZ-NB2 probe) of IcaZ. IcaZ_NB probe detected a specific signal of ~400 nt, whereas IcaZ_NB2 probe bound unspecifically. The unspecific nature of this binding was validated in *S. epidermidis* O-47Δ*tRNA*$^{Thr-4}$Δ*icaZ*Δ*icaR*-3′ UTR, where the binding site of IcaZ_NB2 is deleted in the genome of this strain due to the deletion of *icaZ* and still binding was observed (**Fig. III-1**).

At both temperatures, the length of IcaZ was determined to be ~400 nt and the RNA was expressed in early and mid-exponential growth phase. The results were confirmed with *S. epidermidis* strain RP62A (**Fig. III-2**) and the patient isolate PS2 (**Fig. III-7**).
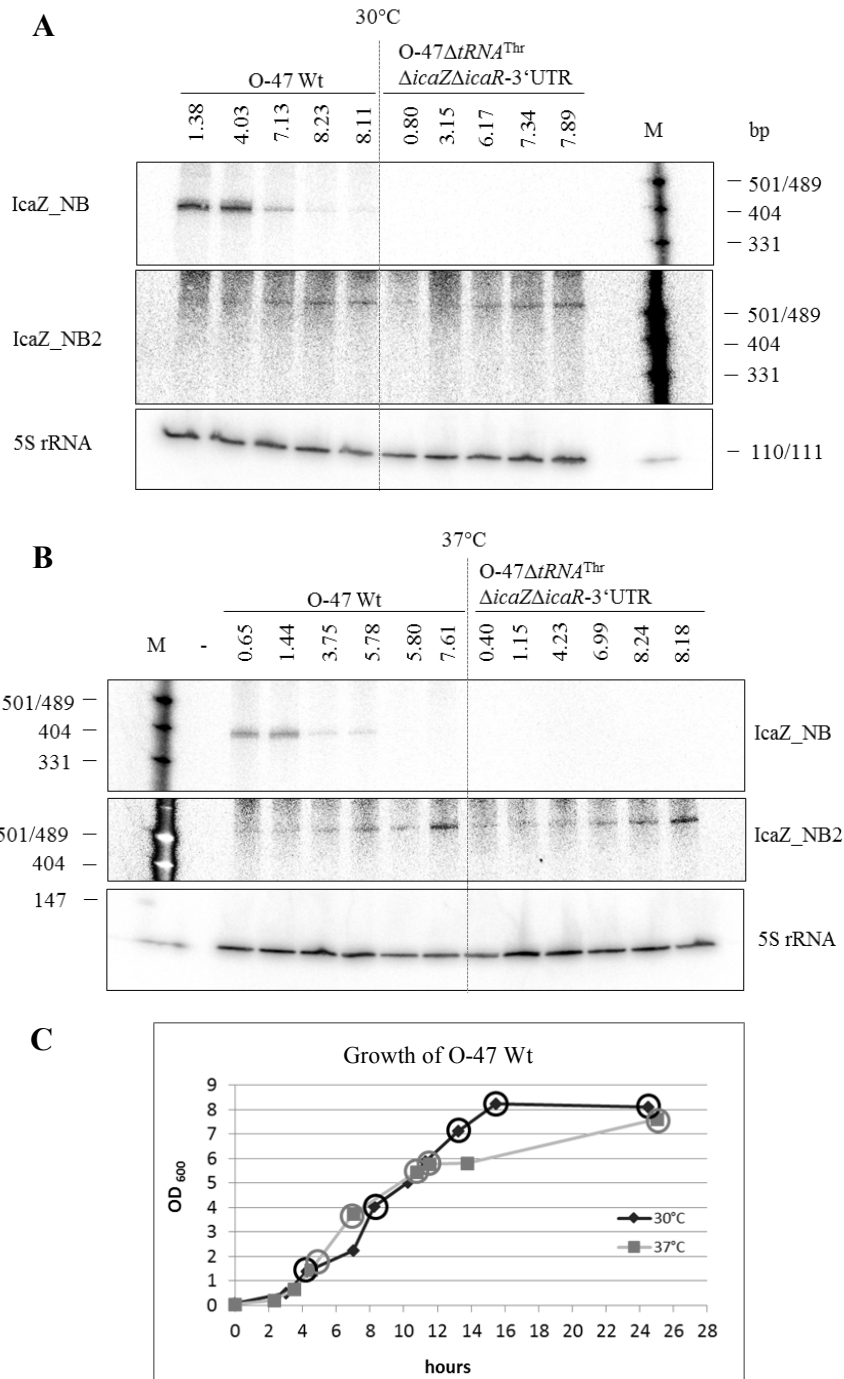
Fig. III-1: Expression of IcaZ in *S. epidermidis* O-47 at 30°C and 37°C

Total RNA was sampled at 30°C (**A**) or 37°C (**B**) and Northern blotting of 10 µg total RNA was carried out. The samples were taken at indicated OD_{600}. Denaturing 8.3M urea/6% PAA gels were run for 1h 45min at 300V. The separated RNA was blotted and subsequently linked to a nylon membrane. IcaZ_NB radioactively end-labelled probe

bound specifically to IcaZ transcripts. 5S rRNA was used as loading control. pUC Mix Marker, 8, ready-to-use (#SM0303) from Fermentas (DNA marker) indicates the band sizes. (**C**) Growth curves of *S. epidermidis* O-47 in TSB medium under shaking conditions at 30°C and 37°C. The optical density of the growing bacterial culture was measured at 600 nm (OD$_{600}$) wavelength and samples were taken at indicated time points. *S. epidermidis* O-47$\Delta tRNA^{Thr-4}\Delta icaZ\Delta icaR$-3' UTR was used as control strain for primer specificity.

Northern blot results of O-47 Wt indicated that IcaZ is more expressed at 30°C. This assumption was confirmed in strain RP62A (**Fig. III-2**). Thus, this RNA seems to be expressed in a temperature-dependent manner.

Additional to the experiments with shaking conditions, the expression of IcaZ was analysed under static conditions to allow the bacteria to adhere to the surface. With this experiment, biofilm forming conditions were simulated and IcaZ expression was analysed with regard to biofilm formation. **Fig. III-3** displays the flow scheme for the experiment. The results obtained with static conditions were in agreement with the results of the experiments under shaking conditions. Here, IcaZ was also expressed at early and mid-exponential growth phase, whereas after 24h nearly no expression of IcaZ was measurable.
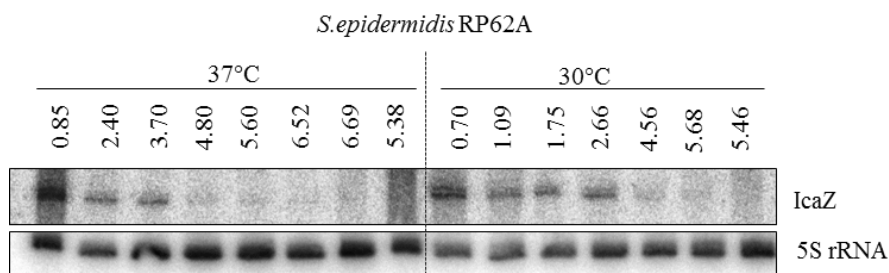
Fig. III-2: Temperature dependent IcaZ expression in *S. epidermidis* RP62A

Northern blot of 10 µg total RNA from *S. epidermidis* RP62A. Samples were taken at different growth phases (indicated OD$_{600}$). IcaZ was detected with radioactively labelled ds-DNA probe. 5S rRNA was used as loading control.
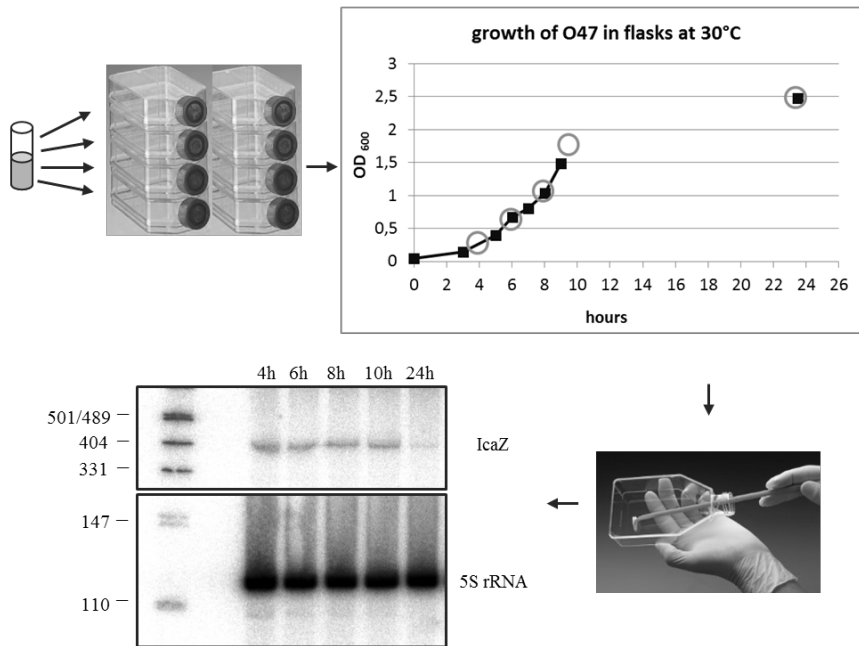
Fig. III-3: Flow scheme of static growth experiment of *S. epidermidis* Wt at 30°C

An ONC of *S. epidermidis* O-47 was inoculated in equal parts into flasks and then cultivated at 30°C under static conditions. The growth of the culture was measured at indicated time points (t_4, t_6, t_8, t_{10}, t_{24}) in hours and the total RNA of adherent and non-adherent cells was isolated. Northern blotting was performed with 15 µg of total RNA. IcaZ transcript and 5S rRNA were detected with radioactively labelled IcaZ-dsDNA and 5SrRNA probes. The quality of the RNA samples was measured with Agilent 2100 Bioanalyzer. The RNA integrity numbers (RIN) showed values of 9.8-10.

1.1.2 *Transcript length*

The length of IcaZ was reassessed, because Northern blots of this work (**Fig. III-1-3**) showed a band size of ~400 nt which conflicted with the results of Dr Eckart, who determined the length of IGR*ica*-RNA with 487 nt. Therefore, the length was analysed using rapid amplification of cDNA ends (RACE) from a circularised IcaZ RNA template (cRACE).

For this purpose, total RNA of *S. epidermidis* O-47 and RP62A was isolated from the exponential growth phase at 30°C and 37°C. The experiment was then processed as described in chapter II-6.8. Two transcription start sites (TSS) for IcaZ were identified, whereas TSS1 was more prominent than TSS2. TSS1 is located at position 2.333.147 in *S. epidermidis* RP62A genome (8 nt downstream of the predicted TSS from Dr Eckart) and TSS2 is at position 2.333.164 (17 nt upstream of TSS1). The 3′ ending of the transcript varied between the sequenced clones, but could be narrowed down to a region of 13 nt (position 2.332.747 to 2.332.759). However, all the transcripts ended after a maximum length of 419 nt and, thus, an overlap of the *icaZ* transcript with the *tRNA*$^{Thr-4}$ transcript in

the antisense direction (chapter I-4) could be excluded. The different temperature conditions during the cultivation of the bacteria did not have an impact on IcaZ length.

The results obtained here were further supported by cRACE data from strains carrying *icaZ* on a plasmid for overexpression of the ncRNA (strain collection codes ML58, ML52 and JE13). Although the different cloning strategies would have allowed *icaZ* transcription to reach different lengths, the RNA length was nearly the same in all three plasmids. None of the cloned and analysed transcripts overlapped with the *tRNA^{Thr-4}* region. This clearly shows that the length of IGR*ica*-RNA is shorter than previously suggested. Thus, the most common length of IcaZ ranges between 402 nt to 419 nt.

Further support for a transcript length of approximately 400 nt is provided by the presence of a terminator sequence in the region, where the *tRNA^{Thr-4}* and *icaZ* genes meet (predicted by the programme ARNold; http://rna.igmors.u-psud.fr/toolbox/arnold/; Gautheret and Lambert, 2001; Lesnik *et al.*, 2001; Macke *et al.*, 2001). The location of this Rho-independent terminator sequence is depicted in **Fig. III-4** (grey). It is assumed that the transcription terminator blocks transcription on both strands, and is used by *tRNA^{Thr-4}* as well as *icaZ*. However, Northern blot analyses showed that longer *icaZ* transcripts were formed, but to a minor proportion, when the expression of *icaZ* was strongly induced.
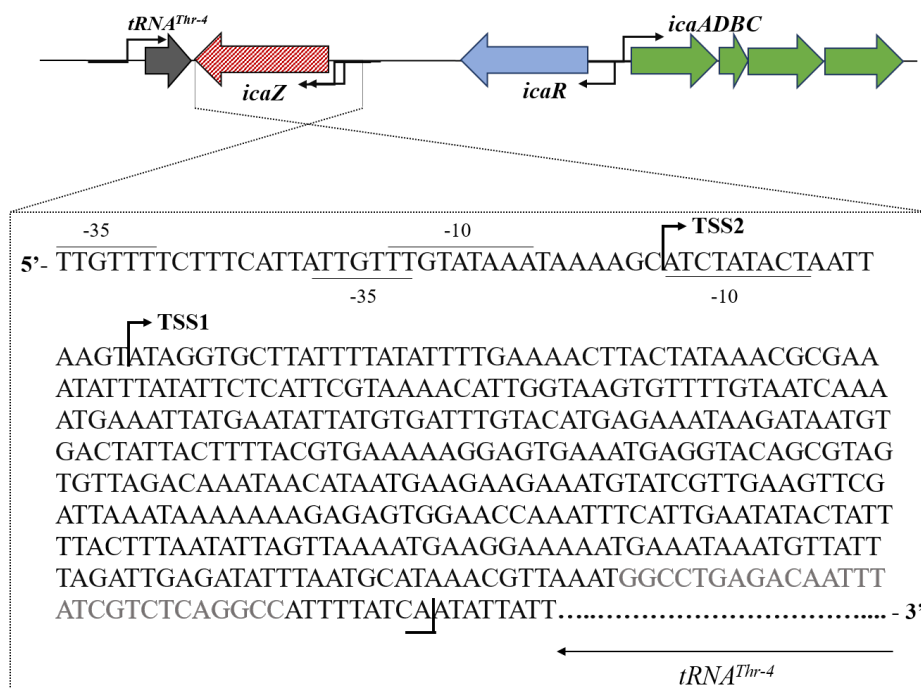
Fig. III-4: Genomic localisation of *icaZ* gene and its sequence

Displayed is the genomic localisation of *icaZ* within the IGR*ica*, the intergenic region between *tRNA^{Thr-4}* and *icaR*. The transcription start sites TSS1 and TSS2 as well as the determined 3′ ends are annotated based on cRACE data. The termination signal, which was predicted by programme ARNold, is highlighted in grey.

1.1.3   *IcaZ is a primary transcript and not a read-through from the adjacent icaR gene*

Primary transcript enrichment with subsequent deep sequencing of the previously prepared cDNA library was carried out in order to distinguish between primary transcripts (5′ triphosphates) and processed transcripts (5′ monophosphates) within an RNA pool. The method is called differential RNA sequencing (Sharma *et al.*, 2010; Sharma and Vogel, 2014). One part of the RNA pool is treated with TEX (Terminator™ 5′-Phosphate-Dependent Exonuclease), a 5′→3′ exonuclease that digests processed RNAs, and the other part is not treated by the enzyme. Upon differential TEX treatment both samples are converted into cDNA and sequenced. If the number of reads is increased for a specific transcript in the treated sample, then the transcript is a primary transcript.

To investigate primary transcripts in *S. epidermidis*, the RNA of *S. epidermidis* PS2 and PS10 was sampled in exponential growth phase (OD_{600} = 1-3) at 37°C and treated with TEX. The four samples, two for each strain (treated and untreated sample) were send for library preparation and sequencing. The bioinformatic RNA-sequencing data analysis, including normalisation of values, was done by Dr Konrad Förstner (head of bioinformatics group within IMIB; CoreUnit SysMed, www.sysmed.uni-wuerzburg.de), who also created the files that were used in this work for data display and scientific analysis. The number of reads for IcaZ increased from 70 in the untreated sample to 110 in the TEX treated sample (1.57x fold), meaning that IcaZ was enriched by the TEX treatment (**Fig. III-5** PS2 panel). This is also shown by the differential analysis in **Fig. III-6**.

The RNA-seq data of *S. epidermidis* PS2 and PS10 moreover confirmed the two distinct transcription start sites of IcaZ, which are marked by arrowheads in **Fig. III-5**. In conclusion, IcaZ is not a read-through by the preceded gene *icaR* and also not a mRNA (3' UTR)-derived RNA.
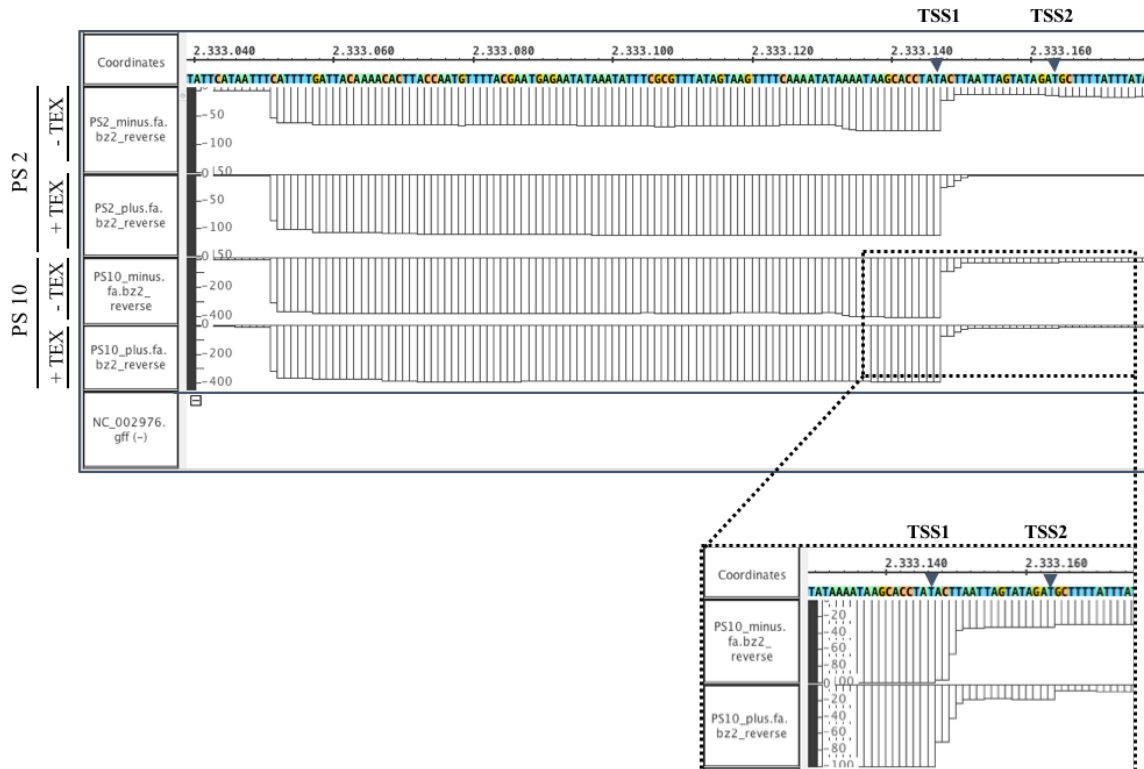
Fig. III-5: Primary transcript enrichment of IcaZ in *S. epidermidis* PS2

The figure shows IcaZ transcript reads from *S. epidermidis* PS2 and PS10 as bars, mapped to the reference genome of *S. epidermidis* RP62A (NC_002976). The data files were displayed with the programme '*Integrated Genome Browser*' (IGB). As the number of IcaZ transcripts increases after TEX treatment, IcaZ is supposed to be a primary transcript. The distinct TSS (marked by arrowheads) are in agreement with the IcaZ 5′-ends determined by the cRACE experiments.
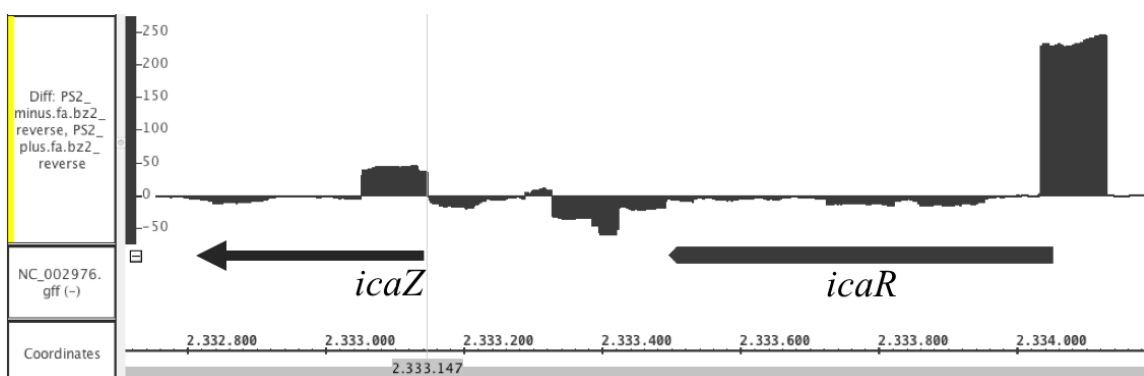
Fig. III-6: Differential analysis of primary transcript enrichment

Shown is the differential analysis of primary and processed transcripts. Primary transcripts, like IcaZ and *icaR* mRNA, are displayed above zero and processed transcripts, like the termination signal of *icaR* mRNA, below zero. RNA-sequencing data of *S. epidermidis* PS2 verified IcaZ as a primary transcript.

1.1.4   *Stability of IcaZ*

The stability of IcaZ is described by the RNA half-live ($t_{1/2}$), which was determined by performing rifampicin assays.

For that, bacterial cells of *S. epidermidis* O-47 were grown in 60 ml TSB medium at 30°C till exponential growth phase (OD_{600} of ~ 1-2). The first sample was taken at time point t_0 and then rifampicin (endconc. 100 µg/ml) was added to the culture. After 1, 2, 4, 8, 16 and 32 min, 2 ml samples each time point were taken and total RNA was isolated following the protocol of chapter II-6.1. 10 µg of isolated RNA from each sample were separated by Northern blot and IcaZ band was detected with specific radioactively labelled probes. The Northern blot data were processed with *GIMP* programme. The signals were measured and the half-live was calculated with *ImageJ*. In **Fig. III-7 A+B**, Northern blots of total RNA from two biological replicates of *S. epidermidis* O-47 are displayed. The half-live of IcaZ was also measured in *S. epidermidis* PS2, in the exponential growth phase at 37°C (**Fig. III-7 C**). The half-lives of IcaZ ranged between 2.7 to 3.3 min in *S. epidermidis* O-47 and 1.8 to 3.1 min in PS2.
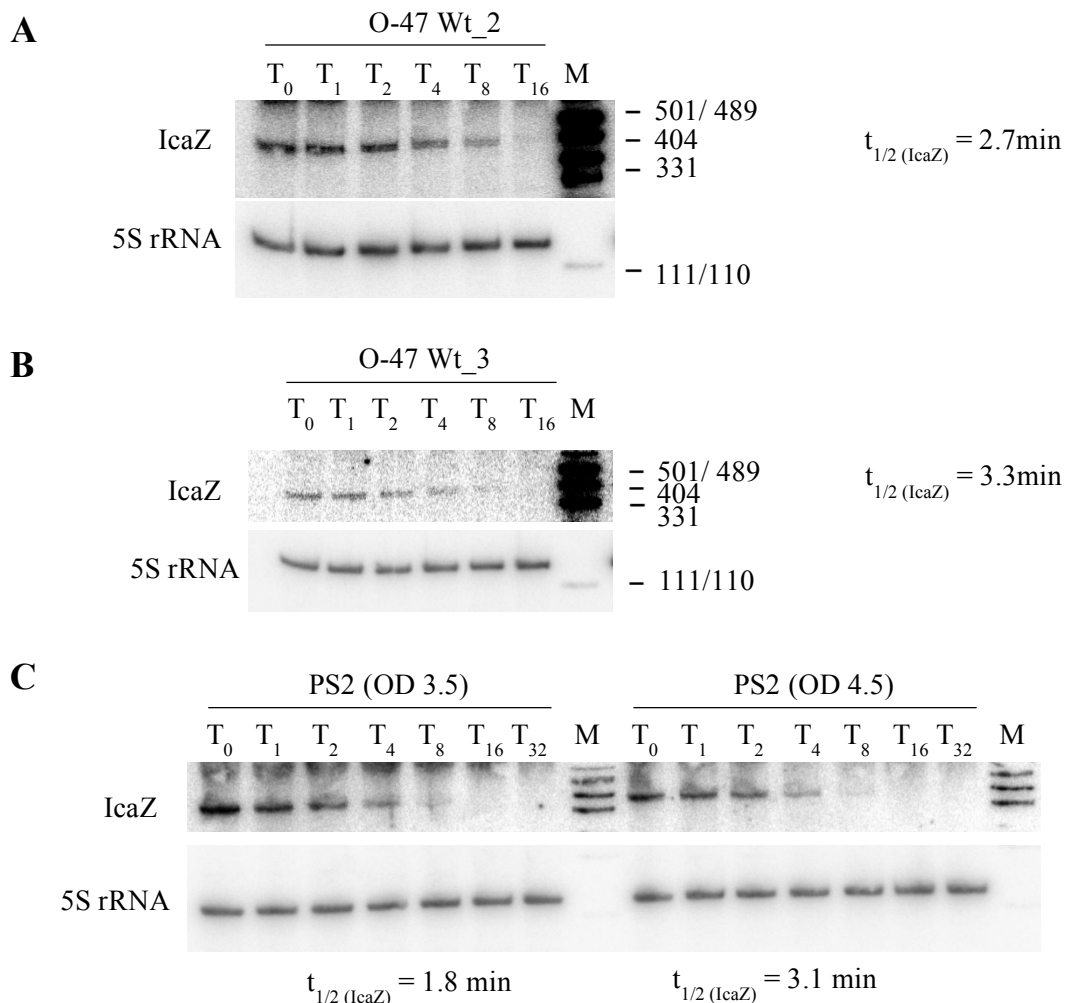
Fig. III-7: Stability of IcaZ by Northern blot analysis

(**A**) NB_IV: RNA at 30°C exp. phase, 6% PAA/ 7M urea, 300V/ 2h 30 min. (**B**) NB_VI: RNA at 30°C exp. phase, 6% PAA/ 7M urea, 300V/ 2h 10 min. (**C**) NB_CLA RNA at 37°C, 10% PAA/ 7M urea, 300V/ 1h 40 min; RNA was sampled by Dr Claudia Lange and Northern blot was carried out by Dr Sonja Schönfelder.

1.1.5   *Promoter activity of P$_{icaZ}$*

The genomic region upstream of *icaZ* was analysed for a promoter sequence by using the online available software BPROM. In addition, *icaZ* promoter activity was analysed *in vivo* and visualised by using the Cerulean reporter system. The promoter region of *icaZ* (P$_{icaZ,}$ 138 bp upstream of *icaZ* TSS1) was inserted upstream of the cerulean gene *cfp* in plasmid pCerulean (chapter II-8.4.4). The obtained plasmid, named pCerulean+icaZprom, was transferred by transformation into various strains and P$_{icaZ}$ activity was measured either by TECAN read out system or confocal laser scanning microscopy (CLSM) during *in vivo* biofilm formation. With both methods, the fluorescence of Cerulean fluorescent protein (CFP) was specifically detected. CFP was produced only when P$_{icaZ}$ was active and the *cfp* gene was transcribed and translated into CFP.

The online tool BPROM (http://www.softberry.com) predicts bacterial promoters and was used to predict σ^{70} dependent promoters within a given nucleotide sequence. The analysed nucleotide sequence comprised 140 nt upstream of the *S. epidermidis* O-47 *icaZ* TSS1. BPROM predicted one promoter sequence with a -10 box and a -35 box within this sequence. A second very similar promoter was predicted manually. Both promoters were located in an adequate position to the TSSs of *icaZ* (**Fig. III-4**).

The region was also analysed for the presence of a σ^{B}-dependent promoter, using the consensus sequence of *B. subtilis* and *S. aureus* (*i.e.* GTTTaa and GGG(A/T)A(A/T) for the -35 and -10 boxes, respectively) (Gertz *et al.*, 2000). Within the analysed nucleotide sequence, no σ^{B} recognition site was detectable.

For the measurement of *P$_{icaZ}$* activity, the cloned Cerulean reporter strain *S. epidermidis* O-47+pCerulean_icaZprom (strain collection code ML13) was inoculated into TSB medium (chapter II-4.5) and analysed by confocal laser scanning microscopy under flow conditions. Sections of the emerging biofilm were scanned hourly (**Fig. III-8 B**). **Fig. III-8 A** displays the records taken after seven, eight and nine hours of bacterial growth. The activity of P$_{icaZ}$ was visualised by detection of CFP fluorescence. Interestingly, the promoter was not active in each bacterial cell, suggesting that the *icaZ* gene is heterogeneously expressed. However, most cells which once had activated the *P$_{icaZ}$* promoter, kept the activity and displayed permanent *icaZ* expression throughout the CLSM recordings. These permanent IcaZ producers are marked with a white arrow in **Fig. III-8**.

A

B

top

bottom
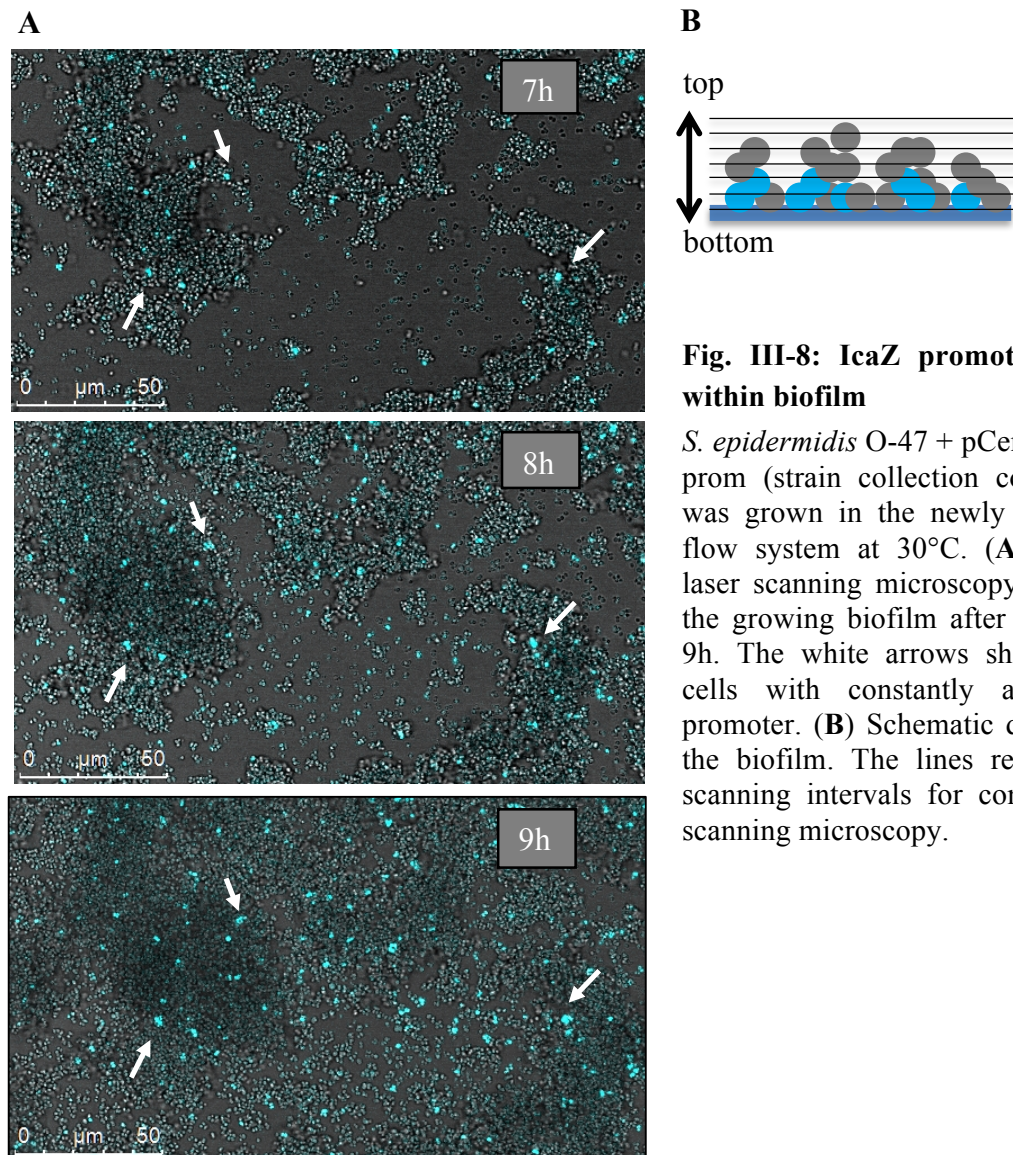
Fig. III-8: IcaZ promoter activity within biofilm

S. epidermidis O-47 + pCerulean_icaZ prom (strain collection code ML13) was grown in the newly established flow system at 30°C. (**A**) Confocal laser scanning microscopy images of the growing biofilm after 7h, 8h and 9h. The white arrows show biofilm cells with constantly active *icaZ* promoter. (**B**) Schematic depiction of the biofilm. The lines represent the scanning intervals for confocal laser scanning microscopy.

1.2 Putative ORFs within IcaZ regulatory RNA

The nucleotide sequence of *S. epidermidis* O-47 *icaZ* was analysed for the presence of possible protein-coding sequences by using the '*find open reading frame*' function of the *CLC Main Workbench* tool. When employing a '*minimum codon length of 12*' and '*all known start codons*' as settings, two short open reading frames of 60 (ORF1) and 99 (ORF2) nucleotides in length were identified. ORF1 had an ATT as start codon and comprised nucleotides 18 to 77 of the icaZ gene, while ORF2 exhibited ATA as a start codon and covered *icaZ* nucleotides 205 to 303. In *S. epidermidis* RP62A, ORF2 was considerably shorter (69 nt) due to the lack of cytosine_251, leading to a frame shift and a stop codon at position 271 (**Tab. III-1**). No significant similarity was found for the deduced amino acid sequence(s) of ORF2, when performing a BLAST search at NCBI using the non-redundant protein sequence data collection. The deduced amino acid sequence of ORF1 displayed

similarities to a number of hypothetical proteins of various organisms, including a putative *S. epidermidis* transposase (NCBI reference sequence ID WP_002504394.1) (see also below). Both ORFs are not preceded by reasonable ribosomal binding sites, making translation unlikely. In agreement with this assumption, experimental studies (performed under supervision of the author) using the addition of Strep-tags to the C-terminus of the peptides, did not reveal convincing evidence for translation of the ORFs into polypeptides (Müller, 2012). Therefore, the *icaZ* gene is suggested to harbour a transcript that is not translated into protein(s) and represents a non-coding RNA rather than a mRNA.

Tab. III-1: Positions and deduced amino acid (aa) sequences of putative open reading frames (ORFs) within *icaZ*

	Position on *icaZ* gene (# of nucleotides)	Nucleotide sequence (5' → 3')	Deduced aa sequence (# of aa residues)
ORF1 (O-47)	18-77 (60)	ATTTTGAAAACTTACTATAAACGCG AAATATTTATATTCTCATTCGTAAA ACATTGGTAA	ILKTYYKREIFIFS FVKHW (19)
ORF1 extended (O-47)	3-77 (75)	AGGTGCTTATTTTATATTTTGAAAA CTTACTATAAACGCGAAATATTTAT ATTCTCATTCGTAAAACATTGGTAA	RCLFYILKTYYK REIFIFSFVKHW (24)
ORF2 (O-47)	205-303 (99)	ATAATGAAGAAGAAATGTATCGTT GAAGTTCGATTAAATAAAAAAAGA GAGTGGAACCAAATTTCATTGAAT ATACTATTTTACTTTAATATTAGTT AA	IMKKKCIVEVRL NKKREWNQISLN ILFYFNIS (32)
ORF2 (RP62A)	205-273 (69)	ATAATGAAGAAGAAATGTATCGTT GAAGTTCGATTAAATAAAAAAAAG AGTGGAACCAAATTTCATTGA	IMKKKCIVEVRL NKKKSGTKFH (22)

Interestingly, when allowing *'any codons'* as translation starts in the CLC open reading frame finding tool, ORF1 was extended at the 5'-end, covering positions 3 to 77 of the *icaZ* gene (**Tab. III-1**). BLAST analysis of the deduced amino acid further supported the above-mentioned similarity to a putative transposase protein detected in a *S. epidermidis* isolate deposited in the NCBI database (sequence ID: EJE28549.1) (**Fig. III-9**).

Fig. III-9: BLAST result for querying the non-redundant protein sequence collection
The Standard Protein BLAST tool was used at NCBI with the deduced amino acid sequence of extended ORF1 (RCLFYILKTYYKREIFIFSFVKHW).

In database-deposited strain *S. epidermidis* NIH05001, the hypothetical protein EJE28549.1 is 132 amino acids in length and displays similarities to bacterial DDE transposases (EJE28549.1). The *IS Finder* data base (https://www-is.biotoul.fr), which contains exclusively sequence information on IS elements and transposons, was queried with this protein sequence. Except for the last 22 amino acid of protein EJE28549.1, a 99 % identity with the C-terminal portion of the transposase of IS*Sep1* was found, indicating that the N-terminus of protein EJE28549.1 is truncated in *S. epidermidis* NIH05001. The 22 amino acids at the C-terminus of EJE28549.1 did not match the IS*Sep1* transposase protein (**Fig. III-10**). However, these additional aa residues corresponded to the deduced amino acid sequence of ORF1 (22 of 25 aa identity) (**Fig. III-10**). IS*Sep1* is a member of the IS*1182* family of IS elements which is widespread among staphylococcal species. IS*Sep1* typically occurs in multiple copies in *S. epidermidis* genomes, many of which being incomplete (https://www-is.biotoul.fr), suggesting that this element serves as common cross over point for recombination and deletion events in the staphylococcal genome. As ORF1 neither matches the IS*Sep1* transposase nor any other known transposase protein, we consider the BLAST result as an accidental alignment to transposases which might reflect a (former) IS*Sep1* insertion in the vicinity of *icaZ* in strain *S. epidermidis* NIH05001.

```
> ISSep1_aa1  Family: IS1182 - Tnp Length=559   Score = 232 bits (592),  Expect
= 2e-74, Method: Compositional matrix adjust.  Identities = 112/113 (99%),
Positives = 112/113 (99%), Gaps = 0/113 (0%)


EJE28549.1 1     MKNYNWEYFKAQINKKLSEPKTKTIYSQRKIDVEPVFGFMKAILGFTRMSVRGIDKAKRE 60
alignment1       MKNYNWEYFKAQINKKLSEPKTKTIYSQRKIDVEPVFGFMKAILGFTRMSVRGIDKAKRE
tnp ISSep1 446   MKNYNWEYFKAQINKKLSEPKTKTIYSQRKIDVEPVFGFMKAILGFTRMSVRGIDKAKRE 505
Orf1             ...........................................................


EJE28549.1 61    LGFVLMALNIRKVTAQRAENNQKNNKKDNFYIISIEIVFFYLSWDFMSHTLFYILKTYYK 120
alignment1       LGFVLMALNIRKVTAQRAENNQKNNKKDNFYIISIEIVFFYLSWDFMSHTL-Y-------
tnp ISSep1 506   LGFVLMALNIRKVTAQRAENNQKNNKKDNFYIISIEIVFFYLSWDFMSHTLSYD...... 559
alignment2                                                          LFYILKTYYK
Orf1             ..........................................RCLFYILKTYYK 12


EJE28549.1 121   REIFIFSFVKHW 132
alignment1       ------------
tnp ISSep1       ............
alignment2       REIFIFSFVKHW
Orf1        13   REIFIFSFVKHW 25
```

Fig. III-10: BLAST research result with protein EJE28549.1

> IS finder platform (https://www-is.biotoul.fr) was used. Alignment1 between EJE28549.1 and the transposase (Tnp) of IS*Sep1* is shown in grey, alignment2 with the deduced aa sequence of ORF1 is highlighted in green.

Another short putative ORF in the close neighbourhood of the *icaZ* gene represents SERP2291 which is annotated as hypothetical protein in the *S. epidermidis* RP62A reference genome (108 nt, position 2.333.271 to 2.333.378). SERP2291 is located upstream of *icaZ* on the opposite (plus) strand and runs into the *icaR* 3'-UTR. The ORF is conserved in *S. epidermidis* O-47 and *S. epidermidis* PS2 and PS10 as well. RNA-seq analyses revealed low expression of SERP2291(50 reads in the untreated pulse-expression sample), but SERP2291 is not preceded by a *bona fide* ribosomal binding site, making the existence as a gene and coding region unlikely.

NCBI Glimmer version 3.02 predicted an ORF on the antisense strand to *icaZ* from nucleotides 271 to 89 (score 5.13). Pulse-expression data showed low amount of transcripts (~150 reads), but subsequent analysis of the translated region with NCBI *blastx 2.5.0* resulted in no identity to any known proteins; it is also not preceded by a *bona fide* ribosomal binding site. Thus, also this predicted ORF is supposed to be non-functional.

In conclusion, IcaZ seems not to harbour any active protein coding regions and therefore seems to be a non-coding RNA (ncRNA), instead of a dual-function RNA or mRNA.

1.3 *icaZ* nucleotide sequence conservation

IGR*ica*-RNA was predicted to be a conserved RNA in *ica*-positive *S. epidermidis*. In this work, the prediction was validated by screening the NCBI database for *icaZ* sequences and by direct sequencing of the *ica*-locus in various strains.

IcaZ sequence was blasted against the '*nucleotide collection*' of NCBI with optimisation '*discontiguous megablast*' by using NCBI *BLASTN 2.6.1+* programme to answer the question in which organisms IcaZ is conserved. The complete sequence was found only in *S. epidermidis* (isolate BPH0662 with 100% identity, strain 1457 and strain RP62A with 99% identity; **Annexe Tab. VIII-1**), but not in other staphylococci. A second blast, this time against '*whole-genome shotgun contigs*' database with limitation to the '*bacillus/staphylococcus* group (taxid: 1385)', was carried out to expand the analysis and include strains, whose genome is not fully assembled. Among the shotgun sequences, IcaZ was also found only in *S. epidermidis* strains. Overall, the database analysis results confirmed that ncRNA IcaZ is conserved among *ica*-locus positive *S. epidermidis* strains. Moreover, the analysis of IcaZ sequence in *S. epidermidis* strains with 99% identity revealed up to four single nucleotide polymorphisms within IcaZ sequence.

The direct sequencing of *icaZ* was carried out with isolates that had been sampled by nasal swabs from residents and staff members from a nursing home in Northern Ireland in 2008. Based on diploma thesis results of Dr Claudia Lange, who characterised these isolates molecularly for biofilm genes and phenotypically for biofilm formation, thirty *icaA*- and *icaC*-positive biofilm forming *S. epidermidis* strains were chosen. They were streaked out onto TSB agar plates and *icaZ* genomic region was amplified by colony PCR with primers IGRica1 and icaC_rev1. PCR products less than 5982 bp (product size in strain RP62A) were not analysed, because it was assumed that these strains didn't contain the whole *icaADBC* operon. In five strains, *icaZ* was detected with a sequence conservation of 96.39%. Within *icaZ* sequence, four single nucleotide polymorphisms were identified. Interestingly, these strains contained either the *icaZ* sequence of *S. epidermidis* O-47 (3 of 5 isolates) or RP62A (2 of 5 isolates), as most of the sequences from the database analysis. The different nucleotides are marked in **Fig. III-12**.

1.4 Secondary structure prediction and visualisation

The secondary structure of ncRNA IcaZ from *S. epidermidis* O-47 was predicted using the *Mfold* web server (http://unafold.rna.albany.edu/?q=mfold/RNA-Folding-Form2.3; Waugh *et al.*, 2002; Zuker, 2003; Zuker M, 1998). *icaZ* nucleotide sequence, starting from TSS 1, was folded by the programme *Mfold* (version 4.7) at 30°C (**Fig. III-12**) and 37°C (**Annexe Fig. VIII-3**).

The secondary structure exhibited a very long and therefore strong stem loop from nucleotides 4-146 (stem loop 1) and shorter stem loops from nucleotides 148-172 (stem loop 2), nucleotides 178-225 (stem loop 3), nucleotides 232-261 (stem loop 4), nucleotides 265-322 (stem loop 5), nucleotides 325-354 (stem loop 6) and nucleotides 359-400 (stem loop 7). Each stem loop contained 1-5 loops. These loops are single stranded and thus potential interaction sites with mRNAs, regulatory RNAs or proteins. Stem loop 1 comprised two more nucleotides at 37°C (nucleotides 2-147), whereas stem loops 2-7 were identical at both temperatures. So, the overall structure of folded IcaZ at 37°C was nearly the same as at 30°C. There were no differences in the folded form concerning the loops.

The single nucleotide polymorphisms, which were identified by *icaZ* nucleotide sequence conservation analysis, were minor variations within the sequence with no consequences for altering the overall structure.

RNA sequencing data analysis of *S. epidermidis* PS2/ PS10 and pulse expression data analysis of *S. epidermidis* O-47 (chapter III-1.1.3) uncovered the accumulation of transcript reads at the middle of *icaZ* starting from nucleotide 147, marked by an asterisk (**Fig. III-11**; **Fig. III-12**). It was therefore supposed that stems 2-4 were more stable than the residual parts of IcaZ and were supposed to interact with binding partners.
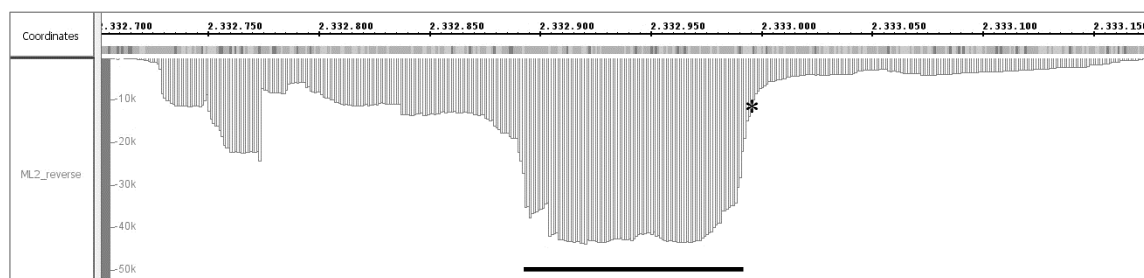
Fig. III-11: Transcript reads of IcaZ after pulse expression

    Transcript reads of strain *S. epidermidis* O-47Δ*tRNA*^{Thr-4}Δ*icaZ*Δ*icaR*-3' UTR carrying the plasmid pCG248_*icaZ*/tRNA (strain collection code JE13) were mapped to *S. epidermidis* RP62A genome reference sequence. Depicted are the transcript reads of IcaZ full nucleotide sequence at the reverse strand. The black line marks accumulated transcripts in the middle of the sequence, starting from nucleotide 147 (marked with an asterisk). The nucleotide sequence of stems 2-4 is enclosed by these transcripts.
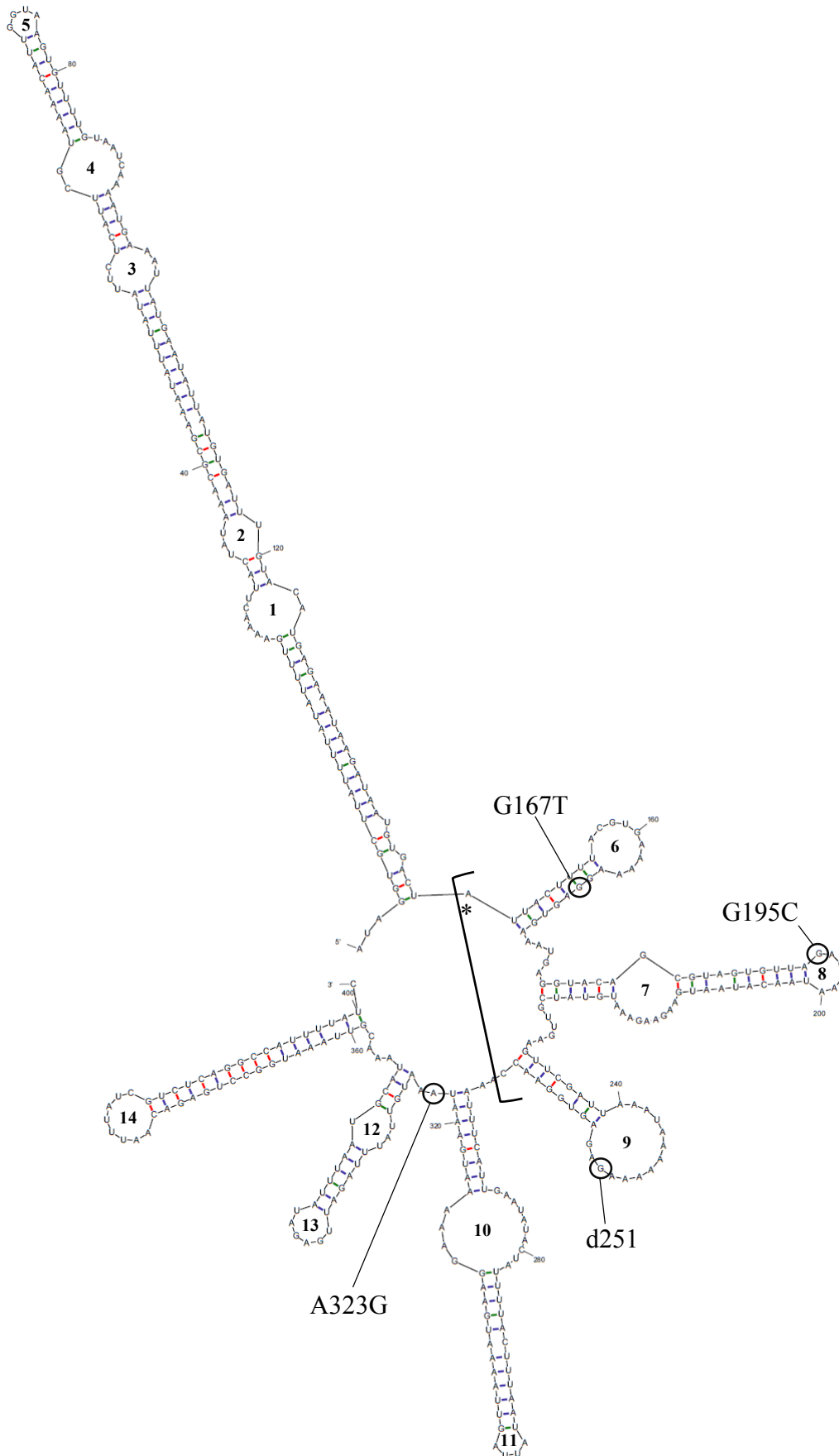
Fig. III-12: Secondary structure of IcaZ at 30°C (predicted by *Mfold*)

Fig. III-12: Secondary structure of IcaZ at 30°C (predicted by *Mfold*)

The figure depicts the secondary structure of IcaZ with the highest free energy value (dG = -98.52), predicted by *Mfold* version 4.7, at 30°C. The marked ribonucleotides are different between IcaZ of *S. epidermidis* RP62A and O-47. These nucleotides were mutated in terms of functional analysis (chapter II-5.5.3 and 8.4.2). The 14 loops of IcaZ secondary structure are numbered consecutively.

2.   IcaZ ncRNA locus in staphylococci and its genomic vicinity

Based on the results provided in the previous section, the annotation of *icaZ* in the vicinity of the *ica*-operon was revised and refined. To get a first insight into the potential function of this ncRNA, an in-depth inspection of the genetic surrounding of the *icaZ* gene was undertaken. As these analyses were crucial for further experimental planning, the results are provided in detail below.

2.1   The adjacent genes *icaR* and *tRNA^{Thr-4}*

2.1.1   *icaR mRNA*

The *icaR* gene, encoding the *ica*-operon repressor IcaR, is located immediately upstream of *icaZ* on the same strand (**Fig. III-4**). The transcript length of *icaR* in *S. epidermidis* came into the focus of this work, when Ruiz de los Mozos *et al.* published that around one-third of the mapped mRNAs in *S. aureus* carry 3′ UTRs longer than 100 nt and that these might have potential regulatory functions (Ruiz de los Mozos *et al.*, 2013). The length of *icaR* was determined or at least predicted in some cases by the authors to be 390 nt in *S. aureus*, 365 nt in *S. epidermidis* RP62A, 482 nt in *S. simiae*, 369 nt in *S. caprae* and 380 nt in *S. capitis*. The deleted regions surrounding IGR*ica*-RNA in mutants, already existing in our group (previously generated by Dr Eckart and F. Herbst; chapter IV-1.1) comprised 71 nt upstream of *icaZ* (calculated from TSS1), suggesting accidental deletion of the most distal part of the putative 3′ UTR of *icaR*, in case such a structure would indeed exist in the *S. epidermidis* strains analysed in this work. The length of *icaR* mRNA was therefore determined experimentally by cRACE in *S. epidermidis* strain O-47, RP62A and in strain O-47Δ*tRNA^{Thr-4}*Δ*icaZ*Δ*icaR*-3′ UTR at 30°C and 37°C, respectively. The experimental procedure is described in chapter II-6.8. cRACE data from wildtypes showed that *icaR* 5′ UTR comprised 74 nt. Pulse-expression data of strain *S. epidermidis* O-47Δ*tRNA^{Thr-4}* Δ*icaZ*Δ*icaR*-3′ UTR carrying pCG248_*icaZ*/tRNA (strain collection code JE13) confirmed the cRACE results for *icaR* 5′ UTR. The pulse-expression data also revealed a long 3′ UTR for *icaR* mRNA, because unlike in other genes (*e.g. geh-1*, SERP2289), an accumulation of transcripts downstream of *icaR* ORF, indicating the transcription terminator, was missing. cRACE experiments of this work confirmed the predicted 365 nt long *icaR* 3′ UTR for *S. epidermidis* RP62A. The ORF of *icaR* in *S. epidermidis* O-47 turned out to be three amino acids shorter (**Fig. III-13** upper zoom-in), than *icaR* ORF of strain RP62A, so that O-47 *icaR* 3′ UTR comprised 374 nt (without stop codon). In both strains, these long *icaR* 3′ UTRs overlap with the 5′-portion of *icaZ* for a maximum of 15 nt (**Fig. III-13** lower zoom-in). The length of *icaR* ORF was also checked by PCR and subsequent DNA sequencing in *S epidermidis* strains 567, 567-1, PS2, PS10 and 307. All strains contained a

longer *icaR* ORF like RP62A, and differed from strain O-47 by three amino acids at the C-terminus (one leucine and two lysine).

Fig. III-13: The length of the adjacent gene *icaR* and *icaR* mRNA in *S. epidermidis*

The figure shows the genomic localisation of tRNA^{Thr-4}, icaZ and icaR and the length of icaZ and icaR mRNA transcripts in S. epidermidis O-47. Circularised RACE was carried out to determine the 5′ and 3′ ends of icaZ transcripts (chapter III-1.1.2) and icaR mRNA transcripts (chapter III-2.1.1). The cRACE results of O-47 and RP62A are depicted schematically. icaR 5′ UTR comprised 74 nt in all sequenced clones. Most of the transcripts exhibited a length of 360-365 nt in strain RP62A and shorter transcripts were detected only to a very minor proportion. It came out, that the length of icaR 3′ UTR was different between O-47 and RP62A and because of that further strains were analysed in this region. The zoom-in on DNA level depicts the different lengths of icaR ORF 3′ end between S. epidermidis strains O-47, RP62A, 307, 567 and the isolates PS2 and PS10. In S. epidermidis O-47, the codon TTA for leucine is changed to stop codon TAA, which results in abortion of translation of icaR and thus in the lack of one leucine and two lysine amino acids at IcaR C-terminal end. Based on the cRACE results, it is known that S. epidermidis harbours very long icaR 3′ UTRs that overlap with the 5′-portion of icaZ for 15 nt and 32 nt, respectively. Black arrow heads indicate the two prominent TSS of icaZ determined by cRACE.

2.1.2 tRNA^{Thr-4}

tRNA^{Thr-4} is located downstream of *icaZ* on the opposite DNA strand. The nucleotide sequence comprises 93 nt, which is unusual compared to tRNA^{Thr1-3}, that comprise only 76 nt. The existence of this annotated tRNA (position 2.332.647 to 2.332.739 in

S. epidermidis RP62A) was analysed among bacteria by using the programme *BLASTN 2.5.1+* from the National Center for Biotechnology Information (NCBI; U.S. National Library of Medicine). For that, the tRNA nucleotide sequence was blasted against NCBI nucleotide collection. Sequence alignments showed that tRNA^{Thr-4} was specific for CoNS, like IcaZ, but did not exclusively exist in *S. epidermidis* genomes. With lower identity but full coverage, it was also detected in *S. capitis* (96%), *S. pasteuri* and *S. warneri* (92%), *S. haemolyticus* (89%), *S. simulans* (82%), *S. sciuri* (coverage 96%; identity 88%) and *S. capitis* (coverage 98%; identity 81%). Among *S. epidermidis,* the *ica*-positive strain RP62A as well as the *ica*-negative strain ATCC 12228 encode *tRNA^{Thr-4}* (**Annexe Tab. VIII-2**). Accordingly, the presence of the *icaADBC*-operon is not a prerequisite for the presence of *tRNA^{Thr-4}*.

From other three threonyl-tRNAs within the *S. epidermidis* RP62A genome, *tRNA^{Thr-1}* and *tRNA^{Thr-2}* are identical to each other and differ from *tRNA^{Thr-3}* in only one nucleotide. In contrast, *tRNA^{Thr-4}* exists as a single copy, distantly located from *tRNA^{Thr1-3}* in the genome. The *bona fide* tRNAs $^{Thr1-3}$ have in common that they are located in tRNA clusters (analysis of genome sequences by *CLC Main Workbench*), which is a usual feature known from *S. aureus* genomes (Green and Vold, 1993). In contrast, *tRNA^{Thr-4}* is found as a single tRNA gene in an intergenic region upstream of the *icaADBC*-operon. The expression of *tRNA^{Thr-4}* in *S. epidermidis* PS2 (~ 110 reads) is comparable to the expression of *tRNA^{Thr2-3}* (~ 130 reads and ~ 110 reads, respectively); *tRNA^{Thr-1}* was more expressed (~ 230 reads). The function of this putative threonyl-tRNA is questionable, because of the unusual length and the similarity to serin-tRNAs. By aligning threonyl-tRNAs and serin-tRNAs of *S. epidermidis* RP62A, it was noticed that *tRNA^{Thr-4}* was more similar to *tRNA^{Ser1-5}* than to *tRNA^{Thr1-3}* (**Fig. III-14**).
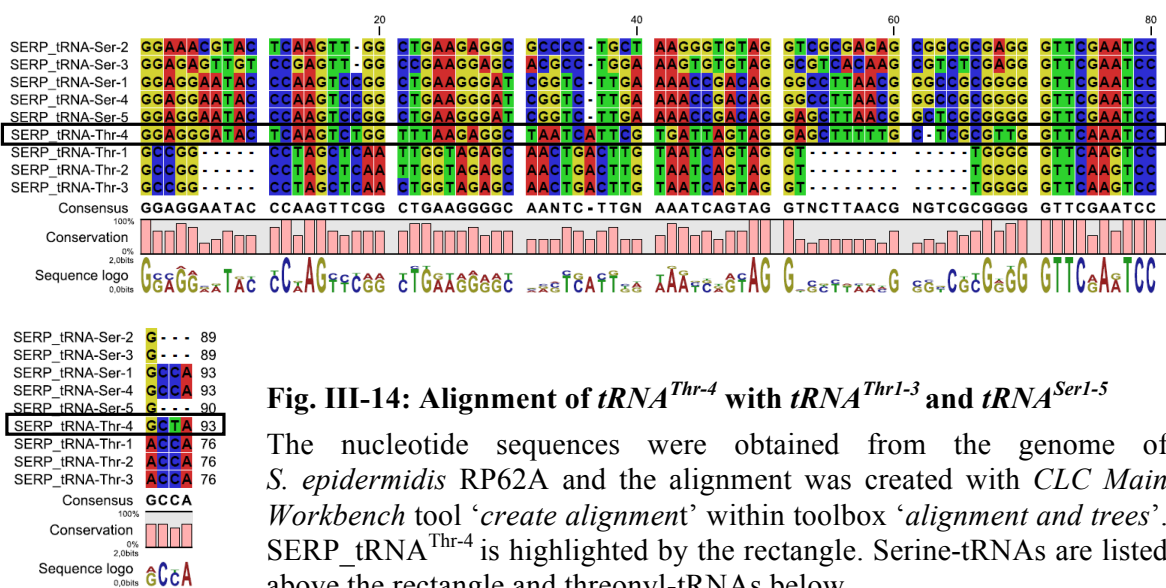
Fig. III-14: Alignment of *tRNA^{Thr-4}* with *tRNA^{Thr1-3}* and *tRNA^{Ser1-5}*
The nucleotide sequences were obtained from the genome of *S. epidermidis* RP62A and the alignment was created with *CLC Main Workbench* tool '*create alignment*' within toolbox '*alignment and trees*'. SERP_tRNA^{Thr-4} is highlighted by the rectangle. Serine-tRNAs are listed above the rectangle and threonyl-tRNAs below.

To decide wether or not tRNA^Thr-4 is a *bona fide* threonyl-tRNA, the nucleotide sequence was analysed and the secondary structure was assembled manually according to the standard tRNA structure form (**Fig. III-15**). Referring to the standard genetic code, the codons ACU, ACC, ACA and ACG (compressed 'ACN') code for the amino acid threonine. Threonyl-tRNAs contain the anticodon AGU, GGU, UGU or CGU. The prognosticated tRNA^Thr-4 contains two of the possible anticodons (CGU and AGU), whereby the codon CGU seems to be more likely than the codon AGU, because of its position within the anticodon stem loop (**Fig. III-15**). The absolute essential cytosine-cytosine-adenine ribonucleotides at the 3′ end (3′ CCA) of the acceptor stem are changed to 3′ CUA, so that it is assumed that further processing of the 3′ end is needed for tRNA^Thr-4 to become fully functional as a tRNA. But, the manually folded stem loops 2-4 seem to be strongly enforced, because of the few base pairings within the stems, compared to the *bona fide* tRNAs, making this structure highly unlikely.
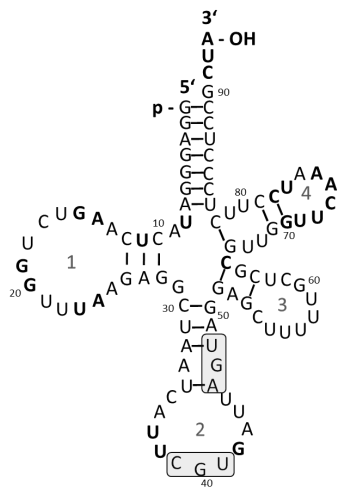
Fig. III-15: Manually folding of tRNA^Thr-4

Depicted is tRNA^Thr-4 with numbered loops: (1) D-loop, (2) anticodon stem loop with highlighted anticodons (rectangle), (3) variable loop and (4) TψC-loop. Conserved ribonucleotides among tRNAs and the 3′ end (3′ CUA) are highlighted in bold.

In addition to the manual folding, the structure of tRNA^Thr-4 was also predicted by *Mfold* RNA folding form at 37°C and RNA folding form (version 2.3) at 37°C and 30°C. tRNA^Thr-1 was used as *bona fide* control. The structure of tRNA^Thr-1 was identical at both temperatures and with both programmes (**Fig. III-16 A-C**). The structure of tRNA^Thr-4 was slightly different at both temperatures and between the two RNA folding programmes at 37°C, but differed greatly from the *bona fide* structure of tRNA^Thr-1 (**Fig. III-16 D-F**). Both anticodons of tRNA^Thr-4 were not or only partly within a loop structure (**Fig. III-16**). In tRNA^Thr-1 the anticodon was freely accessible and an interaction with the mRNA codon was possible. Conclusively, tRNA^Thr-4 didn't fold like *bona fide* tRNAs, *e.g.* tRNA^Thr-1.
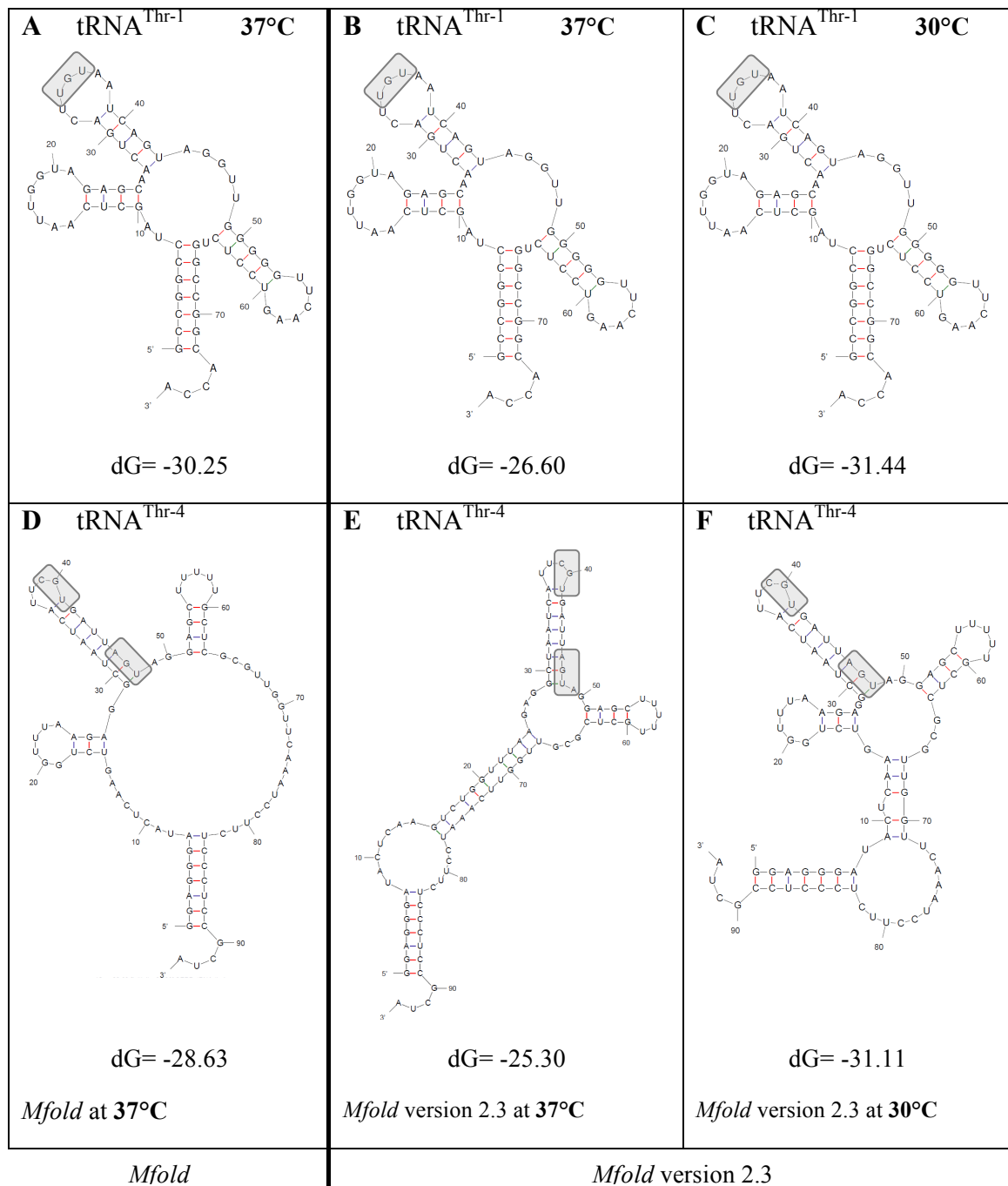
Fig. III-16: Folding of annotated tRNA^{Thr-1} (A-C) and tRNA^{Thr-4} (D-F) of *S. epidermidis* RP62A by *Mfold* RNA folding algorithms

Secondary structure of tRNA^{Thr-1} (**A**) and tRNA^{Thr-4} (**D**) folded with *MFold* RNA folding form at 37°C. RNA folding form (version 2.3) was used to fold the tRNAs at both temperatures: at 37°C for tRNA^{Thr-1} (**B**) and tRNA^{Thr-4} (**E**) and at 30°C for tRNA^{Thr-1} (**C**) and tRNA^{Thr-4} (**F**). Depicted is always the folding result with the highest free energy (Gibbs energy).

Due to the unusual structure, it was speculated that tRNA^{Thr-4} is not a functional tRNA, but rather a regulatory RNA element. The role of tRNAs as RNA sponges was recently identified (Lalaouna *et al.*, 2015b; Ziebuhr and Vogel, 2015) and because both transcripts, tRNA^{Thr-4} and *icaZ*, share a transcription terminator sequence (**Fig. III-17**), the concept of tRNA^{Thr-4} as RNA sponge for IcaZ was addressed.

Does tRNA^{Thr-4} work as a sponge for ncRNA IcaZ or at least has an influence on *icaZ* expression? Both transcripts were analysed in *S. epidermidis* O-47 Wt at 30°C by rifampicin assays, and Northern blots were hybridised with radioactively labelled oligonucleotide probes for the detection of tRNA-ORF and tRNA-3′UTR (**Fig. III-17**).
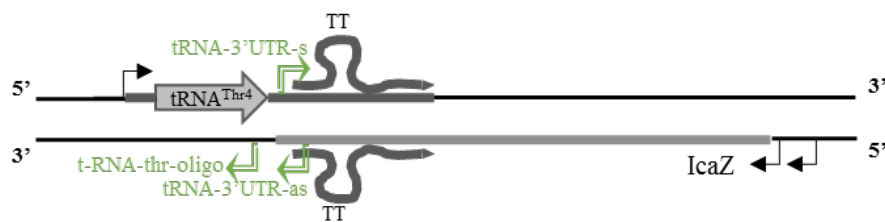
Fig. III-17: Primer binding sites of hybridisation probes for detection of tRNA^{Thr-4}

> Depicted is the genomic localisation of *tRNA^{Thr-4}* in *S. epidermidis ica*-positive strains and the binding sites for the *S. epidermidis* specific, radioactively labelled oligonucleotide probes. The primers used for labelling were: tRNA-thr-oligo, tRNA-3'UTR-as, tRNA-3'UTR-s (green arrows). The transcription terminator loop on both strands is depicted as TT. Bold lines upstream and downstream of *tRNA^{Thr-4}* ORF, which is depicted as grey arrow, symbolize 5′ and 3′ UTRs. Thin arrows indicate promoter regions of *tRNA^{Thr-4}* and *icaZ*.

A signal for the mature tRNA^{Thr-4} was detected with probe tRNA-thr-oligo right below the 110 nt marker band, which was in line with the *tRNA^{Thr-4}* gene length of 93 nt. This excludes any further processing of tRNA^{Thr-4} to the length of *bona fide* tRNAs, *i.e.* tRNA^{Thr-1}. The premature (unprocessed) tRNA^{Thr-4}, still carrying its 3′ UTR, was detected with tRNA-3'UTR-as probe above and below the 147 nt marker band (**Fig. III-18**). The 5′ UTR of tRNA^{Thr-4} comprises 14 nt (TSS at position 2.332.633 in *S. epidermidis* RP62A genome) according to the pulse expression data of *S. epidermidis* O-47Δ*tRNA^{Thr-4}* Δ*icaZ*Δ*icaR*-3′ UTR carrying plasmid pCG248_*icaZ*/tRNA. Together with the ORF and transcription terminator a full length of 167 nt was calculated for the premature tRNA^{Thr-4}.
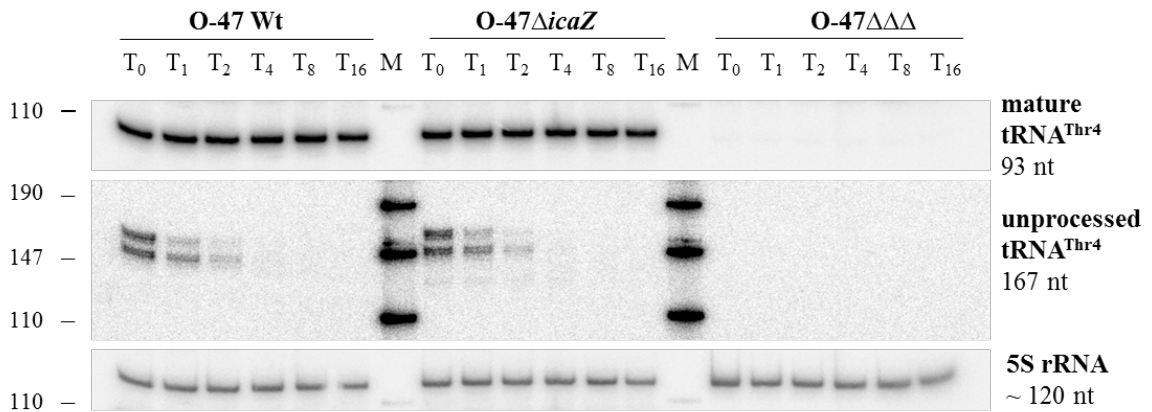
Fig. III-18: Rifampicin Northern blot analysis of several strains for tRNA^{Thr-4}

Total RNA of *S. epidermidis* O-47 Wt, O-47Δ*tRNA^{Thr-4}*Δ*icaZ*Δ*icaR*-3′ UTR (O-47ΔΔΔ; strain collection code FL1Δ2) and O-47Δ*icaZ* (strain collection code ML38) was sampled at 30°C by rifampicin assay. T_0 = uninduced sample at OD$_{600}$ ~ 1-2; T_1-T_{16} = time in min after addition of rifampicin; M = radioactively labelled pUC Mix marker 8. Samples were loaded onto 6% PAA/7M urea gel and electrophoresis was done at 300V for 2h 10 min. Bands were detected by hybridisation of the nylon membrane with radioactively labelled oligonucleotide probes (chapter II-6.5.4). 5S rRNA was used as loading control.

The measured half-live of tRNA^{Thr-4} was >16 min in all analysed strains, which was in agreement with the known half-lives of tRNAs in general. The larger band, indicating the premature tRNA is rapidly degraded during the maturation process. In another Northern blot containing total RNA of O-47 Wt and both *icaZ* mutants with 6% PAA/7M urea, an additional band with a size of < 34 nt was detectable (**Annexe Fig. VIII-7**). This band might represent the segregated tRNA 3′ UTR.

There was no change of half-live in *S. epidermidis* O-47Δ*rnc* (**Fig. V-9**), representing a RNase III deletion mutant. Conclusively, RNase III is not involved in the degradation process. Also, the lack of IcaZ did not have an impact on tRNA^{Thr-4} stability, as demonstrated in strain *S. epidermidis* O-47Δ*icaZ* (strain collection code ML38). No tRNA signal was detected in *S. epidermidis* O-47Δ*tRNA^{Thr-4}*Δ*icaZ*Δ*icaR*-3′ UTR (O-47ΔΔΔ, strain collection code FL1Δ2) due to the deleted *tRNA^{Thr-4}* (**Fig. III-18**).

So far, it is not known, if tRNA^{Thr-4} functions as a regular tRNA or as a regulatory element. But based on the unusual length of 93 nt, the uncharacteristic secondary structure prediction and the stand-alone position in the genome, a function as *bona fide* tRNA seems rather unlikely.

2.2 Summary of the revised *icaZ* locus and its surrounding genes

The previous sections showed that the genes surrounding *icaZ* gene overlap genetically with *icaZ*. **Fig. III-19** shows the *icaZ* gene in context with *tRNA^{Thr-4}* gene and *icaR* gene.
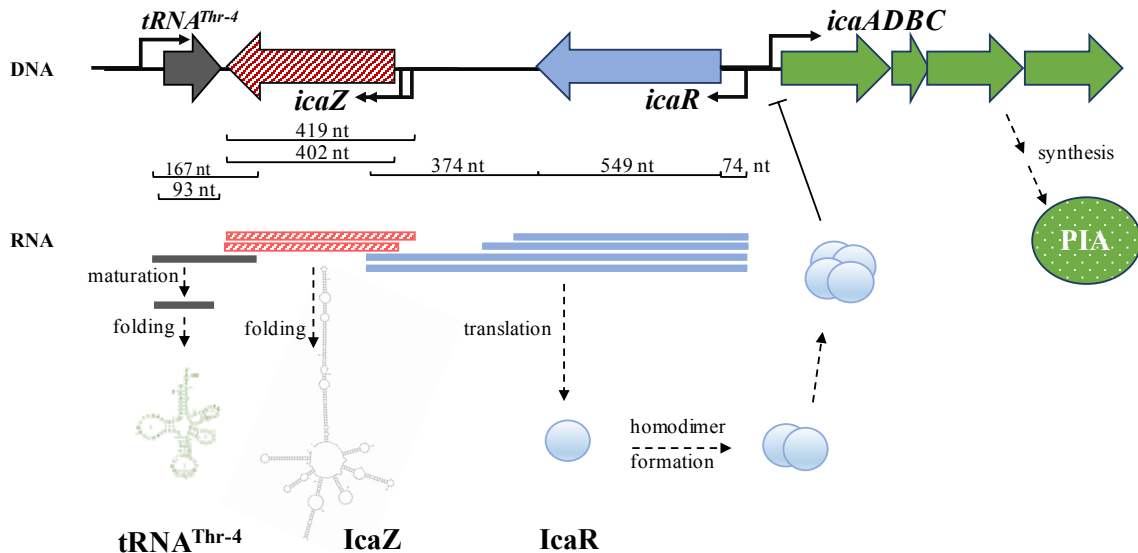
Fig. III-19: *icaZ* locus and genomic vicinity in *ica*-positive *S. epidermidis*

Illustrated is the genomic vicinity of *icaZ* gene in *S. epidermidis* O-47 with transcripts and the determined lengths. This emphasizes the overlap of *icaR* and *icaZ* transcript (blue and red bars) on the one hand and the overlap of the premature tRNA^{Thr-4} and the converging IcaZ (grey and red bars) on the other hand.

2.3 Sequence alignments of *icaZ* vicinity revealed differences between *S. epidermidis* strains

Although the genes are conserved among *ica*-positive *S. epidermidis* strains, single nucleotide polymorphisms exist between different strains. An alignment of the genomic region showed that *icaZ* sequence of strain O-47 differed in four nucleotides from the sequence of RP62A (chapter III-1.3), depicted in **Fig. III-12**. By comparing *icaR*, the *icaADBC*-operon and the DNA sequence upstream of $tRNA^{Thr-4}$, it was noticed that several nucleotides were exchanged or lost (**Fig. III-20**). Four nucleotide changes within *icaR* ORF resulted in two quiet mutations at amino acids D19 and D68 and two amino acid exchanges (N136D and V163I).

icaR 3′ UTR contains three additional SNPs. A huge number of SNPs occurred in *icaA*. However, from biofilm assays of O-47 it is known that PIA, the product of the *ica* proteins, is produced. Conclusively, the mutations and thus the amino acid exchanges are unlikely to have a huge impact on protein functionality.
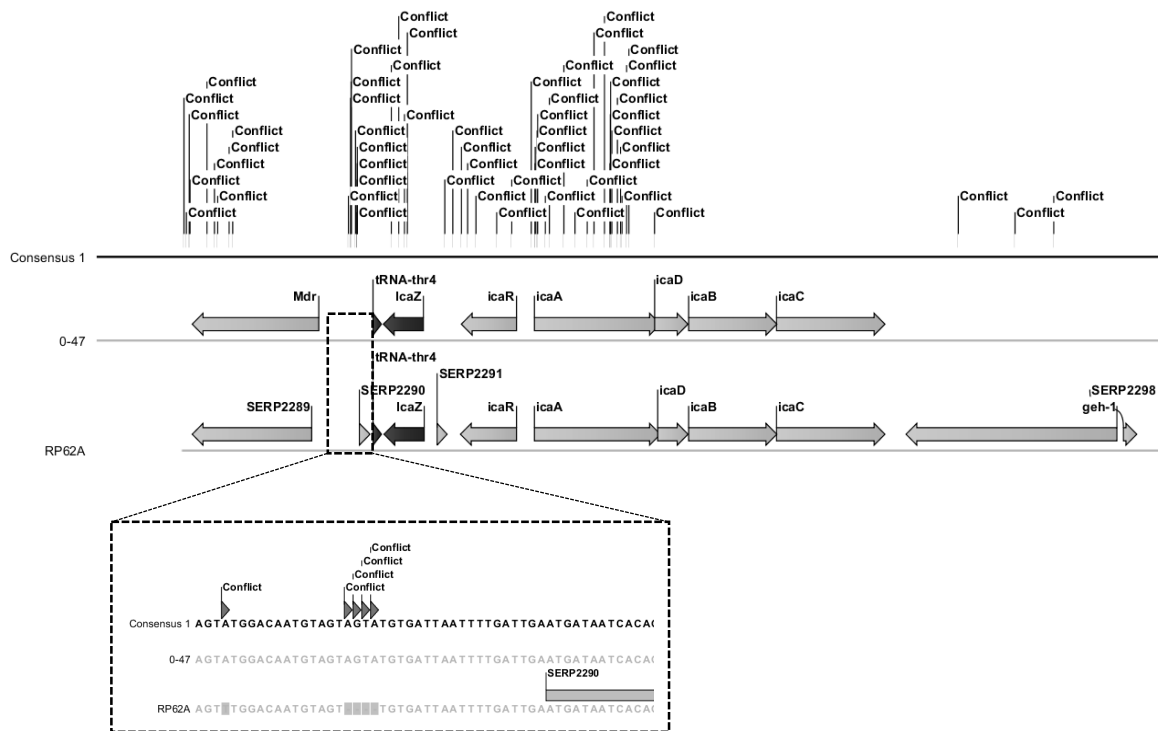
Fig. III-20: Comparison of nucleotide sequences of *icaZ* vicinity between *S. epidermidis* O-47 and RP62A

> The nucleotide sequence of *icaZ* genomic vicinity was compared between two *S. epidermidis* strains, O-47 and RP62A. Conflicts are flagged. The dashed rectangle shows a deletion of 4 nucleotides consecutively upstream of SERP2290 in the genome of RP62A.

Upstream of SERP2290, four nucleotides are deleted in *S. epidermidis* RP62A (**Fig. III-20**). The TSS of SERP2290 is 8 nt upstream of the deleted region, as pulse-expression

data of strain ML13 revealed. Therefore, the 5′ UTR is shortened in RP62A (23 nt, instead of 27 nt in O-47 5′ UTR). But, this putative gene is only weakly transcribed (approx. 60 reads in *icaZ* pulse-expression data).

The nucleotide sequence of SERP2291 is nearly identical, as only amino acid 25 is changed from asparagine to histidine. RNA-seq data showed 320 reads before and 500 reads after *icaZ* pulse expression.

2.4 *S. aureus ica*-operon vicinity lacks *icaZ*

The genomic location of *icaADBC* and *icaR* in *S. aureus* is different to the genomic location in *S. epidermidis*. In *S. aureus*, the *ica* locus is surrounded by *cap* genes and a lipase. The intergenic region between *icaR* and *capC* does not harbour an ORF, according to the published genome of *S. aureus* Newman and others (**Fig. III-21**).
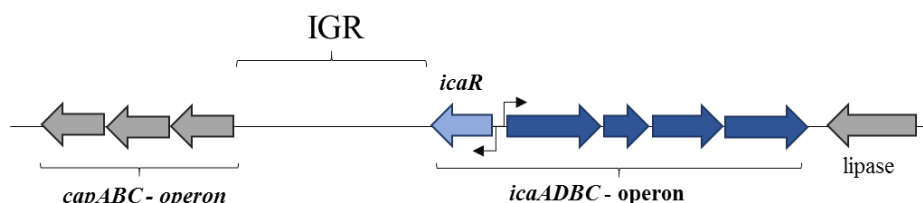
Fig. III-21: Genomic vicinity of *icaADBC*-operon in *S. aureus*

> Schematic overview of the localisation of the *icaADBC*-operon within the genome of *S. aureus*. The intergenic region lacks the *icaZ* nucleotide sequence.

In this work, *S. aureus* Newman was experimentally tested by Northern blot for a transcript originating from the intergenic region. A previously hybridised Northern blot separating total RNA of strains *S. aureus* Newman Wt+pCG248_icaZ/tRNA (strain collection code MF62) and *S. aureus* Newman ΔRNase III+pCG248_icaZ/tRNA (strain collection code MF63) that were generated in this work, was hybridised with a radioactively labelled ds-DNA probe specific for the detection of an IGR transcript.

No transcript could be detected, so that it is assumed that the intergenic region between *capABC* and *icaADBC* of *S. aureus* does not contain any additional transcripts.

3. Summary of Results for Part A

- The new RNA (IcaZ), characterised in this work, is a long non-coding RNA that does not harbour any intact protein coding sequences and, thus, is unlikely to exhibit dual-function.

- IcaZ is specific for *ica*-positive CoNS and is part of the core genome. Neither IcaZ nor any other transcript is encoded in the corresponding IGR*ica* of *S. aureus* (**Fig. III-21**).

- The RNA is genomically located in the vicinity of the *icaADBC*-operon. *icaZ* nucleotide sequence partly overlaps with *icaR* 3′ UTR, but does not overlap with *tRNA^{Thr-4}* antisense sequence (**Fig. III-4**). The orientation was confirmed by cRACE.

- The expression of *icaZ* was verified in *S. epidermidis* O-47, RP62A and in the patient isolates PS2 and PS10 (**Fig. III-1; Fig. III-2; Fig. III-7**). The expression level was strain dependent, but independent of shaking or static conditions (**Fig. III-3**). IcaZ is naturally expressed in early and mid-exponential growth phase at 30°C and 37°C, but with increased expression at 30°C (**Fig. III-1**).

- Transcript length was determined by Northern blot (~400 nt) (**Fig. III-1**) and cRACE. cRACE results from two independent Wt strains (RP62A, O-47) narrowed the transcript size for IcaZ to 401-419 nt. GMOs with *icaZ* overexpression plasmid verified the results.

- Two putative promoters were identified computationally and manually (**Fig. III-4**).

- The *icaZ* promoter activity was confirmed with CFP reporter system (**chapter III-1.1.5**) *in vivo*, measured with Tecan and CLSM (**Fig. III-8**). The promoter is heterogeneously expressed under biofilm forming conditions in a flow system.

- Two TSS for *icaZ* were identified by cRACE (both in RP62A and O-47) at 30°C and 37°C. They were confirmed by RNA-seq analysis of patient isolates PS2 and PS10 at 37°C (**Fig. III-5**).

- A transcription termination signal was predicted bioinformatically that supports the determined length of IcaZ (**Fig. III-4; Fig. III-17**). The terminator structure is assumed to be weak, because longer transcripts (but only in minor proportion) were detected in Northern blots when *icaZ* was overexpressed *in trans* by pulse expression.

- TEX treatment of total RNA from strain PS2 confirmed IcaZ as primary transcript (**Fig. III-5; Fig. III-6**). CFP reporter plasmid confirmed IcaZ as independent transcript (**Fig. III-8**). The transcript is not *icaR* 3′ UTR-derived.

- Transcript stability was determined by rifampicin stability assays and subsequent Northern blotting: $t_{1/2 \text{ IcaZ O-47}}$ = 2.7-3.3 min; $t_{1/2 \text{ IcaZ PS2}}$ = 1.8-3.1 min (**Fig. III-7**).

- *icaZ* nucleotide sequence is conserved among *ica*-positive *S. epidermidis*. Different strains contain a maximum of four single nucleotide polymorphisms within IcaZ sequence.

- The secondary structure of IcaZ was predicted biocomputational. IcaZ exhibits a long stem structure and several loops that might interact with mRNAs, regulatory RNAs or proteins (**Fig. III-12**). Pulse expression analysis revealed an increased number of transcripts containing stem loops 2-4 (**Fig. III-11**).

- The length of *icaR* mRNA UTRs was determined in *S. epidermidis* by cRACE: 74 nt 5′ UTR and 365 nt *icaR* 3′ UTR for RP62A or 374 nt *icaR* 3′ UTR for O-47 due to the loss of three amino acids within *icaR* ORF (**Fig. III-13**). The data were confirmed by pulse expression.

- The putative threonyl-tRNA (tRNA^{Thr-4}) exhibits an unusual secondary structure, distinct from *bona fide* tRNAs. It is not clustered like other tRNAs, but is located as a single gene next to *icaZ* gene. RNA sequencing revealed that tRNA^{Thr-4} is transcribed with a mature length of 93 nt. The tRNA^{Thr-4} transcript was detected right below the 110 nt marker band in Northern blots, whereas shorter bands were not detected, therefore further processing of the transcript is unlikely. The putative tRNA is specific for CoNS and highly conserved in *S. epidermidis*.

IV. Results – Part B 'Functional analysis of IcaZ by classical methods and global approaches'

1. Analysis and generation of *S. epidermidis* IcaZ mutants

For the functional characterisation of IcaZ, a number of deletion mutants had been generated previously to this work. In the light of the new findings concerning the transcript lengths of *icaZ* and its neighbouring genes, the mutants were characterised with respect to transcription of these genes prior to use of these constructs in functional tests.

1.1 Characterisation of genomic *icaZ* deletions in pre-existing mutants

S. epidermidis O-47Δ*tRNA*$^{Thr-4}$Δ*icaZ*Δ*icaR*-3′ UTR (O-47ΔΔΔ; strain collection code FL1Δ2) was generated by F. Herbst. The deletion in this mutant comprised the regions between primers lf2 and rf1 and comprised the whole IGR*ica*-RNA plus 63 nt upstream (71 nt upstream of *icaZ*) and 14 nt downstream (92 nt downstream of *icaZ*), thereby removing almost the entire *tRNA*$^{Thr-4}$ gene except for the first three amino acids and the promoter (**Fig. IV-3**). Of note, due to the cloning strategy, the *icaR* gene harbours a frame shift mutation at the 3′ end of the ORF resulting in an extension of the reading frame by the three additional codons and hence the addition of one leucine and two lysine residues at the C-terminus of the polypeptide. This frame shift mutation occurs naturally in a number of *S. epidermidis* strains such as RP62A and 307 (see **Fig. III-13**).

To check that the deletion of the ncRNA has no negative effect on the neighbouring *icaR* gene, *icaR* mRNA expression was analysed by Northern blots and rifampicin assays (**Fig. IV-1**). These experiments revealed a shorter *icaR* transcript in O-47ΔΔΔ mutant (lower arrow) compared to O-47 Wt (upper arrow), but with an increased initial *icaR* mRNA transcription. Rifampicin assays further indicated that *icaR* mRNA of the mutant was more instable than the *icaR* mRNA of O-47 Wt or RP62A. The abundance of the shortened *icaR* mRNA in O-47ΔΔΔ can be explained by the truncation of the *icaR* 3′ UTR, and the existence and nature of these transcripts was again confirmed by cRACE experiments (data not shown). The detected instability of the *icaR* transcript is likely to be associated with the loss of a termination signal present at the 3′ end of the *icaR* transcript, rendering the RNA

more prone to degradation by RNases. However, there is currently no explanation for the increased initial *icaR* transcription in the mutant compared to the wildtype. In summary, mutant *S. epidermidis* O-47Δ*tRNA*^{Thr-4}Δ*icaZ*Δ*icaR*-3′ UTR (O-47ΔΔΔ) represents a functional triple mutant that is not only defective for IGR*ica*-RNA, but also affects *tRNA*^{Thr-4} expression as well as *icaR* transcript amounts and stability.
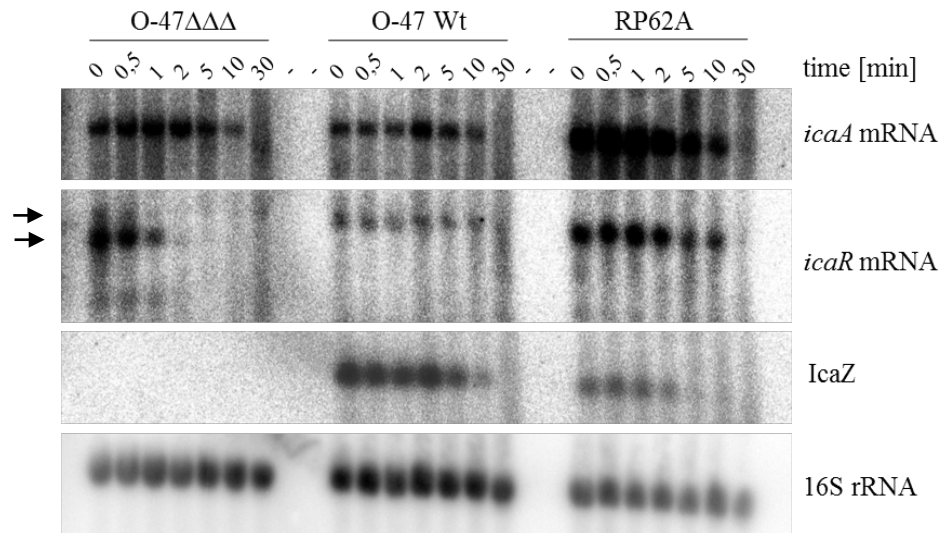
Fig. IV-1: Northern blot analysis for detection of *ica*-transcripts

10 µg of total RNA from *S. epidermidis* strains O-47Δ*tRNA*^{Thr-4}Δ*icaZ*Δ*icaR*-3′ UTR (O-47ΔΔΔ; strain collection code FL1Δ2), O-47 Wt and RP62A, grown in TSB at 30°C until exponential growth phase (OD$_{600}$ ~1), were separated on 1.2% agarose/formaldehyde gel (chapter II-6.4.2) for 4.5h at 100V. RNA was sampled before rifampicin was added (t$_0$) and afterwards at indicated time points (t$_{0.5}$-t$_{30}$). RNA was hybridised with radioactively labelled IcaR ds-DNA probe, IcaA ds-DNA probe, IcaZ ds-DNA probe and 16S rRNA ss-DNA probe. The IcaR ds-DNA probe was generated with primers IcaR-F and IcaR-R (360 bp) and directed against *icaR* mRNA ORF. IcaA ds-DNA probe was generated with primers IcaA-F and IcaA-R (814 bp) and IcaZ ds-DNA probe was generated with primers tRNA_x_as and ica_rev294 (294 bp). Labelling was carried out as described in chapter II-0 and chapter II-6.5.5. Primer Se16SrDNAF was used to detect 16S rRNA as loading control. Black arrows indicate full length *icaR* mRNA transcripts (upper arrow) and the reduced size (lower arrow). Degradation products of *icaR* mRNA transcripts were detected in the mutant, not in the wildtype.

S. epidermidis O-47ΔP$_{tRNA}$^{Thr-4}Δ*tRNA*^{Thr-4}Δ*icaZ*Δ*icaR*-3′ UTR (O-47ΔΔΔΔ; strain collection code FL2Δ1), also created by F. Herbst, comprised the same deletion as in O-47ΔΔΔ, but with an extension into the entire *tRNA*^{Thr-4} locus and its adjacent gene. The deleted region comprised in total the base pairs between primer rf1 and 111 bp upstream of *tRNA*^{Thr-4}.

S. epidermidis 307ΔIGR*ica*-sRNA (strain collection code ME19), created by Dr Martin Eckart, was generated in strain background 307. The deleted region is identical to O-47ΔΔΔ, but carries an erythromycin resistance gene inserted instead of the deleted region.

1.2 Construction of mutant strain O-47ΔicaZ

S. epidermidis O-47Δ_icaZ_ was created to generate a deletion mutant that lacks exclusively IcaZ, but does not affect neighbouring genes and transcripts. The construct was generated several times independently from each other in this work and clones carry strain collection codes ML38, ML39 and ML2.

The marker less deletion of _icaZ_ was accomplished by homologous recombination of _icaZ_ flanking regions from plasmid pBASE6_flankreg_icaZMF with the homologous genomic DNA sequence of strain O-47. To construct the plasmid, the flanking regions of _icaZ_ were amplified by PCR from genomic DNA of _S. epidermidis_ O-47.
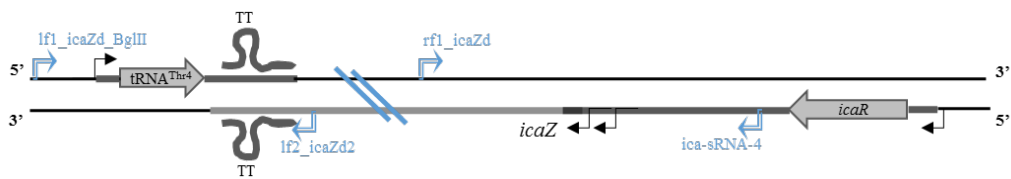
Fig. IV-2: Primer binding sites for the deletion of _icaZ_ middle part

Genomic localisation of _icaZ_ in _S. epidermidis_ O-47 Wt. The flanking regions of _icaZ_ were amplified with Phusion polymerase in 50 µl reaction volume by PCR. Left fragment 'lf' was amplified using primers lf1_icaZd_BglII and lf2_icaZd2 (674 bp); it contains also the transcription termination signal (TT) of _tRNA^{Thr4}_ and _icaZ_. Right fragment 'rf' was amplified by using primers rf1_icaZd and ica-sRNA4_EcoRI (420 bp); it contains 80 bp of _icaZ_ and the upstream region. The double line indicates the deleted part in the middle of _icaZ_ (274 bp). Bold lines upstream and downstream of _tRNA^{Thr-4}_ and _icaR_ ORF symbolize 5′ UTR and 3′ UTR. Thin arrows indicate promoter regions of _tRNA^{Thr-4}_, _icaZ_ and _icaR_.

The two fragments, named 'lf' and 'rf', were connected by overlapping PCR (primers lf1_icaZd_BglII and ica-sRNA4_EcoRI) and the PCR product was then cloned into pBASE6 vector using restriction enzymes BglII and EcoRI by classical cut and paste method. The plasmid was transformed into _E. coli_ DC10B and multiplied by the bacteria. From _E. coli_ DC10B+pBASE6_flankreg_icaZMF (strain collection code MF60), the plasmid was isolated and transferred into _S. epidermidis_ O-47 creating _S. epidermidis_ O-47+pBASE6_flankreg_icaZMF (strain collection code MF61). This strain was used for homologous recombination procedure described in chapter II-8.4.3. The inserted regions in plasmid pBASE6_flankreg_icaZMF recombined with the homologous regions on the genomic DNA, which led to the loss of the middle part of _icaZ_ genomic sequence. Anhydrotetracycline (ATc) addition during growth of the clones caused then the loss of the plasmid and yielded the markerless _icaZ_ deletion mutants _S. epidermidis_ O-47Δ_icaZ_ (strain collection code ML38, ML39 and ML2). Before storage of the mutants in the strain collection, the genomic region surrounding the deletion was checked by PCR.

The advantage of the new *icaZ* mutant *S. epidermidis* O-47Δ*icaZ* is the markerless deletion of only the middle part of *icaZ* (nucleotides 81 to 354 from *icaZ* TSS 1), so that *icaR* and *tRNA*$^{Thr-4}$ sequences remain complete and hence are fully functional (**Fig. IV-3**). That means, any effects seen in the mutant are caused only by the deletion of ncRNA IcaZ. Also, any side effects by introduction of resistance genes can be excluded, because of the markerless deletion. The promoter region of *icaZ* (P$_{icaZ}$) remained within the genome and was not part of the deletion, because this region is part of the *icaR* 3′ UTR.
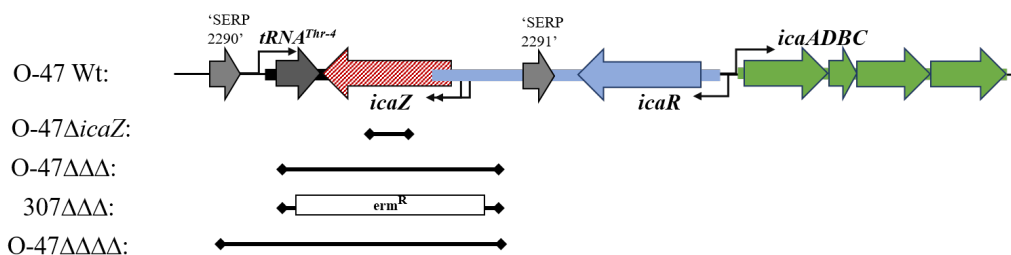
Fig. IV-3: Comparison of *icaZ* deletions in *S. epidermidis* mutants

> The figure depicts schematically the genomic DNA sequence of *S. epidermidis* O-47 Wt for the region surrounding *icaZ*. The deleted regions of *icaZ* mutants are displayed as black lines below the Wt sequence. In O-47Δ*icaZ*, only the middle part of the *icaZ* gene is deleted.

To verify the intact *icaR* mRNA in *S. epidermidis* O-47Δ*icaZ* experimentally, Northern blots were carried out with total RNA of *S. epidermidis* O-47 Wt, O-47Δ*tRNA*$^{Thr-4}$Δ*icaZ*Δ*icaR*-3′ UTR (strain collection code FL1Δ2) and O-47Δ*icaZ* (strain collection code ML38). *icaR* mRNA was detected with radioactively labelled ds-DNA probe. The size of the detected Northern blot band in the new mutant had the same length as the bands detected in the Wt. The shortened *icaR* mRNA of the old mutant O-47ΔΔΔ was still clearly visible. The blots verified the intact *icaR* transcripts of the new mutant O-47Δ*icaZ* (**Fig. IV-4**).
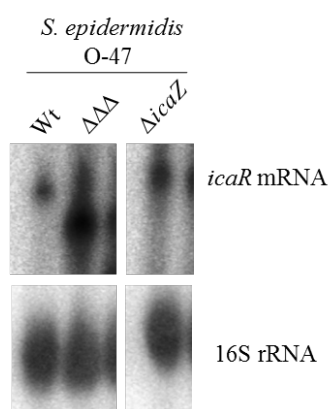
Fig. IV-4: Northern blot with radioactive probe for *icaR* mRNA detection in O-47Δ*icaZ*

10 µg of total RNA from *S. epidermidis* O-47 Wt, *S. epidermidis* O-47Δ*tRNA*$^{Thr-4}$Δ*icaZ*Δ*icaR*-3′ UTR (O-47ΔΔΔ) and the new mutant *S. epidermidis* O-47Δ*icaZ*, from exponential phase at 30°C were separated on a 1.2% agarose gel. Radioactively labelled *icaR* ds-DNA probe detected specifically *icaR* transcript. Radioactive labelled 16S rRNA primer was used to detect 16S rRNA as loading control.

1.3 Biochemical analysis of IcaZ deletion mutant

API Staph tests: API Staph is a standardised system from bioMérieux for the identification of staphylococcal and micrococcus species, based on 20 miniaturised biochemical reactions. The bacteria were inoculated into the microtubes and grew 18-20h at 37°C. During growth, the bacteria metabolised the substrates of the microtubes. This resulted in spontaneous colour change or the colour change was revealed after the addition of special reagents, provided with the test system. This colour was translated into a numerical code that gave the species name and the likelihood in percentage.

S. epidermidis O-47 Wt and IcaZ deletion mutant O-47$\Delta tRNA^{Thr-4}\Delta icaZ\Delta icaR$-3′ UTR (O-47$\Delta\Delta\Delta$; strain collection code FL1Δ2) were identified by code 6606112, being *S. epidermidis* to 93.7%. The deletion of *icaZ* did not influence these selected 20 biochemical reactions, because the test results were identical between Wt and mutant (**Fig. IV-5**). The test was repeated with same results for both strains, but ADH reaction was positive. Thus, the code changed to 6606113, which was even a better identification for *S. epidermidis* (97.9%).
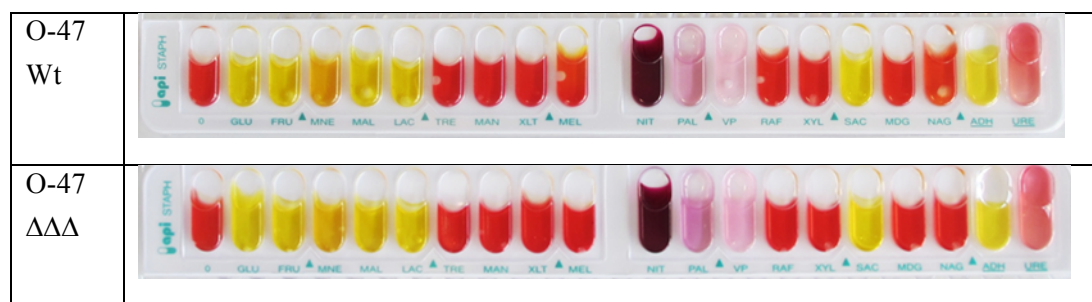
O-47 Wt	
O-47 ΔΔΔ	

Fig. IV-5: Biochemical analysis of O-47 Wt and O-47 triple mutant

ONC of *S. epidermidis* O-47 Wt and O-47$\Delta tRNA^{Thr-4}\Delta icaZ\Delta icaR$-3′ UTR (O-47$\Delta\Delta\Delta$; strain collection code FL1Δ2) were setup in TSB medium at 37°C. 60 µl of the ONC were added to the API Staph medium, mixed and then filled into the wells of the API Staph test. The last two slots for adenine dehydrogenase and urease were covered with immersion oil to achieve anaerobic conditions. The test stripe was placed in a wetted chamber and incubated o/n at 37°C. NIT, PAL and VP reactions were supplemented with the additives, given with the test stripes, and evaluation of the reactions was carried out according to the instructions of bioMérieux.

Milk agar test: The growth of *S. epidermidis* O-47 Wt and *icaZ* deletion mutant O-47$\Delta tRNA^{Thr-4}\Delta icaZ\Delta icaR$-3′ UTR (O-47$\Delta\Delta\Delta$; strain collection code FL1Δ2) was analysed on milk agar plates. After growth at 30°C and 37°C, both strains were surrounded by a clearing zone, which indicated that proteases were expressed (temperature-independently) by both strains (**Fig. IV-6**). Conclusively, the *agr*-system is intact and the deletion of *icaZ* has no effect on the *agr*-system, which regulates the expression of proteases.
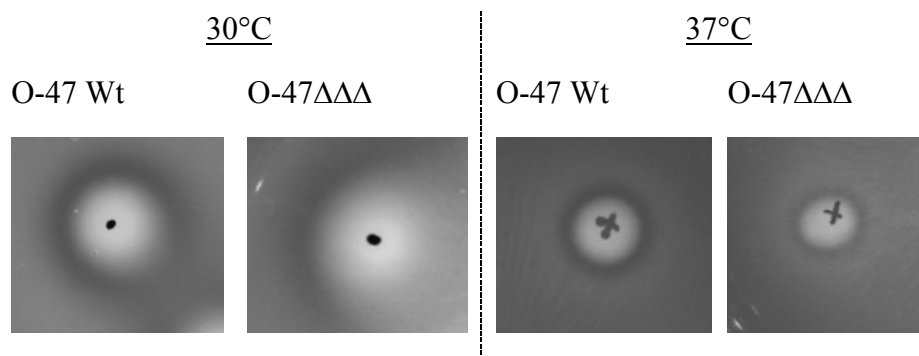
Fig. IV-6: Effect of IcaZ deletion on *agr*-system analysed with milk agar test

  S. epidermidis O-47 Wt and *icaZ* deletion mutant O-47$\Delta tRNA^{Thr-4}\Delta icaZ\Delta icaR$-3′ UTR (O-47$\Delta\Delta\Delta$; strain collection code FL1Δ2) were grown overnight on milk agar at 30°C and 37°C respectively. The appearance of the clearing zone surrounding both strains, formed through the degradation of proteins by proteases, which are under the control of the *agr*-system, indicated that *icaZ* deletion has no effect on the *agr*-system.

Oxidative stress: For functional analysis, H_2O_2 stress tests were carried out. *S. epidermidis* O-47 Wt and IcaZ deletion mutant O-47$\Delta tRNA^{Thr-4}\Delta icaZ\Delta icaR$-3′ UTR (O-47$\Delta\Delta\Delta$; strain collection code FL1Δ2) were grown o/n on TSB agar containing a disk that was basted with 10 µl of 0.23% and 0.46% H_2O_2 solution. The inhibition zones were measured manually (in mm). Results are listed in **Tab. IV-1**. Three independent experiments revealed that the mutant was slightly more sensitive to the applied H_2O_2 solutions at both temperatures.

Tab. IV-1: Results of H_2O_2 inhibition assay

  The table lists the measured inhibition zones in mm for growth with 0.23% and 0.46% H_2O_2 of *S. epidermidis* O-47 Wt and O-47$\Delta tRNA^{Thr-4}\Delta icaZ$ $\Delta icaR$-3′ UTR (O-47$\Delta\Delta\Delta$; strain collection code FL1Δ2). The inhibition assay was performed in triplicates, each at 30°C and 37°C.

		0.23% H_2O_2		0.46% H_2O_2	
Temperature	**Biol. replicate**	**O-47 Wt**	**O-47$\Delta\Delta\Delta$**	**O-47 Wt**	**O-47$\Delta\Delta\Delta$**
30°C	1	26 mm	27 mm	31 mm	32-34 mm
	2	26 mm	27-31 mm	-	37 mm
	3	23 mm	25 mm	30-31 mm	31 mm
37°C	1	18 mm	19 mm	18 mm	22 mm
	2	17 mm	17 mm	20 mm	21 mm
	3	20 mm	22 mm	25 mm	28 mm

1.4 IcaZ deletion mutants reveal a distinct biofilm negative phenotype

1.4.1   *Phenotype on Congo red agar and MgCl$_2$-agar*

Congo red agar (CRA) is a standard method for phenotypic analysis of biofilm forming strains. The method was first described by Freeman *et al.*, 1989, and later the ingredients were further modified by Kaiser *et al.*, 2013. Biofilm forming colonies appear dry and black with an uneven edge, whereas non-biofilm forming colonies have a smooth surface, a red to pink colour and an even edge.

All IcaZ mutants were analysed on CRA and displayed a distinct biofilm negative phenotype in comparison to *S. epidermidis* O-47 Wt (**Fig. IV-7 A-C**). Usually, when the sequence of an RNA is deleted, the resulting phenotype is not that distinct and often results in a 'molecular phenotype'. In this case, the effect of the deletion was clearly obvious and therefore is called a 'macroscopic phenotype'. Due to the fact, that the main patho-mechanism of *S. epidermidis*, which is biofilm formation, is hampered due to the deletion of ncRNA IcaZ, we concluded that this RNA must be very important for biofilm regulation.

In former times, comparisons of strains on Congo red agar concerning the phenotype were done by comparison of *S. epidermidis* or *S. aureus* strains with *S. carnosus* TM300. *S. carnosus* TM300 does not possess the *icaADBC*-operon that is necessary for PIA production and is therefore a strain for comparison to biofilm negative strains. But, as mostly *S. epidermidis* is analysed here, *S. epidermidis* ATCC 12228 is a much better strain for comparison, because the strain also lacks the *icaADBC*-operon, but most importantly, it is the same species. In this work, the initial CRA assays and biofilm assays were carried out with *S. carnosus* TM300 and the later ones with *S. epidermidis* ATCC 12228. Therefore, both strains were used as biofilm negative control strains in this work, depending on the execution time of the experiments (**Fig. IV-7 E-F**). *S. epidermidis* RP62A was always taken as biofilm positive control strain (**Fig. IV-7 D**).

S. epidermidis O-47 Wt and IcaZ mutants

A O-47 Wt   **B** O-47ΔΔΔ   **C** O-47Δ*icaZ*

control strains

D RP62A   **E** ATCC 12228   **F** TM300
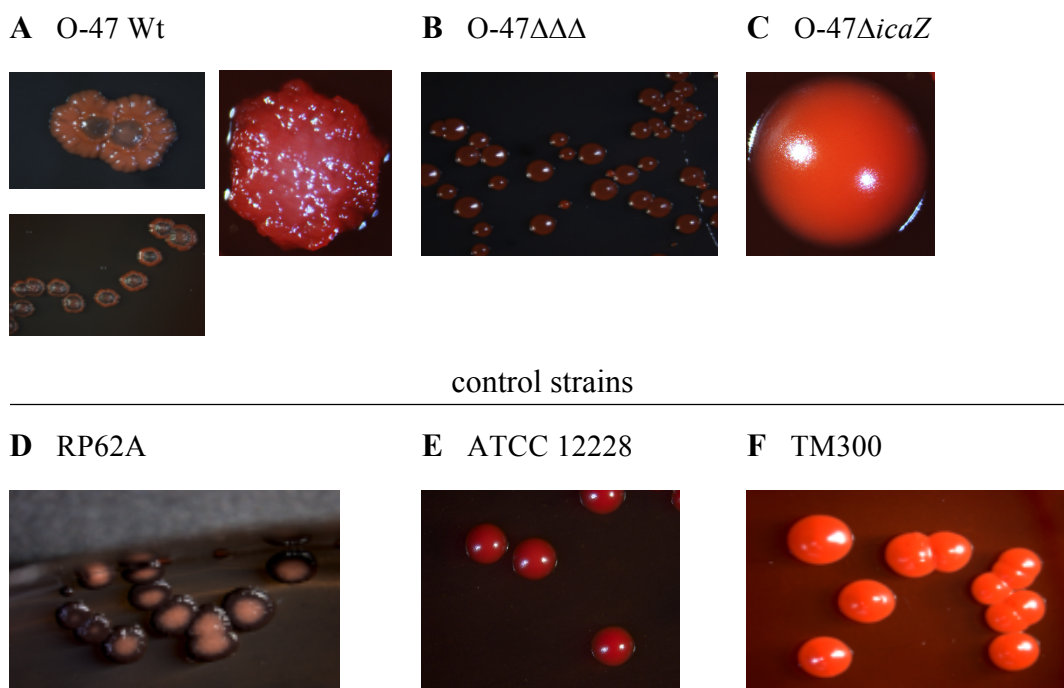
Fig. IV-7: Phenotype of *S. epidermidis* on Congo red agar

Single colonies were either obtained through plating out dilution series or by dilutional streak of the strains onto CRA. Bacteria grew at least o/n at 30°C or 37°C until appropriate colony size was obtained. The agar plates were then further incubated at RT or at 4°C. Colonies were analysed by binocular microscopy. Strains: (**A**) *S. epidermidis* O-47, (**B**) *S. epidermidis* O-47Δ*tRNA^{Thr-4}*Δ*icaZ*Δ*icaR*-3′ UTR (O-47ΔΔΔ; strain collection code FL1Δ2), (**C**) *S. epidermidis* O-47Δ*icaZ* (strain collection code ML38), (**D**) *S. epidermidis* RP62A as positive control, (**E**) *S. epidermidis* ATCC 12228 as negative control, (**F**) *S. carnosus* TM300 as negative control. Biofilm forming colonies appear dry and black with an uneven edge, whereas non-biofilm forming colonies are smooth, red/pink and even.

The phenotype of the mutants was also analysed on 100 mM MgCl$_2$-agar. This agar was used before to induce biofilm formation of *S. aureus* (AG Lopez, IMIB, personal communication). However, the mutant strains showed the same phenotype on MgCl$_2$-agar as the Wt (**Fig. IV-8**).

A O-47 Wt   **B** O-47ΔΔΔ   **C** O-47Δ*icaZ*   **D** ATCC 12228
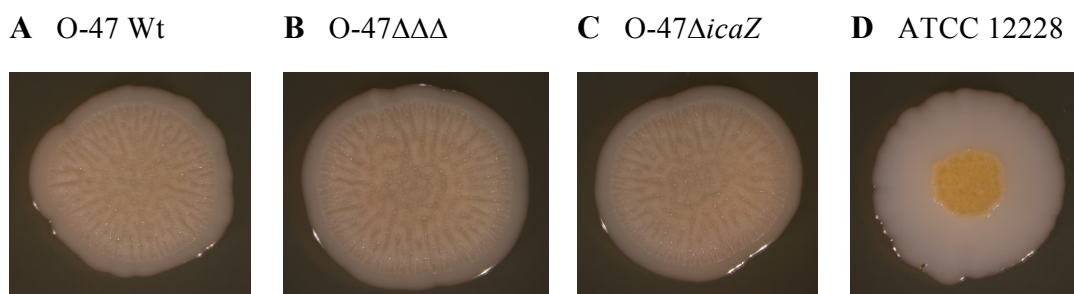
Fig. IV-8: Phenotype of IcaZ mutants on biofilm inducing MgCl$_2$-agar

The strains grew on LB standard agar, mixed with 100 mM MgCl$_2$, for 7d at 30°C. The phenotype was photographed with the digital camera connected to the binocular microscope. (**A**) *S. epidermidis* O-47 Wt, (**B**) *S. epidermidis* O-47Δ*tRNA*$^{Thr-4}$ Δ*icaZ* Δ*icaR*-3′UTR (O-47ΔΔΔ; strain collection code FL1Δ2), (**C**) *S. epidermidis* O-47Δ*icaZ* (strain collection code ML38), (**D**) *S. epidermidis* ATCC 12228 as negative control.

1.4.2   *Deletion of icaZ has no effect on cell shape*

Scanning electron microscopy (SEM) was carried out to compare the cell shape of *S. epidermidis* O-47 Wt and O-47Δ*tRNA*$^{Thr-4}$Δ*icaZ*Δ*icaR*-3′ UTR (O-47ΔΔΔ; strain collection code FL1Δ2). The bacterial cells were prepared according to the protocol of chapter II-4.1. Both strains exhibited a regular coccoidal cell shape (**Fig. IV-9 A+B, Aa**) and cell division (**Fig. IV-9 Ab-f, Ba-f**). Conclusively, the deletion has no impact on cell shape and division. An impact on growth was also excluded.
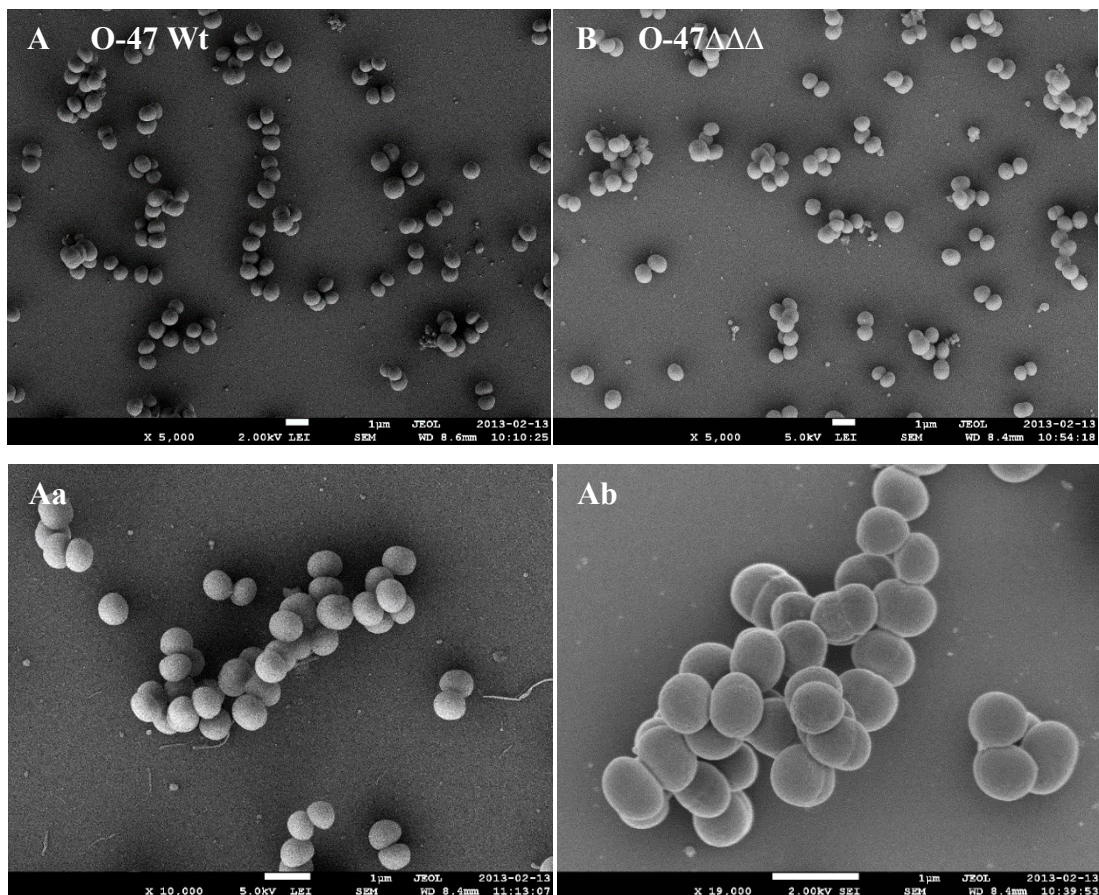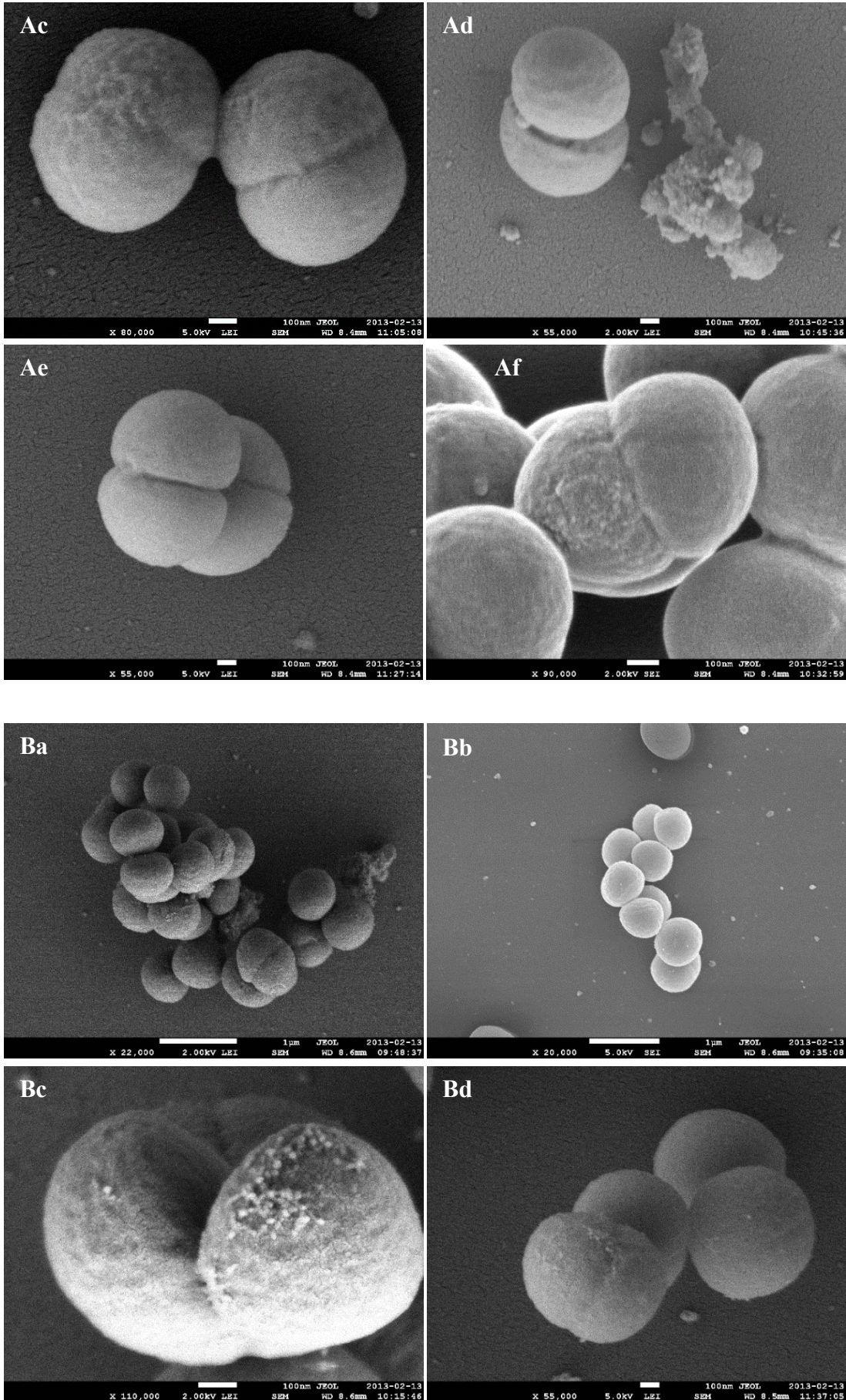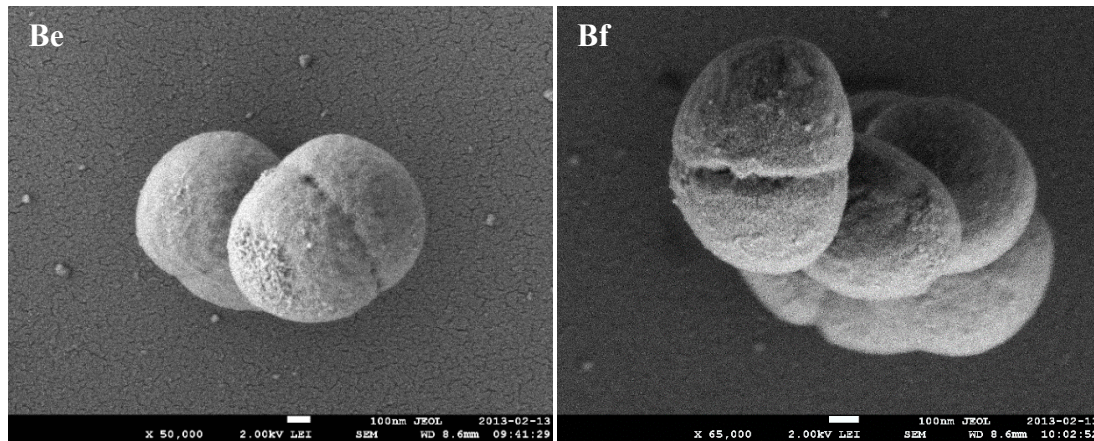
Fig. IV-9: Cell shape and division of *S. epidermidis* O-47 Wt and IcaZ mutant

SEM of exponential phase cells of *S. epidermidis* O-47 Wt (**A, Aa-Af**) and *S. epidermidis* O-47Δ*tRNA^{Thr-4}*Δ*icaZ*Δ*icaR*-3′UTR (O-47ΔΔΔ; strain collection code FL1Δ2, **B, Ba-Bg**) at 37°C. The bacterial cells were prepared according to the protocol of chapter II-4.1. SEM imaging was carried out at the Biocenter of University of Würzburg. Pictures were taken with 5-110x magnification. The white bar beneath each picture either indicates 1 μm (a,b) or 100nm (c-f) in size, as indicated.

1.4.3   *Classical crystal violet biofilm formation assays reveal reduced production of polysaccharides in IcaZ mutants*

Classical crystal violet biofilm formation assays were carried out, according to the protocol of chapter II-4.3, to analyse the composition of the biofilm. They were used to differentiate between total biofilm, the polysaccharide content and the amount of proteins within the biofilm by degradation of the components with proteinase K or sodium periodate ($NaIO_4$). The assays were conducted at two temperatures, at 30°C to mimic human skin conditions and at 37°C to mimic infection conditions (*e.g.* after entering the blood stream).

For a comprehensive analysis, all existing *icaZ* mutants were analysed by classical biofilm assays. The deletion mutant 307ΔIGR*ica*-sRNA produced much less total biofilm than the corresponding Wt. Polysaccharides of the biofilm matrix were reduced in this mutant, but not the amount of proteins (**Fig. IV-10 A**). Biofilm assays of *S. epidermidis* O-47Δ*tRNA^{Thr-4}*Δ*icaZ*Δ*icaR*-3′ UTR (O-47ΔΔΔ; strain collection code FL1Δ2) confirmed these results (**Fig. IV-10 B**) and moreover biofilm formation assays of *S. epidermidis* O-47Δ*icaZ* (strain collection codes ML38 and ML2) repeatedly revealed an even more distinct biofilm negative phenotype (**Fig. IV-10 C**). The total biofilm and particularly the polysaccharide amount was almost abolished, when compared to O-47 Wt.

Conclusively, the macroscopic distinct biofilm negative phenotype of the mutants was attributable to the deletion of ncRNA IcaZ alone, since the effect was also observed (even enhanced) if only the middle part of *icaZ* was deleted. These results underline the importance of ncRNA IcaZ as a regulator for biofilm formation in *S. epidermidis*.
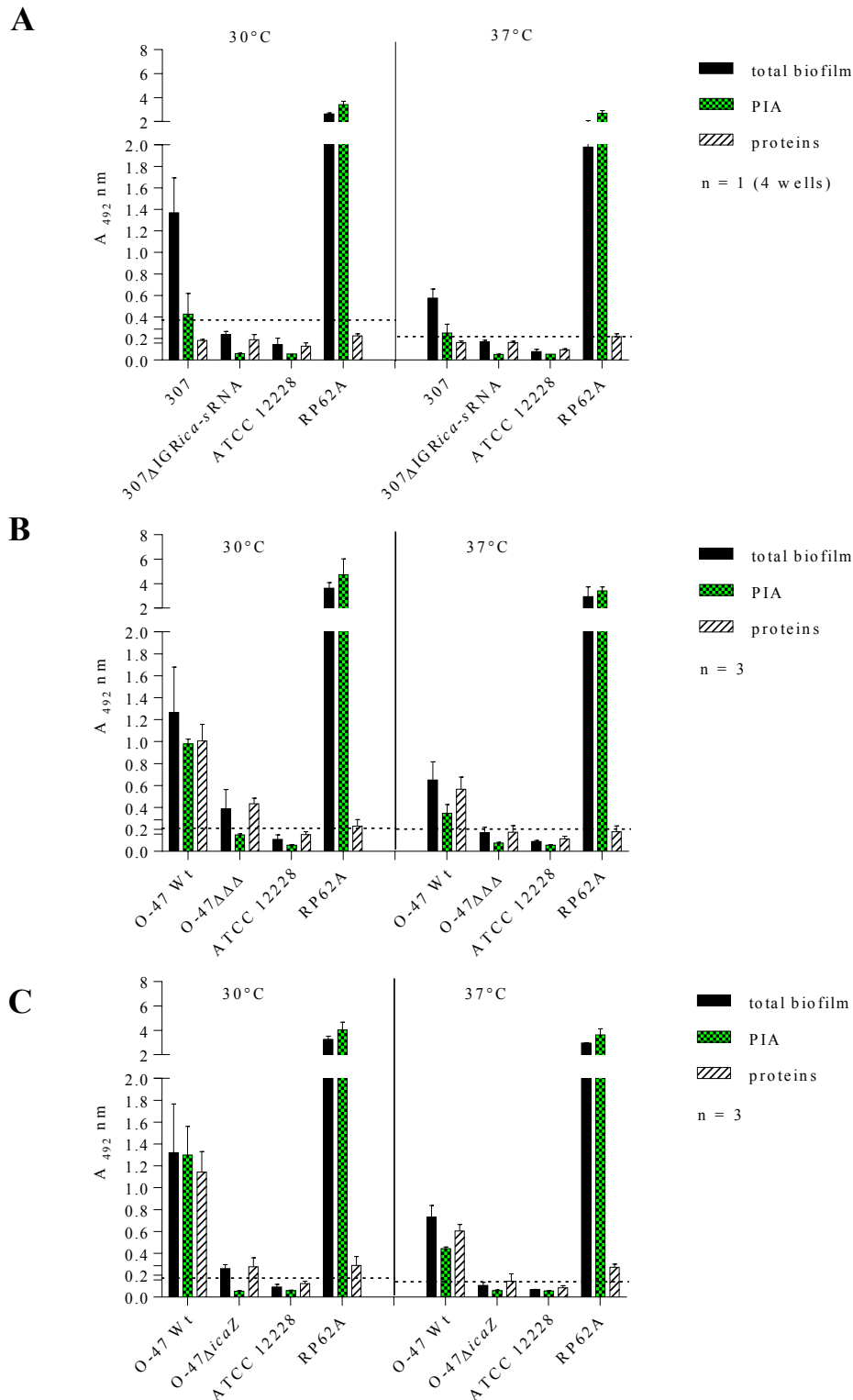
Fig. IV-10: Biofilm formation of *S. epidermidis* O-47 Wt and *icaZ* mutants

Bacterial strains were grown in TSB at 30°C and 37°C. Crystal violet plate assays were performed according to the standard procedure. *S. epidermidis* ATCC 12228 and *S. epidermidis* RP62A were used as biofilm negative and biofilm positive control strains. The dashed lines represent 2x mean of ATCC 12228 total biofilm as cut off for biofilm formation. The data represent one biological replicate (n=1) (A) and three biological replicates (n = 3) (B, C), respectively.

1.5 Real time *in vivo* biofilm formation analysis reveals new insights into biofilm development of O-47 Wt and IcaZ mutants

The flow system for *in vivo* biofilm formation analysis in real time was established in the laboratory with the help of Prof Kai Thormann, who kindly provided the peristaltic pump and gave technical advice. The flow experiments were conducted together with Dr Sonja Schönfelder.

Fig. IV-11 and **Fig. IV-12** depict the installation of the flow system. The emerging biofilms in the six chambers of the slide were observed through the confocal laser scanning microscope, which was connected to the computer system. The slide (7 in Fig. IV-11) was placed onto the microscopic stage, which was surrounded by a heatable box to establish specific temperature conditions (see Fig. IV-12 B, D). It was connected to the inflow tubing (6 in Fig. IV-11) that transported the fresh media from the media reservoirs (1) into the chamber slide, powered by the peristaltic pump (3). A bubble trap (5) was installed between the peristaltic pump and the chamber slide, to get rid of air bubbles within the system, which would disrupt the biofilm in the chamber slide. On the other side, the chamber slide was connected to the outflow tubing (8) that transported the used media into the waste flask (9).
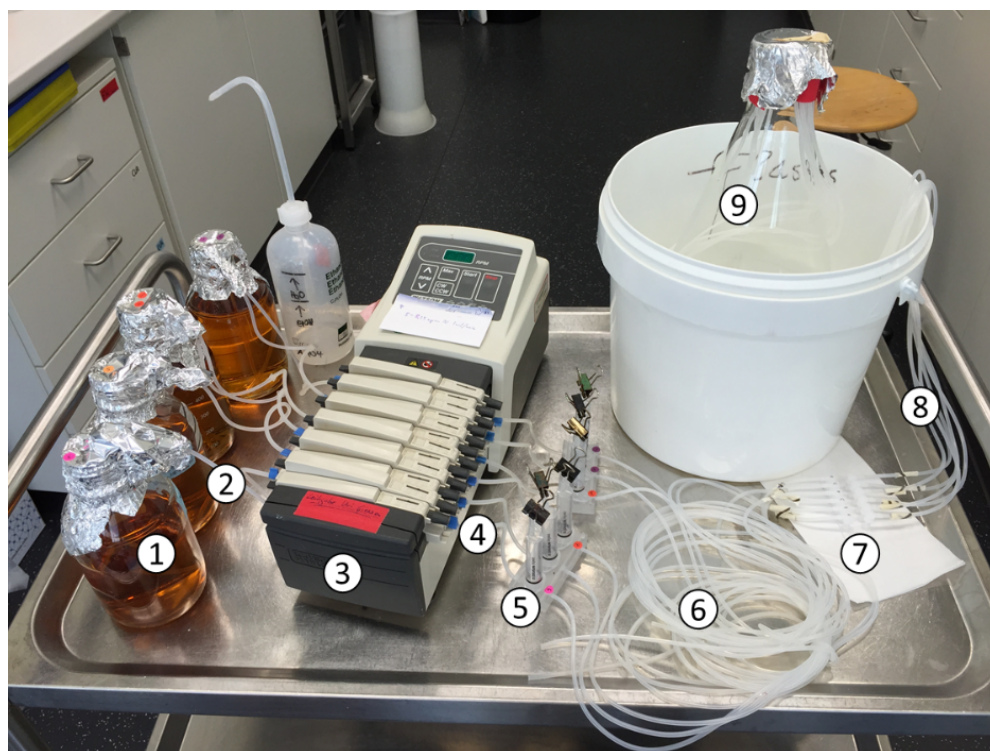
Fig. IV-11: Flow system installation

   The flow system includes the medium reservoir (1), the medium tubing (2), the peristaltic pump (3), the pump tubing (4), the bubble traps (5) the inflow tubing (6), the six-chamber slide (7), the outflow tubing (8) and the waste flask (9). The components were assembled on a transportable table (chapter II-4.5.2) and installed next to the confocal laser scanning microscope (Fig. IV-12).
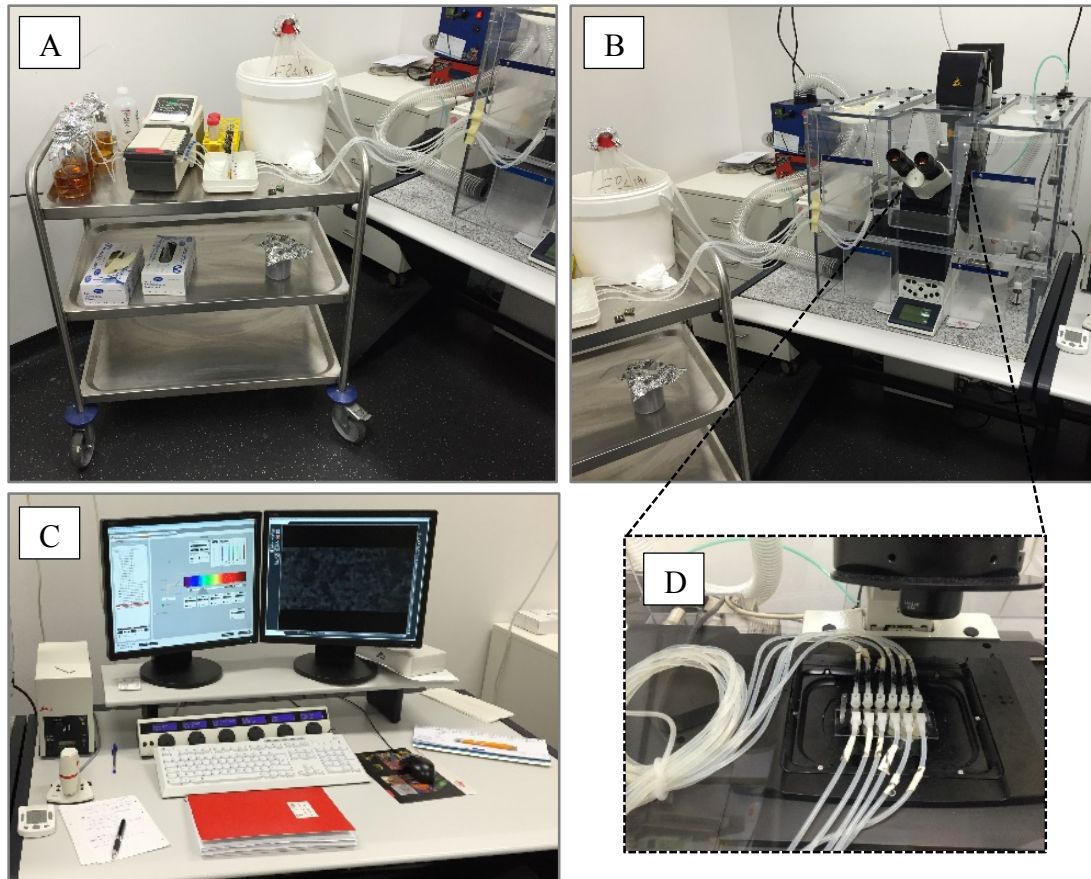
Fig. IV-12: Experimental setup for *in vivo* biofilm formation analysis

(**A**) Peristaltic pump, provided by Prof Kai Thormann, with medium reservoir (left), bubble traps (right) and inflow tubing towards the microscope, as well as outflow tubing going from the slide on the microscopic stage into the waste flask. (**B**) CLSM overview with heater (left) and flexible tube from the heater to the incubator around the microscope. (**C**) Computer station next to the CLSM with the control panel of the microscopic stage. (**D**) Zoom-in of the six-chamber slide with inflow tubing (above) lying in circles and outflow tubing (underneath) upon the microscopic stage.

The experimental setup was prepared as stated in chapter II-4.5. Biofilm growth analysis was conducted with strain *S. epidermidis* O-47 Wt + pCerulean_icaZprom (strain collection code ML13) in chamber 1-5 and *S. epidermidis* O-47 $\Delta tRNA^{Thr-4}\Delta icaZ\Delta icaR$-3′ UTR (O-47ΔΔΔ; strain collection code FL1Δ2) in chamber 6. The bacteria were inoculated at $OD_{600} \sim 0.05$ and allowed to settle down for 1h. The first scan was taken before starting the flow at 0.5 rpm, the second scan right after (**Fig. IV-13**). The next scans were taken hourly of all six chambers. The strains were grown in the chamber slide at 30°C.

One hour after inoculation of the bacteria, nearly the same number of cells settled to the bottom of the slide, but when the flow was initiated, more cells of *S. epidermidis* O-47Δ*tRNA*^Thr-4^Δ*icaZ*Δ*icaR*-3′ UTR (O-47ΔΔΔ; strain collection code FL1Δ2) were washed away (**Fig. IV-13**), while *S. epidermidis* O-47 Wt + pCerulean_icaZprom (strain collection code ML13) was better attached to the surface. Cell-cell adhesion led to the emergence of cell clusters after four hours, which formed into biofilm structures within approximately ten to twelve hours (**Fig. IV-14**). On the other hand, after 4 hours of flow, the mutant still struggled to form cell clusters and twelve hours after flow initiation the biofilm structure was un-incisive in comparison to the biofilm of *S. epidermidis* O-47 Wt+pCerulean_icaZprom (strain collection code ML13) (**Fig. IV-13** and **Fig. IV-14**).
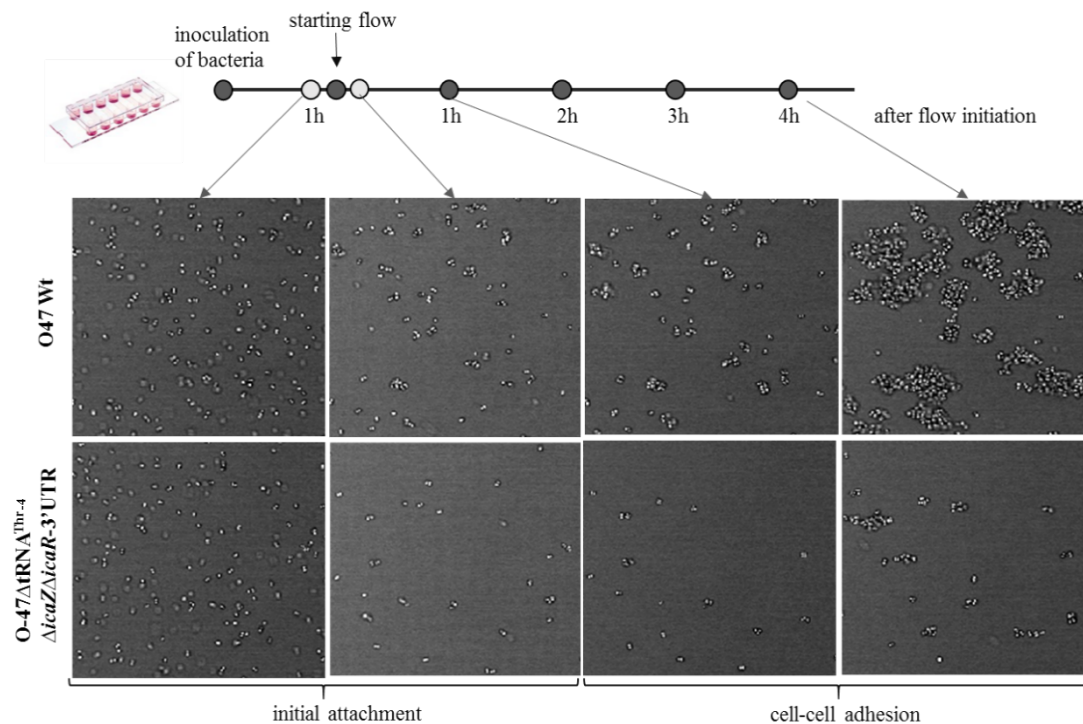
Fig. IV-13: Initial attachment and cell-cell adhesion of *S. epidermidis* O-47 Wt + pCerulean_icaZprom and O-47Δ*tRNA*^Thr-4^Δ*icaZ*Δ*icaR*-3′ UTR

Depicted are the first four hours of biofilm development including initial attachment and cell-cell adhesion phase of O-47 Wt carrying the cerulean reporter plasmid and the IcaZ mutant strain at 30°C. Cells are viewed with the transmission channel.
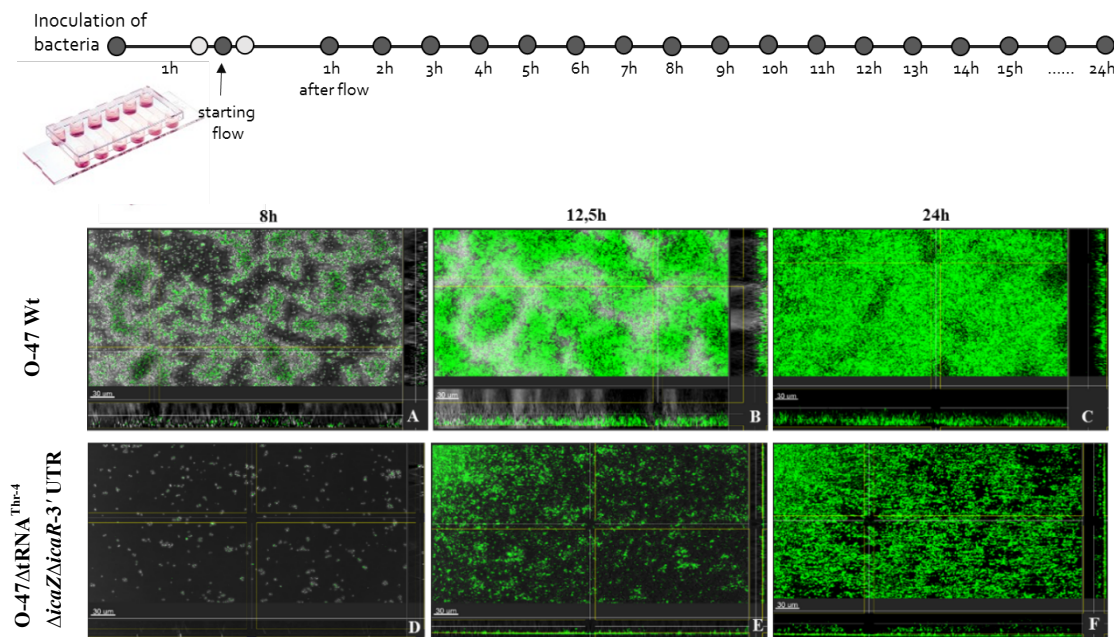
Fig. IV-14: Biofilm formation of O-47 Wt and IcaZ mutant under flow conditions

3D view and side view of the emerging biofilm, analysed by CLSM. The polysaccharides within the biofilm matrix were stained with fluorescently labelled wheat germ agglutinin (WGA-OregonGreen488). Depicted are time points t = 8h, t = 12.5h and t = 24h. The experimental setup is described in chapter II-4.5.2. After finishing the experiment, the strains from the chamber slide were streaked out onto Congo red agar for experimental control. A mix-up of bacterial strains or contamination, thus, was excluded.

The experiment under flow conditions revealed that the mutant had clear defects in initial adherence to the chamber slide surface and decreased cell-cell adherence and therefore was not able to form a proper biofilm under flow, whereas the Wt formed a strong biofilm.

In a second experiment, biofilm growth analysis was conducted with strain *S. epidermidis* O-47Wt+pCerulean_icaZprom (strain collection code ML13) in chambers 1-4, *S. epidermidis* O-47 $\Delta tRNA^{Thr-4}\Delta icaZ\Delta icaR$-3′ UTR (O-47ΔΔΔ; strain collection code FL1Δ2) in chamber 5 and *S. epidermidis* O-47 $\Delta icaZ$ (strain collection code ML38) in chamber 6. The results from the first experiment were confirmed (data not shown).

2. Investigations of biofilm formation after *in-trans* expression of IcaZ

The deletion of ncRNA IcaZ led to a macroscopic, distinct biofilm negative phenotype. To investigate, if the biofilm positive phenotype can be restored, IcaZ overexpression strains were cloned in this work. The RNA was therefore expressed *in trans* from a plasmid. Different plasmids were constructed for this purpose and transformed or transduced into the mutants and also into various *S. epidermidis* or *S. aureus* wildtypes (**Tab. IV-2**). As plasmid backbone, the vector pCG248 was used (Helle *et al.*, 2011; chapter II-6.6.1). The vector contains the $P_{xyl/tet}$ system that allows inducible gene expression of the downstream inserted gene. The encoded repressor binds to the promoter and represses transcription unless released by anhydrotetracycline (ATc). In the experiments, ATc was added to the bacterial culture to induce gene expression of *icaZ*. To exclude any side effects of ATc itself on biofilm formation, the influence of ATc on the biofilm formation of *S. epidermidis* O-47 was analysed in biofilm formation pre-experiments at 30°C and 37°C. The addition of either ATc or PBS had no influence on the biofilm amount and composition of O-47 Wt and IcaZ mutant *S. epidermidis* O-47Δ*tRNA*$^{Thr-4}$Δ*icaZ*Δ*icaR*-3′ UTR (O-47ΔΔΔ; strain collection code FL1Δ2) (**Fig. IV-15**).
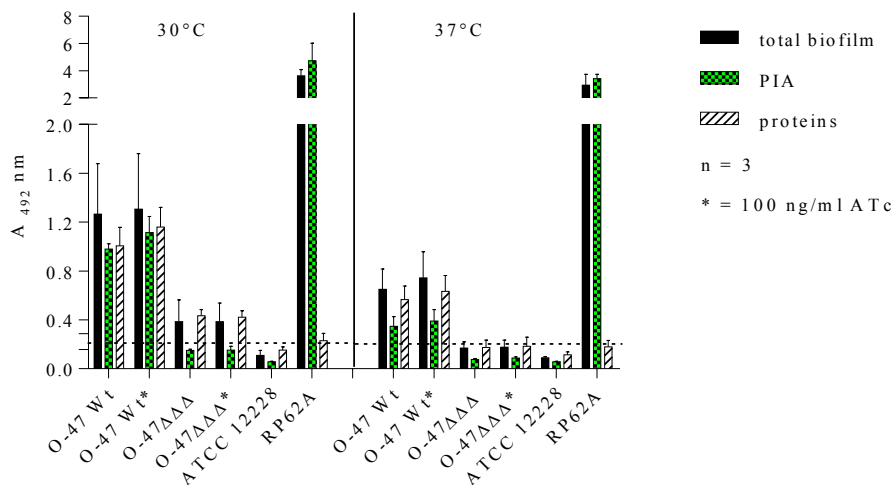
Fig. IV-15: Biofilm formation assay control for the exclusion of an influence by ATc

Biofilm formation assays were carried out according to the standard protocol. Strains were grown in TSB at 30°C and 37°C. 100 ng/ml ATc (indicated by asterisk) were added to the bacterial cultures.

Tab. IV-2: List of plasmids for IcaZ *in-trans* expression

Plasmids contain O-47 *icaZ* gene sequence with or without additional nucleotides at the endings (see table).

Plasmid	Description
pCG248_icaZ/tRNA	ATc-inducible expression vector with *icaZ* and *tRNA*$^{Thr-4}$ with P$_{tRNA}$$^{Thr-4}$ (14 bp upstream of *icaZ* TSS1 until 599 bp downstream of *icaZ* TSS1)
pCG248_icaZ	ATc-inducible expression vector with *icaZ* (14 bp upstream of *icaZ* TSS1 until 478 bp downstream of *icaZ* TSS1)
pCG248_icaZs	ATc-inducible expression vector with *icaZ* (14 bp upstream of *icaZ* TSS1 until 407 bp downstream of *icaZ* TSS1)
pCG248_icaZs_ΔTT	ATc-inducible expression vector with *icaZ* (14 bp upstream of *icaZ* TSS1 until 407 bp downstream of *icaZ* TSS1) and without TT of vector backbone
pCG248c_icaZsML_ΔTT	ATc-inducible expression vector with *icaZ* (from TSS1 until 407 bp downstream of TSS1), without TT of vector backbone and without second binding site for TetR
pCG248c_ΔTT	ATc-inducible expression vector without TT of vector backbone and without second binding site for TetR
pCG248_icaZ/tRNA/SERP2290	ATc-inducible expression vector with *icaZ*, *tRNA*$^{Thr-4}$ with P$_{tRNA}$$^{Thr-4}$ and SERP2290 with P$_{SERP2290}$ (14 bp upstream of *icaZ* TSS1 until 731 bp downstream of *icaZ* TSS1)
pCG248_ΔTT	ATc-inducible expression vector without TT of vector backbone

2.1 Effect of *in-trans icaZ* overexpression in *S. epidermidis* O-47 IcaZ mutants

2.1.1 *S. epidermidis* O-47ΔtRNA^{Thr-4}ΔicaZΔicaR-3' UTR

In this work, various IcaZ overexpression plasmids were generated (**Tab. IV-2**). The first plasmids (pCG248_icaZs; pCG248_icaZ; pCG248_icaZ/tRNA) contained IGR*ica*-RNA in three length variations. Biofilm formation assays with *S. epidermidis* O-47ΔΔΔ carrying these plasmids (strain collection codes MF58, MF52 and JE13) were carried out at two temperatures (30°C and 37°C) according to the standard protocol (chapter II-4.3). The results of these assays were equal and showed that the plasmid carrying the shortest length of the RNA was as effective as the other two plasmids (**Fig. IV-16 A**; **Annexe Fig. VIII-8**). Conclusively, the effects were caused by IcaZ alone and not by tRNA^{Thr-4}, therefore only the effects of plasmid pCG248_*icaZ*s were further investigated.

It first seemed as if biofilm formation, especially the polysaccharides within the extracellular matrix, could be restored by expressing the RNA from a plasmid **(Fig. IV-16 A)**. Dot blot assays with a specific PIA-antibody then verified the polysaccharides as PIA **(Fig. IV-16 B)**. Interestingly, these effects were temperature dependent, because no increase of biofilm formation after ATc addition at 37°C was observed, but clearly at 30°C. The overexpressed RNA from strains MF58, MF52 and JE13 was verified by cRACE and it turned out that the RNA contained additional nucleotides from the vector backbone at the 5′ UTR. Downstream of the MCS, in which the RNA was inserted, the vector contained a transcription termination signal, because this vector was initially purposed by Helle *et al.* to overexpress proteins. The transcription terminator that is formed in the generated mRNA makes sure that genes lacking a termination signal are transcriptionally stopped. In the case of overexpressing RNA though, this transcription terminator (TT) is problematic, if the RNA reads through, because the additional nucleotides might change the secondary structure and thus influence the function of the regulatory RNA. The effect caused by the additional 5′ UTR nucleotides on RNA secondary structure was analysed by *Mfold*. These structure predictions revealed no substantial change in the overall secondary structure at both folding temperatures (30°C and 37°C; **Annexe VIII-9**). The additional 3′ UTR nucleotides due to the transcription terminator were likely to change the structure and therefore the vector had to be cleaned from these additional nucleotides. Plasmids, which are cleaned off the additional 5′ UTR nucleotides contain 'pCG248**c**' instead of 'pCG248' in the name and plasmids without the TT are named 'ΔTT'.
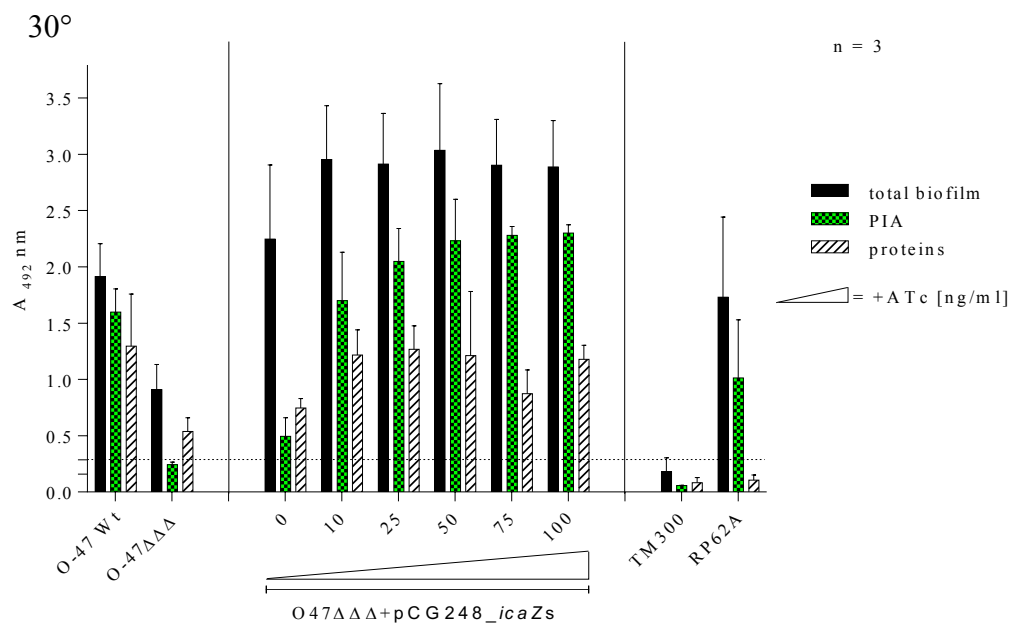
A
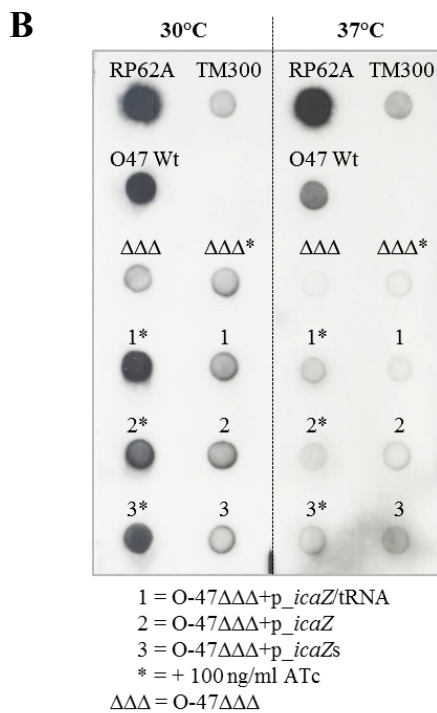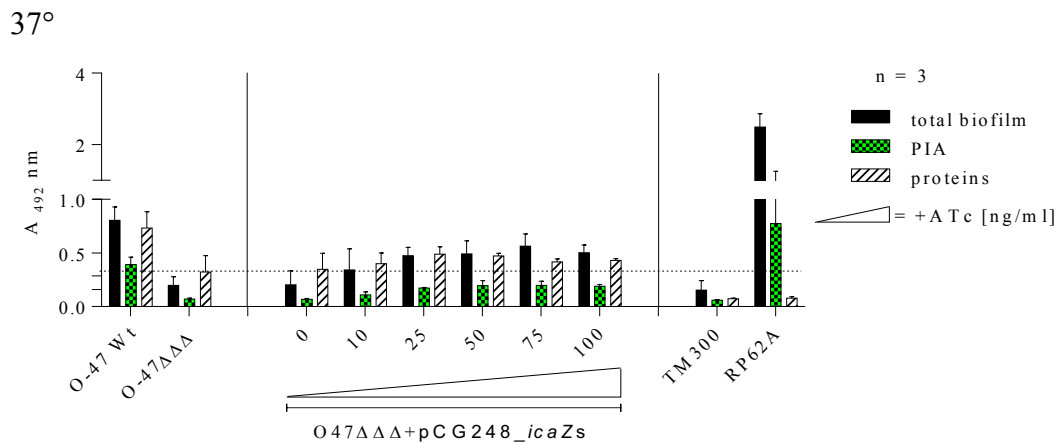
Fig. IV-16: Biofilm formation and dot blot assay of O-47ΔΔΔ carrying *icaZ* overexpression plasmids I

(**A**) Biofilm formation assay results of *S. epidermidis* O-47ΔΔΔ+pCG248_icaZs (strain collection code MF58) from three independent experiments (n = 3) at 30°C (top) and 37°C (bottom). Each experiment was carried out in quadruplicate. The expression of *icaZ* was induced by the addition of ATc with indicated concentrations ranging from 10 ng/ml to 100 ng/ml. (**B**) PIA specific antibody confirmed polysaccharides as PIA by dot blot analysis. Assays were carried out as described in chapter II-7.2.

The biofilm formation at 30°C of strains carrying the new plasmids is shown in **Fig. IV-17**. PIA was clearly diminished in O-47ΔΔΔ compared to O-47 Wt (**Fig. IV-17 a**) as shown before. The biofilm composition of strains carrying the plasmids was equal to the biofilm formation of the mutant, so that no plasmid effect was observed. In **Fig. IV-17 b+c**, strains carried a plasmid with IcaZ that had 5′ UTR extra nucleotides and were with (b) or without (c) 3′ UTR TT. Both strains showed increased biofilm formation after ATc addition, but more biofilm was produced when the TT was absent. The strain without TT and without the additional *icaZ* 5′ UTR nucleotides (**Fig. IV-17 d**) produced only slightly more biofilm than the strain with the 5′ UTR nucleotides (**Fig. IV-17 c**). Thus, the additional 5′ UTR nucleotides seemed not to influence the function of IcaZ, whereas the TT did influence the function.

But, the strain containing the control plasmid (**Fig. IV-18 e**) also showed elevated biofilm formation after ATc induction. A possible explanation might be that this plasmid replicates far more often than the other constructs, because due to the TT deletion downstream of the MCS the *ori* genes, directly located downstream of the MCS, were now overexpressed. A massive production of plasmid DNA could have caused stress for the bacteria, which could well lead to elevated biofilm production. Unfortunately, the results were not clear enough, so that an *in trans* effect of IcaZ is debatable. Maybe a plasmid with a nonsense sequence instead of *icaZ*, but still containing a TT downstream of the promoter would be a better control plasmid.
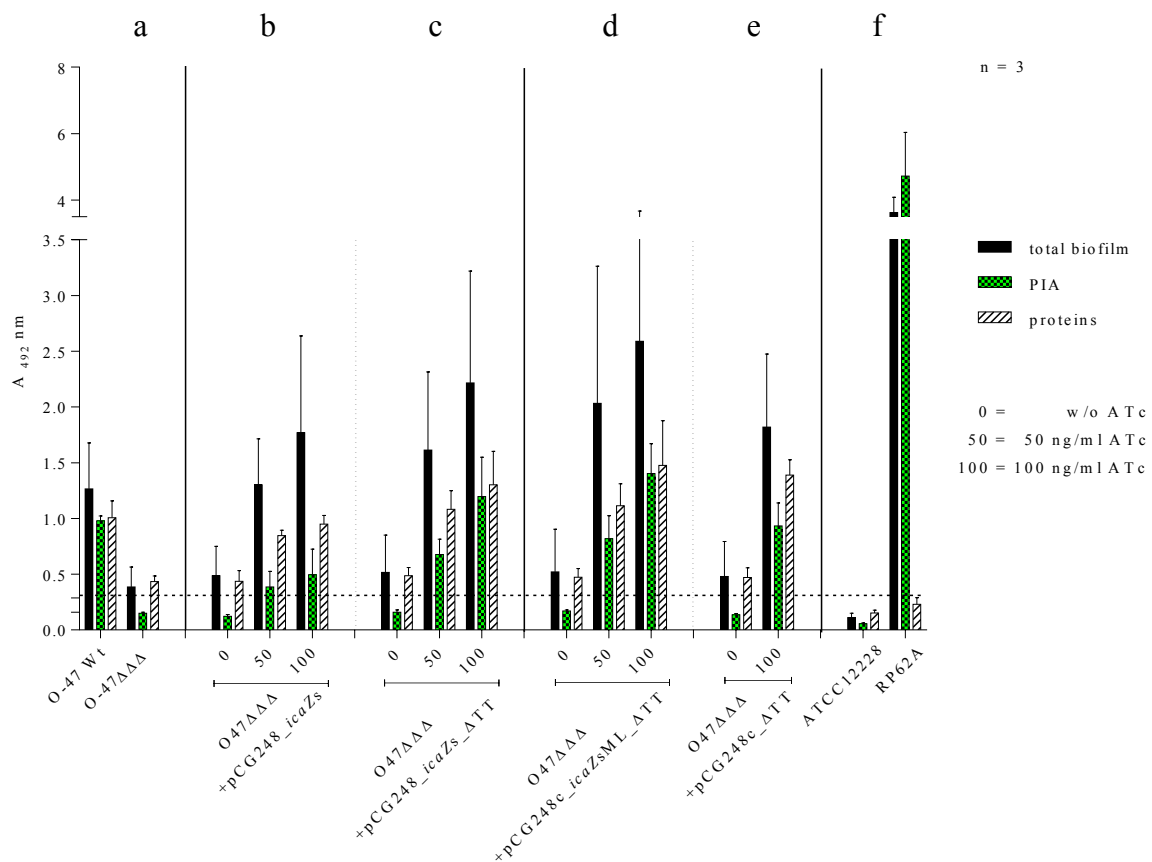
Fig. IV-17: Biofilm formation of O-47ΔΔΔ carrying *icaZ* overexpression plasmids II

Classical biofilm formation assays were carried out in TSB medium at 30°C (n = 3). **a**) *S. epidermidis* O-47 Wt and corresponding *icaZ* mutant O-47Δ*tRNA*^Thr-4^Δ*icaZ*Δ*icaR*-3′UTR (O-47ΔΔΔ; strain collection code FL1Δ2). **b**) *icaZ* complementing strain O-47ΔΔΔ +pCG248_icaZs (strain collection code MF58). **c**) *icaZ* complementing strain O-47ΔΔΔ +pCG248_icaZs_ΔTT (strain collection code ML78). **d**) *icaZ* complementing strain O-47ΔΔΔ+pCG248c_icaZsML_ΔTT (strain collection code ML72). **e**) Control strain O-47ΔΔΔ+pCG248c_ΔTT (strain collection code ML79), plasmid without *icaZ*, but with supposed increased plasmid replication due to the deleted TT that was upstream of *repF* and *ori* pT181. **f**) Control strains for crystal violet assay: biofilm-negative *S. epidermidis* ATCC 12228 and biofilm-positive *S. epidermidis* RP62A.

2.1.2 *S. epidermidis* O-47$\Delta P_{tRNA}^{Thr-4}\Delta tRNA^{Thr-4}\Delta icaZ\Delta icaR$-3′ UTR

The effect of IcaZ overexpression was also analysed in the mutant (O-47$\Delta\Delta\Delta\Delta$) that lacks in addition to *tRNA*$^{Thr-4}$, *icaZ* and *icaR*-3′ UTR, the *tRNA*$^{Thr-4}$ promoter and the coding sequence of the gene upstream of *tRNA*$^{Thr-4}$. In this strain, *icaZ* overexpression with plasmid pCG248_icaZ/tRNA/SERP2290 had no effect, not even an unspecific increase in biofilm formation. The strain remained completely biofilm negative like the mutant. The same was observed with plasmid pCG248_icaZs, pCG248_icaZ and pCG248_icaZ/tRNA carrying strains (data not shown). Interestingly, the loss of 'SERP2290'-sequence in O-47 could not be complemented by the plasmid, although its own promoter was part of the insert (P$_{SERP2290}$). SERP2290 of *S. epidermidis* RP62A is annotated only as a hypothetical protein. Why this strain remained completely biofilm negative was not further investigated in this work.
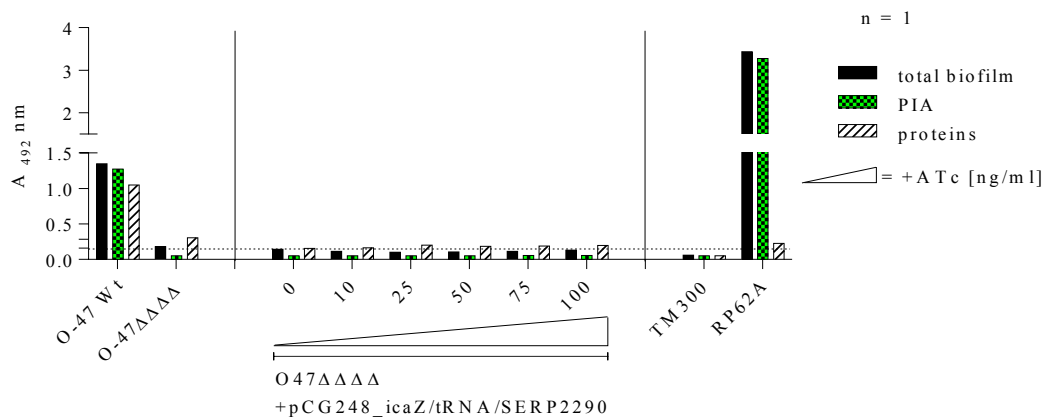
Fig. IV-18: IcaZ overexpression in *S. epidermidis* O-47$\Delta\Delta\Delta\Delta$

Biofilm assay was carried out in quadruplicate, but was not repeated, because the biofilm assays of the other strains (strain collection codes MF53, MF54 and MF59) showed no biofilm formation.

2.1.3 *S. epidermidis* O-47$\Delta icaZ$

In the background of the newly generated mutant, *icaZ* overexpression could not restore biofilm formation after induction by ATc (**Fig. IV-19 A**). This result differed from the results obtained from the triple mutant *S. epidermidis* O-47 $\Delta tRNA^{Thr-4}\Delta icaZ\Delta icaR$-3′ UTR (O-47$\Delta\Delta\Delta$), in which an increase of biofilm formation was measurable after induction of *icaZ* expression and in which also unspecific effects from the control plasmid were measured (chapter IV-2.1.1). To control if IcaZ is actually expressed in O-47$\Delta icaZ^2$+pCG248c_*icaZ*sML (strain collection code ML4), a Northern blot was carried out. The blot validated the massive production of ncRNA IcaZ after addition of ATc (**Fig. IV-19 B**).

A

B
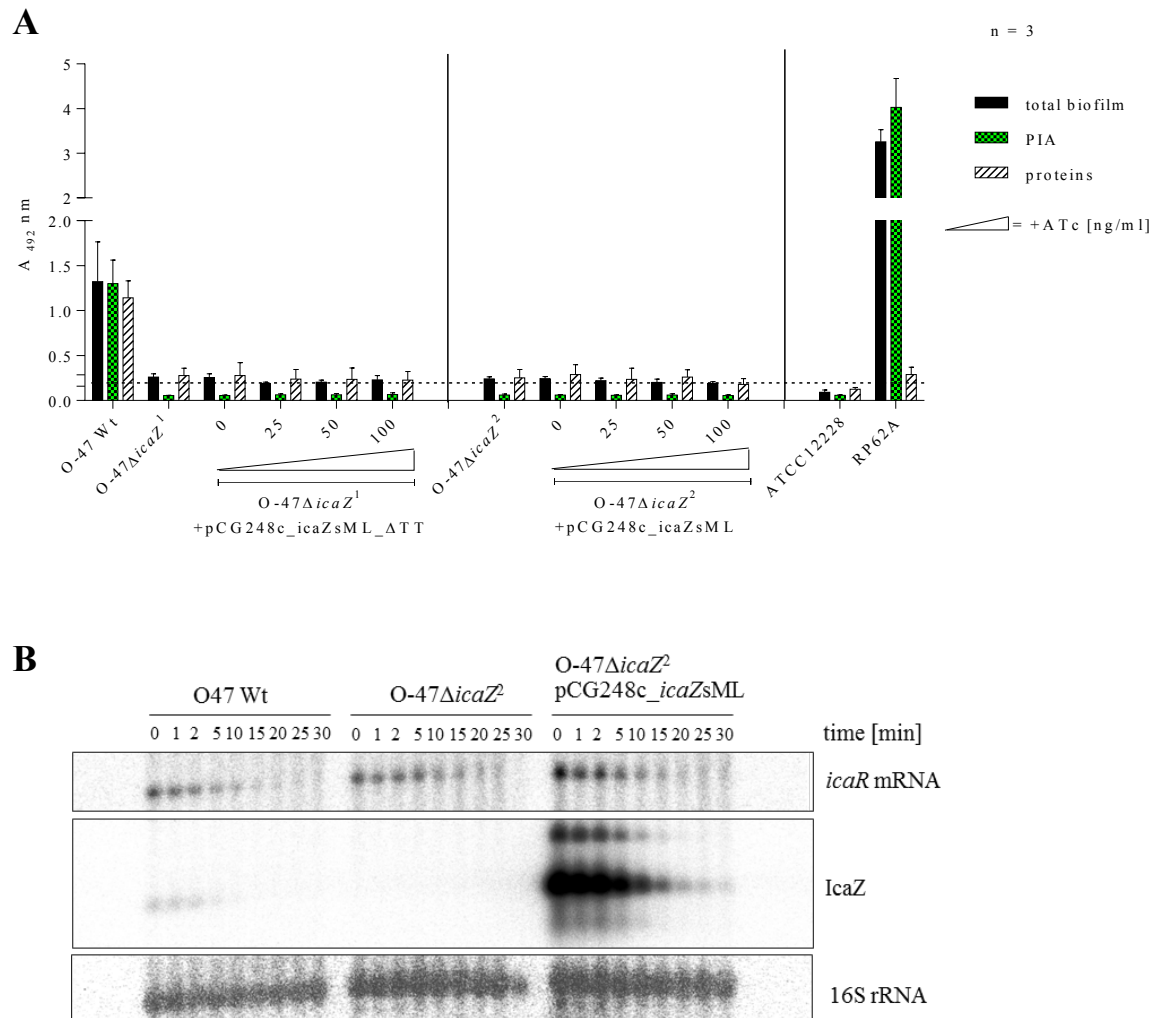
Fig. IV-19: IcaZ overexpression in *S. epidermidis* O-47ΔicaZ

(**A**) Crystal violet biofilm formation assay of *S. epidermidis* O-47 Wt, the mutants O-47Δ*icaZ*[1] (strain collection code ML38) and O-47Δ*icaZ*[2] (strain collection code ML2), the control strains RP62A and ATCC 12228, and the IcaZ overexpression strains O-47ΔicaZ[1]+pCG248c_*icaZ*sML_ΔTT (strain collection code ML80) and O-47ΔicaZ[2]+pCG248c_*icaZ*sML (strain collection code ML4) at 30°C. In both mutant strains, the same region is deleted. They were cloned independently from each other. (**B**) Rifampicin stability assay with total RNA of O-47 Wt, the mutant O-47Δ*icaZ*[2] (strain collection code ML2) and the IcaZ overexpression strain O-47ΔicaZ[2] +pCG248c_*icaZ*sML (strain collection code ML4) at 30°C. t_0 = probe sampling before addition of rifampicin in Wt and mutant; in strain ML4 10 min after ATc addition, but also before addition of rifampicin; t_{1-30} = probe sampling after addition of rifampicin. Detection of transcripts: detection of *icaR* mRNA was carried out with radioactively labelled ds-DNA probe (PCR product of primer IcaR_F and IcaR_R; 360 bp) and for IcaZ (PCR product of IGRica_for120 and IGRica_rev294; 175 bp); 16S rRNA was detected with radioactively labelled oligonucleotide S.epi16S-rrsA_for.

2.2 Effect of *in trans* IcaZ overexpression in *S. epidermidis* Wt strains

2.2.1 *S. epidermidis* PS2

S. epidermidis PS2 is a patient isolate that carries *icaZ-icaR-icaADBC* in its genome, but displays only a weak biofilm positive phenotype, mainly protein-mediated. In *S. epidermidis* PS2, the introduction of the plasmids pCG248_icaZs_ΔTT and pCG248_ΔTT led to an increase in biofilm formation, also without previous induction of IcaZ expression (0 ng/ml ATc). After addition of ATc, the biofilm formation increases strongly, especially PIA-mediated, but also in the control strain (**Fig. IV-20**), which again lacks the TT that was upstream of *repF* and *ori* pT181.
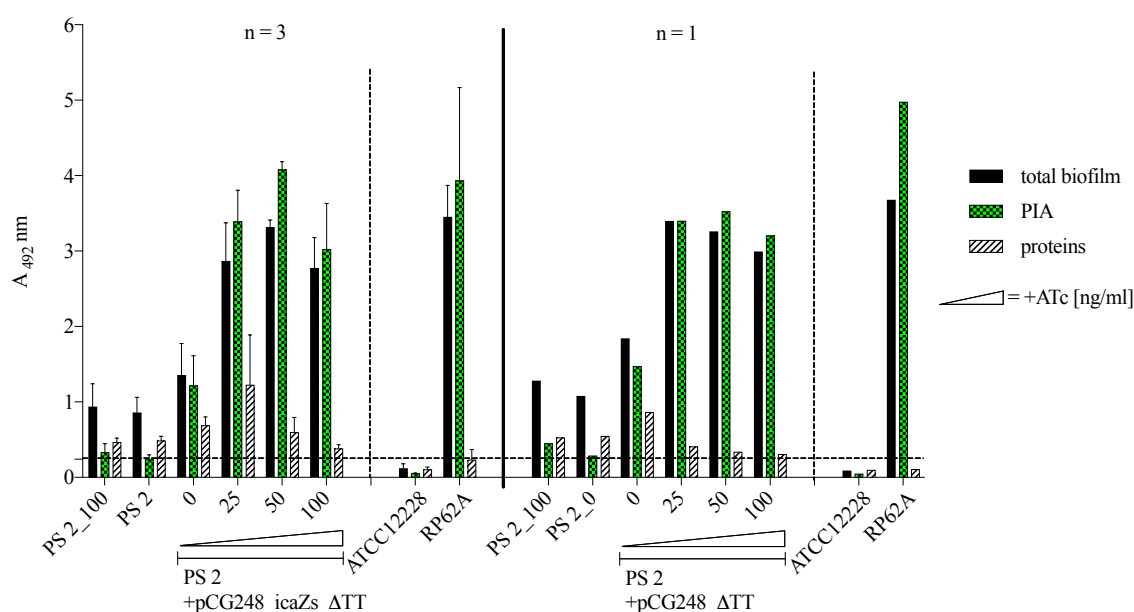
Fig. IV-20: IcaZ overexpression in *S. epidermidis* PS2

Crystal violet biofilm formation assay of *S. epidermidis* PS2, the IcaZ overexpression strains PS2+pCG248_icaZs_ΔTT (strain collection code ML63) and PS2 +pCG248_ΔTT (strain collection code CLA034) and the control strains RP62A and ATCC 12228 at 30°C. The effect of ATc on PS2 was also measured (PS2_100). ATc has no effect on the Wt strain.

2.2.2 *S. epidermidis* ATCC 12228 and Tü3298

In both *ica*-negative strains, *S. epidermidis* ATCC 12228 and Tü3298, the overexpression of IcaZ *in trans* had no effect on biofilm formation, not even an unspecific effect from the plasmid backbone (data not shown). This supports the fact that all PIA-biofilm observed before is indeed mediated by the *ica*-operon, which is absent in these strains.

2.2.3 *S. epidermidis 567 and 567-1*

S. epidermidis 567 is a clinical *icaADBC-* and *agrBDCA*-positive strain isolated from a catheter-related urinary tract infection. The derivate *S. epidermidis* 567-1 lacks an intact *agr* quorum sensing system, because P2 and P3 promoters had been exchanged to an erythromycin resistance cassette (Batzilla *et al.*, 2006). The adjacent genes *agrB* and *RNAIII* were also deleted in parts. Both strains were used to analyse biofilm formation after dose-dependent expression of *icaZ*. The assays revealed that with increased IcaZ production, more PIA (and thus total biofilm) was formed, whereas the protein part remained unchanged (**Fig. IV-21**). This effect was *agr*-independent.
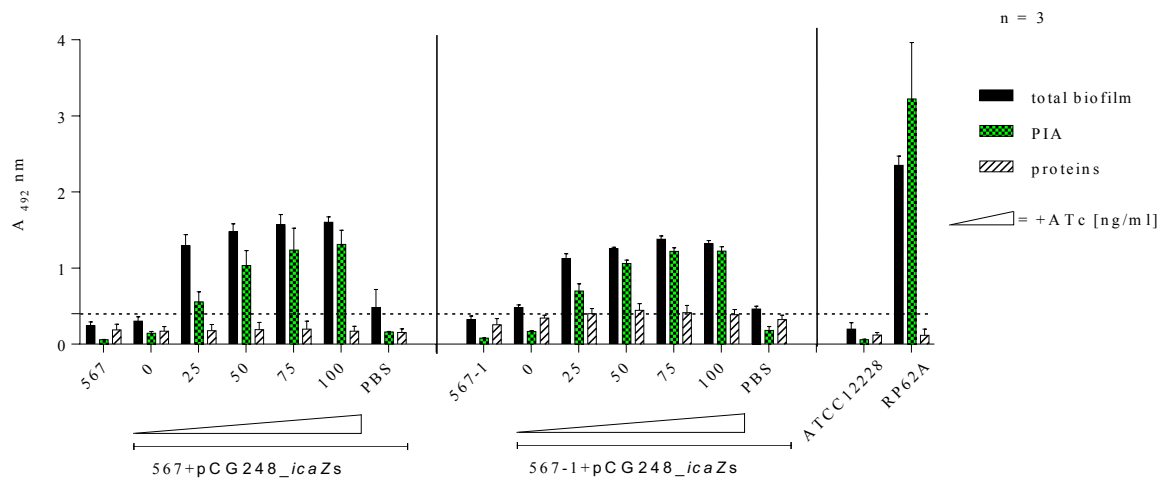
Fig. IV-21: IcaZ overexpression in *S. epidermidis* 567 and 567-1

> *S. epidermidis* 567 and 567-1 (strain collection codes H12 and H25; Batzilla *et al.*, 2006) were used to generate 567+pCG248_*icaZ*s (strain collection code ML14) and 567-1+pCG248_*icaZ*s (strain collection code ML15). Both strains carry an IcaZ-overexpression plasmid, but differ in the *agr*-system, because 567-1 is an *agr* mutant. The biofilm formation of these strains after IcaZ overexpression was analysed to decipher the influence of the *agr*-system.

2.2.4   *S. epidermidis O-47Δrnc*

IcaZ *in-trans* overexpression was analysed in *S. epidermidis* O-47Δ*rnc* strain, having natural *icaZ* expression but no RNase III enzyme. The controls (O-47 Wt and O-47Δ*rnc* with addition of ATc) verify that the addition of ATc itself has no influence on biofilm formation. Also, the overexpression of *icaZ* had no effect on biofilm production. Interestingly, the deletion of RNase III in O-47Δ*rnc* led to a slightly increased amount of proteins within the biofilm matrix, compared to O-47 Wt (**Fig. IV-22**).
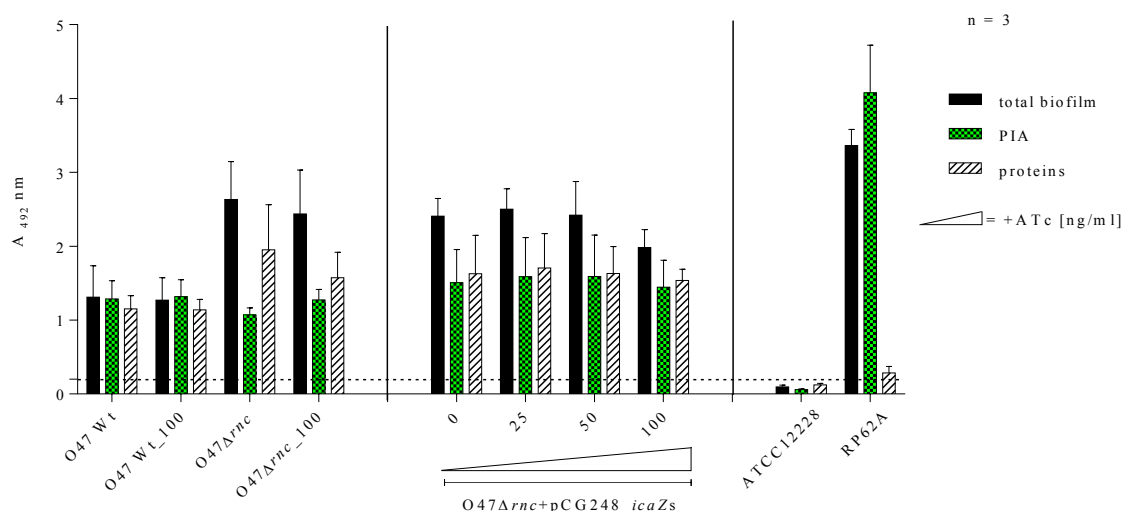
Fig. IV-22: IcaZ overexpression in *S. epidermidis* O-47Δ*rnc*

   Displayed are the results of three independently performed biofilm assays (n = 3) of *S. epidermidis* O-47 Wt, RNase III mutant O-47Δ*rnc* (strain collection code ML40), *icaZ* overexpression strain O-47Δ*rnc*+pCG248_*icaZ*s (strain collection code ML44) and the control strains RP62A and ATCC 12228.

2.3 Effect of *in trans* IcaZ overexpression in *S. aureus* Wt strains

IcaZ was overexpressed in *S. aureus* RN4220 Wt and Newman Wt to analyse, if IcaZ influences biofilm formation in *S. aureus*. In both strains IcaZ overexpression had no effect on biofilm formation. Strain Newman produced nearly no biofilm at all. Strain RN4220 had very minor biofilm production at 30°C (**Fig. IV-23**).
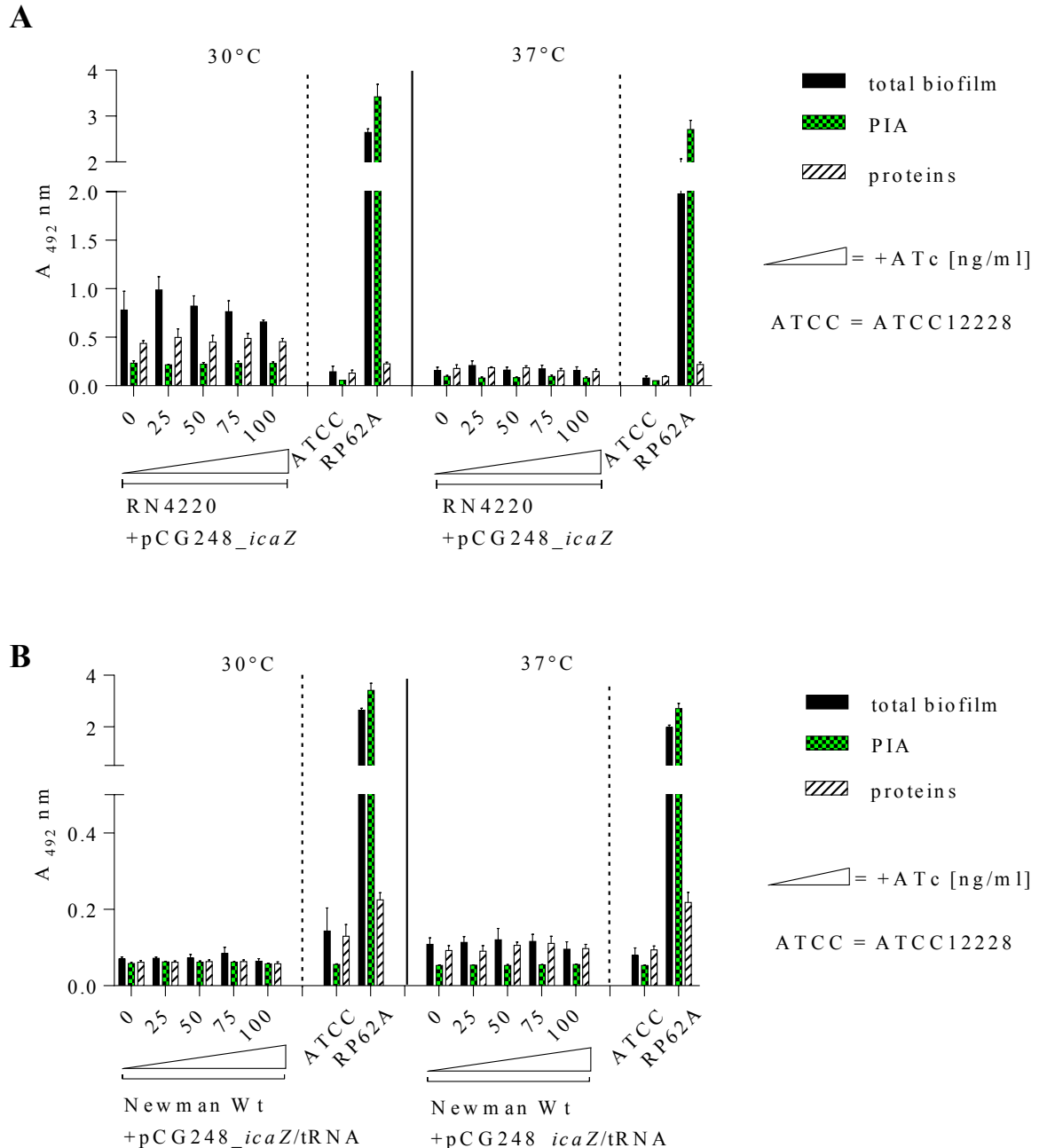
Fig. IV-23: Biofilm formation assays with *icaZ* overexpression in *S. aureus* strains

Strains were grown in TSB at 30° and 37°C. One biological sample in quadruple is depicted. (**A**) *S. aureus* RN4220+pCG248_*icaZ* (strain collection code JE4). (**B**) *S. aureus* Newman Wt+pCG248_*icaZ*/tRNA (strain collection code MF62).

2.4 Influence of site-directed mutagenesis within IcaZ sequence on biofilm formation in *S. epidermidis* O-47 Wt

Data of this work showed that the nucleotide sequence of IcaZ from *S. epidermidis* differs in four nucleotides to the sequence of *S. epidermidis* RP62A (nucleotides are highlighted in **Fig. III-12**). Initial biofilm formation assays with strains expressing either O-47-*icaZ* sequence or RP62A-*icaZ* sequence from the $P_{xyl/tet}$ inducible system of plasmid pCG248 let to hypothesise that RP62A-IcaZ is less functional than O-47-IcaZ, because biofilm formation could not be restored. To analyse this, the four nucleotides were mutated (**Tab. IV-3**) and biofilm assays were carried out, in which the total biofilm amount was measured. All strains showed similar biofilm formation, so that it is assumed that the mutated nucleotides have no relevance for the function of ncRNA IcaZ. But, it is to mention that the tested strains carried genomic IcaZ, while expressing the mutated form from the plasmid. Maybe a mutant background would be better for this analysis.

Tab. IV-3: List of plasmids

> *Plasmids contain O-47 *icaZ* gene sequence with additional nucleotides at the endings (14 bp upstream of *icaZ* TSS1 until 407 bp downstream of *icaZ* TSS1; cloned with BglII and XmaI into pCG248 vector backbone).

Host	Plasmid	Description	Strain collection code
O-47	pCG248_icaZs_G168T	ATc-inducible expression vector with *icaZ** gene incl. G168T mutation	ML31
	pCG248_icaZs_G168T+G196C	ATc-inducible expression vector with *icaZ** gene incl. G168T mutation and G196C mutation	ML32
	pCG248_icaZs_G168T+A323G	ATc-inducible expression vector with *icaZ** gene incl. G168T mutation and A323G mutation	ML33
	pCG248_icaZs_d251	ATc-inducible expression vector with *icaZ** gene incl. deletion of nucleotide pos. 251	ML34
	pCG248_icaZs	ATc-inducible expression vector with *icaZ** gene	ML35
	pCG248_icaZs_d251+A323G	ATc-inducible expression vector with *icaZ** gene incl. deletion of nucleotide pos. 251 and A323G mutation	ML36

3. Target identification and analysis by global approaches

The functional analysis also aimed at the identification of targets that are directly regulated or at least influenced indirectly by ncRNA IcaZ. A primary target is defined by Vogel and Wagner as an mRNA or protein with which the ncRNA physically interacts and whose function, stability or translation it affects. The ncRNA base pairs with the target, which is then translationally inhibited or degraded because of being bound by the antisense RNA. If the targeted mRNA encodes a protein that functions as a transcription factor that regulates downstream genes, the downstream effects are secondary and these affected downstream genes are not primary targets (Vogel and Wagner, 2007). For the identification and analysis of primary targets and secondary effects, several global approaches were conducted previously to and within this work (microarrays, transcriptomics from IcaZ pulse expression, proteomics).

The obtained data were analysed together with PD Dr Wilma Ziebuhr and served as initial step of target identification. In the following sections, the results of these investigations are summarised (see figure legends for author references).

3.1 Microarray analysis

Microarray analysis were carried out with *S. epidermidis* O-47 Wt and O-47ΔΔΔ to study the transcriptional differences after IcaZ deletion. The experiments were conducted previously to this work, so that the data were obtained and data analysis was done with the support of PD Dr Wilma Ziebuhr in the initial phase of this work.

Total RNA was isolated of early exponential phase cells (OD_{600} = 1.85-2.66) from *S. epidermidis* O-47 Wt and *S. epidermidis* O-47Δ*tRNA*$^{Thr-4}$Δ*icaZ*Δ*icaR*-3′ UTR at 30°C and 37°C by Dr Sonja Schönfelder. For each strain and each temperature, the RNA of three biological replicates was sampled. The RNA integrity number (RIN) that gave information about RNA quality was measured with Agilent Bioanalyzer after DNase treatment. RIN ranged from values of 8.6 till 9.5, signifying the RNA quality. 20 μg of DNA-free RNA were sent to the collaboration partners Prof Jacques Schrenzel and Dr Patrice Francois (Geneva). The obtained data were then pre-analysed and provided by PD Dr Wilma Ziebuhr (**Fig. IV-24**).

Differently regulated genes were sorted into pathways and the data revealed significant differences in the gene expression of the main metabolic pathways between Wt and IcaZ mutant (**Fig. IV-24 A**). As phenotypic analysis results showed that biofilm formation was influenced by *icaZ* deletion (**Fig. IV-7; Fig. IV-10; Fig. IV-13; Fig. IV-14**), pathways involved in the synthesis of biofilm components or cell wall synthesis were focused on and the regulator of the *ica*-operon, IcaR, was considered to be involved. **Fig. IV-24 B** depicts the selected differentially regulated genes between the strains with inclusion of the

temperature. Temperature independent was the absence of *aap* transcript in the mutant and the increased expression of *icaR*. Aap protein that is responsible for initial attachment to a surface (Buttner *et al.*, 2015) and IcaR, the repressor of *icaADBC* leading to diminished PIA synthesis, could both be the reason for the biofilm negative phenotype of the IcaZ mutant and were therefore possible targets for IcaZ.
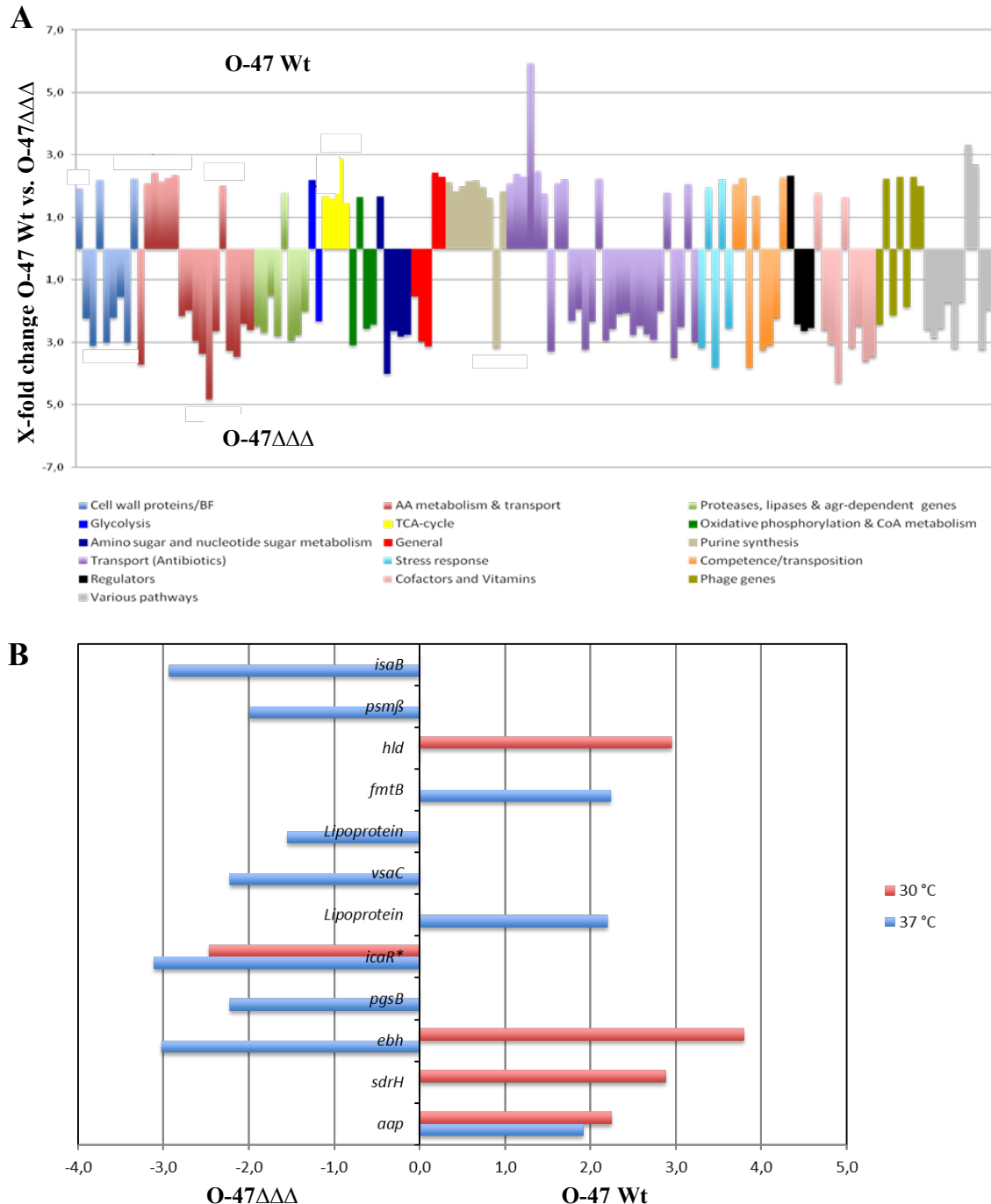
Fig. IV-24: Microarray analysis revealed significant differences in metabolic pathways

(**A**) X-fold change of differentially regulated genes sorted into metabolic pathways. (**B**) Selected genes upregulated in either Wt (positive axis) or IcaZ mutant *S. epidermidis* O-47Δ*tRNA^{Thr-4}*Δ*icaZ*Δ*icaR*-3′ UTR (abbreviated as O-47ΔΔΔ; strain collection code FL1Δ2; negative axis).

3.2 Proteome analysis

Proteome analysis was carried out in collaboration with group members of Prof Dr Susanne Engelmann previously to this work. Intracellular and extracellular proteins from exponential and stationary phase cells of *S. epidermidis* O-47 Wt and *S. epidermidis* O-47Δ*tRNA*$^{Thr-4}$Δ*icaZ*Δ*icaR*-3′ UTR (O-47ΔΔΔ) were sampled at 30°C and 37°C by Dr Sonja Schönfelder in 2011. For each strain, each growth phase and each temperature three biological samples were taken. The samples were sent to Prof Dr Susanne Engelmann in Greifswald, experiments were carried out by the technical assistant and data preparation was done by Swantje Reiß.

For the mutant strain two biological replicates and for the Wt strain three biological replicates were analysed. 12 single comparisons (A-L) and two control analysis (M-N) delivered insight into the expression of 385 identified proteins, which represented 67% of detected proteins (**Tab. IV-4**). Comparisons A and C revealed interesting facts about the protein expression in exponential growth phase at 37°C and 30°C. At 37°C, the protein contents of mutant and Wt were similar (Tab. IV-4 comparison A), but not at 30°C (Tab. IV-4 comparison C). **Fig. IV-25** displays the 2D gel images of comparison C.

Tab. IV-4: Overview of results from single comparisons from 2D gel data analysis

12 individual analysis and two control analysis were performed based on the 2D gels by Swantje Reiss. She listed the results in this table.

	comparison	strain	temp.	growth phase	Label 2x sig.	rep.	ind.	differences
A)	WT vs. Mut	compare	37°C	exp. phase	22	11 (WT)	11 (Mut)	no
B)	WT vs. Mut	compare	37°C	stat. phase	20	6 (WT)	14 (Mut)	no
C)	WT vs. Mut	compare	30°C	exp. phase	164	60 (WT)	104 (Mut)	**yes**
D)	WT vs. Mut	compare	30°C	stat. phase	5	3 (WT)	2 (Mut)	**no**
E)	37°C vs. 30°C	WT	compare	exp. phase	62	23 (37°C)	39 (30°C)	**some**
F)	37°C vs. 30°C	WT	compare	stat. phase	127	30 (37°C)	97 (30°C)	yes
G)	37°C vs. 30°C	Mut	compare	exp. phase	189	73 (37°C)	116 (30°C)	**yes**
H)	37°C vs. 30°C	Mut	compare	stat. phase	111	24 (37°C)	87 (30°C)	yes
I)	exp. vs. stat.	WT	37°C	compare	289	173 (exp.)	116 (stat.)	yes
J)	exp. vs. stat.	WT	30°C	compare	134	40 (exp.)	94 (stat.)	yes
K)	exp. vs. stat.	Mut	37°C	compare	296	194 (exp.)	102 (stat.)	yes
L)	exp. vs. stat.	Mut	30°C	compare	18	12 (exp.)	6 (stat.)	**no**
M)	WT (stat.) vs. Mut (exp.)		30°C		18	8 (WT)	10 (Mut)	**no**
N)	WT (stat.) vs. Mut (exp.)		37°C		303	105 (WT)	198 (Mut)	**yes**

A

B
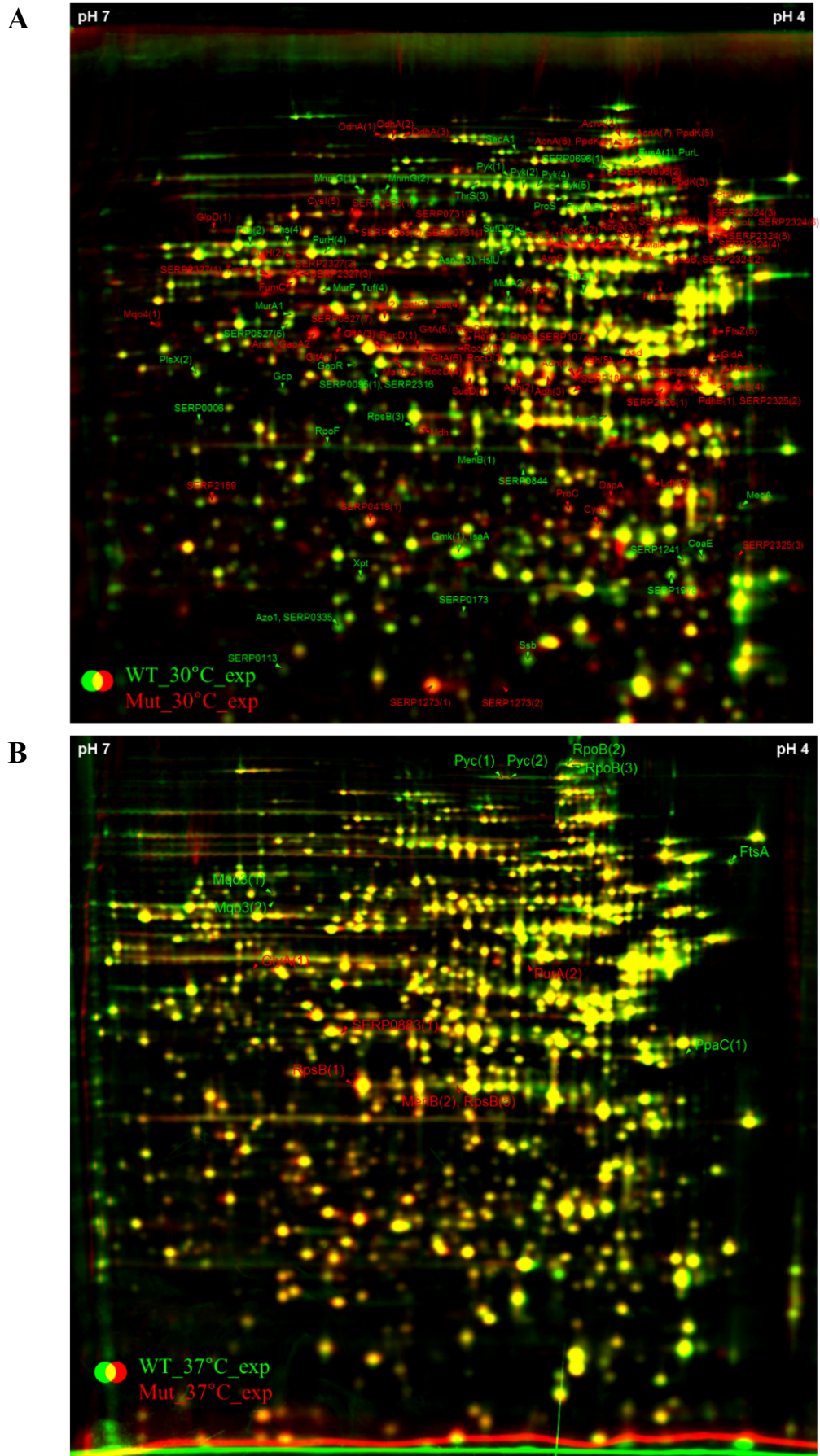
Fig. IV-25: 2D image of exponential phase proteins of O-47 Wt and O-47ΔΔΔ

Depicted are the 2D gel images (created by Delta2D – http://www.decodon.com) of exponential phase proteins from strains *S. epidermidis* O-47 Wt and O-47Δ*tRNA*$^{Thr-4}$ Δ*icaZ*Δ*icaR*-3′ UTR (O-47ΔΔΔ) at 30°C (**A**) and 37°C (**B**). Upregulated proteins in the Wt are marked in green; upregulated proteins in the mutant are marked in red. The images were kindly provided by Swantje Reiß.

Comparison C compared proteins of exponential phase at 30°C between Wt and IcaZ mutant and was therefore most striking. 116 of 164 picked proteins that were either two-fold induced or repressed could be identified (**Annexe Tab. VIII-2**). Upregulated genes were mapped to Kegg pathways using online platform (http://www.genome.jp /kegg/tool/map_pathway2.html). The proteome profile of O-47 Wt showed that peptidoglycan synthesis and purine metabolism were upregulated, indicating DNA replication and growth of the bacteria. These results matched protein expression patterns typical for the exponential growth phase. Surprisingly, in the mutant, almost all proteins of the TCA cycle and other stationary phase proteins were expressed at exponential growth phase.

Carbons are mainly used for peptidoglycan synthesis that is necessary for growth during the exponential growth phase. The TCA cycle is then downregulated and any carbon excess is directed to the overflow metabolism resulting in the production and export of lactate and acetate. In stationary growth phase, when nutrients become scarce, the overflow products are reimported and used for energy and metabolite production. The TCA cycle is then upregulated (**Annexe Fig. VIII-5**). Conclusively, the proteomic data revealed an abnormal exponential phase proteome for the mutant. The results from microarrays and proteomics were summarized in **Fig. IV-26** and raised the following questions. Why does the IcaZ mutant display this abnormal proteome profile in the exponential growth phase? Is the mutant restricted in growth? The latter question was answered by Tecan growth analysis and, indeed, the growth curves of the mutant showed slightly decreased growth when compared to the Wt. This led to suggest a defect in sugar sensing or the involvement of a master regulator like CcpA. The impact of different glucose concentrations on *icaZ* promoter expression was therefore tested in this work (see chapter V-3 for further details).
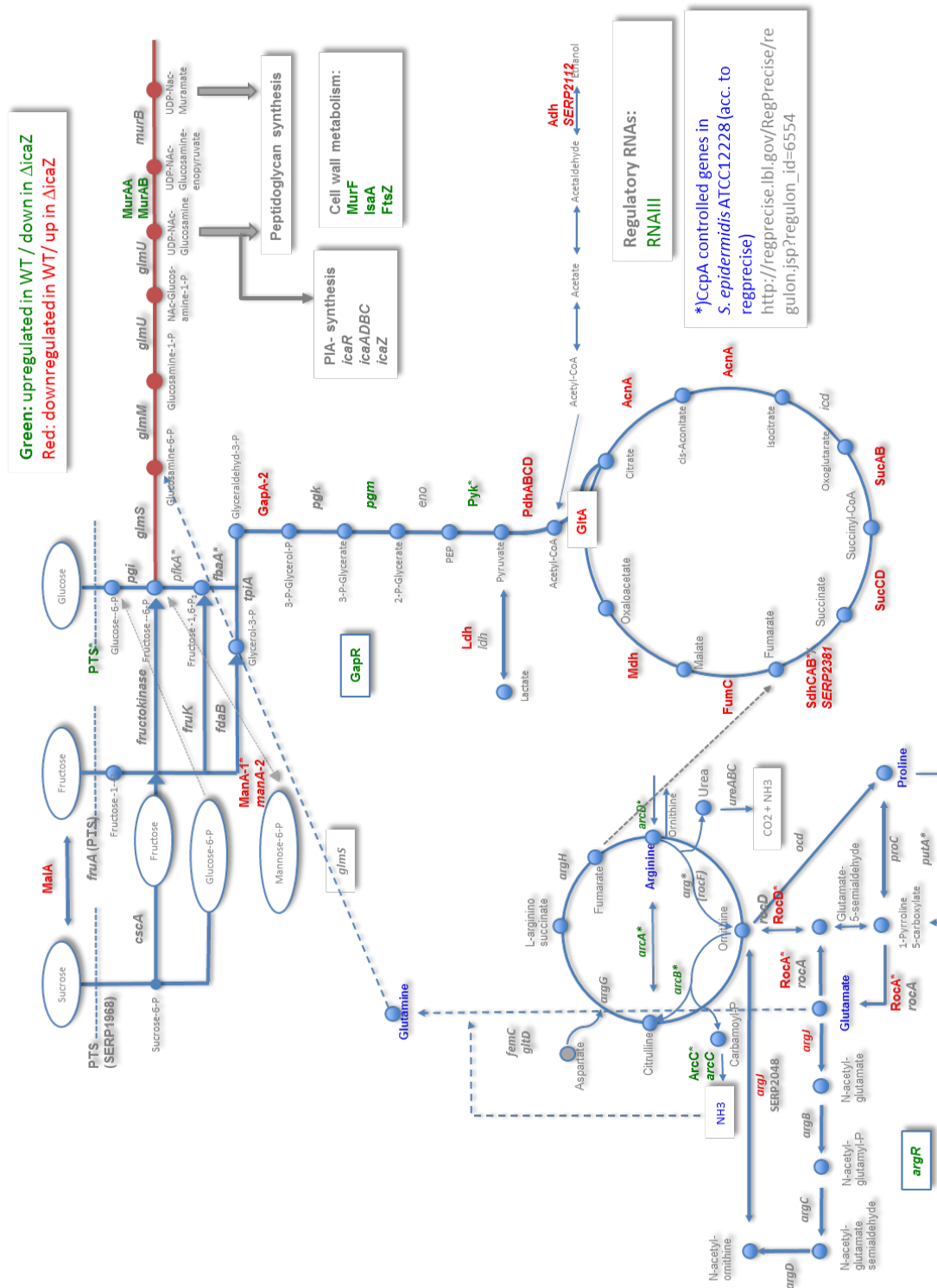
Fig. IV-26: Transcriptome and proteome of *S. epidermidis* O-47 Wt and O-47ΔΔΔ at 30°C in the exponential growth phase

The scheme displays the results from transcriptomic and proteomic analysis of O-47 Wt and O-47ΔΔΔ at 30°C in the exponential growth phase. It was created and provided by PD Dr Wilma Ziebuhr. The main metabolic pathways for the use of carbons are shown (*i.e.* glycolysis, TCA cycle). Genes and enzymes coloured in green are upregulated in the Wt. When coloured in red, then they are upregulated in the mutant.

3.3 Pulse expression analysis

Transcriptome and proteome data gave information on the metabolism of *S. epidermidis* Wt and IcaZ mutant, but since the Wt is a biofilm forming strain and the mutant lacks biofilm formation, it was difficult to associate the data with putative direct interaction partner of IcaZ. A direct fishing method was therefore pursued to identify interaction partners or give at least some hints on the regulatory network(s) IcaZ might be involved in. Thus, pulse-expression of IcaZ followed by RNA-sequencing was therefore performed in collaboration with Prof Cynthia Sharma's laboratory.

The pCG248 vector system was chosen for IcaZ overexpression. Plasmid pCG248_*icaZ*/tRNA that was used for biofilm assays before, was used for pulse expression of IcaZ. The plasmid is an ATc-inducible expression vector that contains IGRica-RNA + 6 nt, tRNA^{Thr-4} and P$_{tRNAThr-4}$. The strain *S. epidermidis* O-47ΔtRNA^{Thr-4}$\Delta icaZ\Delta icaR$-3' UTR +pCG248_icaZ/tRNA (strain collection code JE13) was grown under static conditions at 30°C until exponential growth phase. Static conditions were chosen in this experiment to mimic biofilm forming conditions *e.g.* to allow the bacteria to adhere to a surface (the flask bottom). The temperature was chosen, because IcaZ expression and biofilm formation were shown to be increased at 30°C, in comparison to 37°C. Also, the proteome data of exponential growth phase showed the most differences in gene expression at 30°C. These conditions should provide the best opportunities for expression of both, the potential targets and IcaZ.

IcaZ expression was induced for 10 min in the treated sample and non-induced in the reference sample (chapter II-6.6.2). Total RNA was isolated and the expression was validated by Northern blot (**Annexe Fig. VIII-10**). After rDNaseI-treatment, the quality of the DNA-free RNA was checked with Agilent 2100 Bioanalyzer (**Annexe VIII-11**). Set 1 was used for subsequent RNA-sequencing analysis, because of the very good quality measured through the RIN number of each RNA sample. RNA-sequencing data files and the statistical analysis were prepared and provided by Dr Konrad Förstner for further analysis. The volcano plot depicts the points-of-interest, which are transcripts having a large magnitude of fold change and high statistical significance (**Fig. IV-27**). The reads were sorted for their p-value and then for log$_2$ fold change (**Tab. IV-5**). The first three hits are *icaZ, tRNA^{Thr-4}* and 'SERP2290' transcripts; their high read numbers can be explained due to the plasmid copy number. Data files were visualised with the programme '*Integrated Genome Browser*' (IGB) and aligned to the reference sequence of *S. epidermidis* RP62A. Up- and downregulated genes were then analysed.
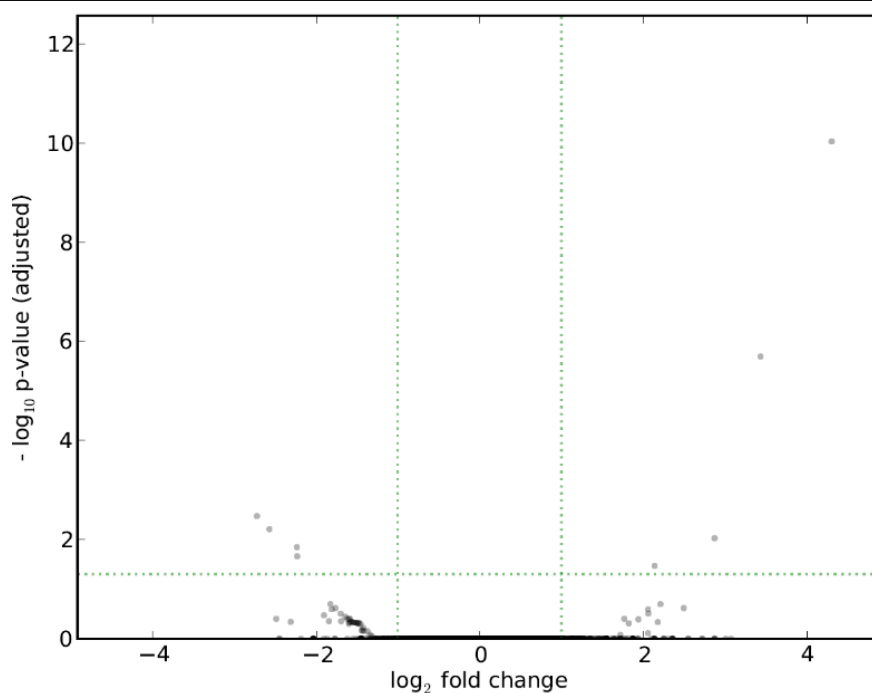
Fig. IV-27: Volcano plot for pulse expression data

Uninduced sample versus induced sample. The upper right and left corner contain the points-of-interest. Each point displays a transcript having large magnitude fold-change (x axis) and high statistical significance (y axis). The horizontal dashed line shows where p = 0.05. Points above the line have p < 0.05 and are therefore statistically relevant.

Most of the hits show genes, which code for hypothetical proteins. Interestingly, an antisense transcript to *eno*, the gene coding for enolase, was upregulated (**Fig. IV-28 A**). The increased expression of *eno* antisense transcript could lead, because of base pairing of the transcript with *eno* mRNA, to the sequestration of *eno* mRNA and thus to a reduced number of transcripts. Translation of *eno* mRNA would be decreased, so that enolase enzyme would be diminished. Enolase is an important enzyme in the metabolic pathway glycolysis that catabolizes reactions in both directions. If this enzyme is diminished, the carbons could not be introduced into the TCA cycle, but could be used instead for PIA production (**Fig. IV-28 B**, indicated by black arrow). The gene *eno* is part of an operon encoding glycolysis enzymes. RNA sequencing data also showed a second antisense transcript, which could inhibit *gapA* and *pgk* mRNA (**Fig. IV-28 A**). *gapA* is the first gene of the operon and encodes the glyceraldehyde-3-phosphate dehydrogenase (GAPDH). This key glycolytic enzyme facilitates the oxidative phosphorylation of glyceraldehyde-3-phosphate to 1,3-diphosphoglycerate during glucose metabolism. The inhibition of the glycolysis pathway and a shifting of carbohydrates instead towards PIA synthesis, would explain the biofilm results of *icaZ* overexpression strains (chapter IV-2).

Tab. IV-5: List of reads with x-fold change after *icaZ* pulse expression

Reads were mapped to the reference genome of *S. epidermidis* RP62A (NC_002976.3).

After *icaZ* expression	Orientation of counted reads relative to the strand location of the annotation	Sequence name	Feature	Start	End	Strand	Fold Change	log2 Fold Change	p-value	YP_number	SERP_number	Function
up	anti-sense	NC_002976.3	CDS	2332514	2332627	+	30,24	4,92	5,20417E-17	YP_189840.1	SERP 2290	hypothetical protein
	anti-sense	NC_002976.3	tRNA	2332647	2332739	+	19,76	4,30	3,61434E-14		-	-
	sense	NC_002976.3	CDS	2332514	2332627	+	10,82	3,44	1,17925E-09	YP_189840.1	SERP 2290	hypothetical protein
	sense	NC_002976.3	CDS	1653965	1655344	+	7,32	2,87	1,08738E-05	YP_189192.1	SERP1627	hypothetical protein
	anti-sense	NC_002976.3	CDS	451418	452722	+	4,40	2,14	5,90555E-05	YP_188039.1	SERP 0446	Enolase
down	sense	NC_002976.3	CDS	2217830	2218135	-	0,21	-2,23	3,37733E-05	YP_189740.1	SERP 2184	hypothetical protein
	sense	NC_002976.3	CDS	918967	919068	+	0,21	-2,24	1,92736E-05	YP_188487.1	SERP 0908	hypothetical protein
	anti-sense	NC_002976.3	CDS	1910009	1910335	+	0,17	-2,57	5,95377E-06	YP_189447.1	SERP 1886 - SERP 1887	SugE protein
	sense	NC_002976.3	CDS	1909922	1910014	-	0,15	-2,72	2,6069E-06	YP_189446.1	SERP 1885	hypothetical protein

A

B
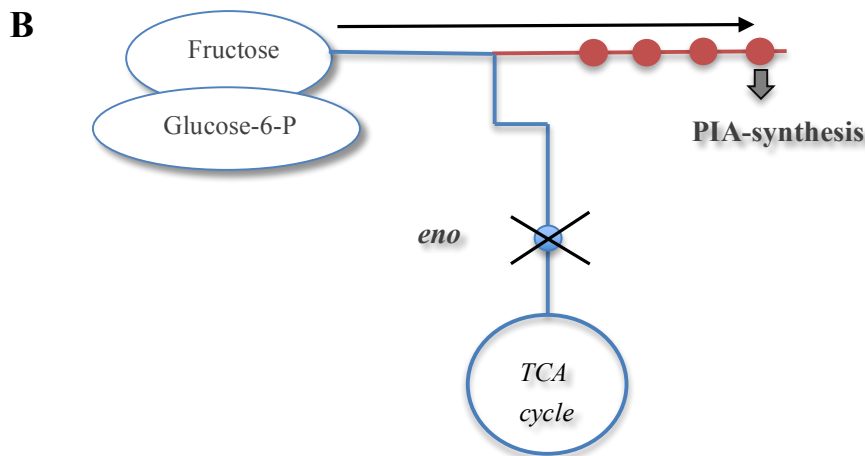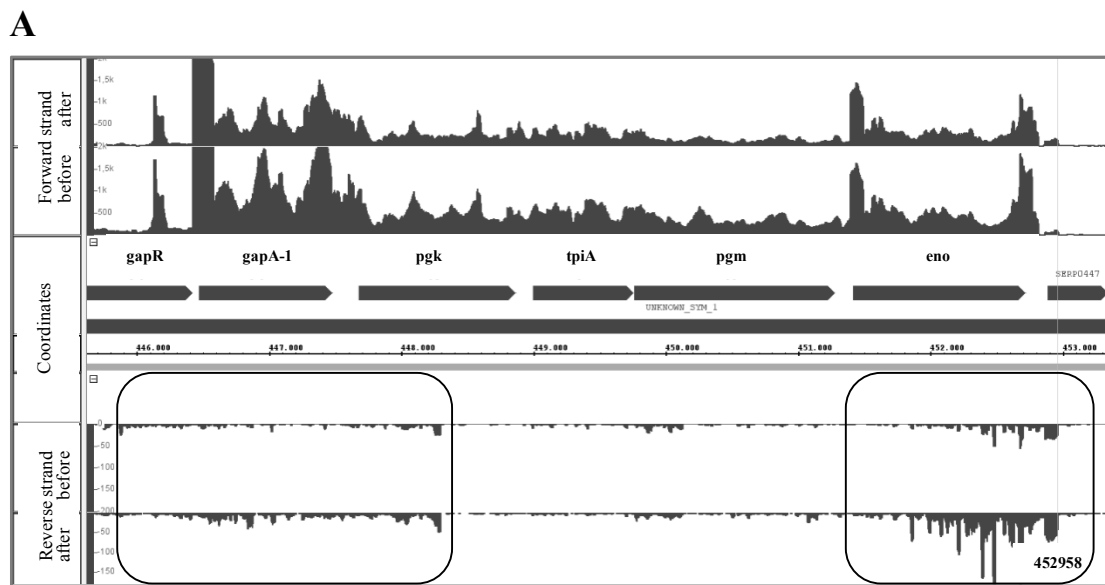
Fig. IV-28: Enolase antisense transcript enriches after IcaZ pulse expression

(**A**) IGB screenshot. Depicted are the transcripts of the *gap*-operon before and 10 min after IcaZ pulse expression. (**B**) Schematic depiction of the pathways shown in Fig. IV-26. Localisation of enolase in glycolysis metabolic pathway. Enolase-antisense transcript could sequester enolase mRNA, leading to reduced Enolase enzymes (cross). Carbons cannot be used by glycolysis and could be used for PIA synthesis instead (arrow).

3.4 Bioinformatical target predictions

As IcaZ is assumed to be a regulatory RNA and could regulate other RNAs by base pairing, bioinformatic analysis was carried out to determine possible interaction partners of IcaZ. For that, several programmes were used (*e.g. TargetRNA2*, *IntaRNA*, *RNApredator*). *TargetRNA2* and *RNApredator* are web based programmes that calculate optimal hybridisation scores for sRNA–target RNA hybrids. A ranking list of candidate mRNAs is then given by the programmes (Vogel and Wagner, 2007). In this work, both sequences (RP62A-IcaZ and O-47-IcaZ) were blasted against *S. epidermidis* RP62A genome to find putative interaction partners, because a full genome of O-47 was not available. The results are listed in **Tab. IV 6** and by using *IntaRNA*, the following mRNAs showed an interaction with IcaZ (**Tab. IV-8**). The candidates were then tested by EMSA (chapter V-1.1.1). *icaR* mRNA as interaction partner was most promising, because four interaction sites with IcaZ were predicted. Latest predictions using the RNA sequences of IcaZ and *icaR* 5′ 3′ UTR fusion product revealed further interaction sites than the aforesaid mentioned. By using the STRING network, it was analysed with which other proteins the predicted interaction partner of IcaZ interact or are co-expressed. Thereby, the genes SERP1897, SERP1126 and SERP0959 encoding hypothetical proteins may be are related to sugar metabolism (hits 2,3 and 8 of Tab. IV-6).

Tab. IV-6: Predicted interaction partners by programme *TargetRNA2*

O-47-IcaZ sequence or RP62A-IcaZ sequence was blasted against *S. epidermidis* RP62A genome. The settings were: 80 nt before start codon and 20 nt after; seed length 7 nt; sRNA window size 13 nt; interaction region 20 nt; filter size 400 and p-value 0.05. The hits are ranked with decreasing energy. STRING network was used to find functional partners of the interaction partners of IcaZ (marked with *).

Input	Rank	Synonym	Energy	Pvalue	sRNA_start	sRNA_stop	mRNA_start	mRNA_stop	Function	Predicted Functional Partners*
RP62A-IcaZ	1	SERP1867	-10.75	0.016	246	258	-60	-47	Hypothetical protein (44 aa)	SERP1866
O-47-IcaZ (also RP62A)	2	SERP1897	-10,02	0.023	255	261	-41	-32	Hypothetical protein (111 aa)	murQ; SERP1900 (PTS system); SERP1901 (RpiR family phosphosugar binding transcriptional regulator)
O-47-IcaZ (also RP62A)	3	SERP1126	-9,61	0.028	246	259	-35	-22	Hypothetical protein (229 aa)	SERP1313 (polysaccharide biosynthesis protein), SERP1125, cshB, nfo, sigA, SERP0835, addB, addA, mrnC, dnaG
O-47_IcaZ (also RP62A)	4	SERP1003	-9,41	0.031	248	259	-79	-68	thyA (Thymidylate synthase, 318 aa)	folA, folA-2, tdk, tmk, ComE, glyA, SERP0035, folD, gcvT, nrdF-2
RP62A-IcaZ	5	SERP0894	-9,03	0.037	208	225	-22	-6	Hypothetical protein (41 aa)	SERP0893, SERP0895
O-47-IcaZ (also RP62A)	6	SERP0219	-8.89	0.039	244	259	-79	-63	vraA (Long chain fatty acid CoA ligase, 453 aa)	fruA; SERP0414 (Glycosyl transferase); icaB
O-47-IcaZ (also RP62A)	6	SERP1351	-8,89	0.039	208	219	5	16	Hypothetical protein (302 aa)	SERP1350, metK
O-47-IcaZ (also RP62A)	7	SERP1646	-8,69	0.042	207	218	-17	-6	Hypothetical protein (153 aa)	SERP1640-1645, SERP1647, xhlB, SERP1649
O-47-IcaZ (also RP62A)	8	SERP0959	-8,59	0.044	245	259	-48	-34	Phosphate ABC transporter permease; Part of the binding-protein-dependent transport system for phosphate; probably responsible for the translocation of the substrate across the membrane (308 aa)	SERP0958, pstS, pstB, SERP0956, SERP2358, SERP2031, SERP0385, SERP1498, walR; srrA
O-47-IcaZ (also RP62A)	9	SERP0920	-8,55	0.045	208	219	5	16	Choline/carnitine/betaine transporter (546 aa)	mscL, betA

Tab. IV-7: Results of *RNApredator*

IcaZ sequence of *S. epidermidis* O-47 was blasted against RP62A genome (NC_002976).

Select	Rank	Energy [kJ/mol]	z-Score	Interaction [dot-bracket]	mRNA [Start]	mRNA [End]	sRNA	Gene Annotation	Locus Tag	Strand	Genomic Coordinates	Accession	Replicon
☐	1.	-26.56	-4.75	(dot-bracket)	-174	-145	22-51	hypothetical protein SERP2291	SERP2291	+	2333071-2333378	NC_002976	chromosome
☐	2.	-23.73	-4.08	(dot-bracket)	-151	-124	1-28	hypothetical protein SERP2291	SERP2291	+	2333071-2333378	NC_002976	chromosome
☐	3.	-21.12	-3.45	(dot-bracket)	-194	-166	43-71	hypothetical protein SERP2291	SERP2291	+	2333071-2333378	NC_002976	chromosome
☐	4.	-17.12	-2.49	(dot-bracket)	2078	2097	208-229	penicillin binding protein 2	SERP1020	+	1063649-1066060	NC_002976	chromosome
☐	5.	-16.76	-2.41	(dot-bracket)	270	287	175-192	glycosyl transferase; group 1 family protein	SERP1028	-	1075673-1074331	NC_002976	chromosome
☐	6.	-16.69	-2.39	(dot-bracket)	-194	-170	158-178	transcriptional regulator; putative	SERP0247	+	256169-256938	NC_002976	chromosome
☐	7.	-16.45	-2.33	(dot-bracket)	21	43	63-85	hypothetical protein SERP0337	SERP0337	-	339502-338622	NC_002976	chromosome
☐	8.	-16.15	-2.26	(dot-bracket)	-198	-169	63-88	cell wall surface anchor family protein	SERP2162	+	2191298-2192088	NC_002976	chromosome
☐	9.	-15.86	-2.19	(dot-bracket)	-132	-104	236-263	cobalamin synthesis protein; putative	SERP0080	+	67169-68571	NC_002976	chromosome
☐	10.	-15.85	-2.19	(dot-bracket)	151	164	251-264	hypothetical protein SERP1772	SERP1772	+	1816231-1816691	NC_002976	chromosome
☐	11.	-15.71	-2.16	(dot-bracket)	18	45	307-335	CBS domain containing protein	SERP0507	+	493671-494896	NC_002976	chromosome
☐	12.	-15.68	-2.15	(dot-bracket)	-153	-137	247-263	hypothetical protein SERP0472	SERP0472	-	472878-472490	NC_002976	chromosome
☐	13.	-15.52	-2.11	(dot-bracket)	-127	-110	158-174	hypothetical protein SERP1833	SERP1833	-	1862865-1862552	NC_002976	chromosome
☐	14.	-15.50	-2.1	(dot-bracket)	500	510	253-263	cobalt transport family protein	SERP0660	-	656608-655569	NC_002976	chromosome
☐	15.	-15.36	-2.07	(dot-bracket)	77	105	160-187	truncated IS1272 transposase	SERP0638	-	632752-632421	NC_002976	chromosome
☐	16.	-15.32	-2.06	(dot-bracket)	253	272	166-184	hypothetical protein SERP1771	SERP1771	-	1816454-1815745	NC_002976	chromosome
☐	17.	-15.23	-2.04	(dot-bracket)	292	311	176-195	major facilitator family transporter	SERP0025	-	22353-20789	NC_002976	chromosome
☐	18.	-15.21	-2.04	(dot-bracket)	-158	-144	158-172	secretory antigen precursor SsaA related protein	SERP2120	+	2144422-2145053	NC_002976	chromosome
☐	19.	-15.08	-2	(dot-bracket)	877	898	176-197	CRISPR associated Csm4 family protein	SERP2458	-	2513169-2512055	NC_002976	chromosome
☐	20.	-15.08	-2	(dot-bracket)	-183	-162	241-262	sulfate permease family protein	SEA0024	-	21256-19505	NC_006663	plasmid pSERP
☐	21.	-15.05	-2	(dot-bracket)	193	212	153-172	universal stress protein	SERP2220	+	2256802-2257433	NC_002976	chromosome
☐	22.	-15.05	-2	(dot-bracket)	401	420	299-319	DNA processing protein DprA; putative	SERP0815	+	818535-819607	NC_002976	chromosome

Tab. IV 7: Results of *RNApredator* (*continued*)

#			Structure				Annotation	Gene	Strand	Coordinates	Accession	Location
23.	-15.02	-1.99	(((((((((((...(&.))))))))))))	-146	-132	246-260	phosphopantothenoylcysteine decarboxylase/phosphopantothenate cysteine ligase	SERP0778	+	776424-777823	NC_002976	chromosome
24.	-14.97	-1.98	((((((((((&.))))))))))	-135	-124	249-260	hypothetical protein SERP0615	SERP0615	-	610609-610224	NC_002976	chromosome
25.	-14.92	-1.97	(((((.(((((&.))))))))))	510	524	251-264	hypothetical protein SERP0809	SERP0809	-	813959-811159	NC_002976	chromosome
26.	-14.64	-1.9	((...(((((.(.(((((((((&.))))))))).).)))))).))	-149	-121	160-187	acetyltransferase	SERP0637	-	632526-631904	NC_002976	chromosome
27.	-14.64	-1.9	(((((((.(((((((((&.)))))))))).))))))	421	442	5-26	N acetylglucosamine 6 phosphate deacetylase	SERP0360	+	359064-360436	NC_002976	chromosome
28.	-14.63	-1.9	(((((((((((.....(((((((&.))))))...)))))))).))))	-166	-141	155-180	thermonuclease precursor family protein	SERP0891	+	902867-903603	NC_002976	chromosome
29.	-14.63	-1.9	(((((((.(((((((((&.))))))))).))))))	472	488	166-182	hypothetical protein SERP0276	SERP0276	-	282583-281490	NC_002976	chromosome
30.	-14.57	-1.88	(((((((.((((((((((((&.))))))))))))))))))	-34	-14	163-182	hypothetical protein SERP0512	SERP0512	+	499346-499935	NC_002976	chromosome
31.	-14.54	-1.87	(((((((((((&.)))))))))))	566	578	251-263	cell division protein FtsA	SERP0750	+	748046-749640	NC_002976	chromosome
32.	-14.45	-1.85	((...((((((((((&.)))))))))).))	189	206	167-182	arsenical pump membrane protein	SERP2430	+	2487850-2489339	NC_002976	chromosome
33.	-14.41	-1.84	(((((((.(((((((((&.))))))))))))))	-182	-164	247-262	hypothetical protein SERP0280	SERP0280	-	283419-283013	NC_002976	chromosome
34.	-14.39	-1.84	(((((.(((.(((((((((&.)))))))))).)))).))))	-55	-42	152-175	ribonuclease III	SERP0799	+	798390-799327	NC_002976	chromosome
35.	-14.37	-1.83	((((((.(((((((((((&.)))))))))...))))))	227	247	149-171	50S ribosomal protein L5	SERP1819	-	1856722-1855963	NC_002976	chromosome
36.	-14.34	-1.83	(((.((.(((((((((&.))))))))).))))	168	185	167-183	OsmC/Ohr family protein	SERP1286	+	1329853-1330493	NC_002976	chromosome
37.	-14.30	-1.82	(((((((((((....((&.))))))))).)))))	193	216	151-172	universal stress protein	SERP2220	+	2256802-2257433	NC_002976	chromosome
38.	-14.29	-1.82	(((.((((.((((.-((((((((((&.))))))))).)))).))))	-175	-150	163-184	adhesion lipoprotein; putative	SERP2081	-	2109235-2108088	NC_002976	chromosome
39.	-14.22	-1.8	(((((((((((&.))))))))))	458	468	250-260	hypothetical protein SERP2199	SERP2199	-	2233652-2232343	NC_002976	chromosome
40.	-14.19	-1.79	((.(((((((.((((((((((&.)))))).)))))).))))))	-130	-110	210-229	hypothetical protein SERP0351	SERP0351	-	352264-351447	NC_002976	chromosome
41.	-14.08	-1.76	(((((((((...(((.((&.))).)..))).))))))))	-198	-176	242-263	hypothetical protein SERP1306	SERP1306	+	1355833-1356347	NC_002976	chromosome
42.	-14.02	-1.75	(((((((((.((((.(((((((((&.)))))).)))).)))))...))))))	933	961	152-180	iron compound ABC transporter; permease protein	SERP1775	-	1820172-1819007	NC_002976	chromosome
43.	-14.02	-1.75	((((((((((&.))))))))))	27	40	218-231	HAD superfamily hydrolase	SERP0740	+	736752-737638	NC_002976	chromosome
44.	-13.87	-1.71	((((((---(((((((.(((((((((&.))).)))))))))))))))))))	541	569	158-183	hypothetical protein SERP0106	SERP0106	-	91339-90027	NC_002976	chromosome
45.	-13.82	-1.7	(((((.((((.-(((((((.-((((.((((&.))).))))))))))))).))))	322	351	162-189	hypothetical protein SERP1471	SERP1471	-	1537402-1536645	NC_002976	chromosome

Tab. IV 7: Results of *RNApredator* (*continued*)

Select	Rank	Energy [kJ/mol]	z-Score	Interaction [dot-bracket]	mRNA [Start]	mRNA [End]	sRNA	Gene Annotation	Locus Tag	Strand	Genomic Coordinates	Accession	Replicon
☐	46.	-13.80	-1.7	(((((((((((((((((((((((((((((((&)))))))))))....))))))))))	815	837	326-353	anthranilate phosphoribosyltransferase	SERP0939	+	955856-957051	NC_002976	chromosome
☐	47.	-13.79	-1.7	(((((((((((((((((((((((((&)))))))))).)))).))))).))	-77	-52	158-184	hypothetical protein SERP1897	SERP1897	+	1918892-1919427	NC_002976	chromosome
☐	48.	-13.78	-1.69	(((((((.....(((((((.((((((&))))))..))))).))))))))	-183	-156	158-181	penicillin V acylase; putative	SERP0227	-	236799-235619	NC_002976	chromosome
☐	49.	-13.78	-1.69	((((((((((((&)))))))))))))	247	258	251-262	gufA protein; putative	SERP0382	-	381338-380323	NC_002976	chromosome
☐	50.	-13.78	-1.69	((((((..((((((((&.)))))))..))))))	-159	-142	155-172	pyrroline 5 carboxylate reductase	SERP1065	+	1109203-1110218	NC_002976	chromosome
☐	51.	-13.76	-1.69	(((((((((((&.))))))))))))	445	455	175-185	O succinylbenzoic acid CoA ligase	SERP1358	-	1415882-1414258	NC_002976	chromosome
☐	52.	-13.75	-1.69	(((((((..((((&)))).))))))))	-139	-125	246-260	aldehyde dehydrogenase	SERP1456	+	1521551-1523130	NC_002976	chromosome
☐	53.	-13.73	-1.68	(((.-((((((((((&)))))))))))...))	136	153	167-185	hypothetical protein SERP0569	SERP0569	-	563341-562770	NC_002976	chromosome
☐	54.	-13.72	-1.68	(((((((((((((&)))))))).))).))))))))	-137	-122	164-180	fibronectin/fibrinogen binding protein	SERP0775	-	775180-773283	NC_002976	chromosome
☐	55.	-13.71	-1.68	(((((((((((&))))))))))	2377	2387	175-185	leucyl tRNA synthetase	SERP1318	-	1380055-1377441	NC_002976	chromosome
☐	56.	-13.65	-1.66	(((((((((.------((((&.))).))))))))...))))))))	-188	-160	158-180	hypothetical protein SERP0741	SERP0741	-	738385-737745	NC_002976	chromosome
☐	57.	-13.62	-1.65	(((((((((((((((((((&))))))))))......))))))	1424	1445	299-324	monovalent cation/H+ antiporter subunit A	SERP0538	-	523124-520519	NC_002976	chromosome
☐	58.	-13.62	-1.65	(((((((((((((...-((((((&)))))).))))))))))))	26	47	158-177	lysozyme domain containing protein	SERP0043	-	40212-39203	NC_002976	chromosome
☐	59.	-13.59	-1.65	(((((((((((...((((&))).-)))).)))))))))))	259	283	168-193	hypothetical protein SERP2384	SERP2384	+	2433580-2434886	NC_002976	chromosome
☐	60.	-13.58	-1.64	((((((((&.))))))))	-197	-190	251-258	hypothetical protein SERP1140	SERP1140	-	1178489-1177300	NC_002976	chromosome
☐	61.	-13.56	-1.64	(((((((((((((&.))))))))))))))	443	460	6-23	hypothetical protein SERP1763	SERP1763	-	1801989-1800854	NC_002976	chromosome
☐	62.	-13.55	-1.64	((((((((.(((((((&))))))).))))))))	11	31	299-319	hypothetical protein SERP1118	SERP1118	+	1157713-1158014	NC_002976	chromosome
☐	63.	-13.50	-1.63	((((((((((((((((((&))))).))).))))))))	-109	-89	236-257	resolvase; putative	SEA0025	+	20970-21712	NC_006663	plasmid pSERP
☐	64.	-13.49	-1.62	(((((((((......(((((&.&))))))).)))).))))))))	756	779	160-182	acetolactate synthase; large subunit; biosynthetic type	SERP1666	+	1704508-1706411	NC_002976	chromosome
☐	65.	-13.48	-1.62	(((((((((((((((((((.((((&))).)).)).)))....)))))))))	-147	-124	236-261	type III leader peptidase family protein	SERP1226	-	1259979-1259069	NC_002976	chromosome
☐	66.	-13.48	-1.62	(((((((((....((((&)))).....))))))))	678	695	166-183	tRNA pseudouridine synthase A	SERP1800	-	1845904-1844901	NC_002976	chromosome
☐	67.	-13.47	-1.62	(((((((..(((((((&))))).)))).)))))))))	-158	-135	176-196	hypothetical protein SERP2135	SERP2135	+	2160707-2161047	NC_002976	chromosome
☐	68.	-13.46	-1.62	(((((-------((((((&.)))))))...))))))	115	137	158-179	PTS system; IIBC components	SERP1290	-	1336340-1334668	NC_002976	chromosome
☐	69.	-13.37	-1.59	((((((((......((((&.)))).....))))))))	863	881	212-229	sensor histidine kinase	SERP0313	+	315951-317191	NC_002976	chromosome
☐	70.	-13.36	-1.59	((((((((((((((&))))))))))))))))	373	392	218-235	bifunctional homocysteine S methyltransferase/5,10 methylenetetrahydrofolate reductase protein	SERP0035	-	32736-30698	NC_002976	chromosome

Tab. IV 7: Results of *RNApredator* (*continued*)

#	ΔG	ΔG	start	end	position	description	locus	strand	coordinates	accession	location
71.	-13.35	-1.59	506	534	195-222	hypothetical protein SERP0495	SERP0495	-	485429-484369	NC_002976	chromosome
72.	-13.33	-1.59	866	881	328-343	dipeptidase PepV	SERP1310	-	1360810-1359201	NC_002976	chromosome
73.	-13.32	-1.58	456	479	206-229	hypothetical protein SERP1050	SERP1050	-	1098271-1097109	NC_002976	chromosome
74.	-13.32	-1.58	-88	-70	240-257	bicyclomycin resistance protein	SERP2014	+	2031413-2032812	NC_002976	chromosome
75.	-13.31	-1.58	-63	-53	175-185	rhodanese like domain containing protein	SERP1317	-	1377615-1377104	NC_002976	chromosome
76.	-13.30	-1.58	68	92	157-180	hypothetical protein SERP0425	SERP0425	-	428034-427742	NC_002976	chromosome
77.	-13.29	-1.58	77	93	248-264	Na+/H+ antiporter NhaC	SERP1881	-	1907250-1905553	NC_002976	chromosome
78.	-13.29	-1.58	1116	1134	211-231	hypothetical protein SERP0605	SERP0605	-	598651-597258	NC_002976	chromosome
79.	-13.29	-1.58	810	825	304-319	ABC transporter, permease protein	SERP2203	-	2239783-2237571	NC_002976	chromosome
80.	-13.27	-1.57	321	328	251-258	tagG protein; teichoic acid ABC transporter protein; putative	SERP0297	+	299151-300163	NC_002976	chromosome
81.	-13.27	-1.57	467	490	167-193	short chain dehydrogenase/reductase family oxidoreductase	SERP2379	-	2426735-2425762	NC_002976	chromosome
82.	-13.27	-1.57	-119	-98	246-261	hypothetical protein SERP0617	SERP0617	-	612096-611678	NC_002976	chromosome
83.	-13.27	-1.57	-181	-152	236-260	sulfate permease family protein	SEA0024	-	21256-19605	NC_006663	plasmid pSERP
84.	-13.26	-1.57	248	272	213-239	Holliday junction DNA helicase RuvA	SERP1206	-	1246027-1245225	NC_002976	chromosome
85.	-13.24	-1.56	729	740	248-259	glycine dehydrogenase subunit 1	SERP1101	-	1145880-1144334	NC_002976	chromosome
86.	-13.23	-1.56	-149	-127	159-178	transcriptional regulator CzrA	SERP1755	+	1791623-1792164	NC_002976	chromosome
87.	-13.22	-1.56	439	454	123-138	N acetylmuramoyl L alanine amidase	SERP1330	-	1393105-1392054	NC_002976	chromosome
88.	-13.22	-1.56	-176	-155	209-230	methionine sulfoxide reductase A	SERP0931	-	949209-948493	NC_002976	chromosome
89.	-13.21	-1.56	-141	-129	247-259	fmhA protein	SERP2001	+	2019016-2020463	NC_002976	chromosome
90.	-13.19	-1.55	-183	-165	158-177	hypothetical protein SERP0102	SERP0102	-	88358-87880	NC_002976	chromosome
91.	-13.18	-1.55	70	86	212-228	hypothetical protein SERP2139	SERP2139	-	2166307-2166003	NC_002976	chromosome
92.	-13.16	-1.54	-158	-139	162-178	hypothetical protein SERP1969	SERP1969	+	1988514-1989091	NC_002976	chromosome
93.	-13.14	-1.54	384	402	166-183	cadmium resistance family protein	SERP1370	-	1426285-1427468	NC_002976	chromosome
94.	-13.14	-1.54	277	285	250-258	cytochrome oxidase assembly protein	SERP0705	-	703864-702756	NC_002976	chromosome
95.	-13.14	-1.54	-62	-37	277-303	2 dehydropantoate 2 reductase	SERP2022	-	2042326-2041194	NC_002976	chromosome
96.	-13.13	-1.54	-100	-83	125-145	pyridine nucleotide disulfide oxidoreductase family protein	SERP0242	-	250587-249056	NC_002976	chromosome
97.	-13.12	-1.53	-199	-175	121-146	CroCl family transcriptional regulator	SERP0012	+	7956-8725	NC_002976	chromosome
98.	-13.12	-1.53	44	64	236-257	hypothetical protein SERP0894	SERP0894	-	905740-905415	NC_002976	chromosome
99.	-13.11	-1.53	214	234	335-355	hypothetical protein SERP1448	SERP1448	-	1513927-1513101	NC_002976	chromosome

By using *IntaRNA*, the following mRNAs showed an interaction with IcaZ (**Tab. IV-8**). The candidates were then tested by EMSA (chapter V-1.1.1). *icaR* mRNA as interaction partner was most promising, because four interaction sites with IcaZ were predicted.

Tab. IV-8: Possible interaction partners with binding site position in IcaZ

Position in IcaZ	mRNA fragment
01-10	5′ *icaR**
95-112	5′ *icaR**
115-133	3′ *icaR**
135-146	5′ *ebh*
139-149	5′ *ctsR*
156-187	5′ *icaA*
163-182	5′ *hcrA*
274-283	3′ *icaR* (ORF)*
278-306	5′ *murA*

Listed are the mRNA fragments, whose nucleotide sequences were used for the prediction of an interaction with IcaZ and for which an interaction site was predictable by *IntaRNA*. The position of the interacting sequence of IcaZ is given. For *icaR* mRNA, four interaction sites were found (marked with *).

4. Summary of Results for Part B

- A number of *icaZ* deletion mutants were tested in this chapter demonstrating differences with respect to *icaZ* and neighbouring gene expression.

- O-47ΔΔΔ is a triple mutant affecting, in addition to *icaZ*, also neighbouring *tRNA^{Thr-4}* and *icaR* mRNA expression. Due to partial deletion of *icaR* 3′ UTR in this mutant, *icaR* mRNA is shorter, more instable, but stronger expressed than in the Wt (**Fig. IV-1**).

- O-47ΔΔΔΔ corresponds to the triple mutant, but lacks additionally the entire *tRNA^{Thr-4}* gene (**Fig. IV-3**).

- The newly generated mutant (O-47Δ*icaZ),* lacks exclusively IcaZ and leaves neighbouring gene expression intact (**Fig. IV-2; Fig. IV-3; Fig. IV-4**).

- Abolishment of *icaZ* in any of the mutants results in a clearly biofilm negative phenotype, which is mainly because of the loss of PIA production (**Fig. IV-7; Fig. IV-10**).

- Loss of PIA-mediated biofilm formation occurs both under static and flow conditions.

- Lack of IcaZ does not influence growth rate, cell shape and quorum-sensing activity (**Fig. IV-6; Fig. IV-9**).

- O-47ΔΔΔ is slightly more sensitive to oxidative stress than the Wt (**Tab. IV-1**).

- Restoration of PIA-mediated biofilm formation upon providing *icaZ* complementation from plasmids revealed inconsistent results in the various mutant backgrounds (**Fig. IV-16; Fig. IV-17; Fig. IV-18; Fig. IV-19**):
    - In O-47ΔΔΔ biofilm formation was restored, but also by an empty vector control.
    - In O-47ΔΔΔΔ biofilm formation was not restored.
    - In O-47Δ*icaZ* biofilm formation was not restored, neither by the *icaZ* bearing plasmid nor by the empty vector control.

- IcaZ *in trans* expression from plasmid increased biofilm formation in *S. epidermidis* PS2, strain 567 and its isogenic *agr*-mutant 567-1. Regarding the results from 567 and 567-1, IcaZ is assumed to act independently of the *agr* quorum sensing system.

- IcaZ *in trans* expression from plasmid did not increase biofilm formation in *icaADBC*-negative *S. epidermidis* ATCC 12228 and Tü 3298, nor in *icaADBC*-positive *S. aureus* Newman and RN4220.

- Transcription profiling by microarray analysis of O-47 Wt in comparison with O-47ΔΔΔ revealed, in addition to differential expression of numerous metabolic genes, upregulation of *icaR* in the mutant at 30°C and 37°C, whereas *aap* and *sdrH* were downregulated, and *ebh* being expressed in a temperature-dependent manner (**Fig. IV-24**).

- Proteome analysis of O-47 Wt and O-47ΔΔΔ revealed most varying proteome patterns in the exponential growth phase at 30°C (**Fig. IV-25**). Metabolic protein expression patterns obtained in the O-47ΔΔΔ exponential growth stage correspond to a typical stationary-phase signature, suggesting a premature entry of the mutant into stationary growth, which would metabolically disable PIA-mediated biofilm formation (**Fig. IV-26**).

- Pulse-expression of *icaZ* in O-47ΔΔΔ followed by RNA-seq resulted in the enrichment of only a limited number of transcripts from which an enolase gene anti-sense transcript was the most interesting one (**Tab. IV-5; Fig. IV-28**).

- Bioinformatic search for putative IcaZ mRNA interaction partners identified *icaR* mRNA as a potential interaction partner (**Tab. IV-8**).

V. Results – Part C 'Establishing and challenging a hypothetical biofilm regulation model involving ncRNA IcaZ'

1. Hypothetic model of PIA biofilm regulation by ncRNA IcaZ

The experiments done so far clearly show that IcaZ positively influences PIA-mediated biofilm formation. However, the mechanism by which the ncRNA accomplishes this effect remained elusive. Bacterial biofilm formation usually requires the activation of distinct metabolic patterns to enable extracellular matrix production. Hence, the varying biofilm phenotypes of wildtype and *icaZ* mutants make it difficult to identify direct IcaZ mRNA targets by the aforementioned global approaches, as these targets may be masked by the generally different metabolic status of the biofilm-forming wildtype and the biofilm-negative *icaZ* mutants. Nevertheless, the combined data of these analyses suggested an involvement of *icaR* in IcaZ-mediated biofilm control. Thus, *icaR* featured as differentially regulated gene in the transcriptome analyses and was predicted as a target by bioinformatic approaches. In the light of its close genetic localisation and overlap with the *icaZ* transcript, subsequent experimental work therefore focussed on *icaR* and its possible functional relation to IcaZ.

Fig. V-1 displays a hypothetic model of PIA biofilm regulation by IcaZ in *S. epidermidis*. The distinct biofilm negative phenotype of the *icaZ* mutants (**Fig. IV-7; Fig. IV-10; Fig. IV-13; Fig. IV-14**) and the biofilm positive phenotype of the wildtype can be explained by this model, in which ncRNA IcaZ regulates *icaR* mRNA through a direct base-pairing mechanism. Bioinformatical interaction predictions, which were carried out before, revealed four interaction sites within IcaZ that might interact with *icaR* mRNA. By using *IntaRNA*, the following mRNAs showed an interaction with IcaZ (**Tab. IV-8**). The candidates were then tested by EMSA (chapter V-1.1.1). *icaR* mRNA as interaction partner was most promising, because four interaction sites with IcaZ were predicted.

Thus, in the wildtype, IcaZ is expressed and base pairs with mainly the *icaR* 5'- and 3'-UTRs, thereby inhibiting translation of the *icaR* mRNA. Lack of the repressor protein IcaR

results in *icaADBC* operon expression and subsequent PIA production. The complex of IcaZ and *icaR* mRNA may undergo degradation by RNase III, a RNA double strand-specific ribonuclease that is known to degrade the *icaR* mRNA autoregulation complex in *S. aureus* (chapter I-3.2.2). In contrast, in *icaZ* mutants the IcaR repressor is expressed and blocks *icaADBC* transcription by binding to the *icaADBC* promoter, resulting in efficient inhibition of PIA production and a biofilm-negative phenotype.

This model was experimentally challenged. For simplification, it does not yet consider environmental factors that may influence IcaZ synthesis or the involvement of other *ica*-operon regulators. Some of this putative factors and regulators were experimentally addressed in this work as well and the data are also provided in this chapter.

A *S. epidermidis* O-47 Wt:

B *S. epidermidis* O-47Δ*icaZ*:
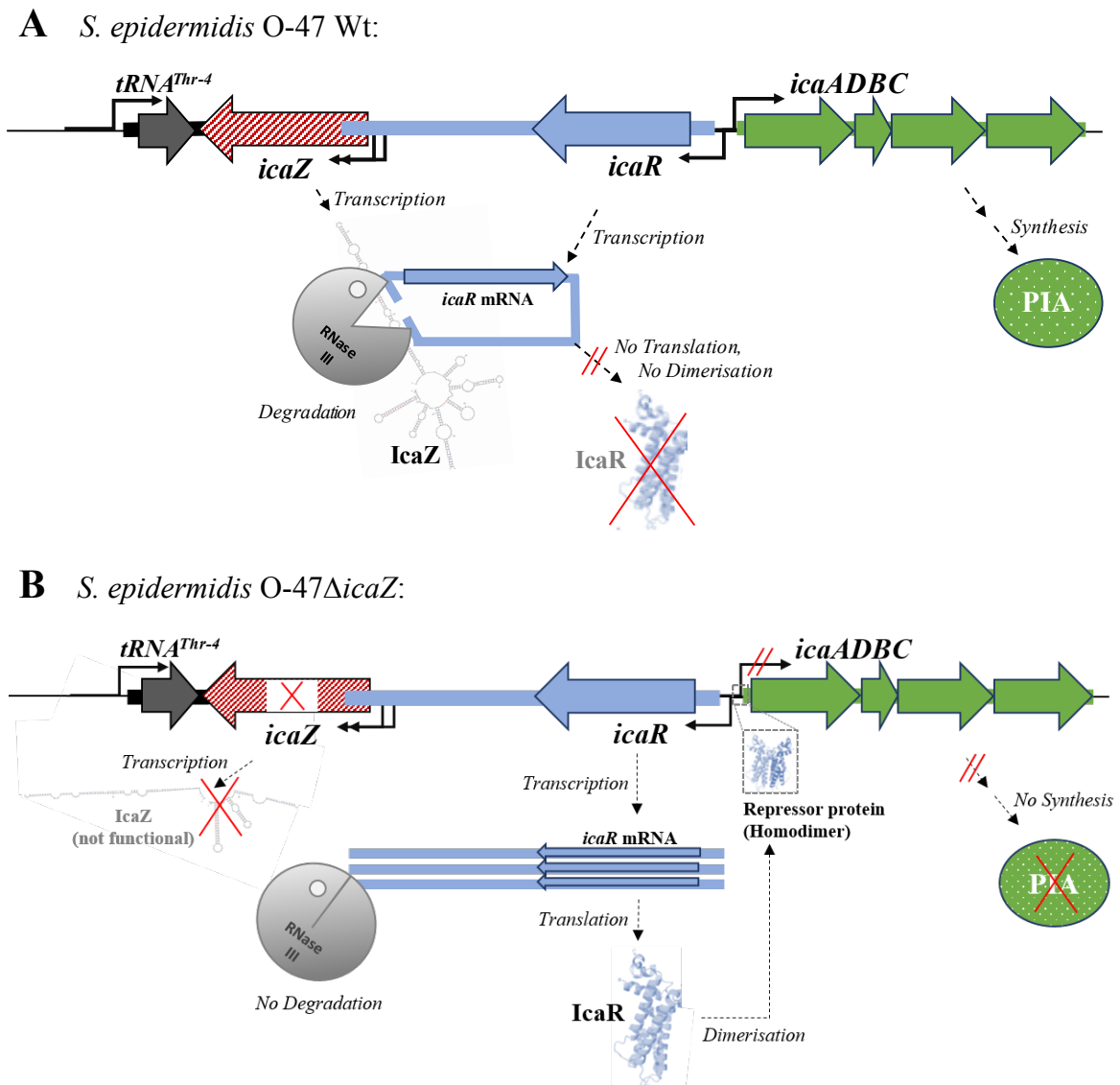
Fig. V-1: Hypothetic model of PIA biofilm regulation by ncRNA IcaZ in *S. epidermidis*

DNA elements that are located on the sense strand (5′ to 3′ orientation) are shifted to the background, whereas DNA elements that are located on the antisense strand are shifted to the front. The crystal structure of IcaR was taken and modified from Jeng *et al.*, 2008 (Figure 1A). (**A**) Regulation of PIA synthesis in *S. epidermidis* O-47 Wt. IcaZ interacts with 5′ UTR and 3′ UTR of *icaR* mRNA, thereby indirectly represses the translation of *icaR*. Consequently, IcaR is not synthesised and *icaADBC* transcription cannot be blocked by IcaR. PIA synthesis takes place and a biofilm can be formed. (**B**) Regulation of PIA synthesis in *S. epidermidis* O-47Δ*icaZ*. In absence of functional IcaZ, IcaR can be translated and represses the transcription of *icaADBC*.

1.1 Indirect regulation of *icaADBC*-operon expression in *S. epidermidis* by post-transcriptional regulation of *icaR* mRNA translation by IcaZ

1.1.1 *Classical EMSA reveals no base-pairing interaction between IcaZ and the tested RNA targets*

The experiments were carried out with 4 nM radioactively labelled RNA and 0-1000 nM target RNA. Tested target RNAs included RNAs for which an interaction was bioinformatically predicted or which were apparent in the global approaches. The list of *in vitro* transcripts is in **Annexe Tab. VIII-6**.

The initial classical EMSAs were carried out with IGR*ica*-RNA and *icaR*-5′ UTR (IVT$_1$) or *icaR*-5′ UTR (IVT$_2$), respectively. Both *in vitro* transcribed RNAs were denatured and renatured together at 37°C for 15 min. The complex was loaded onto a native 6% PAA gel and electrophoresis was carried out for 3h in 0.5X TBE at 300V. No band shift was visible (data not shown). For the next EMSAs, the renaturation temperature was changed to 30°C and a 4% PAA gel was used to better separate the fragments. Electrophoresis time was extended to 4h. Several EMSAs were carried out, but IcaZ showed no interaction with *icaR*-3′ UTR (IVT$_3$), *murAA*-5′ UTR (IVT$_4$) and *icaR*-5′ UTR (IVT$_1$ and IVT$_2$). The same procedure, but using a 6% PAA gel was carried out to analyse the interaction of IcaZ with *ebh*-5′ UTR (IVT$_6$), *hrcA*-5′ UTR (IVT$_7$), *ctsR*-5′ UTR (IVT$_8$) and *icaA*-5′ UTR (IVT$_9$), but also with these targets no band shift could be detected. The protocol was modified again. Labelled IcaZ (IVT$_{17}$) was renatured with the target at 37°C, either *ctsR*-5′ UTR (IVT$_8$) or *murAA*-5′ UTR (IVT$_4$), and then separated on a 4% PAA gel for 6h and 22min. Other assays contained the labelled IcaZ (IVT$_{17}$), which was renatured for 5 min at 30°C and then added to the denatured target on ice, *icaR*-5′ UTR (IVT$_1$ and IVT$_2$) or *icaR*-3′ UTR (IVT$_3$) or *icaA*-5′ UTR (IVT$_9$), and subsequently incubated at 30°C for 15 min (4% PAA gel/ 6-6.5h). Further assays contained labelled targets (IVT$_{2-5}$), which were incubated with renatured IcaZ at 30°C for 15 min and then separated on 6% PAA gel for 3-3.5h. Also with these gel shift assays, a band shift was not detectable.

To technically test the method, using a different buffer, *icaR* 5′ UTR and *icaR* 3′ UTR of *S. aureus* were incubated together and classical EMSA was carried out. The positive gel shift result (**Fig. V-2 left**) verified the general suitability of the procedure so that experimental mistakes could be ruled out.

1.1.2   *No autoregulation of icaR mRNA in S. epidermidis*

The autoregulation of *icaR* mRNA was shown for *S. aureus* by Ruiz de los Mozos *et al.*, 2013. In this work, the interaction of *S. aureus icaR* 5′ UTR and *icaR* 3′ UTR was verified experimentally and served here as proof of principle for the classical gel shift protocol to show that the negative results described in the previous section were not a result of any experimental mistakes. In a parallel assay, the same protocol was used to analyse, if *icaR* mRNA of *S. epidermidis* can also undergo autoregulation. The transcripts used for the assays are listed in **Annexe Tab. VIII-7**. The assays were carried out as described in chapter II-6.7.5.1.

The interaction of *icaR*-5′ UTR (IVT$_{23}$) with *icaR*-3′ UTR (IVT$_{24}$) was successfully verified for *S. aureus in vitro* (**Fig. V-2**). Interestingly, *icaR*-5′ UTR (IVT$_{18}$) and *icaR*-3′ UTR (IVT$_{20}$) of *S. epidermidis* did not interact (**Fig. V-2**), so that, conclusively, there is no autoregulation for *icaR* mRNA of *S. epidermidis*. This result raised the question, how *icaR* mRNA is regulated and if IcaZ is involved in *icaR* mRNA autoregulation or even facilitates the interaction of *icaR* 5′ UTR and *icaR* 3′ UTR.
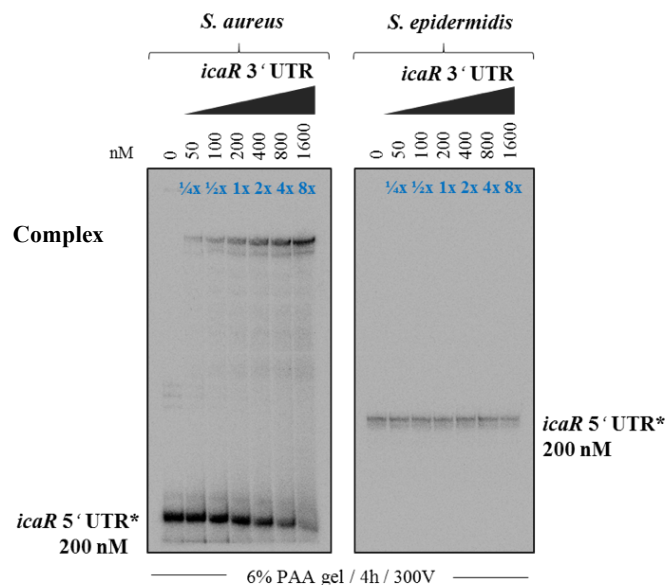
Fig. V-2: (No) auto-regulation of *icaR*-mRNA

> The classical gel shifts were performed with radioactively (*) labelled *icaR*-5′ UTR and *icaR*-3′ UTR of either *S. aureus* 8325 (**left**) or *S. epidermidis* O-47 (**right**). An interaction of the UTRs was detected for *S. aureus*, but not for *S. epidermidis*. The detailed protocol is given in chapter II-6.7.5.1.

1.1.3 *By application of 'live' in-vitro transcription prior to EMSA, icaR mRNA was identified to be an interaction partner for IcaZ, but not icaA mRNA*

Because of the strong secondary structures of IcaZ, it was assumed that an interaction between *in vitro* transcribed (pre-folded) RNAs (as it is the case in classical EMSAs) is not possible or is at least less efficient, so that IcaZ is not able to interact with the target by choice under classical conditions and needs either help by a chaperone or modified reaction conditions that facilitate an interaction. Three of the four potential binding sites of IcaZ possibly used for the interaction with *icaR* mRNA were located within the strong stem loop 1, which we hypothesise forms very rapidly after transcription. Moreover, the interacting nucleotides within *icaR* mRNA were also sequestered due to secondary structure folding, as revealed by secondary structure prediction of *icaR* mRNA (**Annexe Fig. VIII-13**).

To facilitate the interaction between IcaZ and the targets, the reaction conditions were modified by including a 'live' *in vitro* transcription reaction that took place in presence of the re-folding interaction partner. The advantage of this new protocol was that both transcripts were not pre-folded yet (or refolded) and therefore had the opportunity to interact with each other. A similar approach was used before by Dr Sonja Schoenfelder regarding a different project (Schoenfelder *et al.*, 2013; Schoenfelder, 2014). The principle was adopted, meaning, each reaction contained one interaction partner in denatured form (or more), the T7 DNA template of the other interaction partner, T7 polymerase for the *in vitro* transcription of the RNA and the reaction buffer. The denatured interaction partner renatured in the presence of the just *in vitro* transcribed RNA of the other partner (**Fig. V-4**).

The original protocol had to be changed completely to adapt to conditions suitable for very long RNAs. Both RNAs, IcaZ and *icaR* mRNA, were too long to be separated entirely on a 6% PAA gel, therefore they were fractionated prior to their usage in the assay. Pulse-expression analysis previously revealed a more stable region within IcaZ (stem loops 2-4), so that the beginning of this region was taken to divide IcaZ into two parts (figuratively), named 'IcaZ part 1' and 'IcaZ part 2' (**Fig. V-3**). This was experimentally carried out by amplifying the two parts of IcaZ from genomic DNA and adding a T7 promoter site at the 5′ end of each part. The T7 DNA templates for both parts were amplified from *S. epidermidis* O-47 genomic DNA with primers T7_IGRica_MF and IGRtr-1_RT_rev for the amplification of 'IcaZ part 1' and T7-3_IGRica_MF and tRNA-3'UTR-s for 'IcaZ part 2'. The protocol for the *in vitro* transcription of the RNAs from T7 DNA templates is described in chapter II-6.7.1. The T7 transcript 'IcaZ part 1' comprised the first stem loop (172 nt) and 'IcaZ part 2' comprised stem loops 2-7 (262 nt) (**Fig. V-3**).
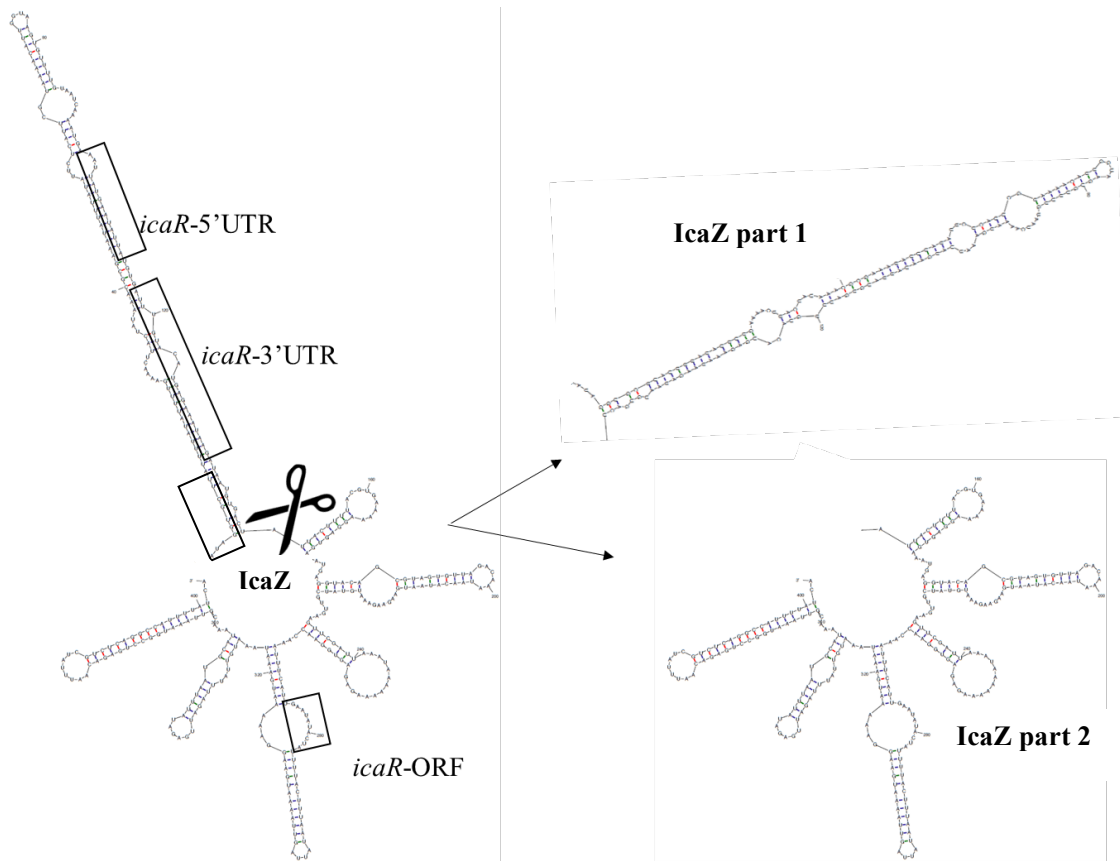
Fig. V-3: Partitionment of ncRNA IcaZ for application in EMSAs

   Pulse-expression analysis of IcaZ revealed a more stable part after the first stem loop. The beginning of this region was used to cut the RNA into two parts (figuratively). Experimentally, both parts were amplified separately and transcribed from T7-promoter. IcaZ part 1 included the interaction sites for *icaR* 5′ UTR and *icaR* 3′ UTR. IcaZ part 2 included the interaction site for *icaR* ORF.

Due to the length of *icaR* mRNA (~1000 nt), this RNA had to be shortened as well. This was done by amplifying only the UTRs, or in the case of the fusion product, by leaving nearly the whole ORF out. The PCR product for the T7 transcript '*icaR*-5′ UTR' was amplified with primers ML_icaR5'_T7-F3 and MF_icaR5'_R (176 bp PCR product, 157 nt RNA). The PCR product for the T7 transcript '*icaR*-3′ UTR' was amplified with primers MF_icaR3'_T7-F and ML_icaR3'_R2 (429 bp PCR product, 411 nt RNA). A third transcript '*icaR*-5′3′ fusion product' (IVT$_{19}$, **Annexe Tab. VIII-4**) was made of the linked *icaR* mRNA UTRs (IVT$_{19lf}$ and IVT$_{19rf}$). That means, *icaR*-5′ UTR was combined with the *icaR* 3′ UTR whereas the *icaR* 3'UTR also contained a small part of the 3′ end of the ORF to cover also the third predicted interaction site. The secondary structure folding of the fusion product was analysed with *Mfold* prior to the usage in EMSAs to check, if it folds like *icaR* 5′ UTR and *icaR* 3′ UTR fragments (**Annexe Fig. VIII-12**). The four interaction sites in *icaR* mRNA, for base-pairing with IcaZ, were predicted with *IntaRNA* (Busch *et*

al., 2008; Wright *et al.*, 2014). The interaction sequences and the amount of released free energy during interaction is depicted in **Annexe Fig. VIII-6**.
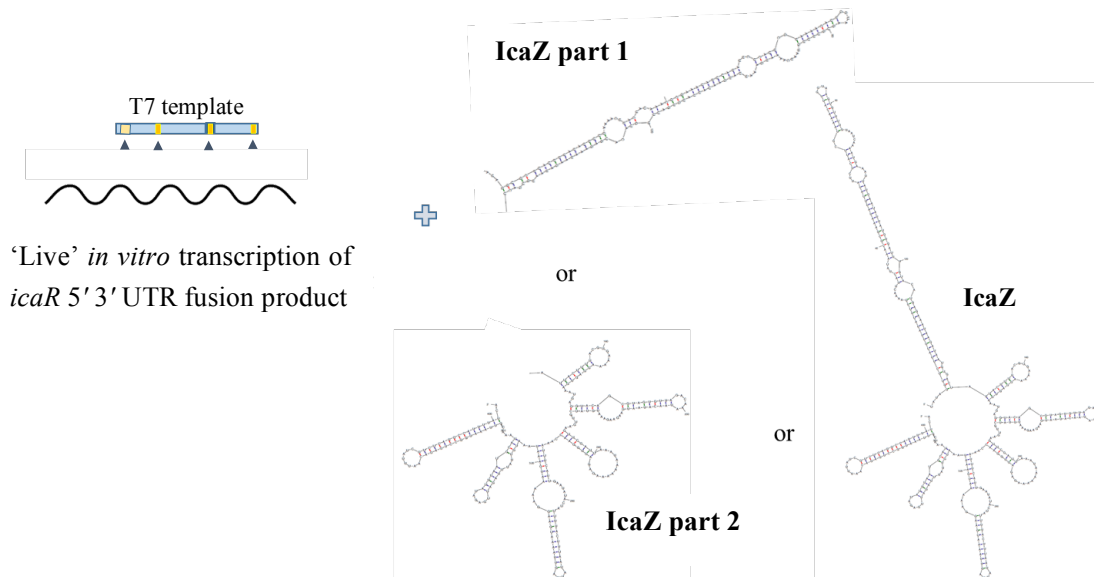
Fig. V-4: Schematic depiction of "live" IVT method

> The principle of 'live' *in vitro* transcription followed by EMSA was adapted from Dr Sonja Schoenfelder. In this work, the interaction partner '*icaR*-5′ 3′ UTR fusion product' was *in vitro* transcribed, while IcaZ or parts of IcaZ were present and folded or re-folded at the same time (Fig. V-5 A-D). The three interaction sites within '*icaR*-5′ 3′ UTR fusion product' are marked with an arrowhead. The experiment was also carried out *vice versa* transcribing *icaZ* in the presence of various *icaR* mRNA species (Fig. V-5 E).

The (interaction-) reactions were performed in the PCR cycler at 30°C or 37°C. For that, a defined amount of radioactively labelled RNA was mixed with 1 pmol of T7 DNA template. T7 polymerase then transcribed the specific RNA, while the interaction partner re-folded at the same time. The reactions were incubated up to 12h at the indicated temperature and were then separated on native 4% or 6% PAA gels for up to 7h, depending of the size of the transcripts and the supposed interaction complex.

Fig. V-5 shows the results of the EMSAs with radioactively labelled IcaZ or IcaZ parts and live *in vitro* transcribed *icaR*-5′ 3′ UTR or *icaR*-3′ UTR. Only IcaZ part 1 gave a band shift, when incubated with *icaR*-5′ 3′ UTR, but not IcaZ part 2 (**Fig. V-5 A+B**). The interaction was validated with an additional gel shift assay containing full length IcaZ and *icaR*-5′ 3′ UTR fusion product (**Fig. V-5 C**). The interaction seemed to be driven by the *icaR*-5′ UTR, because the *icaR*-3′ UTR showed only weak interaction with full length IcaZ (**Fig. V-5 D**). These assays were repeated, revealing the same results. The interaction was validated with the *vice versa* reaction, in which the target RNA, *icaR*-5′ 3′ UTR fusion product, was radioactively labelled and full length IcaZ was live *in vitro* transcribed. Also by this approach, an interaction complex was detectable (**Fig. V-5 E**).

In contrast to the results with target *icaR*-5′3′UTR, an interaction between full length IcaZ and *icaA*-5′UTR could not be verified by application of the same conditions (**Fig. V-5 F**). Interaction of IcaZ with the fusion product was therefore considered to be specific for the fusion product *icaR*-5′ 3′ UTR, but not for other adjacent targets such as *icaA*-5' UTR. Conclusively, 'live' *in vitro* transcription followed by EMSA identified *icaR* mRNA as an interaction partner of IcaZ.

E

F

*: γ-ATP	nc : reaction without template
pc**: IVT control + α-UTP	: dilution of template for IVT
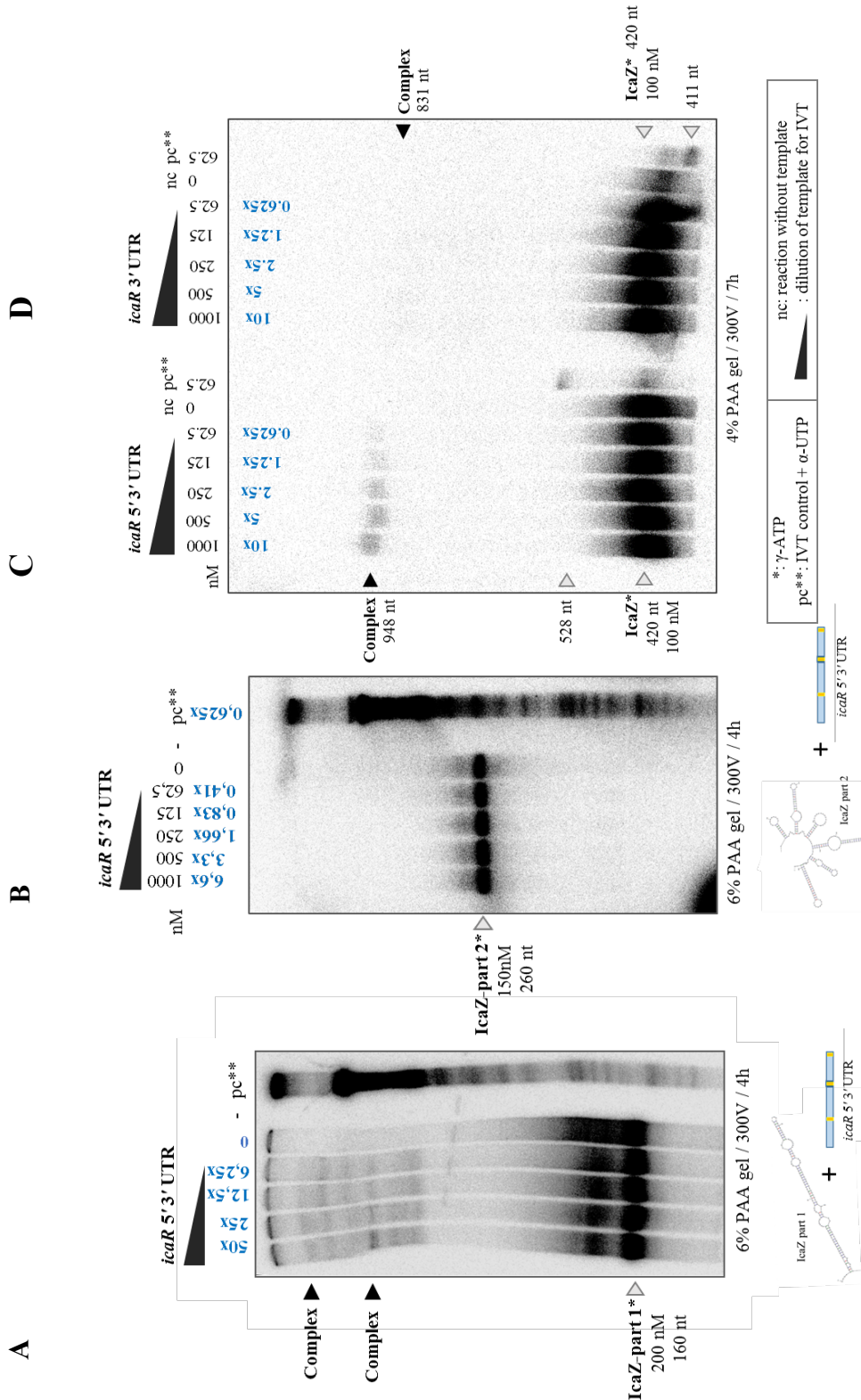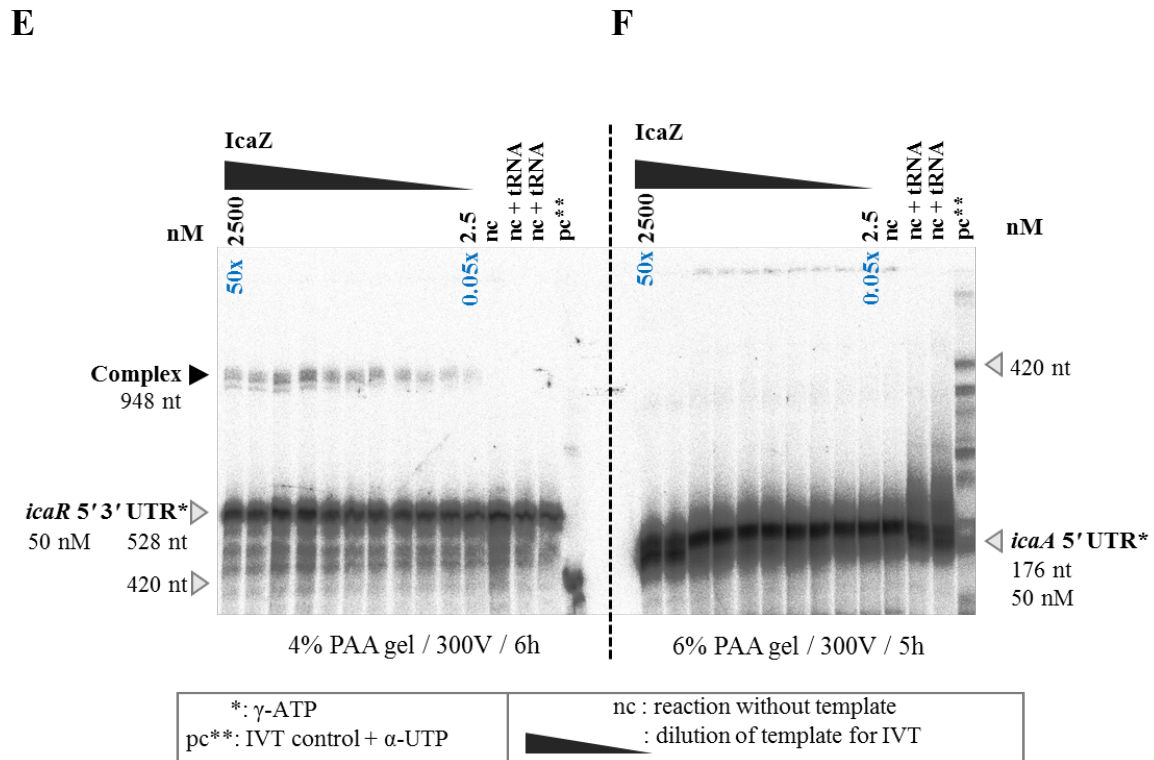
Fig. V-5: Interaction of *icaR* mRNA with IcaZ analysed by EMSA

For these electrophoretic mobility shift assays (EMSAs), the advanced protocol was applied (chapter II-6.7.5.2). The conditions for gel electrophoresis are written below each gel. For each reaction, the successful IVT was controlled (see figure legend pc**). (**A**) Radioactively labelled IcaZ-part 1 refolded, while *icaR* 5′ 3′ UTR fusion product was transcribed *in vitro*. The secondary structure of the used transcript is depicted below the gel. A weak band shift was detectable. (**B**) Radioactively labelled IcaZ-part 2 refolded, while *icaR* 5′ 3′ UTR fusion product was transcribed *in vitro*. The secondary structure of the used transcript is depicted below the gel. (**C**) Radioactively labelled full length IcaZ refolded, while *icaR* 5′ 3′ UTR fusion product was transcribed *in vitro* (37°C, 2 h 10 min). The amount of produced RNA was calculated based on a control experiment. The size of the interaction complex was calculated to be 849 nt. The positions of the detected signals fit this size. (**D**) Radioactively labelled full length IcaZ refolded, while *icaR* 3′ UTR was transcribed *in vitro* (37°C, 2 h 10 min). The amount of produced RNA was calculated based on a control experiment. A very weak band shift was detectable. (**E**) *Vice versa* reaction to **C**. Radioactively labelled *icaR* 5′ 3′ UTR fusion product refolded, while full length IcaZ was transcribed *in vitro*. The size of the interaction complex was calculated to be 849 nt. The positions of the detected signals fit this size. (**F**) Control reaction with target *icaA* 5′ UTR. Radioactively labelled *icaA* 5′ UTR refolded, while full length IcaZ was transcribed *in vitro*. No band shift was detectable.

1.1.4 *Visualisation of the interaction between IcaZ and icaR mRNA by GFP-reporter plasmids*

The idea of using two-plasmid systems for studying post-transcriptional control of gene expression *in vivo* originated from Urban and Vogel (Urban and Vogel, 2007; 2009). Based on an advanced version by Corcoran et al. (Corcoran *et al.*, 2012), the plasmid pCN33_pami_gyrB_gfp was created by the group of Prof Brice Felden (Université de Rennes, France), who kindly provided the plasmid. In two-plasmid systems, the sRNA is expressed from an inducible promoter, while the 5′ UTR of the target mRNA is expressed constitutively from a second plasmid. The 5′ UTR of the target mRNA is fused to green fluorescent protein to reflect target gene expression. An interaction of the induced sRNA with the target 5′ UTR results in a decrease or increase of GFP fluorescence.

Such a two-plasmid system, providing the ncRNA *in trans*, was not suitable for analysing IcaZ and *icaR* mRNA interaction, because IcaZ was supposed to interact *in cis* during (or shortly after) transcription was taking place (chapter V-1.1.3; **Fig. V-5**). This hypothesis was based on the one hand on the results of the classical biofilm assays that did not show a significant effect on biofilm formation when IcaZ was expressed *in trans* from the ATc-inducible pCG248 plasmid system (chapter IV-2), and on the other hand on EMSAs demonstrating that IcaZ and *icaR* mRNA interacted only when both RNAs were not pre-transcribed, but adopted their structure simultaneously in the presence of each other (chapter V-1.1.3). Also, the ratio between IcaZ and *icaR* mRNA transcripts should not be significantly changed in the assay, in order to mimic natural expression conditions. Using the highly active P_{ami} promoter for *icaR* expression would result in unnaturally high amounts of *icaR* mRNA, so that a reduction of GFP fluorescence (due to a supposed interaction with IcaZ) might be difficult to detect. Therefore, the native promoter of *icaR* (P_{icaR}) was cloned into GFP reporter plasmids. As start codon for GFP translation, the start codon TTG from *icaR* ORF was used. Because the GFP-reporter system had to be further developed, a total of three novel plasmid constructs were generated in this work (see **Tab. V-1** at the end of this section).

The first generation of plasmids for the visualisation of IcaZ/*icaR* mRNA interaction by the GFP reporter were named pCN33_P_{icaR}_5'UTR-*icaR*_TTG-*gfp*_3'UTR-*icaR*_*icaZ* and pCN33_P_{icaR}_5'UTR-*icaR*_TTG-*gfp*_3'UTR-*icaR*_*icaZ*del. Each of the plasmids combined the principle of the two-plasmid system in one vector. They contained the backbone of plasmid pCN33_P_{ami}_gyrB_gfp. The vector was enzymatically digested with KpnI-HF and PstI-HF to yield pCN33 backbone without P_{ami}_*gyrB*_*gfp*. The new inserts were integrated into this vector backbone yielding the plasmids listed in **Tab. V-1**.

First, the GFP reporter plasmid system was analysed in an E. coli background. Both promoters, P_{icaZ} and P_{icaR}, were checked for activity. *icaR* expression was analysed in *E. coli*

DC10B+pCerulean_icaZprom (strain collection code ML1), containing the *icaZ* promoter fused to *cfp*. This plasmid was used before to analyse P$_{icaZ}$ expression in *S. epidermidis* O-47 Wt to verify ncRNA IcaZ as a *icaR*-independent RNA (see chapter III-1.1.5). In strain ML1, the cerulean fluorescence increased during growth compared to the wildtype (**Fig. V-6 A**).

Conclusively, the promoter P$_{icaZ}$ can be expressed in *E. coli*, but it is not known if its regulation is the same as in *S. epidermidis*. P$_{icaR}$ expression was measured in *E. coli* DC10B+pCN33_PicaR_5' UTR-icaR_TTG-gfp_TT (strain collection codes ML82 and ML83) by detecting GFP fluorescence. This control construct only included promoter and 5′ UTR of *icaR* fused to *gfp,* but not its 3′ UTR to exclude any regulatory effects of this distal part of the transcript, and was simply used to visualize P$_{icaR}$ activity. Because a signal was clearly detectable for P$_{icaR}$, the strains carrying the 1st-generation plasmids (strain collection codes ML84-ML87) were tested. GFP fluorescence was detectable (at 30°C and 37°C in LB medium), but unfortunately, there was no clear pattern, because the two identical clones, which both carried the partly deleted *icaZ* on the GFP reporter plasmid (strains ML86 and ML87) exhibited highly divergent GFP fluorescence (**Fig. V-6 B**). It was supposed that the copy effect of the plasmids or a missing regulator was the reason for the inconsistent *icaR* expression in these clones. In conclusion: the GFP-reporter system was not reliable for use in the *E. coli* background.

A

P$_{icaZ}$ expression in LB ± Amp100 at 37°C

CFP fluorescence (Ex 430nm / Em 485nm)

time [h]

■ E. coli DC10B   ● E. coli DC10B + pCerulean_icaZprom (ML1)

B

P$_{icaR}$ expression in LB ± Amp^{100} at 37°C

GFP fluorescence (Ex 485 nm/ Em 535 nm)

time [h]
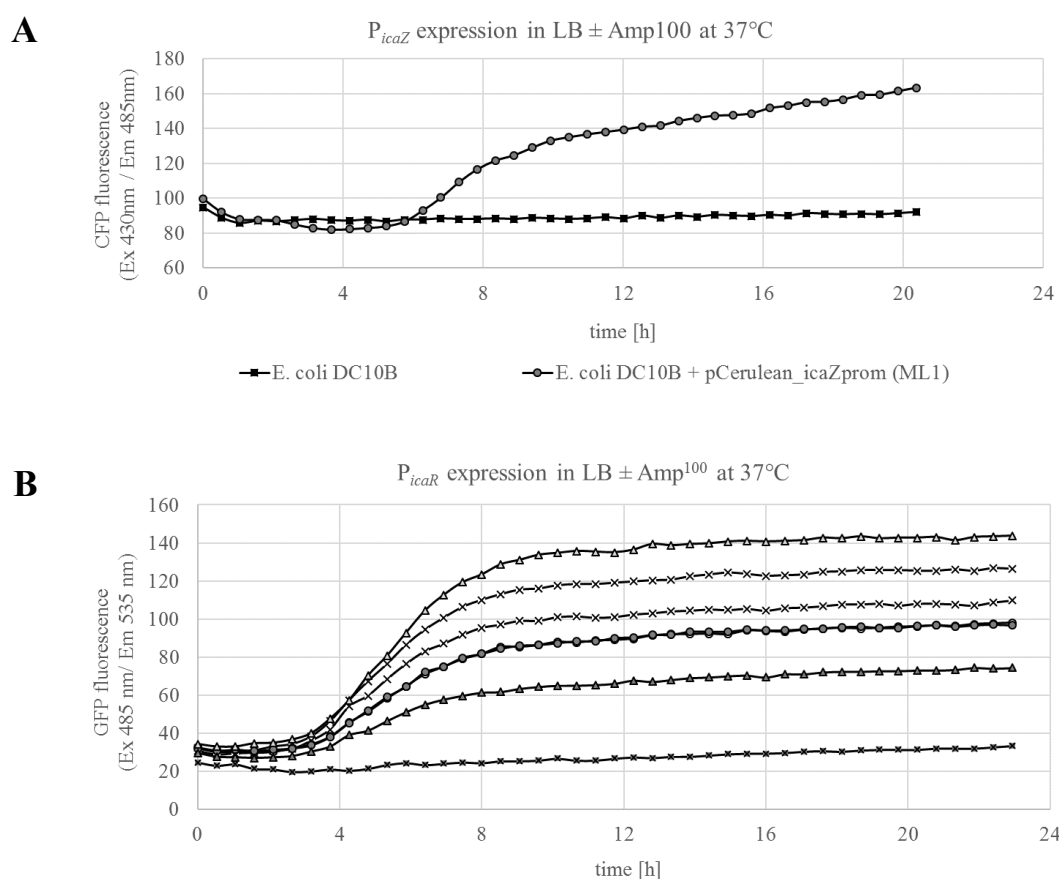
—*—E. coli DC10B

—×—E. coli DC10B + pCN33_PicaR_5'UTR-icaR_TTG-gfp_TT (ML82)

—×—E. coli DC10B + pCN33_PicaR_5'UTR-icaR_TTG-gfp_TT (ML83)

—○—E. coli DC10B + pCN33_PicaR_5'UTR-icaR_TTG-gfp_3'UTR-icaR_icaZ (ML84)

—●—E. coli DC10B + pCN33_PicaR_5'UTR-icaR_TTG-gfp_3'UTR-icaR_icaZ (ML85)

—△—E. coli DC10B + pCN33_PicaR_5'UTR-icaR_TTG-gfp_3'UTR-icaR_icaZdel (ML86)

—▲—E. coli DC10B + pCN33_PicaR_5'UTR-icaR_TTG-gfp_3'UTR-icaR_icaZdel (ML87)

Fig. V-6: P$_{icaZ}$ and P$_{icaR}$ expression in *E. coli* background

Strains were grown in LB medium at 37°C, containing Amp^{100} when required. (**A**) P$_{icaZ}$ activity was measured in *E. coli* DC10B+pCerulean_icaZprom (strain collection code ML 1). CFP fluorescence was measured by Tecan analyser at 485 nm wavelength. An increase in fluorescence was detected after 6 h of growth, when compared to the negative control strain *E. coli* DC10B. (**B**) P$_{icaR}$ activity was measured in the GFP control strains (strain collection codes ML82 and ML83), in the GFP reporter constructs with *icaZ* (strain collection codes ML84 and ML85) and with partly deleted *icaZ* (strain collection codes ML86 and ML87), but without a clear pattern.

Next, the GFP reporter plasmid system was analysed in S. aureus background. The *S. aureus* PS187Δ*hsdR*Δ*sauUSI* served in general as a shuttle strain for the transduction of plasmids from *S. aureus* to *S. epidermidis* via phage 187. Here, the strain was used to test, if the GFP reporter system works in *S. aureus* and if the interaction of IcaZ and *icaR* mRNA can be verified here. For the analysis of P$_{icaZ}$ expression, strains *S. aureus* PS187Δ*hsdR*Δ*sauUSI*+pCerulean_IcaZprom (strain collection codes ML96 and ML97) were used. Surprisingly, P$_{icaZ}$ expression was measurable in the *S. aureus* background (**Fig. V-7 A**), but P$_{icaR}$ expression instead was not detectable. GFP fluorescence was measurable with the control plasmid carrying P$_{ami}$ fused to *gfp*, ruling out technical issues, but not with P$_{icaR}$ fused to *gfp* (**Fig. V-7 B**). Also, the test strains, *S. aureus* PS187Δ*hsdR*Δ*sauUSI* carrying ‘pCN33_P$_{icaR}$_5'UTR-*icaR*_TTG-*gfp*_3'UTR-*icaR_icaZ*’ (strain collection codes ML88, ML90, ML92 and ML93) or ‘pCN33_P$_{icaR}$_5'UTR-*icaR*_TTG-*gfp*_3'UTR-*icaR_icaZ*del’ (strain collection codes ML89, ML91), showed the same fluorescence curve as the control strain without plasmid (*S. aureus* PS187Δ*hsdR*Δ*sauUSI*). Consequently, P$_{icaR}$ from *S. epidermidis* seems not to be expressed in *S. aureus* and, thus, the interaction of IcaZ and *icaR* mRNA could not be analysed in *S. aureus* background which might be due to the lack of unknown factors necessary for P$_{icaR}$ expression, such as binding site(s) for *icaR* or *ica*-operon regulator(s).

A

P_{icaZ} expression in TSB ± Cm^{30} at 37°C

Legend:
- S. aureus 187 ΔhsdR ΔsauUSI + pCerulean_icaZprom (ML96)
- S. aureus 187 ΔhsdR ΔsauUSI + pCerulean_icaZprom (ML97)
- S. aureus 187 ΔhsdR ΔsauUSI

B

P_{icaR} expression in TSB ± Erm^{12,5} at 37°C

Legend:
- S. aureus 187 ΔhsdR ΔsauUSI + pCN33_Pami_gyrB_GFP (ML94)
- S. aureus 187 ΔhsdR ΔsauUSI + pCN33_Pami_gyrB_GFP (ML95)
- S. aureus 187 ΔhsdR ΔsauUSI + PicaR_5'UTR-icaR_TTG-gfp_TT (ML98)
- S. aureus 187 ΔhsdR ΔsauUSI + PicaR_5'UTR-icaR_TTG-gfp_TT (ML99)
- S. aureus 187 ΔhsdR ΔsauUSI

Fig. V-7: Analysis of P_{icaZ} and P_{icaR} expression in *S. aureus*

(**A**) Depicted is the P_{icaZ} expression of the strains in TSB ± CM^{30} (similar results were obtained in LB medium ± CM^{30}) (**B**) Technical control via P_{ami} expression of GFP measurement (ML94 and ML95), control strains for P_{icaR} measurement without an interaction partner, lacking *icaR* 3' UTR (strains ML98 and ML99) and the wildtype without plasmid as reference, all grown in TSB ± CM^{30}. ML98 and ML99 appear as one line, close to the wildtype, because the measured GFP fluorescence was nearly identical.

For the analysis in S. epidermidis, three different *S. epidermidis* strains were used to analyse P_{icaR} activity; the *ica*-negative ATCC 12228, the *ica*-positive O-47 Wt and O-47Δ*rnc*. But, as in *S. aureus*, GFP fluorescence was measurable only in strains carrying GFP fused to P_{ami} (data not shown). The detected GFP fluorescence signal of the *ica*-positive strains was very weak and independent of the temperature, so that P_{icaR} expression had to be improved. To do so, the plasmids were extended for the region between *icaR* and *icaA* and also for the first 22 amino acids of *icaA* ORF. A stop codon and the terminator sequence of gene SA2206 of *S. aureus* were added downstream of the truncated *icaA* ORF

to avoid any transcript formation due to the inserted *icaA* promoter (2nd generation plasmids). In a next step, an LVA-tag was integrated at the 3′ end of *gfp* to generate an unstable GFP that allowed the detection of rapid changes in the fluorescence. These GFP-improved plasmids with an extended P$_{icaR}$ region (3rd generation plasmids) were named 'pCN33_SA2206TT_*icaA*-trunc_P$_{icaR}$_5'UTR-*icaR*_TTG-*gfp*-mut(LVA)_3'UTR-*icaR_icaZ*' and 'pCN33_SA2206TT_*icaA*-trunc_P$_{icaR}$_5'UTR-*icaR*_TTG-*gfp*-mut(LVA)_3'UTR-*icaR*_ *icaZ*del' (**Fig. V-8**).
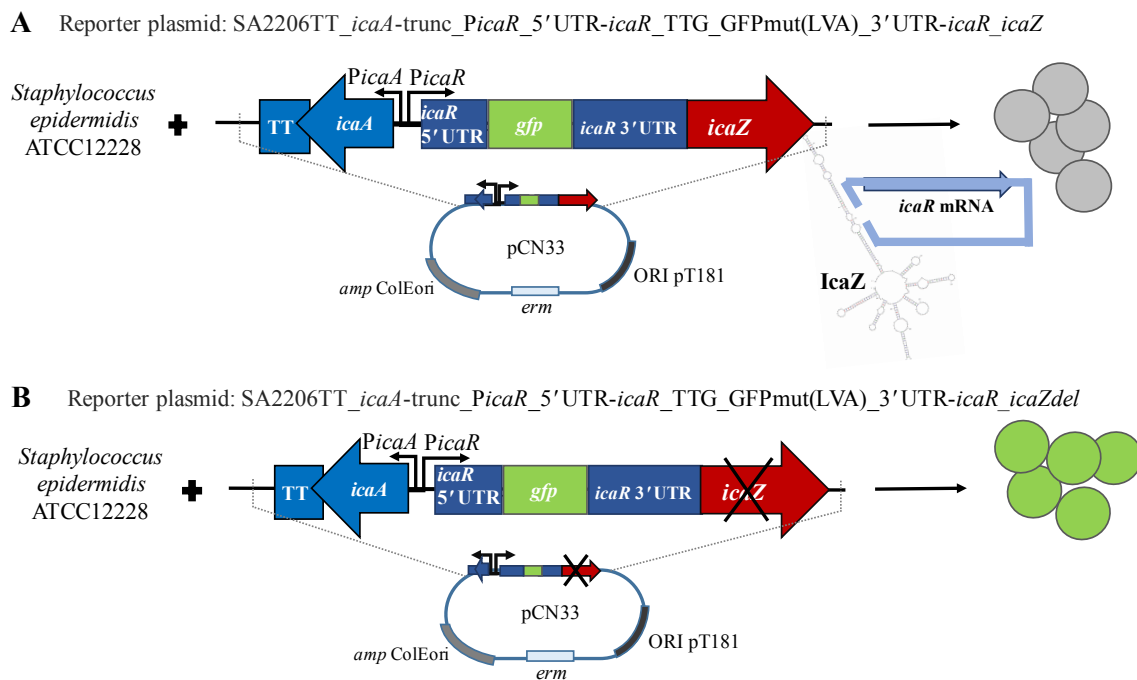
Fig. V-8: Cloning scheme for GFP-reporter plasmids (3rd generation)

Depicted is the improved GFP reporter plasmid and the supposed reaction after induced expression of IcaZ. The plasmid system was introduced into *S. epidermidis* ATCC 12228. Two variants were constructed; one of them contained the intact IcaZ sequence (top) and the other contained a non-intact IcaZ sequence (bottom). The *gfp* sequence contained an LVA-tag, which leads to an unstable GFP, so that non-degraded proteins don't sequester a quick change in *gfp* translation by IcaZ. According to the model, described in Fig. V-1, an interaction between IcaZ and *icaR* mRNA would lead to a decrease in GFP fluorescence due to the sequestration and degradation of *gfp* mRNA, whereas a non-interaction would lead to GFP fluorescence, because *gfp* mRNA can be translated into GFP.

The plasmids were constructed in *E. coli*, transferred into *S. aureus* and then transferred into *S. epidermidis* ATCC 12228. Unfortunately, GFP fluorescence did not improve upon the changes made in this class of plasmids, hence the interaction between IcaZ and *icaR* mRNA could not be analysed using the GFP reporter system. Possible reasons and additional improvements are mentioned in the discussions section.

Tab. V-1: List of GFP-reporter plasmids and plasmid carrying strains

Generation	Plasmid name	Plasmid description	Purpose	Plasmid carrying strain (strain collection code)			
				E. coli DC10B	*S. aureus* PS187 ΔhsdRΔsauUSI	*S. epidermidis* O-47	*S. epidermidis* ATCC12228
-	pCN33_P*ami*_*gyrB*_*gfp* (obtained from Prof. B. Felden)	*gyrB*-5'UTR fused to *gfp* under control of P*ami*	Control plasmid for *gfp* expression	V30	ML94-95	ML103-104	-
-	pCN33_P*icaR*_5'UTR-*icaR*_TTG-*gfp*_TT	*icaR*-5'UTR fused to *gfp* with *icaR*-start codon (TTG) under control of own promoter (P*icaR*)	Control plasmid for P*icaR* promoter expression	ML82-83	ML98-99	ML107-109	-
I	pCN33_P*icaR*_5'UTR-*icaR*_TTG-*gfp*_3'UTR-*icaR*_*icaZ*	*icaR*-5'UTR fused to *gfp* with *icaR*-start codon (TTG) under control of own promoter (P*icaR*) and *icaZ* downstream of *icaR*-3'UTR	GFP reporter for *IcaZ-icaR*-mRNA interaction with P*icaR* and stable GFP	ML84-85	ML88, ML90, ML92-93	ML105-106	-
	pCN33_P*icaR*_5'UTR-*icaR*_TTG-*gfp*_3'UTR-*icaR*_*icaZ*del	*icaR*-5'UTR fused to *gfp* with *icaR*-start codon (TTG) under control of own promoter (P*icaR*) and *icaZ* without middle part downstream of *icaR*-3'UTR	GFP reporter control for loss of *IcaZ-icaR*-mRNA interaction with P*icaR* and stable GFP	ML86-87	ML89, ML91	ML101-102	-
II	pCN33_SA2206TT_*icaA*-trunc_P*icaR*_5'UTR-*icaR*_TTG-*gfp*_3'UTR-*icaR*_*icaZ*	*icaR*-5'UTR fused to *gfp* with *icaR*-start codon (TTG) under control of own promoter (P*icaR*) with part of *icaA* and TT and *icaZ* downstream of *icaR*-3'UTR	GFP reporter for *IcaZ-icaR*-mRNA interaction with extended P*icaR*	ML118	-	-	-
	pCN33_SA2206TT_*icaA*-trunc_P*icaR*_5'UTR-*icaR*_TTG-*gfp*_3'UTR-*icaR*_*icaZ*del	*icaR*-5'UTR fused to *gfp* with *icaR*-start codon (TTG) under control of own promoter (P*icaR*) with part of *icaA* and TT and *icaZ* without middle part downstream of *icaR*-3'UTR	GFP reporter control for loss of *IcaZ-icaR*-mRNA interaction with extended P*icaR*	ML119	-	-	-
III	pCN33_SA2206TT_*icaA*-trunc_P*icaR*_5'UTR-*icaR*_TTG-*gfp*-mut(LVA)_3'UTR-*icaR*_*icaZ*	*icaR*-5'UTR fused to unstable *gfp* with *icaR*-start codon (TTG) under control of own promoter (P*icaR*) with part of *icaA* and TT and *icaZ* downstream of *icaR*-3'UTR	GFP reporter for *IcaZ-icaR*-mRNA interaction with extended P*icaR* and unstable GFP	ML123, ML128-129	ML131-134	-	ML137-138, ML130
	pCN33_SA2206TT_*icaA*-trunc_P*icaR*_5'UTR-*icaR*_TTG-*gfp*-mut(LVA)_3'UTR-*icaR*_*icaZ*del	*icaR*-5'UTR fused to unstable *gfp* with *icaR*-start codon (TTG) under control of own promoter (P*icaR*) with part of *icaA* and TT and *icaZ* without middle part downstream of *icaR*-3'UTR	GFP reporter control for loss of *IcaZ-icaR*-mRNA interaction with extended P*icaR* and unstable GFP	ML121	ML126-127	-	ML135-136

1.2 Investigation of RNase III involvement

1.2.1 *Cloning of S. epidermidis O-47Δrnc and the complementing strain*

Cloning of S. epidermidis O-47Δrnc:

Strain HS02, *S. epidermidis* O-47+pBASE6_flankreg _rnc, was constructed by Heike Schreier (Schreier, 2014) under supervision of the author. The plasmid consists of pBASE6 backbone and the flanking regions of *rnc* gene from *S. epidermidis* O-47. The transcript lengths of *rnc* adjacent genes were calculated from pulse-expression data of strain JE13 (O-47 background) to ensure that the deletion of *rnc* had no negative effect on the adjacent genes. Primer used for cloning are listed in **Annexe Tab. VIII-5**. Strain HS02 was used by the author for homologous recombination of regions flanking *rnc* on the plasmid with the homologous regions of *rnc* within the genome of *S. epidermidis* O-47 (chapter II-8.4.3). The successful double crossover caused the marker less deletion of *rnc* and resulted in *S. epidermidis* O-47Δ*rnc* (strain collection code ML40). The strain was verified by PCR and sequencing.

Cloning of S. epidermidis O-47 rnc complementing strain:

The strategy and primer design for cloning of *rnc* complementing strain were provided by the author to Jonas Helmreich, who performed subsequent cloning of plasmid pBASE6_rnc under the supervision of Dr Claudia Lange. For that, the PCR product was amplified from *S. epidermidis* O-47 genomic DNA with primer rnc_BglII_for and rnc_EcoRI_rev, giving a product size of 1118 bp. The product was digested with BglII and EcoRI and ligated with the previously digested and dephosphorylated pBASE6 vector. The resulting plasmid pBASE6_*rnc* contained *rnc* under control of its own promoter P*rnc* within the MCS of pBASE6 vector. The plasmid of strain *E. coli* DC10B+pBASE6_*rnc* (strain collection code CLA072) was then transferred by the author to *S. aureus* PS187Δ*hsdR*Δ*sauUSI* by electroporation method, generating strains ML124-125 and from there it was transferred via phage transduction into strain ML40 to generate *S. epidermidis* O-47Δ*rnc*+pBASE6_*rnc* (strain collection codes ML139-140). The complementing strains were tested by PCR for the successful incorporation of the plasmid and for genomic *rnc* deletion. The sequencing results were proven with the programme *CLC Main Workbench*.

1.2.2   *Role of RNase III in the degradation of various transcripts*

The double stranded endoribonuclease RNase III was shown to degrade the autoregulation complex of *icaR* mRNA in *S. aureus* (Ruiz de los Mozos *et al.*, 2013). For *S. epidermidis*, an interaction of *icaR* mRNA and IcaZ was suggested, therefore we analysed the effect of *rnc* deletion in *S. epidermidis* O-47 on these transcripts. An effect of IcaZ *in-trans* overexpression in *S. epidermidis* O-47Δ*rnc* on the biofilm formation was investigated previously by classical crystal violet biofilm assays (chapter IV-2.2.4). Thereby, an effect of IcaZ on the biofilm amount and composition was not observed.

Rifampicin Northern blots were performed with total RNA from *S. epidermidis* O-47 Wt and O-47Δ*rnc* to analyse, if *rnc* deletion influences the RNA stability of various transcripts, *i.e. icaR* mRNA, the putative threonyl-tRNA tRNA^{Thr-4}, ncRNA IcaZ and small RNA RsaE. The small, non-coding RNA RsaE was found to be expressed in late exponential phase in *S. aureus* (Geissmann *et al.*, 2009) and also in the exponential phase in *S. epidermidis*.

If RNase III is involved in the degradation of these transcripts, they would be more stable in the mutant strain. As this was not observed, RNase III was concluded to not be involved in the degradation process (**Fig. V-9 A+C**). A possible increase in the transcription rate was also not detected, because the thickness of the bands in T_0 samples was equal (**Fig. V-9 B**).

With these rifampicin stability assays, it was not tested, if RNase III is able to cleave an interaction complex of *icaR* mRNA and IcaZ as the Northern blots are carried out using denaturing PAA gels. To investigate this, an *in vitro* cleavage assay with radioactively labelled interaction complex and purified *S. epidermidis* RNase III, subsequently followed by gel analysis, could be performed.
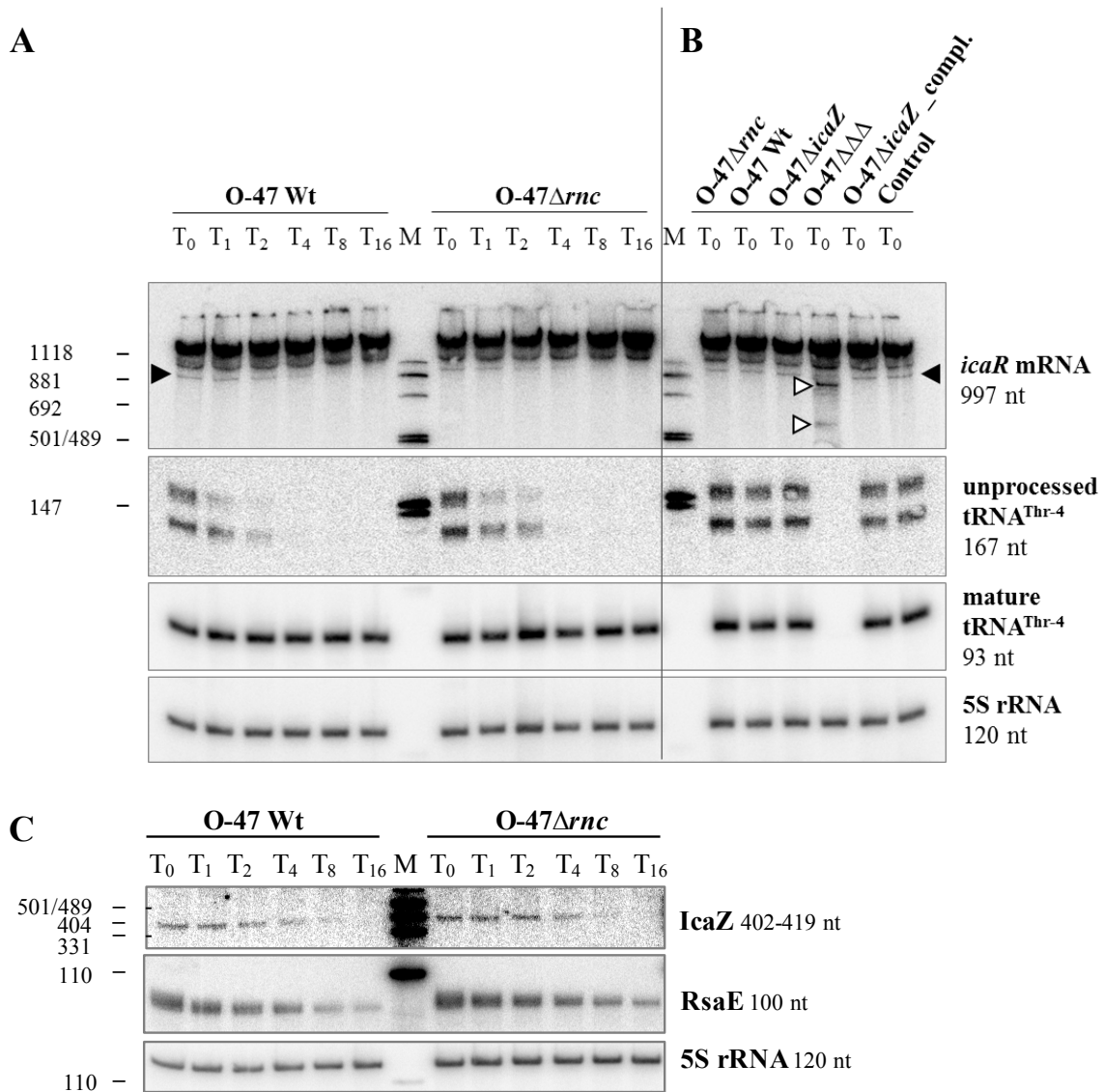
Fig. V-9: Rifampicin Northern blot of total RNA from *S. epidermidis* O-47 Wt and *rnc* mutant

(**A+B**) The Northern blot represents one of three independent biological replicates. It depicts the RNA stabilities of *icaR* mRNA and tRNA^{Thr-4} from *S. epidermidis* O-47 Wt and O-47Δ*rnc* (strain collection code ML40), O-47Δ*icaZ* (strain collection code ML38), O-47Δ*tRNA*$^{Thr-4}$Δ*icaZ*Δ*icaR*-3′ UTR (strain collection code FL1Δ2), O-47Δ*icaZ* complementing strain ML80 and the control strain ML47, carrying the empty plasmid. Total RNA was sampled in TSB medium at 30°C in exponential growth phase. The first sample was taken before rifampicin was added [endc.: 100 ng/ ml], then after indicated minutes. RNA was isolated using the standard protocol and 10 µg were separated on 5% PAA/ 7M urea gel at 300V for 2h. RNA bands were detected using radioactively labelled IcaR ds-DNA probe, tRNA-3'UTR_as oligo (detecting unprocessed tRNA^{Thr-4}), t-RNA-thr-oligo (detecting mature tRNA^{Thr-4}) and 5SrRNA oligo (detecting 5S rRNA) as loading control. (**C**) The Northern blot represents one of three independent biological replicates. It depicts the RNA stabilities of IcaZ and RsaE from *S. epidermidis* O-47 Wt and O-47Δ*rnc* (strain collection code ML40). Sampling of RNA as in A+B, but separated on 6%PAA/ 7M urea gel at 300V for 2h 10min. RNA bands were detected using radioactively labelled IcaZ ds-DNA probe, RsaE_Oligo new and 5SrRNA oligo.

2. Effect of IcaZ deletion and overexpression on transcript number and mRNA stability of known *ica*-operon regulators

Several protein regulators, *i.e.* SarA, IcaR and TcaR, have been published to bind upstream of *icaADBC*-operon between *icaA*, the first gene of the operon, and *icaR* (see chapter I-2.3.2; **Tab. I-2**). The binding sites of these regulatory proteins partly overlap with each other (**Fig. V-10),** so that the following questions arose: Which regulators bind at the same time or which one binds first, second, third etc.? Do they influence each other, because of their three-dimensional structure? Are the above listed regulators even expressed in the exponential growth phase, so that they have the possibility to interact with IcaZ?

IcaR functions as tetramer and negatively regulates *icaA*. If the supposed IcaZ-*icaR* mRNA interaction leads to a reduction of IcaR monomers, the repression of the *icaADBC*-operon would be reduced. But TcaR, which is a MarR family binding protein with ss-DNA binding ability (Chang *et al.*, 2012) that acts also as a repressor, could inhibit *icaA* transcription theoretically, even when IcaR is missing. Rifampicin Northern blots were performed to analyse the expression of these regulators in the exponential growth phase, when IcaZ is expressed. For that, total RNA from *S. epidermidis* O-47, O-47Δ*icaZ* and the complementing strain was used. *icaR* mRNA was detected, but *tcaR* mRNA was not although several independent hybridisation approaches were conducted. It was concluded that TcaR is not present in the exponential growth phase and that the repressor is therefore no interaction partner for IcaZ and not relevant for PIA biofilm regulation by IcaZ (**Fig. V-11**).

SarA acts as a homodimer and is a positive regulator of *icaA* and PIA biofilm formation, and SarA protein has its binding site next to IcaR in P*icaR-icaA* (**Fig. V-10 A**). *sarA* mRNA was detected on the Northern blots, therefore could represent a possible interaction partner for IcaZ. The deletion of IcaZ had no influence on neither *sar*A nor *icaR* transcript numbers or their stabilities (**Fig. V-11**). Identical results were obtained from the complementary strain ML80 upon *icaZ* pulse-expression. It is concluded that IcaZ does not affect *sarA* or *icaR* gene expression on transcriptional level. A post-transcriptional effect on mRNA stability that was expected at least for *icaR* mRNA was not observed. Moreover, TcaR and SarA do not inhibit each other regarding the binding of P*icaR-icaA* in the exponential growth phase, because TcaR is not present.

= TSS of *icaA* = TSS of *icaR*

Fig. V-10: DNA binding sites of *icaADBC*-operon regulators

(**A**) Schematic overview of the binding sites upstream of *icaA* (within P$_{icaR-icaA}$ region) for *icaADBC*-operon regulators of *S. epidermidis*. The regulators are depicted as spheres, whereat the functional regulators are dimers (*i.e.* SarA and TcaR) or tetramers (*i.e.* IcaR) (see legend below the rectangle). (**B**) Depicted is the double stranded nucleotide sequence of P$_{icaR-icaA}$ region from *S. epidermidis* RP62A. The nucleotide sequences of RP62A and O-47 are identical for this genomic region, except for one nucleotide within IcaR binding site (*icaA* ORF -31). The open reading frames for *icaR* and *icaA* are depicted in yellow; binding sites for TcaR in grey; binding sites for SarA in green and for IcaR in blue. The arrows mark the transcription start sites of *icaA* and *icaR*.

Fig. V-11: Rifampicin Northern blot of total RNA from *S. epidermidis* O-47, O-47Δ*icaZ* and the complementing strain

Northern blot of total RNA from *S. epidermidis* O-47, O-47Δ*icaZ* (strain collection code ML38) and IcaZ complementing strain *S. epidermidis* O-47Δ*icaZ*+pCG248c_*icaZ*sML_ΔTT (strain collection code ML80). RNA was sampled from exponential growth phase in TSB medium at 30°C. The first sample in the complementing strain was taken before ATc [endc.: 100 ng/ ml] was added (T_{00}), then further samples were taken before (T_0) and after rifampicin addition [endc.: 100 μg/ ml] at indicated time points in minutes (T_1-T_{16}). ATc was not added to the culture medium of the wildtype and the mutant. The RNA was isolated using the standard protocol and 10 μg were separated on 5% PAA/ 7M urea gel at 300V for 2h. RNA bands were detected using radioactively labelled IcaR, IcaZ and SarA ds-DNA probes. 5S rRNA was detected with 5SrRNA oligo as loading control.

3. IcaZ expression is increased by ethanol, but not by NaCl or glucose

The previous sections aimed at analysing factors that are regulated by ncRNA IcaZ. Here, the emphasis was on unravelling the factors that influence or regulate ncRNA IcaZ. Ethanol and NaCl were tested as stimuli, because both were demonstrated previously to influence *icaR* expression negatively. The regulatory factor(s) mediating this effect, however, are/is still unknown (O'Gara, 2007). Glucose was described as a positive effector for PIA-biofilm production via (again) an unknown regulatory circuit. However, it is hypothesised that glucose might facilitate PIA production indirectly through its role in central carbon metabolism and as a substrate for PIA precursor synthesis rather than by directly influencing *icaADBC* operon expression (O'Gara, 2007). In the light of the unusual carbon utilisation proteome signature detected in the *icaZ* triple mutant in the exponential growth phase at 30°C, the effect of glucose on *icaZ* expression was tested as well.

For investigating the influence of ethanol, NaCl and glucose on *icaZ* expression, the cerulean reporter system was used. Plasmid pCerulean_icaZprom was constructed by integrating P_{icaZ} in front of the cerulean gene in plasmid pCerulean. The generated plasmid was transferred into *S. epidermidis* O-47 to generate *S. epidermidis* O-47+pCerulean_icaZprom (strain collection code ML13). This strain was stimulated during growth with ethanol, NaCl and different concentrations of glucose.

The effects of the additives were analysed by cerulean fluorescence measurement with Tecan analyser and cerulean fluorescence detection by confocal laser scanning microscopy (CLSM). As shown in **Fig. V-12 B**, ethanol had a positive effect on P_{icaZ}, during exponential growth. Thus, between 4h-7h of growth cerulean expression was highly increased at 37°C. This increase in cerulean expression was also detectable at 30°C, but between 6h-11h due to slower growth of the culture at lower temperature (data not shown). A slight increase of cerulean fluorescence was also detectable with supplementation of NaCl, whereas the addition of glucose had no effect on P_{icaZ} activity (**Fig. V-12 B**).

Confocal laser scanning microscopy was used to verify the results obtained with the Tecan analyzer. For that, the strain was grown overnight in TSB medium at 37°C. The culture was diluted to $OD_{600} \sim 0.05$ and further grown to exponential growth phase with addition of ethanol or NaCl. *S. epidermidis* O-47 Wt was used as negative control for cerulean fluorescence (**Fig. V-13 A**). The signal intensity was adjusted to the background fluorescence of these cells. Strain *S. epidermidis* O-47+pCerulean_icaZprom showed cells that expressed IcaZ and cells that did not express the ncRNA (**Fig. V-13 B**). The heterogeneous expression of P_{icaZ} was shown before (**Fig. III-8**). After addition of ethanol, all cells expressed IcaZ (**Fig. V-13 C**). In contrast, addition of NaCl had no significant effect as the cells expressed IcaZ in a similar heterogeneous pattern as the control strain (**Fig. V-13 D**).

A

B
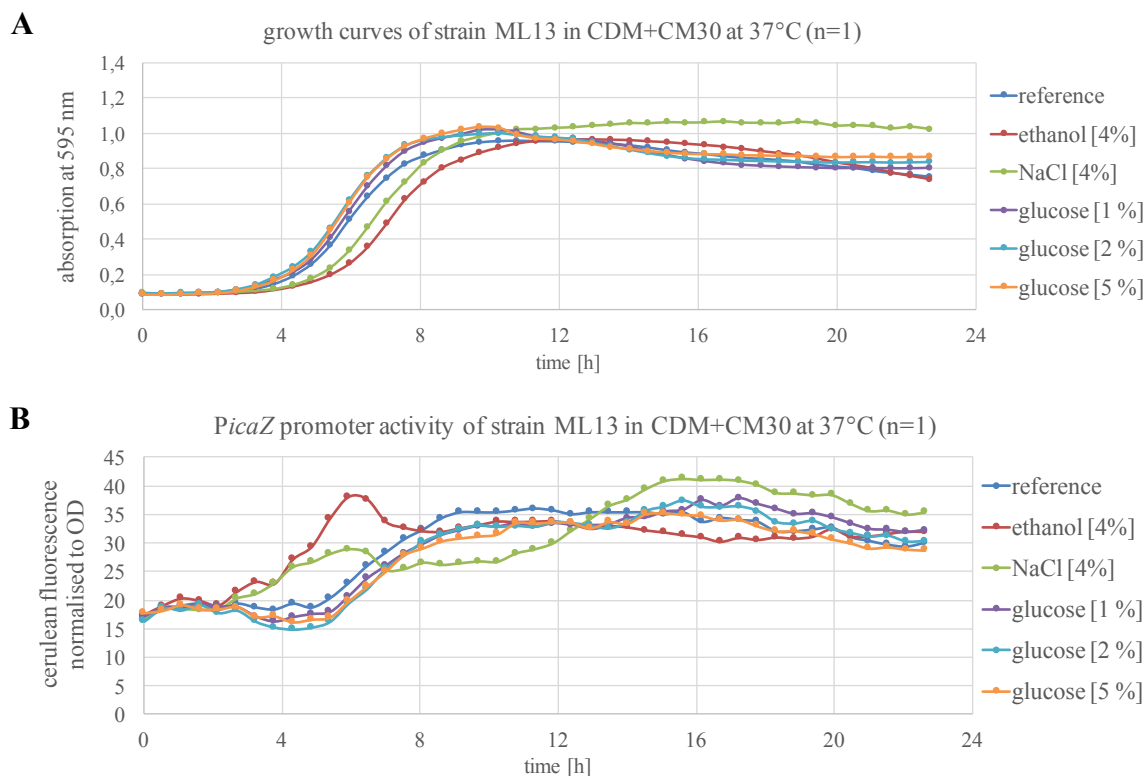
Fig. V-12: Influence of medium additives on P$_{icaZ}$ expression

For Tecan cerulean read out, strains were grown in chemically defined medium (CDM) with or without ethanol, NaCl and glucose at 30°C and 37°C. The growth curves of 37°C are depicted in (**A**). The fluorescence of cerulean was measured with excitation wavelength at 430 nm and emission wavelength at 485 nm for Tecan read out. The gain was set manually to 50. The fluorescence was normalised to the growth (**B**). One biological replicate is shown as representative. The experiment was done in duplicate.
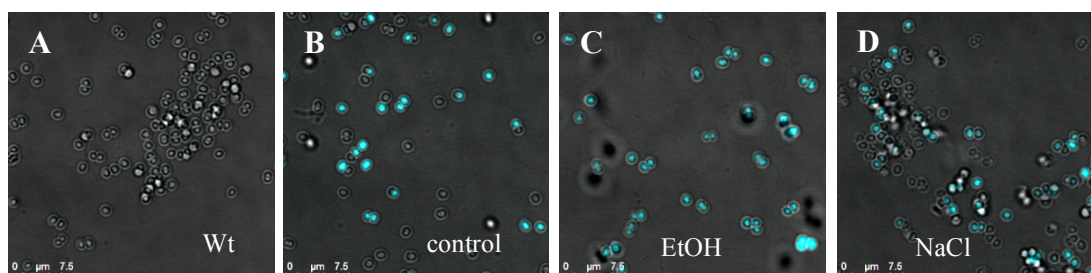
Fig. V-13: Influence of medium additives on IcaZ expression (CLSM)

For CLSM analysis, the laser power of the confocal laser scanning microscope was adjusted to *S. epidermidis* O-47 Wt as negative control (**A**). *S. epidermidis* O-47 +pCerulean_icaZprom (strain collection code ML13) was grown at 37°C in plain TSB (**B**) or with the addition of 4% ethanol (**C**) or 4% NaCl (**D**).

4. Summary of Results for Part C

- Based on the results of part A and B, a hypothetic model for the regulation of PIA biofilm formation by ncRNA IcaZ was proposed (**Fig. V-1**).

- Classical electrophoretic mobility shift assays revealed that *S. epidermidis icaR* 5′UTR and *icaR* 3′UTR do not interact and thus *S. epidermidis icaR* mRNA does not undergo autoregulation as in *S. aureus*. The autoregulation of *S. aureus icaR* mRNA was validated experimentally in strain *S. aureus* 8235 and served as positive control for the gel shift assays (**Fig. V-2**).

- An interaction of IcaZ with *icaR* mRNA was identified: A gel shift was observed for radioactively labelled full length IcaZ and *in vitro* transcribed *icaR* 5′3′UTR fusion product and *vice versa* (**Fig. V-5 C+E**). Radioactively labelled IcaZ-part 1 showed a weak band shift with *in vitro* transcribed *icaR* 5′3′UTR fusion product (**Fig. V-5 A**), whereas IcaZ-part 2 did not (**Fig. V-5 B**). An interaction between radioactively labelled *icaA* 5′UTR and *in vitro* transcribed full length IcaZ was experimentally ruled out (**Fig. V-5 F**) and served as negative control.

- In collaboration with Dr Ingrid Tessmer (RVZ, Würzburg), atomic force microscopy (AFM) was successfully used to visualise IcaZ secondary structure variants (**Annexe Fig. VIII-4**). Inconclusive results, however, were obtained for RNA-RNA interactions, concluding that the technique is less suitable for this purpose (data not shown; experimental procedure in Annexe-Supplementary experiment).

- GFP-reporter plasmids were created and further developed to analyse the interaction of IcaZ and *icaR* mRNA (**Tab. V-1; Fig. V-8**). Unexpectedly, the overall GFP fluorescence in staphylococcal backgrounds was too low, so that the interaction could not be analysed with this system.

- The experiments, nevertheless, provided some interesting insights for future experimental planning:
  - The *icaZ* promoter is active in *E. coli* DC10B and *S. aureus* PS187Δ*hsdR*Δ*sau*USI host backgrounds.
  - In contrast, the *S. epidermidis icaR* promoter P*icaR* is active in *E. coli* DC10B, but not in *S. aureus* PS187Δ*hsdR*Δ*sauUSI*.

- The RNase III mutant, *S. epidermidis* O-47Δ*rnc*, and the *rnc* complementing strain, *S. epidermidis* O-47Δ*rnc*+pBASE6_rnc, were generated in this work (chapter II-8.4.3 and chapter V-1.2.1) and used for the analysis of an involvement of RNase III on transcript degradation. The deletion of RNase III did not affect transcript stability of tRNA^{Thr-4}, *icaR* mRNA, IcaZ or RsaE (**Fig. V-9**).

- The effect of *icaZ* deletion and overexpression on the transcript number of *ica*-operon regulators was analysed:

- o SarA and IcaR are expressed during exponential growth phase. Neither the deletion of IcaZ, nor its overexpression had an impact on the transcription of *sarA* and *icaR* or their mRNA transcript stabilities (**Fig. V-11**).
- o TcaR is not expressed during the exponential growth phase and therefore an unlikely interaction partner of IcaZ or regulatory factor for IcaZ (**Fig. V-11**).

- The generated cerulean reporter system for P*icaZ* expression was used to analyse the effect of ethanol, NaCl and glucose. In contrast to glucose, the addition of NaCl and ethanol to the culture medium caused an increase in P*icaZ* expression, which was measured by Tecan system (**Fig. V-12**). The effect of ethanol was verified by confocal laser scanning microscopy (**Fig. V-13**). Ethanol was discovered to be a positive trigger for *icaZ* expression.

- The regulatory network of PIA biofilm formation was enlarged by ncRNA IcaZ, which is suggested to be a positive regulator for *ica*-operon expression by regulating *icaR* mRNA through direct binding.

VI. Discussion

This work characterises IcaZ, the first non-coding RNA that is found in the near surrounding of the intercellular adhesin (*ica*) locus of *Staphylococcus epidermidis*, and reveals its function as the regulator of the regulator of PIA-mediated biofilm formation.

1. Ica-positive *S. epidermidis* harbour a lncRNA, named IcaZ, downstream of *icaR* repressor gene

1.1 The intergenic region downstream of *icaR* harbours a transcript named IcaZ

The intergenic region between *icaR* and $tRNA^{Thr-4}$ was shown initially in our group by Northern blot analysis to harbour a transcript of 400-500 nt (487 nt; Eckart, 2006). In this work, by using circular RACE, the exact 5′ and 3′ ends of this transcript, named IcaZ, were determined and the length was corrected to 402-419 nt in *S. epidermidis* O-47 (401 nt in *S. epidermidis* RP62A). The *icaZ* gene is transcribed in early- and mid-exponential growth phase from two transcription start sites (TSS 1 or TSS 2) that were determined by *BPROM* prediction and verified experimentally by transcriptome analysis of *S. epidermidis* PS2. Transcription of *icaZ* stops after a Rho-independent transcription terminator sequence that is shared with the converging gene $tRNA^{Thr-4}$. Consequently, *icaZ* does not overlap with the $tRNA^{Thr-4}$ ORF as supposed by Eckart, 2006.

Because the preceding gene *icaR* was shown to have a very long 3′ UTR in *S. aureus* (Ruiz de los Mozos *et al.*, 2013), the length of *icaR* mRNA was also determined with cRACE for *S. epidermidis* O-47. Due to its length of 374 nt (365 nt in RP62A), *icaR* 3′ UTR was shown to overlap with *icaZ* for up to 32 nt, hence the promoter of *icaZ* (P*icaZ*) is located within *icaR* 3' UTR. As small RNAs can be 3' UTR derived (Svensson and Sharma, 2016), IcaZ was proven to be a primary transcript, rather than the result of a read-through by *icaR* gene, by two independent approaches: (i) treatment of RNA with the 5' monophosphate-dependent RNase TEX removed all transcripts derived from processing events containing a 5'monophosphate and enriched the RNA pool for primary transcripts containing a 5'triphosphate (Sharma *et al.*, 2010; Sharma and Vogel, 2014). This confirmed IcaZ as a primary transcript in the transcriptome data of *S. epidermidis* PS2. (ii) functionality of the

promoter region of *icaZ* gene (P*icaZ*) in *S. epidermidis* O-47 was verified using a *cfp*-reporter system that contained the Cerulean gene under the control of P*icaZ*. Confocal laser scanning microscopy was applied to detect Cerulean fluorescence in single cells. P*icaZ* was hereby shown to be active in cells that attached to the surface and were the starting point for cell-cell accumulation and later biofilm formation. The fluorescence signal was detectable over several hours in subpopulations of cells. This contrasted with data from *S. epidermidis* PS2, in which the same *cfp*-reporter plasmid, but for the P*RsaE* was used. P*RsaE* was heterogeneously expressed and cells were often found to switch off within 30 min while new cells switched on (Dr Sonja Schoenfelder, unpublished data). We therefore assumed that P*icaZ* was permanently active in these subpopulations over several hours. Bleaching of the fluorescence protein was not applied here. The promoter activity of P*icaZ* reflects rather a constant low-level need of IcaZ in certain cell clusters involved in attachment and biofilm formation.

In conclusion, IcaZ was clearly identified as an independent RNA and not as a read-through by the preceding *icaR* gene, nor a 3' UTR derived RNA. Due to the obtained data regarding the length of IcaZ and the neighbouring genes, the annotated localisation of *icaZ* was revised (see **Fig. III-19**).

1.2 IcaZ is specific for *ica*-positive *S. epidermidis* and is part of the *ica*-locus

NCBI database screening for IcaZ nucleotide sequence demonstrated that IcaZ is specific for *S. epidermidis* harbouring concomitantly the *icaADBC*-operon and the repressor gene *icaR*, suggesting that IcaZ is an inherent part of the *ica*-locus. Ica-negative *S. epidermidis* and other CoNS species lack IcaZ and surprisingly the ncRNA is also not present in *S. aureus*, although all sequenced *S. aureus* genomes encode *icaADBC* and *icaR* genes, as well as a long intergenic region (IGR) downstream of *icaR*. Interestingly, the IGR does also not contain any other transcripts*,* as shown here by Northern blot analysis, suggesting significant differences concerning the *ica*-locus structure and regulation between *S. aureus* and *S. epidermidis*.

In *S. epidermidis*, IcaZ is located right next to the $tRNA^{Thr-4}$ gene, which is conserved among *S. epidermidis* regardless of *icaADBC* presence and to a lesser extend in other CoNS species, whereas this putative threonyl-tRNA is not present in *S. aureus*. Due to their genetic conservation, tRNA genes have been shown to serve as common insertion sites for mobile genetic elements such as phages or pathogenicity islands (Katz *et al.*, 2016). Interestingly, *ica*-positive and *ica*-negative *S. epidermidis* strains differ in the region downstream of $tRNA^{Thr-4}$, exactly after the $tRNA^{Thr-4}$ nucleotide sequence, suggesting that the *ica*-locus was integrated precisely at this genomic site (Eckart, 2006). IcaZ is thus supposed to be part of this mobile *ica*-locus.

However, the *ica*-genes of *S. epidermidis* have not been found on plasmids so far. For *S. aureus,* it was shown recently that *ica*-like genes were located on plasmid pAFS11 from a bovine methicillin-resistant *S. aureus* (MRSA) isolate (Fessler *et al.*, 2016). While the nucleotide sequences shared no similarities, the amino acid sequences identified the gene products as Ica proteins with 64.4-76.9% homology to *S. aureus* strains Mu50, Mu3 and N315 and 96.2-99.4% homology to *S. sciuri* NS1, revealing a horizontal gene transfer from *S. sciuri* to *S. aureus* (Fessler *et al.*, 2016). This example shows that *ica*-genes can be mobile.

1.3 *icaZ* gene exists in two alleles in *ica*-positive *S. epidermidis*

The *icaZ* gene was found to exist in two allelic forms, which differ only in four nucleotides. The genomes that were analysed either experimentally or computationally, were assigned to carry either the RP62A-*icaZ* gene sequence or the O-47-*icaZ* gene sequence. To examine, if the nucleotide exchanges influence the functionality of ncRNA IcaZ, plasmids with correct O-47 *icaZ* gene sequence or with single nucleotide mutations were generated and biofilm formation assays were carried out with strains carrying these plasmids.

S. epidermidis O-47Δ*tRNA*^{Thr-4}Δ*icaZ*Δ*icaR*-3′ UTR (O-47ΔΔΔ) overexpressing RP62A-IcaZ showed less biofilm formation than the triple mutant strains with O-47-IcaZ overexpression, suggesting that the exchanged nucleotides have an impact on RNA functionality. However, since the expression of these plasmids in O-47 wildtype genetic background had no impact on biofilm formation and the nucleotide exchanges had no effect on the predicted secondary structure (compared by *MFold*), the results remain inconclusive.

1.4 IcaZ is suggested to be a long non-coding RNA (lncRNA)

The *icaZ* nucleotide sequence does not harbour a long open reading frame, suggesting that IcaZ represents a non-coding RNA, which according to its length classifies as long ncRNA (Ma *et al.*, 2013). Occasionally, lncRNAs may encode short oligopeptides (*e.g.* the effector molecule of the staphylococcal Agr-quorum-sensing system, RNAIII, encodes the delta-hemolysin gene *hld*) and thus exhibit dual function (Novick *et al.*, 1993; Bronesky *et al.*, 2016). IcaZ indeed harbours two short open reading frames which lack, however, *bona fide* ribosomal binding sites. Preliminary experiments introducing Strep-tags to the C-terminus of the peptides did not reveal convincing evidence for efficient translation of the ORFs into polypeptides (Müller, 2012; Nosocomial Infections, IMIB, Würzburg). Moreover, blasting the putative ORFs against NCBI database using *protein blast*, did not reveal any similar protein matches in the database of NCBI.

Nevertheless, IcaZ stem loop 2 came into focus when secondary structure predictions by *MFold* using 3′ end truncated IGR*ica*-RNA nucleotide sequence (413 nt from TSS) revealed a loose base pairing in stem loop 2 at 30°C compared to 37°C (see **Annexe Fig.**

VIII-13). A closer look at the nucleotide sequence of IcaZ stem loop 2 revealed that the stem contains four uridines in a row that pair with a G-rich region that is followed by ORF2. Interestingly, the sequence is identical to a known Shine-Dalgarno sequence of an RNA thermometer (Narberhaus *et al.*, 2006; see **Annexe Fig. VIII-14**).

By definition, RNA thermometers are complex RNA structures that change their conformation in response to temperature (Narberhaus *et al.*, 2006). A drop of temperature was shown to induce translation by loosening the base pairing of the RNA thermometer and exposing the SD sequence. Moreover, they likewise can sense small molecules (Chowdhury *et al.*, 2006; Narberhaus *et al.*, 2006; Rossmanith and Narberhaus, 2016). A model RNA thermometer is the ROSE-element (repressor of heat-shock gene expression), which is present in small heat-shock genes in Gram-negative bacteria. Hereby, elevated temperature of 42°C induces the transformation and the release of the SD sequence. An involvement of RNase III in binding and structural transition leading to translation stimulation, but not degradation, was also supposed (Altuvia *et al*. 1989).

In IcaZ, the second G within the putative SD sequence (AAG<u>G</u>AG) in stem loop 2 is one of the four nucleotides that are different between *S. epidermidis* O-47- and RP62A-IcaZ (see chapter VI-1.3). If the sequence is a functional SD sequence, then the G167T exchange would probably reduce or inhibit translation of ORF2. This would explain the diminished biofilm in RP62A-IcaZ overexpressing strains, presupposed the putative peptide is a positive regulator. Also, the loss of nucleotide 251 (G; calculated from IcaZ TSS1), which is located within ORF2, could influence the amino acid structure of the putative protein and might lead to a non-functional protein in RP62A. The putative ORF 2, ranging from position 205 until 303 within IcaZ of O-47, has the amino acid sequence 'I M K K K C I V E V R L N K K R E W N Q I S L N I L F Y F N I S Stop'. Because of the deleted nucleotide, it is reduced to 'I M K K K C I V E V R L N K K K S G T K F H Stop' in RP62A-IcaZ, which leads to a shortened length.

Another RNA thermometer, the 'fourU'-thermometer, was identified first in Salmonella *agsA*, which codes for a heat-shock protein (Waldminghaus *et al.*, 2007). In *agsA* mRNA, four uridines pair with the SD sequence and control the translation of the downstream ORF until high temperature opens the structure to facilitate ribosome binding. The authors reported that mutations within the element affected the translation *in vivo*. This supports the idea that the G167T exchange could inhibit translation of ORF2 in RP62A-IcaZ. Kortmann and Narberhaus, 2012, further mentioned in their review that a few key features are necessary for proper function of a fourU element. These include a destabilising mismatch pair at the bottom of the fourU motif that is required for melting of the helix, a stabilising GC base pair at the top that serves as molecular clamp, and Mg^{2+} binding sites (**Fig. VI-1 A**). By comparison of IcaZ stem 2 with *agsA*, the stabilising GC pair is missing

so that there might be no remote effect via the hydration shell or the hydration shell is formed differently. A second Mg^{2+} binding site next to the fourU element is also missing (**Fig. VI-1 B**).

But, as this example is from *Salmonella*, it could work differently in *Staphylococcus*. This assumption is supported by a review, in which it is stated that there is no sequence conservation among RNA thermometers, although belonging to ROSE- or fourU-elements (Grosso-Becera *et al.*, 2015). However, the putative SD sequence is in suboptimal distance to the downstream located, predicted ORF2 (+35 nt) and more data and experiments are necessary to further analyse this aspect. Although we cannot entirely rule out the possibility of short peptide-encoding regions in *icaZ* at this time, we consider the transcript preliminarily as a non-coding RNA with regulatory function and not as a dual-RNA or mRNA.
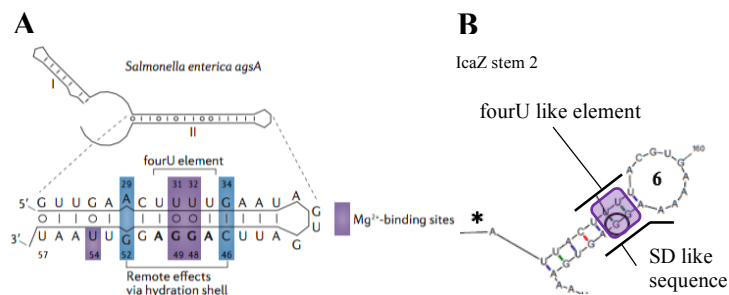
Fig. VI-1: FourU thermo-sensor of *agsA* and putative fourU element of IcaZ

A) *Salmonella enterica agsA* taken from Kortmann and Narberhaus, 2012 (part of figure 2).
B) *Staphylococcus epidermidis* IcaZ stem loop 2 (taken from Fig. III-15).

2. Functional role of ncRNA IcaZ and its effect on biofilm formation

2.1 IcaZ is critically involved in PIA-mediated biofilm formation

Regular detection of IcaZ in biofilm forming strains and its association with the *ica* locus led to the assumption that the ncRNA might play a role in PIA-mediated biofilm formation. Indeed, markerless deletions of either the complete *icaZ* sequence or only its middle part as in mutant O-47Δ*icaZ*, caused a distinct macroscopic, biofilm-negative phenotype with predominantly diminished PIA biofilm. Sequencing of the deletion bordering genes *tRNA^{Thr-4}* and *icaR,* and *icaADBC,* confirmed their integrity. To ensure that the observed phenotype is only due to the deletion of the *icaZ* gene and not the consequence of other secondary mutations in the genome, two further Δ*icaZ* mutants were generated independently, which showed the same biofilm-negative phenotype as strain O-47Δ*icaZ*, thereby ruling out additional mutations as the cause of the observed phenotype.

The composition of the biofilm of wildtype and mutant was deciphered *in vitro* by classical crystal violet assays which revealed the clear reduction of polysaccharides in the mutant. These results were verified *in vivo* by confocal laser scanning microscopy. The growing biofilm was here analysed in real time and PIA was detected by staining with fluorescent Wheat Germ Agglutinin (WGA). In addition, shear stress was applied to the cultures using a peristaltic pump that produced a medium flow to simulate a dynamic infection environment. Shear stress was shown before to specifically induce PIA-biofilm (Weaver *et al.*, 2012). Here, it was used to trigger polysaccharide formation especially in the mutant. Before starting the flow, both the wildtype and the mutant could get in touch with the chamber slide surface, but when the fluid flow was started, most of the IcaZ mutant colonies were torn away. While the wildtype formed bacterial clusters that further emerged as a complete biofilm with channels and towers, the mutant formed only flat cell layers and had lost its biofilm forming ability (**Fig. IV-14**).

Conclusively, the experiments revealed a tremendous inability of the mutant to attach to the chamber slide surface and to other bacterial cells (**Fig. IV-13**). Surface attachment and colonisation of catheters are mediated amongst others through the accumulation associated protein Aap (Vandecasteele *et al.*, 2003). Microarray analysis showed that *aap* mRNA was diminished transcribed in the mutant in the exponential growth phase compared to the wildtype and thus is less translated into Aap. The *in vivo* experiments moreover revealed that extracellular polysaccharides were also highly diminished in the mutant. As almost all extracellular polysaccharides in staphylococci are part of the polysaccharide intercellular adhesin (PIA), which connects the bacterial cells within a biofilm, it is likely that the absence of Aap and PIA are reasons for the inability of the mutant to form a proper biofilm.

As the genetic requirements for Aap or PIA formation are still present in the *icaZ* mutant and a malfunction of the *ica*-operon can be excluded, the reason for the biofilm negative phenotype must solely be due to a regulatory effect of IcaZ. In general, it is remarkable that the deletion of a ncRNA elicits such a virulence defect and does not only cause a 'molecular phenotype', like in most cases when small RNAs are deleted (Barquist *et al.*, 2016).

2.2 Lower temperatures of 30°C increased biofilm formation and IcaZ expression

Interestingly, all biofilm assays of this work showed that *S. epidermidis* produced more biofilm, especially more polysaccharides (PIA) at 30°C, than at 37°C.

Generally, elevated temperatures (>37°C) are assumed to enhance biofilm production and the only report claiming that also lower temperatures increase biofilm formation in some *S. epidermidis* strains was published by Fitzpatrick *et al.*. The enhanced biofilm formation was asserted by the authors to be *ica*-independent and not to be associated with the activation of the *icaADBC*-operon (Fitzpatrick *et al.*, 2005).

Here, we showed by Northern blot analysis and by standard biofilm assays that IcaZ expression and PIA synthesis both increased at lower temperatures in *S. epidermidis* and thus the biofilm increase was *ica*-dependent. As lower temperatures of 30-33°C are known environmental factors for the commensal lifestyle *e.g.* on the skin, PIA-biofilm not only seems to be beneficial for an infection environment, but also for commensal growth in this organism. In *S. aureus* in contrast, we observed that only the protein portion within the biofilm varied upon temperature shift, highlighting again the difference of biofilm composition among different species of staphylococci.

2.3 IcaZ overexpression *in trans* restored biofilm formation dependant on the mutant

The deletion of IcaZ in the mutant strains was complemented by inducible expression of the ncRNA from vector pCG248 carrying different length of IGR*ica*-RNA or IcaZ. The expression was induced by addition of anhydrotetracycline (ATc) to the culture medium and biofilm composition was measured after 18-20h by crystal violet method. Interestingly, a complementation of the biofilm formation was observed for mutant O-47ΔΔΔ, but not for O-47Δ*icaZ*. The amount of PIA-biofilm increased dose-dependently in IcaZ overexpressing strains MF52, MF58 and JE13 (**Fig. IV-16**; **Fig. VIII-9**), when ATc was added to the growth medium. As negative controls served the bacterial cultures without ATc, because due to the binding of the repressor protein TetR to the two repressor binding sites on plasmid pCG248, the promotor P$_{xyl/tet}$ was blocked and IcaZ was not expressed (confirmed by Northern blot analysis). From these results, it was assumed that IcaZ complements the biofilm *in trans* at least in mutant O-47ΔΔΔ.

As the RNA produced in these constructs carried additional nucleotides at the 5′ and 3′ ends, because of the position of the transcription start site and a transcriptional terminator (TT)

from the plasmid backbone, these sequences were deleted from the plasmid to ensure expression of the actual IcaZ sequence. The deletion of the 5′ nucleotides included the second repressor binding site, leaving the plasmid leaky, meaning that small amounts of the RNA were expressed even without the addition of ATc (which resulted in RNA levels comparable to a classical complementation without induction). To generate a correct control plasmid, the pCG248 vector was also cleaned from these nucleotides and from the TT. The generated plasmid pCG248c_ΔTT unexpectedly induced biofilm formation in O-47ΔΔΔ background like the IcaZ overexpression plasmids, but again not in O-47Δ*icaZ*. However, due to the deleted sequences in the control plasmid, an induction of Pxyl/tet now let to a read-through into *repF* and *oriC*. It is therefore likely that upon ATc induction the control plasmid was replicated far more often than the plasmid carrying IcaZ, which contains its own transcription terminator sequence. This increase in plasmid replication would cause stress for the cells, which results in increased biofilm formation. Nevertheless, in mutant O-47ΔΔΔ the effect on PIA-biofilm after IcaZ overexpression was still more prominent than the effect of the control plasmid.

Taken together, the results indicated that IcaZ can complement the biofilm negative phenotype *in trans* in the O-47ΔΔΔ mutant, but cannot exert any function expressed *in trans* in the O-47Δ*icaZ* mutant. The difference between these mutants is firstly a truncated *icaR*-3′ UTR in O-47ΔΔΔ which leads to a very short lived *icaR* mRNA. This might explain, why mutant O-47Δ*icaZ* with the intact *icaR* mRNA, allowing plenty of IcaR translation, forms even less biofilm than the triple mutant. At the same time, only if the structure of *icaR* is affected by the truncated 3′ UTR in the triple mutant and most RNA molecules are quickly degraded, an *in trans* complementation with IcaZ suffices to block most of IcaR translation and results in biofilm formation. A second more technical aspect might be grounded in the other difference between these mutants. As only the middle part of IcaZ is deleted in O-47Δ*icaZ*, the first 80 nt at the 5′-end are present followed by the transcription terminator; both areas are absent in O-47ΔΔΔ. This first 80 nt are a perfect antisense transcript to IcaZ being transcribed from the plasmid and after base pairing with *in trans* IcaZ could interfere with its regulatory function. To address this technical problem, a second variation of *icaZ* deletion would be needed that contains only the very first 32 nt, which overlap with the *icaR* 3′UTR, to reduce this supposed antisense effect to a minimum.

2.4 Towards the identification of IcaZ interaction partners

2.4.1 *Location of involved regulatory systems*

The overexpression of IcaZ was analysed in various staphylococcal backgrounds to locate the involved regulatory systems. *S. aureus* was chosen because of its lack of IcaZ and the low biofilm forming ability compared to *S. epidermidis*. Crystal violet assays showed that IcaZ overexpression was not able to trigger biofilm formation in *S. aureus* RN4220 and in

strain Newman (**Fig. IV-23**). We concluded that the interaction partner for IcaZ must be specific for *S. epidermidis*. Biofilm formation could also not be triggered in the *ica*-operon lacking strains *S. epidermidis* ATCC 12228 and Tü3298, indicating that IcaZ function does not depend on proteinaceous factors necessary for biofilm formation. If IcaZ would induce biofilm formation *ica*-independently, then biofilm formation should have been induced in these stains. As this was not the case, these results underpin the theory that IcaZ functions *ica*-dependent.

To analyse, if IcaZ function depends on the *agr* quorum sensing system, *S. epidermidis* strain 567 and its isogenic *agr*-mutant (Batzilla *et al.*, 2006) were used for IcaZ overexpression. Deletion of *agr* caused a slight increase of proteins within the biofilm, but IcaZ overexpression did not change the biofilm composition (**Fig. IV-21**). After IcaZ overexpression, the strains produced dose-dependently more biofilm, especially PIA, but there were no differences between the wildtype and the *agr*-mutant. Conclusively, IcaZ functions *agr*-independently.

2.4.2 *Fishing methods for target identification*

The first sRNAs were found on mobile genetic elements such as plasmids, phages and transposons, where they controlled the replication process and the transposition (Brantl, 2007). To elucidate the potential of RNA-mediated regulation, several genome-wide studies, firstly in *E. coli*, were performed to identify potential sRNA candidates. Amongst others, these studies used comparative genomics, computational searches for promoter and terminator sequences in intergenic regions and secondary structure predictions. Transcripts were proved for activity using high density and tiling arrays as well as RNomics (shotgun cloning or microarray analysis of cDNA). Global sequencing approaches such as next-generation sequencing additionally revealed an enormous number of novel noncoding transcripts. 'Differential RNA-seq' was used to identify primary transcripts and to determine transcriptional start sites; 'RIP-seq (RNA-immuno-precipitation-sequencing)' helped to identify RNA-protein interactions and was very effective for Hfq and RNase III. More sequencing applications are the global mapping of transposon insertion sites (transposon sequencing) and the analysis of translatomes by applying ribosome profiling (reviewed in Svensson and Sharma, 2016). Nowadays, hybridisation based technologies are replaced by quantitative RNA-seq and the discovery number of novel transcripts increases continuously. Beside the identification of sRNAs, their functional analysis is revealed by using comparative transcriptomics of sRNA deletion and overexpression strains (Svensson and Sharma, 2016). Both methods were also applied in this work.

Microarray data of O-47 Wt and *icaZ* triple mutant showed that the mutant did not express proteins relevant for attachment and accumulation, like the cell wall-anchored accumulation associated protein (*aap*) and SdrH, which explains (in parts) the inability to

adhere to the chamber slide surface and to other cells. Ebh/ebp was differentially regulated in the mutant (absent at 30°C, present at 37°C) and therefore a target candidate for IcaZ interaction. The triple mutant also produced far more *icaR* transcript than the wildtype, which could also explain the biofilm negative phenotype, because of the negative regulation of *icaA* expression by repressor IcaR. However, the transcriptomes of wildtype and mutant differed excessively due to the differences in biofilm phenotype and a direct target for IcaZ could not be determined by this approach. Considering the immense biochemical differences between a biofilm former and a non-biofilm former, this result was not surprising.

Proteomic analysis of this work revealed that the triple mutant displayed an unusual exponential phase proteome at 30°C in comparison to the wildtype, whereas the proteomes were indifferent at 37°C. At 30°C, stationary phase proteins (*i.e.* TCA cycle) were upregulated in the mutant already in the exponential growth phase and not only in stationary phase. Because of these temperature related differences, IcaZ was supposed to regulate in a temperature-dependent manner. As glucose limitation is a trigger for the cells to change growth phases, it was further supposed that the mutant lacks sugar detection and therefore shifts to a stationary metabolic status. The global regulator CcpA (catabolite control protein A) came into focus then, because CcpA coordinates central metabolism and biofilm formation in *S. epidermidis* (Sadykov *et al.*, 2011). CcpA both regulates TCA cycle activity and conveys signals associated with the TCA cycle to PIA/PNAG biosynthetic genes. But so far, no direct connection between IcaZ and CcpA could be identified.

Pulse expression of IcaZ was executed then as a direct fishing method for the identification of IcaZ interaction partners and computational target predictions as well as interaction predictions were carried out. Latest identified *icaR* mRNA (beside others) as the most promising target. Four interaction sites were identified for the binding of *icaR* mRNA with IcaZ and the interaction was then analysed and verified by electrophoretic mobility shift assays.

3. Placement and importance of ncRNA IcaZ within the regulatory network of *ica*-dependent biofilm formation

3.1 *S. epidermidis* and *S. aureus* differ in the ability of *icaR* mRNA to perform autoregulation

Both staphylococci, *S. aureus* and *S. epidermidis*, encode the functional regulator of the *icaADBC*-operon IcaR, but *icaR* mRNA itself differs in length and nucleotide sequence. *S. epidermidis icaR* mRNA exhibits a total length of 997 nt, determined here experimentally by cRACE for strain O-47 (5′ UTR: 74 nt; ORF: 549 nt; 3′ UTR: 374 nt) and RP62A (5′ UTR: 74 nt; ORF: 558 nt; 3′ UTR: 365 nt). The length of *icaR* mRNA of *S. aureus* is 72 nt 5′ UTR, 561 nt ORF and 390 nt 3′ UTR (Ruiz de los Mozos *et al.*, 2013). Thus, both staphylococcal species have very long *icaR* UTRs.

5′ UTRs longer than 20-40 nt are assumed to be able to act in a regulatory manner (Svensson 2016) and also long 3′ UTR were shown to include regulatory functions (Ruiz de los Mozos *et al.*, 2013). Ruiz de los Mozos *et al.* actually showed for *S. aureus* that *icaR* mRNA acts as auto-regulator by intramolecular or intermolecular interaction of 5′ and 3′ UTR (**Fig. VI-2**), leading to a complex that is subsequently degraded by RNase III. In contrast to *S. aureus,* such an interaction was experimentally excluded in this work for *S. epidermidis* by electrophoretic mobility shift assays (**Fig. V-2**). Our results were in line with the predictions of Ruiz de los Mozos *et al.*, 2013. The corresponding *icaR* UTR nucleotide sequences differ completely between the two species and because an auto-regulation in *S. epidermidis* was excluded for *icaR* mRNA, the mRNA was suggested to need another factor for regulation.
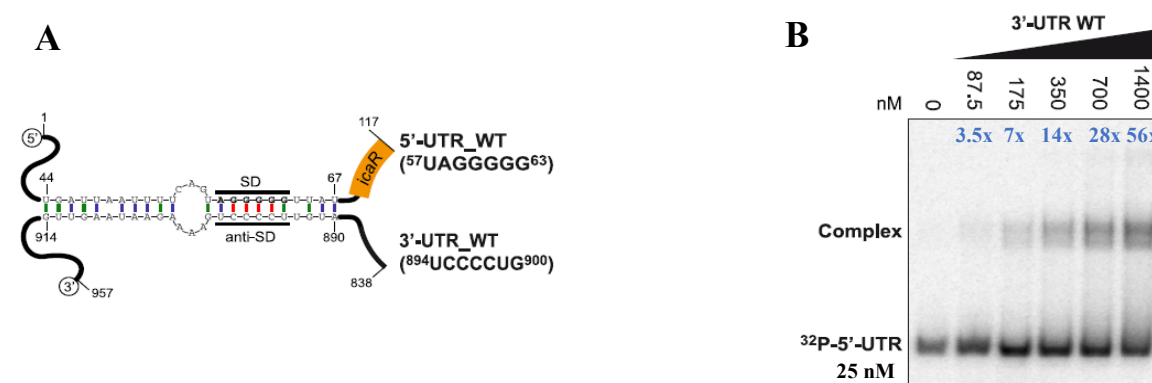
Fig. VI-2: Interaction between *icaR* 3′ UTR and the Shine-Dalgarno region of *icaR* mRNA in *S. aureus*

The figure was modified from Ruiz de los Mozos *et al.*, 2013 (Figure 5). (**A**) Schematic representation of the intramolecular interaction of *icaR* 5′ UTR and *icaR* 3′ UTR of *S. aureus*. (**B**) Gel shift analysis show the complex formation of *icaR* 5′ UTR and *icaR* 3′ UTR. The radioactively labelled *icaR* 5′ UTR was applied in a concentration of 25 nM.

3.2 *S. epidermidis icaR* mRNA is regulated by ncRNA IcaZ

3.2.1 *Electrophoretic mobility shift assays revealed IcaZ ncRNA to bind to icaR mRNA, but not to icaA mRNA*

Electrophoretic mobility shift assays carried out with IcaZ and potential interaction partners, unravelled IcaZ as a regulator of *icaR* mRNA translation by direct base pairing. In the deletion mutant, the loss of IcaZ as negative regulator of IcaR would have led to a fully functional IcaR protein, which would repress, as a tetramer, the expression of *icaA*. This would explain the macroscopic biofilm negative phenotype of the mutant. In the wildtype, IcaZ facilitates biofilm formation by post-transcriptional negative regulation of *icaR* mRNA subsequent to environmental stimuli. The interaction sites in *icaZ-* and *icaR* transcripts were predicted bioinformatically (**Fig. VIII-6**; **Fig. V-5**) and cRACE data verified that they exist in the transcripts (chapter III-1.1.2 and 2.1.1). Live-*in vitro* transcription EMSAs verified an interaction between IcaZ and *icaR* mRNA, whereas no gel shift was observed when IcaZ and *icaA* mRNA were incubated together (chapter V-1.1.3).

3.2.2 *GFP-reporter system for analysis of IcaZ icaR mRNA interaction*

The influence of IcaZ interaction on *icaR* translation was planned to be verified by a GFP-reporter system, where the native locus of *icaR-icaZ* was cloned onto a plasmid with an exchange of the *icaR* ORF for *gfp* as a readout for translation. Unfortunately, *icaR* promoter activity was not detectable, although various approaches were carried out to improve the system. As *icaR* ORF contains the alternative start codon TTG, which is a weaker signal for translation initiation than ATG (Gualerzi and Pon, 2015), ribosomes need additional sequences downstream of the start codon (an AAA and a downstream box) to correctly position the reading frame and to efficiently translate *icaR* mRNA into IcaR. The hitherto existing plasmid generations lack these (necessary) sequence elements for translation initiation. 4th generation plasmids are currently under construction and are enlarged to include these structural elements. The lack of these elements would explain why GFP fluorescence in strains, carrying the previous GFP reporter plasmids, was hardly detected.

3.3 Interplay at the *icaR* 5'UTR between small RNA RsaE and ncRNA IcaZ

It was shown recently that *S. epidermidis icaR* 5′ UTR interacts with the small RNA RsaE in classical electrophoretic mobility shift assays (Dr Sonja Schoenfelder, unpublished data). RsaE is a small conserved RNA of approximately 100 nt, which was identified in *S. aureus* (Geissmann *et al.*, 2009; Bohn *et al.*, 2010) and is located between the genes SA0859 and SA0860 in *S. aureus* N315. The sRNA is expressed in late exponential phase and thought to regulate the transition from exponential to stationary phase by downregulation of the TCA cycle. Expression is suggested to be independent of SigB, SarA or Agr (Bohn *et al.*,

2010). In *S. epidermidis*, RsaE is conserved and located in the intergenic region between SERP0580 (PepF) and SERP0581 (hypothetical protein) in strain RP62A. The small RNA is expressed (at least) in the exponential growth phase in *S. epidermidis* O-47 (**Fig. V-9 C**), like ncRNA IcaZ, and differentially expressed in the biofilm of *S. epidermidis* PS2 (Dr Sonja Schoenfelder, unpublished data). RsaE is a member of a family of sRNAs that bind to target mRNAs through a conserved C-rich sequence motif (Geissmann *et al.*, 2009) and therefore is thought to bind to the SD sequence of *icaR* mRNA. IcaZ was predicted to bind at the proximal end of the UTR and therefore we excluded that RsaE and IcaZ compete for the same binding site in *icaR* 5′ UTR. Nevertheless, competition assays have shown that increased concentrations of IcaZ displace RsaE from the complex with *icaR* mRNA (Dr Sonja Schoenfelder, unpublished data), suggesting that IcaZ is dominant in its regulatory role compared to RsaE. This might be an explanation, why deletion or overexpression of RsaE in strain O-47 had no effect on biofilm formation (unpublished data), because IcaZ was still present in these mutants.

Recent repetition of the RNA-RNA interaction prediction by *IntaRNA* using IcaZ and *icaR* 5′3′ UTR fusion product as input sequences interestingly revealed further interaction sites in *icaR* UTRs, not focused on before in this work. Amongst others, possible base-pairings between nucleotides 6 to 26 of IcaZ and nucleotides 41 to 61 of *icaR* 5′ UTR (the sequence upstream of *icaR* SD sequence and partly SD sequence) or alternatively nucleotides 8 to 30 of IcaZ and nucleotides 63 to 86 of *icaR* 5′ UTR (the sequence downstream of *icaR* SD sequence and partly SD sequence inclusive *icaR* start codon and the supportive AAA codon) were predicted (**Fig. VI-3**). Both interactions theoretically could block *icaR* mRNA translation initiation or RsaE binding in *S. epidermidis*.

In *S. aureus* genomes, IcaZ is not encoded and *icaR* mRNA was shown to undergo autoregulation, which was excluded in *S. epidermidis*. The sequence alignment of *icaR* 5′ UTR from *S. aureus* N315 and *S. epidermidis* O-47 shows many differences, mostly around the SD sequence, and therewith in the region of possible binding sites of IcaZ. Thus, although not experimentally proven, it is unlikely that IcaZ binds to *S. aureus icaR* mRNA and might be an explanation, why *in-trans* expression of IcaZ from the ATc inducible vector did not induce biofilm formation in *S. aureus*. Moreover, *S. aureus icaR* mRNA 5′ UTR was shown to bind nearly perfectly to its 3′ UTR (**Fig. VI-3**; binding site is marked in blue). So, even if IcaZ from *S. epidermidis* binds to one of the aforesaid regions in *S. aureus icaR* mRNA 5′ UTR, the intramolecular binding of 5′ and 3′ UTR, described by Ruiz de los Mozos *et. al.*, would be stronger. However, these considerations are only speculative and were not experimentally proven in this work.

```
                                                      |————— 41-61 —————|
5´- GUAAUAUUUGUAAUUUUAACUUAAUUUUUCUGUAAUAUAUAUUUUUAGAAAAUUGAAUAA - 3´  S. epidermidis
5´- GAAAUAUUUGUAAUUGCAACUUAAUUUUUCCUGUAACAUAGUGUGAUUAAUUU__UCAG - 3´  S. aureus

    |——— |————— 63-86 —————|
                          *
5´- GGGGGAGAUUUUAGAAUUGAAAGAUAAGAUUAUUGAUAACGCAAUAACCUUAUUUUUCCG - 3´  S. epidermidis
5´- UAGGGGGUUAUAAAAAAUUGAAGGAUAAGAUUAUUGAUAACGCAAUAACCUUAUUUUUCAG - 3´  S. aureus
```
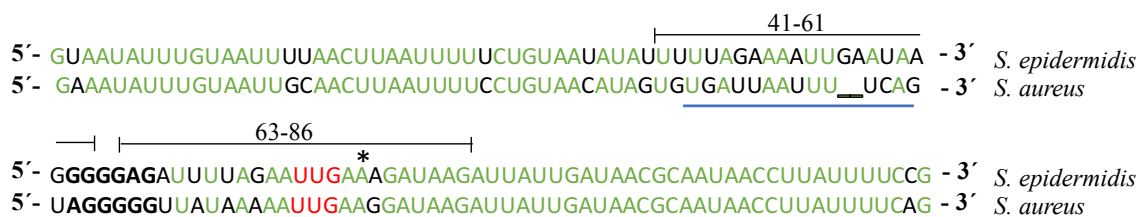
Fig. VI-3: Sequence alignment of *S. epidermidis* and *S. aureus* icaR 5' UTR

Alignment of the nucleotide sequences of *icaR* 5′ UTR of *S. epidermidis* O-47 (74 nt) and *S. aureus* (72 nt). Differences are highlighted in black. The SD sequence is marked in bold. The start codon is marked in red and the supportive AAA by an asterisk. Nucleotides in the *S. aureus* sequence, which bind to *icaR* 3′ UTR are underlined in blue. Possible interaction sites of *S. epidermidis icaR* 5′ UTR with IcaZ are indicated.

3.4 Factors influencing IcaZ expression

3.4.1 *IcaZ expression is influenced by temperature, but not dependent on surface contact*

The expression of *icaZ* was found to be growth phase dependent (exp. growth phase) and temperature dependent. IcaZ was detectable on Northern blots at 30°C and 37°C, but the ncRNA was more prominent at 30°C. Crystal violet biofilm formation assays (performed always under static conditions) also revealed more biofilm formation of the bacteria at 30°C than at 37°C. It was questioned therefore, if static conditions, hence the direct contact of the bacteria to a surface is a trigger for IcaZ synthesis. For that, *icaZ* expression was analysed by Northern blot of total RNA sampled from bacteria incubated under static conditions. The cells grew slower (maybe due to the lower amount of oxygen), but *icaZ* expression was comparable to previous blots for which shaking conditions had been applied. Hence, the surface attachment was excluded as a trigger for *icaZ* expression.

3.4.2 *Reciprocal influence of tRNA^{Thr-4} and icaR on IcaZ or its expression*

Due to the genomic overlap of the neighbouring genes with *icaZ* it was reckoned that the unprocessed tRNA^{Thr-4}, the processed tRNA-3′ end or *icaR* expression might influence IcaZ functionality or synthesis.

The tRNA^{Thr-4}, annotated in *S. epidermidis* RP62A, is specific for CoNS (chapter III-2.1.2) and its presence was found to be independent of the *ica*-operon. Thus, this tRNA is not assumed to be part of the *ica*-locus unlike it is assumed for IcaZ. But, it is also possible that the tRNA was part of the locus in the ancestor before and that *ica*-negatives have lost the *ica*-genes inclusive *icaZ*. Nevertheless, in *S. epidermidis* O-47, tRNA^{Thr-4} is expressed and unlike tRNA^{Thr1-3} located as a single tRNA gene. Because of its length and structure, which is different from the *bona fide* tRNAs tRNA^{Thr1-3}, a function as regular transfer RNA is

debatable and a regulatory role instead is conceivable. The genes, *tRNA^Thr-4* and *icaZ*, are convergently transcribed and share a terminator sequence that was predicted bioinformatically. In consequence, the 3′ end of the non-mature tRNA^Thr-4 and the processed 3′ end (deriving from tRNA^Thr-4 maturation process) form a natural antisense transcript to IcaZ and therefore probably influence IcaZ in matters of its functionality. Both transcripts, the non-mature tRNA^Thr-4 and the processed 3′ end of the tRNA^Thr-4 were detected by Northern blot and thus it is possible that either the one or the other functions as an RNA sponge for IcaZ. An RNA sponge is an RNA fragment that prevents transcriptional noise from a small RNA. This regulatory mechanism of RNAs to act as RNA sponges was reviewed recently (Ziebuhr and Vogel, 2015; Lalaouna *et al.*, 2015b). Beside the involvement of RNA sponges in the control of sugar utilisation (Figueroa-Bossi *et al.*, 2009; Overgaard *et al.*, 2009) and amino acid metabolism (Miyakoshi *et al.*, 2015), tRNA-precursor derived RNA sponges were described as well. Such an RNA fragment, for example, is the 3′ end of the glyW-cysT-leuZ polycistronic tRNA precursor (3′ETS^leuZ) in *E. coli* that was shown to serve another function outside the tRNA pathway, namely to base-pair with RybB or RyhB to alleviate their activity (Lalaouna *et al.*, 2015a; Lalaouna *et al.*, 2015b). Here, the deletion of *icaZ* had no effect on *tRNA^Thr-4* expression and a transcriptional regulation of *tRNA^Thr-4* by IcaZ can be excluded. Nevertheless, the pulse-expression experiment indicated more *tRNA^Thr-4* transcripts after induction of *icaZ* expression, so that a regulatory role by tRNA^Thr-4 on IcaZ should not be fully excluded. Further experiments would be necessary to investigate this in more detail.

Due to the overlapping nucleotide sequences of *icaZ* and *icaR*, it was investigated here, if IcaZ derives from *icaR* 3′ UTR or is a primary transcript and independent of *icaR* transcription. The latter was clearly proven, but it could be subject of further investigations, if *icaZ* expression is influenced by *icaR* transcription simply due to a steric inhibition of IcaZ transcription initiation by the RNA polymerase already transcribing *icaR*.

3.4.3   *IcaZ expression is responsive to environmental stimuli*

Environmental stresses, like high osmolarity (NaCl) and ethanol, as well as glucose are known to regulate PIA (polysaccharide intercellular adhesion) synthesis positively (Conlon *et al.*, 2002a; Knobloch *et al.*, 2004; **Fig. VI-4**). PIA synthesis is carried out by the enzymes encoded by the *icaADBC*-operon, which is regulated (amongst others) by repressor IcaR. The expression of *icaR* on the other hand is negatively regulated in a σ^B-dependent manner by NaCl and in a σ^B-independent manner by ethanol (Knobloch *et al.*, 2001; Knobloch *et al.*, 2004), causing indirectly *ica* expression (**Fig. VI-4)**.
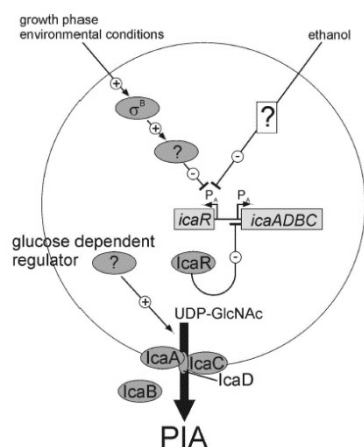
Fig. VI-4: Model of the regulation of PIA synthesis in *S. epidermidis* from Knobloch *et al.* contains unknown factors

Figure was taken from Knobloch *et al.*, 2004. IcaR gene expression is negatively regulated by a σ^B-dependent regulator and by a σ^B-independent regulator, that itself is triggered by ethanol.

The nucleotide sequences of *icaR* and *icaADBC*-operon do not contain sequence homologues to σ^B-dependent promoters, so the regulation of *icaR* by σ^B is thought to be indirect (Knobloch *et al.*, 2001). Ethanol stimulation represses *icaR* transcription but also regulates *icaR* post-transcriptionally, whereas NaCl does not repress *icaR* transcription (Conlon *et al.*, 2002b; Conlon *et al.*, 2002a). The regulation by NaCl was shown to require RsbU, a positive regulator of the global transcription factor σ^B (Knobloch *et al.*, 2001; Knobloch *et al.*, 2004), hence the σ^B-dependent pathway. The repression of *icaR* upon ethanol stress on the other hand was postulated to involve an unknown σ^B-independent intermediate factor (Knobloch *et al.*, 2004; Cue *et al.*, 2012).

As the regulation by these environmental stimuli needs intermediate factors (highlighted in **Fig. VI-4** by question marks), their impact on *icaZ* expression was analysed in this work by using a reporter gene fusion of the *icaZ* promoter to Cerulean gene (strain collection code ML13). The *icaZ* promoter(s) responded to ethanol supplementation with increased Cerulean fluorescence compared to the un-induced sample and responded slightly to NaCl, but not to various concentrations of glucose. IcaZ was therefore excluded to be the wanted glucose dependent regulator. Also, a direct regulation of *icaZ* expression by σ^B was excluded, because the upstream region of *icaZ* does not contain a σ^B-dependent promoter (data not shown), but might be the wanted σ^B-independent intermediate factor regulated by ethanol, as a regulation upon ethanol stimulation was confirmed by the *cfp*-reporter system.

3.5 Proposed regulatory network of biofilm formation in *S. epidermidis*

The regulatory network of biofilm formation is very complex and even differs between staphylococcal species. A detailed list of all known *icaADBC*-regulators of both species, *S. aureus* and *S. epidermidis,* was already given in **Tab. I-2**. The following scheme summarises the current knowledge about the regulatory network governing biofilm formation in *S. epidermidis* including the proposed regulation by the new ncRNA IcaZ **(Fig. VI-5)**. Based on the findings of this work, ncRNA IcaZ is likely to be the aforesaid intermediate factor that fills the gap between ethanol and *icaR* gene in this complex regulatory network (**Fig. VI-4**; **Fig. VI-5**).

Biofilm assays showed contradictory effects of *in trans* expressed IcaZ, depending on the mutant background. Based on the genomic localisation of the RNA and the distinct PIA-negative phenotype of the mutants, the regulation by ncRNA IcaZ was likely to be carried out *in cis* involving the *ica*-operon. Electrophoretic mobility shift assays confirmed an interaction of IcaZ with *icaR* mRNA. Due to this interaction, the translation into functional IcaR repressor protein is unlikely, so that the main regulator of *icaADBC*-operon is inhibited; IcaR is more dominant than the regulation by the Rbf-SarR-SarX axis (Rowe *et al.*, 2016). TcaR was not detected in the exponential growth phase and therefore is not supposed to take over the missing repression of *icaADBC*. With the negative regulators of *icaADBC* inactive, the positive regulator SarA can induce biofilm formation in the wildtype background. When IcaZ as the 'regulator of the regulator of biofilm formation' is missing, IcaR represses the biofilm formation unhindered.

IcaZ expression itself was not affected by the *agr*-quorum sensing system that regulates biofilm formation indirectly through the effector RNA RNAIII and the TCA cycle axis, neither did glucose induce *icaZ* expression, confirming no involvement of IcaZ in this regulatory axis. The strongest effect on IcaZ promoter activity was seen by ethanol. Since ethanol cannot directly bind to DNA and function as transcriptional regulator, an intermediate factor between the stimulus ethanol and induction of IcaZ is supposed to mediate the signal. NaCl slightly increased the expression of *icaZ* as well, making a role of IcaZ in a σ^B-dependent *icaR* regulation possible. Again, an intermediate, regulated by σ^B would be necessary to convey the signal to IcaZ, which itself lacks sequence homologues to σ^B-dependent promoters. Further experiments are needed to clarify the role of σ^B and other transcription factors on the expression of IcaZ.
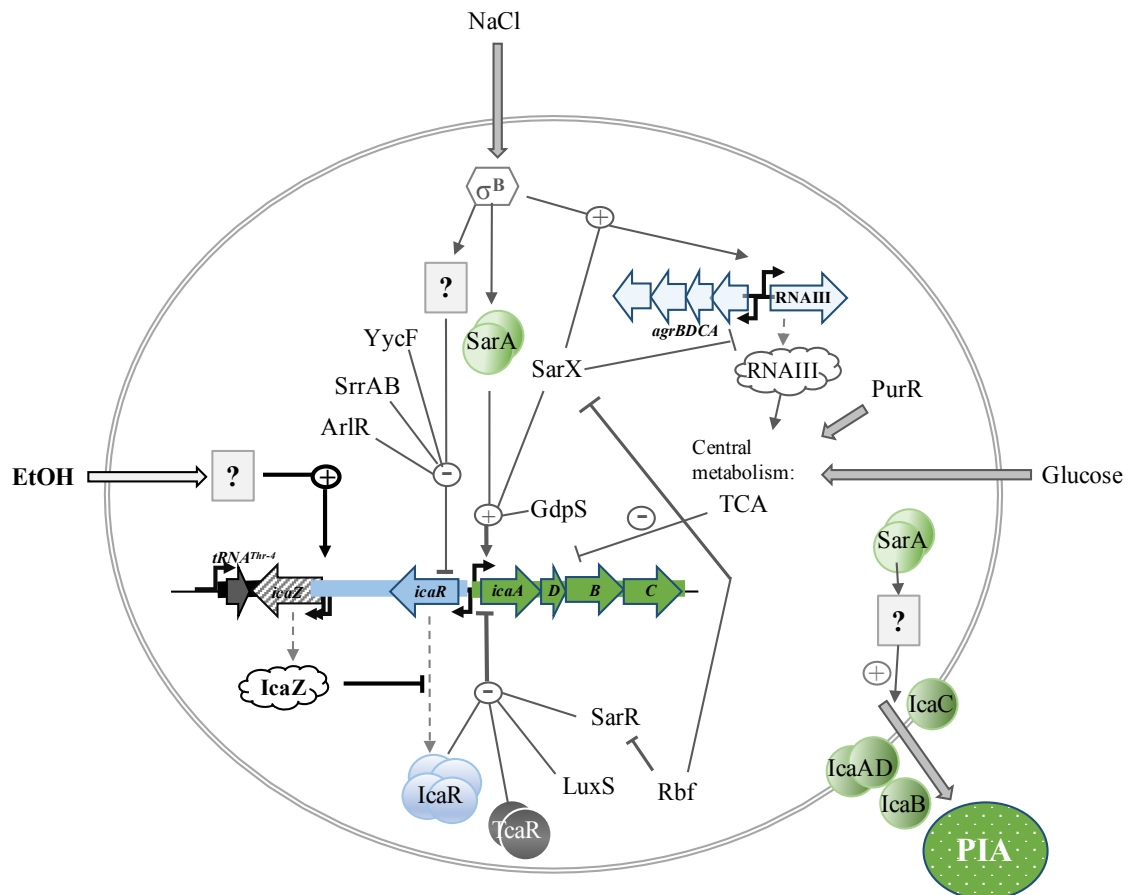
Fig. VI-5: Proposed regulatory network of biofilm formation in *S. epidermidis* including the regulation by ncRNA IcaZ

The figure was created based on O'Gara, 2007. Current literature (reviewed in Tab.I-2) and results from this work (highlighted in bold) were included. The analysed regulators are marked according to the here used scheme.

4. Closing remarks and outlook

This work has given a comprehensive molecular characterization of the new non-coding RNA named IcaZ, which is expressed in the exponential growth phase of *icaADBC*-positive *S. epidermidis* and uncovered its functional role in the regulation of biofilm formation. The RNA was found to regulate *icaR* mRNA by base-pairing interaction at at least four interaction sites that are within the coding region of *icaR* mRNA and its 5′ and 3′ untranslated regions. The interaction is supposed to cause the blockage of *icaR* mRNA translation into functional IcaR repressor protein and in consequence of that, PIA biofilm formation is not repressed by the repressor IcaR, but is synthesized instead. The regulation seemed to be independent of *agrBDCA* quorum sensing system. Environmental factors, like temperature and ethanol were discovered to trigger *icaZ* synthesis, whereas the influence of NaCl was lower and different concentrations of glucose caused no effect. An involvement of RNase III or other already known *icaADBC*-operon regulators (*e.i.* SarA, TcaR) was disproved.

The importance of the regulation by ethanol was mentioned before, as the alcohol-inducible biofilm formation of *S. epidermidis* has potentially profound clinical ramifications, because alcohol is a component of skin disinfectants routinely used in hospitals (Knobloch *et al.*, 2002; Luther *et al.*, 2015; Milisavljevic *et al.*, 2008). To date, the exact regulatory mechanism by ethanol is still unknown, but the here presented results showed that the non-coding RNA IcaZ is triggered by ethanol and itself regulates *icaR* expression, resulting in strong biofilm formation. Conclusively, this work has not only given a comprehensive molecular characterization of the new non-coding RNA named IcaZ, but moreover filled an important gap in the regulatory network of biofilm formation in *S. epidermidis* (**Fig. VI-5**), highlighted biofilm relevant differences to the second most important nosocomial pathogen *S. aureus* and connected the obtained results to current clinical issues.

Recent investigations of our group regarding the regulation of *icaR* 5′ UTR revealed that IcaZ is able to titrate away another small RNA, called RsaE, from *icaR* 5′ UTR. Interestingly, deletion of this RNA in strain O-47 did not result in a biofilm negative phenotype in contrast to the deletion of IcaZ. Thus, at least in strain O-47, the regulation of biofilm formation by IcaZ is hierarchically above the regulation by RsaE (unpublished data). Future work will focus on the exact underlying molecular mechanism of IcaZ binding and the interplay with RsaE or other RNA regulators, identified later to this work, for a more thorough understanding of biofilm regulation in staphylococci.

VII.   References

Arciola, C.R., Campoccia, D., Ravaioli, S. and Montanaro, L. (2015): Polysaccharide intercellular adhesin in biofilm: structural and regulatory aspects. *Front Cell Infect Microbiol*, **5**: p. 7.

Asaad, A.M., Ansar Qureshi, M. and Mujeeb Hasan, S. (2016): Clinical significance of coagulase-negative staphylococci isolates from nosocomial bloodstream infections. *Infect Dis (Lond)*, **48**(5): p. 356-360.

Atkin, K.E., MacDonald, S.J., Brentnall, A.S., Potts, J.R. and Thomas, G.H. (2014): A different path: revealing the function of staphylococcal proteins in biofilm formation. *FEBS Lett*, **588**(10): p. 1869-1872.

Augustin, J. and Gotz, F. (1990): Transformation of Staphylococcus epidermidis and other staphylococcal species with plasmid DNA by electroporation. *FEMS Microbiol Lett*, **54**(1-3): p. 203-207.

Baba, T., Bae, T., Schneewind, O., Takeuchi, F. and Hiramatsu, K. (2008): Genome sequence of Staphylococcus aureus strain Newman and comparative analysis of staphylococcal genomes: polymorphism and evolution of two major pathogenicity islands. *J Bacteriol*, **190**(1): p. 300-310.

Bae, T. and Schneewind, O. (2006): Allelic replacement in Staphylococcus aureus with inducible counter-selection. *Plasmid*, **55**(1): p. 58-63.

Balaban, N. and Novick, R.P. (1995): Translation of RNAIII, the Staphylococcus aureus agr regulatory RNA molecule, can be activated by a 3'-end deletion. *FEMS Microbiol Lett*, **133**(1-2): p. 155-161.

Barquist, L., Westermann, A.J. and Vogel, J. (2016): Molecular phenotyping of infection-associated small non-coding RNAs. *Philos Trans R Soc Lond B Biol Sci*, **371**(1707).

Batzilla, C.F., Rachid, S., Engelmann, S., Hecker, M., Hacker, J. and Ziebuhr, W. (2006): Impact of the accessory gene regulatory system (Agr) on extracellular proteins, codY expression and amino acid metabolism in Staphylococcus epidermidis. *Proteomics*, **6**(12): p. 3602-3613.

Benito, Y., Kolb, F.A., Romby, P., Lina, G., Etienne, J. and Vandenesch, F. (2000): Probing the structure of RNAIII, the Staphylococcus aureus agr regulatory RNA, and identification of the RNA domain involved in repression of protein A expression. *RNA*, **6**(5): p. 668-679.

Bohn, C., Rigoulay, C., Chabelskaya, S., Sharma, C.M., Marchais, A., Skorski, P., Borezee-Durant, E., Barbet, R., Jacquet, E., Jacq, A., Gautheret, D., Felden, B., Vogel, J. and Bouloc, P. (2010): Experimental discovery of small RNAs in

Staphylococcus aureus reveals a riboregulator of central metabolism. *Nucleic Acids Res*, **38**(19): p. 6620-6636.

Brantl, S. (2007): Regulatory mechanisms employed by cis-encoded antisense RNAs. *Curr Opin Microbiol*, **10**(2): p. 102-109.

Brenneis, M., Hering, O., Lange, C. and Soppa, J. (2007): Experimental characterization of Cis-acting elements important for translation and transcription in halophilic archaea. *PLoS Genet*, **3**(12): p. e229.

Bronesky, D., Wu, Z., Marzi, S., Walter, P., Geissmann, T., Moreau, K., Vandenesch, F., Caldelari, I. and Romby, P. (2016): Staphylococcus aureus RNAIII and Its Regulon Link Quorum Sensing, Stress Responses, Metabolic Adaptation, and Regulation of Virulence Gene Expression. *Annu Rev Microbiol*, **70**: p. 299-316.

Busch, A., Richter, A.S. and Backofen, R. (2008): IntaRNA: efficient prediction of bacterial sRNA targets incorporating target site accessibility and seed regions. *Bioinformatics*, **24**(24): p. 2849-2856.

Buttner, H., Mack, D. and Rohde, H. (2015): Structural basis of Staphylococcus epidermidis biofilm formation: mechanisms and molecular interactions. *Front Cell Infect Microbiol*, **5**: p. 14.

Cavanagh, J.P., Wolden, R., Heise, P., Esaiassen, E., Klingenberg, C. and Aarag Fredheim, E.G. (2016): Antimicrobial susceptibility and body site distribution of community isolates of coagulase-negative staphylococci. *APMIS*.

Chambers, J.R. and Sauer, K. (2013): Small RNAs and their role in biofilm formation. *Trends Microbiol*, **21**(1): p. 39-49.

Chang, Y.M., Jeng, W.Y., Ko, T.P., Yeh, Y.J., Chen, C.K. and Wang, A.H. (2010): Structural study of TcaR and its complexes with multiple antibiotics from Staphylococcus epidermidis. *Proc Natl Acad Sci U S A*, **107**(19): p. 8617-8622.

Chang, Y.M., Chen, C.K., Chang, Y.C., Jeng, W.Y., Hou, M.H. and Wang, A.H. (2012): Functional studies of ssDNA binding ability of MarR family protein TcaR from Staphylococcus epidermidis. *PLoS One*, **7**(9): p. e45665.

Chang, Y.M., Ho, C.H., Chen, C.K., Maestre-Reyna, M., Chang-Chien, M.W. and Wang, A.H. (2014): TcaR-ssDNA complex crystal structure reveals new DNA binding mechanism of the MarR family proteins. *Nucleic Acids Res*, **42**(8): p. 5314-5321.

Chatterjee, S.S., Joo, H.S., Duong, A.C., Dieringer, T.D., Tan, V.Y., Song, Y., Fischer, E.R., Cheung, G.Y., Li, M. and Otto, M. (2013): Essential Staphylococcus aureus toxin export system. *Nat Med*, **19**(3): p. 364-367.

Chowdhury, S., Maris, C., Allain, F.H. and Narberhaus, F. (2006): Molecular basis for temperature sensing by an RNA thermometer. *EMBO J*, **25**(11): p. 2487-2497.

Conlon, K.M., Humphreys, H. and O'Gara, J.P. (2002a): icaR encodes a transcriptional repressor involved in environmental regulation of ica operon expression and biofilm formation in Staphylococcus epidermidis. *J Bacteriol*, **184**(16): p. 4400-4408.

Conlon, K.M., Humphreys, H. and O'Gara, J.P. (2002b): Regulation of icaR gene expression in Staphylococcus epidermidis. *FEMS Microbiol Lett*, **216**(2): p. 171-177.

Corcoran, C.P., Podkaminski, D., Papenfort, K., Urban, J.H., Hinton, J.C. and Vogel, J. (2012): Superfolder GFP reporters validate diverse new mRNA targets of the classic porin regulator, MicF RNA. *Mol Microbiol*, **84**(3): p. 428-445.

Costerton, J.W., Geesey, G.G. and Cheng, K.J. (1978): How bacteria stick. *Sci Am*, **238**(1): p. 86-95.

Costerton, J.W., Stewart, P.S. and Greenberg, E.P. (1999): Bacterial biofilms: a common cause of persistent infections. *Science*, **284**(5418): p. 1318-1322.

Cramton, S.E., Gerke, C., Schnell, N.F., Nichols, W.W. and Gotz, F. (1999): The intercellular adhesion (ica) locus is present in Staphylococcus aureus and is required for biofilm formation. *Infect Immun*, **67**(10): p. 5427-5433.

Cue, D., Lei, M.G., Luong, T.T., Kuechenmeister, L., Dunman, P.M., O'Donnell, S., Rowe, S., O'Gara, J.P. and Lee, C.Y. (2009): Rbf promotes biofilm formation by Staphylococcus aureus via repression of icaR, a negative regulator of icaADBC. *J Bacteriol*, **191**(20): p. 6363-6373.

Cue, D., Lei, M.G. and Lee, C.Y. (2012): Genetic regulation of the intercellular adhesion locus in staphylococci. *Front Cell Infect Microbiol*, **2**: p. 38.

Cue, D., Lei, M.G. and Lee, C.Y. (2013): Activation of sarX by Rbf is required for biofilm formation and icaADBC expression in Staphylococcus aureus. *J Bacteriol*, **195**(7): p. 1515-1524.

Cuny, C., Arnold, P., Hermes, J., Eckmanns, T., Mehraj, J., Schoenfelder, S., Ziebuhr, W., Zhao, Q., Wang, Y., Fessler, A.T., Krause, G., Schwarz, S. and Witte, W. (2016): Occurrence of cfr-mediated multiresistance in staphylococci from veal calves and pigs, from humans at the corresponding farms, and from veterinarians and their family members. *Vet Microbiol*.

Duthie, E.S. and Lorenz, L.L. (1952): Staphylococcal coagulase; mode of action and antigenicity. *J Gen Microbiol*, **6**(1-2): p. 95-107.

Duval, M., Simonetti, A., Caldelari, I. and Marzi, S. (2015): Multiple ways to regulate translation initiation in bacteria: Mechanisms, regulatory circuits, dynamics. *Biochimie*, **114**: p. 18-29.

Eckart, M. (2006): Analyse einer chromosomalen Deletion und Entdeckung einer neuartigen nicht-translatierten RNA in Staphylococcus epidermidis.

Eggenhofer, F., Tafer, H., Stadler, P.F. and Hofacker, I.L. (2011): RNApredator: fast accessibility-based prediction of sRNA targets. *Nucleic Acids Res*, **39**(Web Server issue): p. W149-154.

Fessler, A.T., Zhao, Q., Schoenfelder, S., Kadlec, K., Brenner Michael, G., Wang, Y., Ziebuhr, W., Shen, J. and Schwarz, S. (2016): Complete sequence of a plasmid from a bovine methicillin-resistant Staphylococcus aureus harbouring a novel ica-like gene cluster in addition to antimicrobial and heavy metal resistance genes. *Vet Microbiol*.

Figueroa-Bossi, N., Valentini, M., Malleret, L., Fiorini, F. and Bossi, L. (2009): Caught at its own game: regulatory small RNA inactivated by an inducible transcript mimicking its target. *Genes Dev*, **23**(17): p. 2004-2015.

Fitzpatrick, F., Humphreys, H. and O'Gara J, P. (2005): Evidence for low temperature regulation of biofilm formation in Staphylococcus epidermidis. *J Med Microbiol*, **54**(Pt 5): p. 509-510.

Flannagan, R.S., Heit, B. and Heinrichs, D.E. (2016): Intracellular replication of Staphylococcus aureus in mature phagolysosomes in macrophages precedes host cell death, and bacterial escape and dissemination. *Cell Microbiol*, **18**(4): p. 514-535.

Fournier, B. and Hooper, D.C. (2000): A new two-component regulatory system involved in adhesion, autolysis, and extracellular proteolytic activity of Staphylococcus aureus. *J Bacteriol*, **182**(14): p. 3955-3964.

Fournier, B., Klier, A. and Rapoport, G. (2001): The two-component system ArlS-ArlR is a regulator of virulence gene expression in Staphylococcus aureus. *Mol Microbiol*, **41**(1): p. 247-261.

Fournier, B. and Klier, A. (2004): Protein A gene expression is regulated by DNA supercoiling which is modified by the ArlS-ArlR two-component system of Staphylococcus aureus. *Microbiology*, **150**(Pt 11): p. 3807-3819.

Fowler, V.G., Jr., Fey, P.D., Reller, L.B., Chamis, A.L., Corey, G.R. and Rupp, M.E. (2001): The intercellular adhesin locus ica is present in clinical isolates of Staphylococcus aureus from bacteremic patients with infected and uninfected prosthetic joints. *Med Microbiol Immunol*, **189**(3): p. 127-131.

Freeman, D.J., Falkiner, F.R. and Keane, C.T. (1989): New method for detecting slime production by coagulase negative staphylococci. *Journal of clinical pathology*, **42**(8): p. 872-874.

Freese, N.H., Norris, D.C. and Loraine, A.E. (2016a): Integrated genome browser: visual analytics platform for genomics. *Bioinformatics*, **32**(14): p. 2089-2095.

Freese, N.H., Norris, D.C. and Loraine, A.E. (2016b): Integrated genome browser: visual analytics platform for genomics. *Bioinformatics*.

Galdbart, J.O., Allignet, J., Tung, H.S., Ryden, C. and El Solh, N. (2000): Screening for Staphylococcus epidermidis markers discriminating between skin-flora strains and those responsible for infections of joint prostheses. *J Infect Dis*, **182**(1): p. 351-355.

Garzoni, C. and Kelley, W.L. (2009): Staphylococcus aureus: new evidence for intracellular persistence. *Trends Microbiol*, **17**(2): p. 59-65.

Gautheret, D. and Lambert, A. (2001): Direct RNA motif definition and identification from multiple sequence alignments using secondary structure profiles. *J Mol Biol*, **313**(5): p. 1003-1011.

Geissmann, T., Chevalier, C., Cros, M.J., Boisset, S., Fechter, P., Noirot, C., Schrenzel, J., Francois, P., Vandenesch, F., Gaspin, C. and Romby, P. (2009): A search for small noncoding RNAs in Staphylococcus aureus reveals a conserved sequence motif for regulation. *Nucleic Acids Res*, **37**(21): p. 7239-7257.

Gerke, C., Kraft, A., Sussmuth, R., Schweitzer, O. and Gotz, F. (1998): Characterization of the N-acetylglucosaminyltransferase activity involved in the biosynthesis of the Staphylococcus epidermidis polysaccharide intercellular adhesin. *J Biol Chem*, **273**(29): p. 18586-18593.

Gertz, S., Engelmann, S., Schmid, R., Ziebandt, A.K., Tischer, K., Scharf, C., Hacker, J. and Hecker, M. (2000): Characterization of the sigma(B) regulon in Staphylococcus aureus. *J Bacteriol*, **182**(24): p. 6983-6991.

Gill, S.R., Fouts, D.E., Archer, G.L., Mongodin, E.F., Deboy, R.T., Ravel, J., Paulsen, I.T., Kolonay, J.F., Brinkac, L., Beanan, M., Dodson, R.J., Daugherty, S.C., Madupu, R., Angiuoli, S.V., Durkin, A.S., Haft, D.H., Vamathevan, J., Khouri, H., Utterback, T., Lee, C., Dimitrov, G., Jiang, L., Qin, H., Weidman, J., Tran, K., Kang, K., Hance, I.R., Nelson, K.E. and Fraser, C.M. (2005): Insights on evolution of virulence and resistance from the complete genome analysis of an early methicillin-resistant Staphylococcus aureus strain and a biofilm-producing methicillin-resistant Staphylococcus epidermidis strain. *J Bacteriol*, **187**(7): p. 2426-2438.

Gimpel, M. and Brantl, S. (2017): Dual-function small regulatory RNAs in bacteria. *Mol Microbiol*, **103**(3): p. 387-397.

Gordon, R.J. and Lowy, F.D. (2008): Pathogenesis of methicillin-resistant Staphylococcus aureus infection. *Clin Infect Dis*, **46 Suppl 5**: p. S350-359.

Gotz, F. (1990): Staphylococcus carnosus: a new host organism for gene cloning and protein production. *Soc Appl Bacteriol Symp Ser*, **19**: p. 49S-53S.

Green, C.J. and Vold, B.S. (1993): Staphylococcus aureus has clustered tRNA genes. *J Bacteriol*, **175**(16): p. 5091-5096.

Grice, E.A. and Segre, J.A. (2011): The skin microbiome. *Nat Rev Microbiol*, **9**(4): p. 244-253.

Grosso-Becera, M.V., Servin-Gonzalez, L. and Soberon-Chavez, G. (2015): RNA structures are involved in the thermoregulation of bacterial virulence-associated traits. *Trends Microbiol*, **23**(8): p. 509-518.

Gualerzi, C.O. and Pon, C.L. (2015): Initiation of mRNA translation in bacteria: structural and dynamic aspects. *Cell Mol Life Sci*, **72**(22): p. 4341-4367.

Guillet, J., Hallier, M. and Felden, B. (2013): Emerging functions for the Staphylococcus aureus RNome. *PLoS Pathog*, **9**(12): p. e1003767.

Hamill, R.J., Vann, J.M. and Proctor, R.A. (1986): Phagocytosis of Staphylococcus aureus by cultured bovine aortic endothelial cells: model for postadherence events in endovascular infections. *Infect Immun*, **54**(3): p. 833-836.

Heilmann, C., Gerke, C., Perdreau-Remington, F. and Gotz, F. (1996a): Characterization of Tn917 insertion mutants of Staphylococcus epidermidis affected in biofilm formation. *Infect Immun*, **64**(1): p. 277-282.

Heilmann, C., Schweitzer, O., Gerke, C., Vanittanakom, N., Mack, D. and Gotz, F. (1996b): Molecular basis of intercellular adhesion in the biofilm-forming Staphylococcus epidermidis. *Mol Microbiol*, **20**(5): p. 1083-1091.

Helle, L., Kull, M., Mayer, S., Marincola, G., Zelder, M.E., Goerke, C., Wolz, C. and Bertram, R. (2011): Vectors for improved Tet repressor-dependent gradual gene induction or silencing in Staphylococcus aureus. *Microbiology*, **157**(Pt 12): p. 3314-3323.

Holland, L.M., O'Donnell, S.T., Ryjenkov, D.A., Gomelsky, L., Slater, S.R., Fey, P.D., Gomelsky, M. and O'Gara, J.P. (2008): A staphylococcal GGDEF domain protein regulates biofilm formation independently of cyclic dimeric GMP. *J Bacteriol*, **190**(15): p. 5178-5189.

Huebner, J. and Goldmann, D.A. (1999): Coagulase-negative staphylococci: role as pathogens. *Annu Rev Med*, **50**: p. 223-236.

Jefferson, K.K., Cramton, S.E., Gotz, F. and Pier, G.B. (2003): Identification of a 5-nucleotide sequence that controls expression of the ica locus in Staphylococcus aureus and characterization of the DNA-binding properties of IcaR. *Mol Microbiol*, **48**(4): p. 889-899.

Jefferson, K.K., Pier, D.B., Goldmann, D.A. and Pier, G.B. (2004): The teicoplanin-associated locus regulator (TcaR) and the intercellular adhesin locus regulator (IcaR) are transcriptional inhibitors of the ica locus in Staphylococcus aureus. *J Bacteriol*, **186**(8): p. 2449-2456.

Jeng, W.Y., Ko, T.P., Liu, C.I., Guo, R.T., Liu, C.L., Shr, H.L. and Wang, A.H. (2008): Crystal structure of IcaR, a repressor of the TetR family implicated in biofilm formation in Staphylococcus epidermidis. *Nucleic Acids Res*, **36**(5): p. 1567-1577.

Joo, H.S. and Otto, M. (2012): Molecular basis of in vivo biofilm formation by bacterial pathogens. *Chem Biol*, **19**(12): p. 1503-1513.

Kahl, B.C. (2014): Small colony variants (SCVs) of Staphylococcus aureus--a bacterial survival strategy. *Infect Genet Evol*, **21**: p. 515-522.

Kaiser, T.D., Pereira, E.M., Dos Santos, K.R., Maciel, E.L., Schuenck, R.P. and Nunes, A.P. (2013): Modification of the Congo red agar method to detect biofilm production by Staphylococcus epidermidis. *Diagn Microbiol Infect Dis*, **75**(3): p. 235-239.

Kaito, C., Saito, Y., Nagano, G., Ikuo, M., Omae, Y., Hanada, Y., Han, X., Kuwahara-Arai, K., Hishinuma, T., Baba, T., Ito, T., Hiramatsu, K. and Sekimizu, K. (2011): Transcription and translation products of the cytolysin gene psm-mec on the mobile genetic element SCCmec regulate Staphylococcus aureus virulence. *PLoS Pathog*, **7**(2): p. e1001267.

Kaito, C., Saito, Y., Ikuo, M., Omae, Y., Mao, H., Nagano, G., Fujiyuki, T., Numata, S., Han, X., Obata, K., Hasegawa, S., Yamaguchi, H., Inokuchi, K., Ito, T., Hiramatsu, K. and Sekimizu, K. (2013): Mobile genetic element SCCmec-encoded psm-mec RNA suppresses translation of agrA and attenuates MRSA virulence. *PLoS Pathog*, **9**(4): p. e1003269.

Katz, A., Elgamal, S., Rajkovic, A. and Ibba, M. (2016): Non-canonical roles of tRNAs and tRNA mimics in bacterial cell biology. *Mol Microbiol*, **101**(4): p. 545-558.

Kery, M.B., Feldman, M., Livny, J. and Tjaden, B. (2014): TargetRNA2: identifying targets of small regulatory RNAs in bacteria. *Nucleic Acids Res*, **42**(Web Server issue): p. W124-129.

Kloos, W.E. and Musselwhite, M.S. (1975): Distribution and persistence of Staphylococcus and Micrococcus species and other aerobic bacteria on human skin. *Appl Microbiol*, **30**(3): p. 381-385.

Knobloch, J.K., Bartscht, K., Sabottke, A., Rohde, H., Feucht, H.H. and Mack, D. (2001): Biofilm formation by Staphylococcus epidermidis depends on functional RsbU, an activator of the sigB operon: differential activation mechanisms due to ethanol and salt stress. *J Bacteriol*, **183**(8): p. 2624-2633.

Knobloch, J.K., Horstkotte, M.A., Rohde, H., Kaulfers, P.M. and Mack, D. (2002): Alcoholic ingredients in skin disinfectants increase biofilm expression of Staphylococcus epidermidis. *J Antimicrob Chemother*, **49**(4): p. 683-687.

Knobloch, J.K., Jager, S., Horstkotte, M.A., Rohde, H. and Mack, D. (2004): RsbU-dependent regulation of Staphylococcus epidermidis biofilm formation is mediated via the alternative sigma factor sigmaB by repression of the negative regulator gene icaR. *Infect Immun*, **72**(7): p. 3838-3848.

Kortmann, J. and Narberhaus, F. (2012): Bacterial RNA thermometers: molecular zippers and switches. *Nat Rev Microbiol*, **10**(4): p. 255-265.

Lalaouna, D., Carrier, M.C. and Masse, E. (2015a): Every little piece counts: the many faces of tRNA transcripts. *Transcription*, **6**(4): p. 74-77.

Lalaouna, D., Carrier, M.C., Semsey, S., Brouard, J.S., Wang, J., Wade, J.T. and Masse, E. (2015b): A 3' external transcribed spacer in a tRNA transcript acts as a sponge for small RNAs to prevent transcriptional noise. *Mol Cell*, **58**(3): p. 393-405.

Lesnik, E.A., Sampath, R., Levene, H.B., Henderson, T.J., McNeil, J.A. and Ecker, D.J. (2001): Prediction of rho-independent transcriptional terminators in Escherichia coli. *Nucleic Acids Res*, **29**(17): p. 3583-3594.

Li, H., Xu, L., Wang, J., Wen, Y., Vuong, C., Otto, M. and Gao, Q. (2005): Conversion of Staphylococcus epidermidis strains from commensal to invasive by expression of the ica locus encoding production of biofilm exopolysaccharide. *Infect Immun*, **73**(5): p. 3188-3191.

Lowy, F.D. (1998): Staphylococcus aureus infections. *N Engl J Med*, **339**(8): p. 520-532.

Luther, M.K., Bilida, S., Mermel, L.A. and LaPlante, K.L. (2015): Ethanol and Isopropyl Alcohol Exposure Increases Biofilm Formation in Staphylococcus aureus and Staphylococcus epidermidis. *Infect Dis Ther*, **4**(2): p. 219-226.

Ma, L., Bajic, V.B. and Zhang, Z. (2013): On the classification of long non-coding RNAs. *RNA Biol*, **10**(6): p. 925-933.

Mack, D., Fischer, W., Krokotsch, A., Leopold, K., Hartmann, R., Egge, H. and Laufs, R. (1996a): The intercellular adhesin involved in biofilm accumulation of Staphylococcus epidermidis is a linear beta-1,6-linked glucosaminoglycan: purification and structural analysis. *J Bacteriol*, **178**(1): p. 175-183.

Mack, D., Haeder, M., Siemssen, N. and Laufs, R. (1996b): Association of biofilm production of coagulase-negative staphylococci with expression of a specific polysaccharide intercellular adhesin. *J Infect Dis*, **174**(4): p. 881-884.

Macke, T.J., Ecker, D.J., Gutell, R.R., Gautheret, D., Case, D.A. and Sampath, R. (2001): RNAMotif, an RNA secondary structure definition and search algorithm. *Nucleic Acids Res*, **29**(22): p. 4724-4735.

Mann, M., Wright, P.R. and Backofen, R. (2017): IntaRNA 2.0: enhanced and customizable prediction of RNA-RNA interactions. *Nucleic Acids Res*.

Manna, A.C. and Cheung, A.L. (2006): Expression of SarX, a negative regulator of agr and exoprotein synthesis, is activated by MgrA in Staphylococcus aureus. *J Bacteriol*, **188**(12): p. 4288-4299.

McKenney, D., Hubner, J., Muller, E., Wang, Y., Goldmann, D.A. and Pier, G.B. (1998): The ica locus of Staphylococcus epidermidis encodes production of the capsular polysaccharide/adhesin. *Infect Immun*, **66**(10): p. 4711-4720.

Meric, G., Miragaia, M., de Been, M., Yahara, K., Pascoe, B., Mageiros, L., Mikhail, J., Harris, L.G., Wilkinson, T.S., Rolo, J., Lamble, S., Bray, J.E., Jolley, K.A.,

Hanage, W.P., Bowden, R., Maiden, M.C., Mack, D., de Lencastre, H., Feil, E.J., Corander, J. and Sheppard, S.K. (2015): Ecological Overlap and Horizontal Gene Transfer in Staphylococcus aureus and Staphylococcus epidermidis. *Genome Biol Evol*, **7**(5): p. 1313-1328.

Milisavljevic, V., Tran, L.P., Batmalle, C. and Bootsma, H.J. (2008): Benzyl alcohol and ethanol can enhance the pathogenic potential of clinical Staphylococcus epidermidis strains. *Am J Infect Control*, **36**(8): p. 552-558.

Miyakoshi, M., Chao, Y. and Vogel, J. (2015): Cross talk between ABC transporter mRNAs via a target mRNA-derived sponge of the GcvB small RNA. *EMBO J*, **34**(11): p. 1478-1492.

Monk, I.R. and Foster, T.J. (2012): Genetic manipulation of Staphylococci-breaking through the barrier. *Front Cell Infect Microbiol*, **2**: p. 49.

Monk, I.R., Shah, I.M., Xu, M., Tan, M.W. and Foster, T.J. (2012): Transforming the untransformable: application of direct transformation to manipulate genetically Staphylococcus aureus and Staphylococcus epidermidis. *MBio*, **3**(2).

Moormeier, D.E., Bose, J.L., Horswill, A.R. and Bayles, K.W. (2014): Temporal and stochastic control of Staphylococcus aureus biofilm development. *MBio*, **5**(5): p. e01341-01314.

Moran, J.C. and Horsburgh, M.J. (2016): Whole-Genome Sequence of Staphylococcus epidermidis Tu3298. *Genome Announc*, **4**(2).

Morfeldt, E., Taylor, D., von Gabain, A. and Arvidson, S. (1995): Activation of alpha-toxin translation in Staphylococcus aureus by the trans-encoded antisense RNA, RNAIII. *EMBO J*, **14**(18): p. 4569-4577.

Müller, L. (2012): Search for putative coding regions in a novel regulatory RNA of Staphylococcus epidermidis.

Nair, D., Memmi, G., Hernandez, D., Bard, J., Beaume, M., Gill, S., Francois, P. and Cheung, A.L. (2011): Whole-genome sequencing of Staphylococcus aureus strain RN4220, a key laboratory strain used in virulence research, identifies mutations that affect not only virulence factors but also the fitness of the strain. *J Bacteriol*, **193**(9): p. 2332-2335.

Narberhaus, F., Waldminghaus, T. and Chowdhury, S. (2006): RNA thermometers. *FEMS Microbiol Rev*, **30**(1): p. 3-16.

NNIS (1999): National Nosocomial Infections Surveillance (NNIS) System Report, Data Summary from January 1990-May 1999, issued June 1999. A report from the NNIS System. *Am J Infect Control*, **27**(6): p. 520-532.

Novick, R.P., Ross, H.F., Projan, S.J., Kornblum, J., Kreiswirth, B. and Moghazeh, S. (1993): Synthesis of staphylococcal virulence factors is controlled by a regulatory RNA molecule. *EMBO J*, **12**(10): p. 3967-3975.

O'Gara, J.P. (2007): ica and beyond: biofilm mechanisms and regulation in Staphylococcus epidermidis and Staphylococcus aureus. *FEMS Microbiol Lett*, **270**(2): p. 179-188.

Ogawa, S.K., Yurberg, E.R., Hatcher, V.B., Levitt, M.A. and Lowy, F.D. (1985): Bacterial adherence to human endothelial cells in vitro. *Infect Immun*, **50**(1): p. 218-224.

Ogston, A. (1882): Micrococcus Poisoning. *J Anat Physiol*, **16**(Pt 4): p. 526-567.

Otto, M. (2009): Staphylococcus epidermidis--the 'accidental' pathogen. *Nat Rev Microbiol*, **7**(8): p. 555-567.

Otto, M. (2012): Molecular basis of Staphylococcus epidermidis infections. *Semin Immunopathol*, **34**(2): p. 201-214.

Otto, M. (2013): Staphylococcal infections: mechanisms of biofilm maturation and detachment as critical determinants of pathogenicity. *Annu Rev Med*, **64**: p. 175-188.

Overgaard, M., Johansen, J., Moller-Jensen, J. and Valentin-Hansen, P. (2009): Switching off small RNA regulation with trap-mRNA. *Mol Microbiol*, **73**(5): p. 790-800.

Pamp, S.J., Frees, D., Engelmann, S., Hecker, M. and Ingmer, H. (2006): Spx is a global effector impacting stress tolerance and biofilm formation in Staphylococcus aureus. *J Bacteriol*, **188**(13): p. 4861-4870.

Paprotka, K., Giese, B. and Fraunholz, M.J. (2010): Codon-improved fluorescent proteins in investigation of Staphylococcus aureus host pathogen interactions. *J Microbiol Methods*, **83**(1): p. 82-86.

Pokrovskaya, V., Poloczek, J., Little, D.J., Griffiths, H., Howell, P.L. and Nitz, M. (2013): Functional characterization of Staphylococcus epidermidis IcaB, a de-N-acetylase important for biofilm formation. *Biochemistry*, **52**(32): p. 5463-5471.

Qin, L., McCausland, J.W., Cheung, G.Y. and Otto, M. (2016): PSM-Mec-A Virulence Determinant that Connects Transcriptional Regulation, Virulence, and Antibiotic Resistance in Staphylococci. *Front Microbiol*, **7**: p. 1293.

Rachid, S., Ohlsen, K., Wallner, U., Hacker, J., Hecker, M. and Ziebuhr, W. (2000): Alternative transcription factor sigma(B) is involved in regulation of biofilm expression in a Staphylococcus aureus mucosal isolate. *J Bacteriol*, **182**(23): p. 6824-6826.

Ren, G.X., Guo, X.P. and Sun, Y.C. (2017): Regulatory 3' Untranslated Regions of Bacterial mRNAs. *Front Microbiol*, **8**: p. 1276.

Robinson, J.T., Thorvaldsdottir, H., Winckler, W., Guttman, M., Lander, E.S., Getz, G. and Mesirov, J.P. (2011): Integrative genomics viewer. *Nat Biotechnol*, **29**(1): p. 24-26.

Rogers, K.L., Rupp, M.E. and Fey, P.D. (2008): The presence of icaADBC is detrimental to the colonization of human skin by Staphylococcus epidermidis. *Appl Environ Microbiol*, **74**(19): p. 6155-6157.

Rosenbach, F.J. (1884): Mikro-organismen bei den Wund-Infections-Krankheiten des Menschen. Wiesbaden: Bergmann, J. F. 1-122.

Rosenstein, R., Nerz, C., Biswas, L., Resch, A., Raddatz, G., Schuster, S.C. and Gotz, F. (2009): Genome analysis of the meat starter culture bacterium Staphylococcus carnosus TM300. *Appl Environ Microbiol*, **75**(3): p. 811-822.

Rossmanith, J. and Narberhaus, F. (2016): Exploring the modular nature of riboswitches and RNA thermometers. *Nucleic Acids Res*, **44**(11): p. 5410-5423.

Rowe, S.E., Mahon, V., Smith, S.G. and O'Gara, J.P. (2011): A novel role for SarX in Staphylococcus epidermidis biofilm regulation. *Microbiology*, **157**(Pt 4): p. 1042-1049.

Rowe, S.E., Campbell, C., Lowry, C., O'Donnell, S.T., Olson, M.E., Lindgren, J.K., Waters, E.M., Fey, P.D. and O'Gara, J.P. (2016): AraC-type regulator Rbf controls the Staphylococcus epidermidis biofilm phenotype by negatively regulating the icaADBC repressor SarR. *J Bacteriol*.

Ruiz de los Mozos, I., Vergara-Irigaray, M., Segura, V., Villanueva, M., Bitarte, N., Saramago, M., Domingues, S., Arraiano, C.M., Fechter, P., Romby, P., Valle, J., Solano, C., Lasa, I. and Toledo-Arana, A. (2013): Base pairing interaction between 5'- and 3'-UTRs controls icaR mRNA translation in Staphylococcus aureus. *PLoS Genet*, **9**(12): p. e1004001.

Rupp, M.E., Ulphani, J.S., Fey, P.D., Bartscht, K. and Mack, D. (1999a): Characterization of the importance of polysaccharide intercellular adhesin/hemagglutinin of Staphylococcus epidermidis in the pathogenesis of biomaterial-based infection in a mouse foreign body infection model. *Infect Immun*, **67**(5): p. 2627-2632.

Rupp, M.E., Ulphani, J.S., Fey, P.D. and Mack, D. (1999b): Characterization of Staphylococcus epidermidis polysaccharide intercellular adhesin/hemagglutinin in the pathogenesis of intravascular catheter-associated infection in a rat model. *Infect Immun*, **67**(5): p. 2656-2659.

Rupp, M.E., Fey, P.D., Heilmann, C. and Gotz, F. (2001): Characterization of the importance of Staphylococcus epidermidis autolysin and polysaccharide intercellular adhesin in the pathogenesis of intravascular catheter-associated infection in a rat model. *J Infect Dis*, **183**(7): p. 1038-1042.

Sadykov, M.R., Hartmann, T., Mattes, T.A., Hiatt, M., Jann, N.J., Zhu, Y., Ledala, N., Landmann, R., Herrmann, M., Rohde, H., Bischoff, M. and Somerville, G.A. (2011): CcpA coordinates central metabolism and biofilm formation in Staphylococcus epidermidis. *Microbiology*, **157**(Pt 12): p. 3458-3468.

Schaeffer, C.R., Hoang, T.N., Sudbeck, C.M., Alawi, M., Tolo, I.E., Robinson, D.A., Horswill, A.R., Rohde, H. and Fey, P.D. (2016): Versatility of Biofilm Matrix Molecules in Staphylococcus epidermidis Clinical Isolates and Importance of Polysaccharide Intercellular Adhesin Expression during High Shear Stress. *mSphere*, **1**(5).

Schindler, C.A. and Schuhardt, V.T. (1964): Lysostaphin: A New Bacteriolytic Agent for the Staphylococcus. *Proc Natl Acad Sci U S A*, **51**: p. 414-421.

Schoenfelder, S.M., Lange, C., Eckart, M., Hennig, S., Kozytska, S. and Ziebuhr, W. (2010): Success through diversity - how Staphylococcus epidermidis establishes as a nosocomial pathogen. *Int J Med Microbiol*, **300**(6): p. 380-386.

Schoenfelder, S.M., Marincola, G., Geiger, T., Goerke, C., Wolz, C. and Ziebuhr, W. (2013): Methionine biosynthesis in Staphylococcus aureus is tightly controlled by a hierarchical network involving an initiator tRNA-specific T-box riboswitch. *PLoS Pathog*, **9**(9): p. e1003606.

Schoenfelder, S.M. (2014): *In vitro* Transcription (IVT) and tRNA Binding Assay. *Bio-protocol*, **4**(18).

Schoenfelder, S.M., Dong, Y., Fessler, A.T., Schwarz, S., Schoen, C., Kock, R. and Ziebuhr, W. (2016): Antibiotic resistance profiles of coagulase-negative staphylococci in livestock environments. *Vet Microbiol*.

Schreier, H. (2014): RNA-Prozessierung und Genregulation in Biofilm-bildenden Staphylococcus epidermidis.

Schuster, C.F. and Bertram, R. (2016): Toxin-Antitoxin Systems of Staphylococcus aureus. *Toxins (Basel)*, **8**(5).

Seidl, K., Goerke, C., Wolz, C., Mack, D., Berger-Bachi, B. and Bischoff, M. (2008): Staphylococcus aureus CcpA affects biofilm formation. *Infect Immun*, **76**(5): p. 2044-2050.

Sharma, C.M., Hoffmann, S., Darfeuille, F., Reignier, J., Findeiss, S., Sittka, A., Chabas, S., Reiche, K., Hackermuller, J., Reinhardt, R., Stadler, P.F. and Vogel, J. (2010): The primary transcriptome of the major human pathogen Helicobacter pylori. *Nature*, **464**(7286): p. 250-255.

Sharma, C.M. and Vogel, J. (2014): Differential RNA-seq: the approach behind and the biological insight gained. *Curr Opin Microbiol*, **19**: p. 97-105.

Sinha, B. and Fraunholz, M. (2010): Staphylococcus aureus host cell invasion and post-invasion events. *Int J Med Microbiol*, **300**(2-3): p. 170-175.

Svensson, S.L. and Sharma, C.M. (2016): Small RNAs in Bacterial Virulence and Communication. *Microbiol Spectr*, **4**(3).

Thorvaldsdottir, H., Robinson, J.T. and Mesirov, J.P. (2013): Integrative Genomics Viewer (IGV): high-performance genomics data visualization and exploration. *Brief Bioinform*, **14**(2): p. 178-192.

Tu Quoc, P.H., Genevaux, P., Pajunen, M., Savilahti, H., Georgopoulos, C., Schrenzel, J. and Kelley, W.L. (2007): Isolation and characterization of biofilm formation-defective mutants of Staphylococcus aureus. *Infect Immun*, **75**(3): p. 1079-1088.

Uckay, I., Pittet, D., Vaudaux, P., Sax, H., Lew, D. and Waldvogel, F. (2009): Foreign body infections due to Staphylococcus epidermidis. *Ann Med*, **41**(2): p. 109-119.

Urban, J.H. and Vogel, J. (2007): Translational control and target recognition by Escherichia coli small RNAs in vivo. *Nucleic Acids Res*, **35**(3): p. 1018-1037.

Urban, J.H. and Vogel, J. (2009): A green fluorescent protein (GFP)-based plasmid system to study post-transcriptional control of gene expression in vivo. *Methods Mol Biol*, **540**: p. 301-319.

Valle, J., Toledo-Arana, A., Berasain, C., Ghigo, J.M., Amorena, B., Penades, J.R. and Lasa, I. (2003): SarA and not sigmaB is essential for biofilm development by Staphylococcus aureus. *Mol Microbiol*, **48**(4): p. 1075-1087.

Vandecasteele, S.J., Peetermans, W.E., R, R.M., Rijnders, B.J. and Van Eldere, J. (2003): Reliability of the ica, aap and atlE genes in the discrimination between invasive, colonizing and contaminant Staphylococcus epidermidis isolates in the diagnosis of catheter-related infections. *Clin Microbiol Infect*, **9**(2): p. 114-119.

Vanderpool, C.K., Balasubramanian, D. and Lloyd, C.R. (2011): Dual-function RNA regulators in bacteria. *Biochimie*, **93**(11): p. 1943-1949.

Vogel, J. and Wagner, E.G. (2007): Target identification of small noncoding RNAs in bacteria. *Curr Opin Microbiol*, **10**(3): p. 262-270.

von Eiff, C., Peters, G. and Heilmann, C. (2002): Pathogenesis of infections due to coagulasenegative staphylococci. *The Lancet Infectious Diseases*, **2**(11): p. 677-685.

Vuong, C., Kocianova, S., Voyich, J.M., Yao, Y., Fischer, E.R., DeLeo, F.R. and Otto, M. (2004a): A crucial role for exopolysaccharide modification in bacterial biofilm formation, immune evasion, and virulence. *J Biol Chem*, **279**(52): p. 54881-54886.

Vuong, C., Voyich, J.M., Fischer, E.R., Braughton, K.R., Whitney, A.R., DeLeo, F.R. and Otto, M. (2004b): Polysaccharide intercellular adhesin (PIA) protects Staphylococcus epidermidis against major components of the human innate immune system. *Cell Microbiol*, **6**(3): p. 269-275.

Waldminghaus, T., Heidrich, N., Brantl, S. and Narberhaus, F. (2007): FourU: a novel type of RNA thermometer in Salmonella. *Mol Microbiol*, **65**(2): p. 413-424.

Wang, C., Fan, J., Niu, C., Wang, C., Villaruz, A.E., Otto, M. and Gao, Q. (2010): Role of spx in biofilm formation of Staphylococcus epidermidis. *FEMS Immunol Med Microbiol*, **59**(2): p. 152-160.

Wang, L., Li, M., Dong, D., Bach, T.H., Sturdevant, D.E., Vuong, C., Otto, M. and Gao, Q. (2008): SarZ is a key regulator of biofilm formation and virulence in Staphylococcus epidermidis. *J Infect Dis*, **197**(9): p. 1254-1262.

Wang, X., Niu, C., Sun, G., Dong, D., Villaruz, A.E., Li, M., Wang, D., Wang, J., Otto, M. and Gao, Q. (2011): ygs is a novel gene that influences biofilm formation and the general stress response of Staphylococcus epidermidis. *Infect Immun*, **79**(3): p. 1007-1015.

Waters, L.S. and Storz, G. (2009): Regulatory RNAs in bacteria. *Cell*, **136**(4): p. 615-628.

Waugh, A., Gendron, P., Altman, R., Brown, J.W., Case, D., Gautheret, D., Harvey, S.C., Leontis, N., Westbrook, J., Westhof, E., Zuker, M. and Major, F. (2002): RNAML: a standard syntax for exchanging RNA information. *RNA*, **8**(6): p. 707-717.

Weaver, W.M., Milisavljevic, V., Miller, J.F. and Di Carlo, D. (2012): Fluid flow induces biofilm formation in Staphylococcus epidermidis polysaccharide intracellular adhesin-positive clinical isolates. *Appl Environ Microbiol*, **78**(16): p. 5890-5896.

Weisser, M., Schoenfelder, S.M., Orasch, C., Arber, C., Gratwohl, A., Frei, R., Eckart, M., Fluckiger, U. and Ziebuhr, W. (2010): Hypervariability of biofilm formation and oxacillin resistance in a Staphylococcus epidermidis strain causing persistent severe infection in an immunocompromised patient. *J Clin Microbiol*, **48**(7): p. 2407-2412.

Wicke, L. (2015): Manipulation genetisch schwer zugänglicher Staphylokokkenspezies: Etablierung neuer molekularer Werkzeuge und Nachweissysteme.

Widerstrom, M. (2016): Significance of Staphylococcus epidermidis in Health Care-Associated Infections, from Contaminant to Clinically Relevant Pathogen: This Is a Wake-Up Call! *J Clin Microbiol*, **54**(7): p. 1679-1681.

Winstel, V., Liang, C., Sanchez-Carballo, P., Steglich, M., Munar, M., Broker, B.M., Penades, J.R., Nubel, U., Holst, O., Dandekar, T., Peschel, A. and Xia, G.

(2013): Wall teichoic acid structure governs horizontal gene transfer between major bacterial pathogens. *Nat Commun*, **4**: p. 2345.

Winstel, V., Kuhner, P., Krismer, B., Peschel, A. and Rohde, H. (2015): Transfer of plasmid DNA to clinical coagulase-negative staphylococcal pathogens using a unique bacteriophage. *Appl Environ Microbiol*.

Winstel, V., Kuhner, P., Rohde, H. and Peschel, A. (2016): Genetic engineering of untransformable coagulase-negative staphylococcal pathogens. *Nat Protoc*, **11**(5): p. 949-959.

Wright, P.R., Georg, J., Mann, M., Sorescu, D.A., Richter, A.S., Lott, S., Kleinkauf, R., Hess, W.R. and Backofen, R. (2014): CopraRNA and IntaRNA: predicting small RNA targets, networks and interaction domains. *Nucleic Acids Res*, **42**(Web Server issue): p. W119-123.

Wu, Y., Wang, J., Xu, T., Liu, J., Yu, W., Lou, Q., Zhu, T., He, N., Ben, H., Hu, J., Gotz, F. and Qu, D. (2012): The two-component signal transduction system ArlRS regulates Staphylococcus epidermidis biofilm formation in an ica-dependent manner. *PLoS One*, **7**(7): p. e40041.

Wu, Y., Wu, Y., Zhu, T., Han, H., Liu, H., Xu, T., Francois, P., Fischer, A., Bai, L., Gotz, F. and Qu, D. (2015): Staphylococcus epidermidis SrrAB regulates bacterial growth and biofilm formation differently under oxic and microaerobic conditions. *J Bacteriol*, **197**(3): p. 459-476.

Xu, L., Li, H., Vuong, C., Vadyvaloo, V., Wang, J., Yao, Y., Otto, M. and Gao, Q. (2006): Role of the luxS quorum-sensing system in biofilm formation and virulence of Staphylococcus epidermidis. *Infect Immun*, **74**(1): p. 488-496.

Xu, T., Wu, Y., Lin, Z., Bertram, R., Gotz, F., Zhang, Y. and Qu, D. (2017): Identification of Genes Controlled by the Essential YycFG Two-Component System Reveals a Role for Biofilm Modulation in Staphylococcus epidermidis. *Front Microbiol*, **8**: p. 724.

You, Y., Xue, T., Cao, L., Zhao, L., Sun, H. and Sun, B. (2014): Staphylococcus aureus glucose-induced biofilm accessory proteins, GbaAB, influence biofilm formation in a PIA-dependent manner. *Int J Med Microbiol*, **304**(5-6): p. 603-612.

Yu, L., Hisatsune, J., Hayashi, I., Tatsukawa, N., Sato'o, Y., Mizumachi, E., Kato, F., Hirakawa, H., Pier, G.B. and Sugai, M. (2017): A Novel Repressor of the ica Locus Discovered in Clinically Isolated Super-Biofilm-Elaborating Staphylococcus aureus. *MBio*, **8**(1).

Zapotoczna, M., O'Neill, E. and O'Gara, J.P. (2016): Untangling the Diverse and Redundant Mechanisms of Staphylococcus aureus Biofilm Formation. *PLoS Pathog*, **12**(7): p. e1005671.

Zhang, Y.Q., Ren, S.X., Li, H.L., Wang, Y.X., Fu, G., Yang, J., Qin, Z.Q., Miao, Y.G., Wang, W.Y., Chen, R.S., Shen, Y., Chen, Z., Yuan, Z.H., Zhao, G.P., Qu, D., Danchin, A. and Wen, Y.M. (2003): Genome-based analysis of virulence genes in a non-biofilm-forming Staphylococcus epidermidis strain (ATCC 12228). *Mol Microbiol*, **49**(6): p. 1577-1593.

Ziebuhr, W., Heilmann, C., Gotz, F., Meyer, P., Wilms, K., Straube, E. and Hacker, J. (1997): Detection of the intercellular adhesion gene cluster (ica) and phase variation in Staphylococcus epidermidis blood culture strains and mucosal isolates. *Infect Immun*, **65**(3): p. 890-896.

Ziebuhr, W. (2001): Staphylococcus aureus and Staphylococcus epidermidis: emerging pathogens in nosocomial infections. *Contrib Microbiol*, **8**: p. 102-107.

Ziebuhr, W., Hennig, S., Eckart, M., Kranzler, H., Batzilla, C. and Kozitskaya, S. (2006): Nosocomial infections by Staphylococcus epidermidis: how a commensal bacterium turns into a pathogen. *Int J Antimicrob Agents*, **28 Suppl 1**: p. S14-20.

Ziebuhr, W. and Vogel, J. (2015): The end is not the end: remnants of tRNA precursors live on to sponge up small regulatory RNAs. *Mol Cell*, **58**(3): p. 389-390.

Zuker, M. (2003): Mfold web server for nucleic acid folding and hybridization prediction. *Nucleic Acids Res*, **31**(13): p. 3406-3415.

Zuker M, J.A. (1998): Using reliability information to annotate RNA secondary structures. *RNA*.

VIII. Annexe

1. Supplementary figures and tables

Oxidase	Negative							
Novobiocin	Susceptible							
Coagulase	Negative	Positive[1] – variable[2] – negative[3]		Negative				
Species group	Hyicus-Intermedius			Epidermidis-Aureus				
Cluster group	Muscae	Hyicus	Intermedius	Aureus	Epidermidis	Warneri	Haemolyticus	Lugdunensis
Species	S. muscae S. microti S. rostri	S. hyicus[2] S. agnetis[2] S. chromogenes[3] S. felis[3]	S. intermedius[1] S. delphini[1] S. lutrae[1] S. pseudinter- medius[1] S. schleiferi ssp. schleiferi[3] ssp. coagulans[1]	S. aureus ssp. aureus[1] ssp. anaerobius[1] S. simiae[1]	S. epidermidis S. capitis ssp. capitis ssp. urealyticus S. caprae S. saccharoly- ticus	S. warneri S. pasteuri	S. haemolyticus S. devriesei S. hominis ssp. hominis ssp. novobio- septicus S. jettensis S. petrasii ssp. croceilyticus ssp. petrasii	S. lugdunensis

Oxidase	Negative						Positive
Novobiocin	Susceptible		Resistant				
Coagulase	Negative						
Species group	Auricularis	Simulans	Saprophyticus				Sciuri
Cluster group	Auricularis	Simulans-Carnosus	Pettenkoferi-Massiliensis	Saprophyticus	Cohnii-Nepalensis	Arlettae-Kloosii	Sciuri
Species	S. auricularis	S. simulans S. carnosus ssp. carnosus ssp. utilis S. condimenti S. piscifermen- tans	S. pettenkoferi S. massiliensis	S. saprophyticus ssp. saprophy- ticus ssp. bovis S. equorum ssp. equorum ssp. linens S. gallinarum S. succinus ssp. succinus ssp. casei S. xylosus	S. cohnii ssp. cohnii ssp. urealyticus S. nepalensis	S. arlettae S. kloosii	S. sciuri ssp. sciuri ssp. carnaticus ssp. rodentium S. fleurettii S. lentus S. stepanovicii S. vitulinus

Fig. VIII-1: Phylogenetic tree with key diagnostic characteristics

Figure taken from Becker *et al.*, 2014 (Figure 3). Shown are the six species groups of Lamers *et al.*, extended by key diagnostic characteristics.

Abbildung 4.13.: Northern Analyse der intergenischen Region von kommensalen (1, 195; 2, 197; 3, RP62A; 4, O-47; 5, 567; 6, 307) und pathogenen *S. epidermidis*.
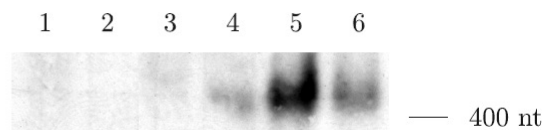
Fig. VIII-2: Northern analysis of IGR from commensal and pathogenic *S. epidermidis*

Figure with figure legend taken from Eckart, 2006 (Figure 4.13).

Tab. VIII-1: IcaZ sequence blast by NCBI *Blastn* (abbreviated results)

Description	Max score	Total score	Query cover	E value	Ident	Accession
Staphylococcus epidermidis isolate BPH0662 genome assembly, chromosome: 1	724	772	100%	0.0	100%	LT571449.1
Staphylococcus epidermidis strain 1457, complete genome	702	750	100%	0.0	99%	CP020463.1
Staphylococcus epidermidis RP62A, complete genome	702	750	100%	0.0	99%	CP000029.1
Schistosoma curassoni genome assembly S_curassoni_Dakar, scaffold SCUD_contig0000174	46.4	46.4	9%	0.58	85%	LM067638.1
PREDICTED: Cyprinodon variegatus voltage-dependent P/Q-type calcium channel subunit alpha-1A-like (LOC107096037), transcript variant X24, mRNA	42.8	42.8	10%	7.1	83%	XM_015392517.1
PREDICTED: Cyprinodon variegatus voltage-dependent P/Q-type calcium channel subunit alpha-1A-like (LOC107096037), transcript variant X23, mRNA	42.8	42.8	10%	7.1	83%	XM_015392516.1
PREDICTED: Cyprinodon variegatus voltage-dependent P/Q-type calcium channel subunit alpha-1A-like (LOC107096037), transcript variant X22, mRNA	42.8	42.8	10%	7.1	83%	XM_015392515.1
PREDICTED: Cyprinodon variegatus voltage-dependent P/Q-type calcium channel subunit alpha-1A-like (LOC107096037), transcript variant X21, mRNA	42.8	42.8	10%	7.1	83%	XM_015392514.1
PREDICTED: Cyprinodon variegatus voltage-dependent P/Q-type calcium channel subunit alpha-1A-like (LOC107096037), transcript variant X19, mRNA	42.8	42.8	10%	7.1	83%	XM_015392511.1
PREDICTED: Cyprinodon variegatus voltage-dependent P/Q-type calcium channel subunit alpha-1A-like (LOC107096037), transcript variant X18, mRNA	42.8	42.8	10%	7.1	83%	XM_015392510.1
PREDICTED: Cyprinodon variegatus voltage-dependent P/Q-type calcium channel subunit alpha-1A-like (LOC107096037), transcript variant X17, mRNA	42.8	42.8	10%	7.1	83%	XM_015392509.1
PREDICTED: Cyprinodon variegatus voltage-dependent P/Q-type calcium channel subunit alpha-1A-like (LOC107096037), transcript variant X16, mRNA	42.8	42.8	10%	7.1	83%	XM_015392508.1
PREDICTED: Cyprinodon variegatus voltage-dependent P/Q-type calcium channel subunit alpha-1A-like (LOC107096037), transcript variant X15, mRNA	42.8	42.8	10%	7.1	83%	XM_015392507.1
PREDICTED: Cyprinodon variegatus voltage-dependent P/Q-type calcium channel subunit alpha-1A-like (LOC107096037), transcript variant X14, mRNA	42.8	42.8	10%	7.1	83%	XM_015392506.1
PREDICTED: Cyprinodon variegatus voltage-dependent P/Q-type calcium channel subunit alpha-1A-like	42.8	42.8	10%	7.1	83%	XM_015392505.1

Tab. VIII-2: Occurrence of *tRNA^{Thr-4}* among staphylococci.

BLASTN 2.5.1+ from NCBI was used to blast tRNA nucleotide sequence against the nucleotide collection database. The table contains an abbreviated list.

Description	Max score	Total score	Query cover	E value	Ident	Accession
Staphylococcus epidermidis isolate BPH0662 genome assembly, chromosome: 1	168	168	100%	1e-38	100%	LT571449.1
Staphylococcus epidermidis strain 949_S8 genome	168	168	100%	1e-38	100%	CP010942.1
Staphylococcus epidermidis strain SEI, complete genome	168	168	100%	1e-38	100%	CP009046.1
Staphylococcus epidermidis PM221 complete genome	168	168	100%	1e-38	100%	HG813242.1
Staphylococcus epidermidis strain SR1 clone step.1005d02 genomic sequence	168	168	100%	1e-38	100%	AF269477.1
Staphylococcus epidermidis RP62A, complete genome	168	168	100%	1e-38	100%	CP000029.1
Staphylococcus epidermidis ATCC 12228, complete genome	168	168	100%	1e-38	100%	AE015929.1
Staphylococcus capitis CR01 complete genome	150	150	100%	3e-33	96%	LN866849.1
Staphylococcus capitis subsp. capitis strain AYP1020, complete genome	150	150	100%	3e-33	96%	CP007601.1
Staphylococcus pasteuri SP1, complete genome	136	136	100%	6e-29	92%	CP004014.1
Staphylococcus warneri SG1, complete genome	136	136	100%	6e-29	92%	CP003668.1
Staphylococcus epidermidis plasmid SAP024A, partial sequence	127	127	96%	3e-26	91%	GQ900469.1
Staphylococcus haemolyticus strain BC05211 SCCmec cassette, complete sequence; and flanking sequence	123	123	100%	4e-25	89%	KX181861.1
Staphylococcus haemolyticus strain Sh29/312/L2, complete genome	123	123	100%	4e-25	89%	CP011116.1
Staphylococcus haemolyticus strain SH32 staphylococcal cassette mec, complete sequence	123	123	100%	4e-25	89%	KF006347.1
Staphylococcus haemolyticus JCSC1435 DNA, complete genome	123	123	100%	4e-25	89%	AP006716.1
Staphylococcus haemolyticus strain S167, complete genome	118	118	100%	2e-23	88%	CP013911.1
Staphylococcus sciuri subsp. sciuri plasmid pACK6, complete sequence	109	109	96%	8e-21	88%	AF093750.2
Staphylococcus simulans bv. staphylolyticus strain NRRL B-2628 plasmid pACK1, complete sequence	87.8	161	100%	3e-14	82%	GU228571.1
Staphylococcus capitis DNA for ALE-1, complete cds	82.4	82.4	98%	1e-12	81%	D86328.1
Staphylococcus simulans strain FDAARGOS_124, complete genome	80.6	80.6	98%	4e-12	80%	CP014016.1
Staphylococcus capitis epr gene, complete cds	75.2	75.2	98%	2e-10	79%	AB000222.2
Staphylococcus simulans lysostaphin (lss) and lysostaphin immunity factor (lif) genes, complete cds, insertion sequence IS1293, complete sequence, and IS257-1 transposase (tnp-1) gene, complete cds	73.4	73.4	100%	6e-10	79%	U66883.1
Staphylococcus aureus endopeptidase-like gene, complete sequence	71.6	71.6	100%	2e-09	79%	EF014432.1
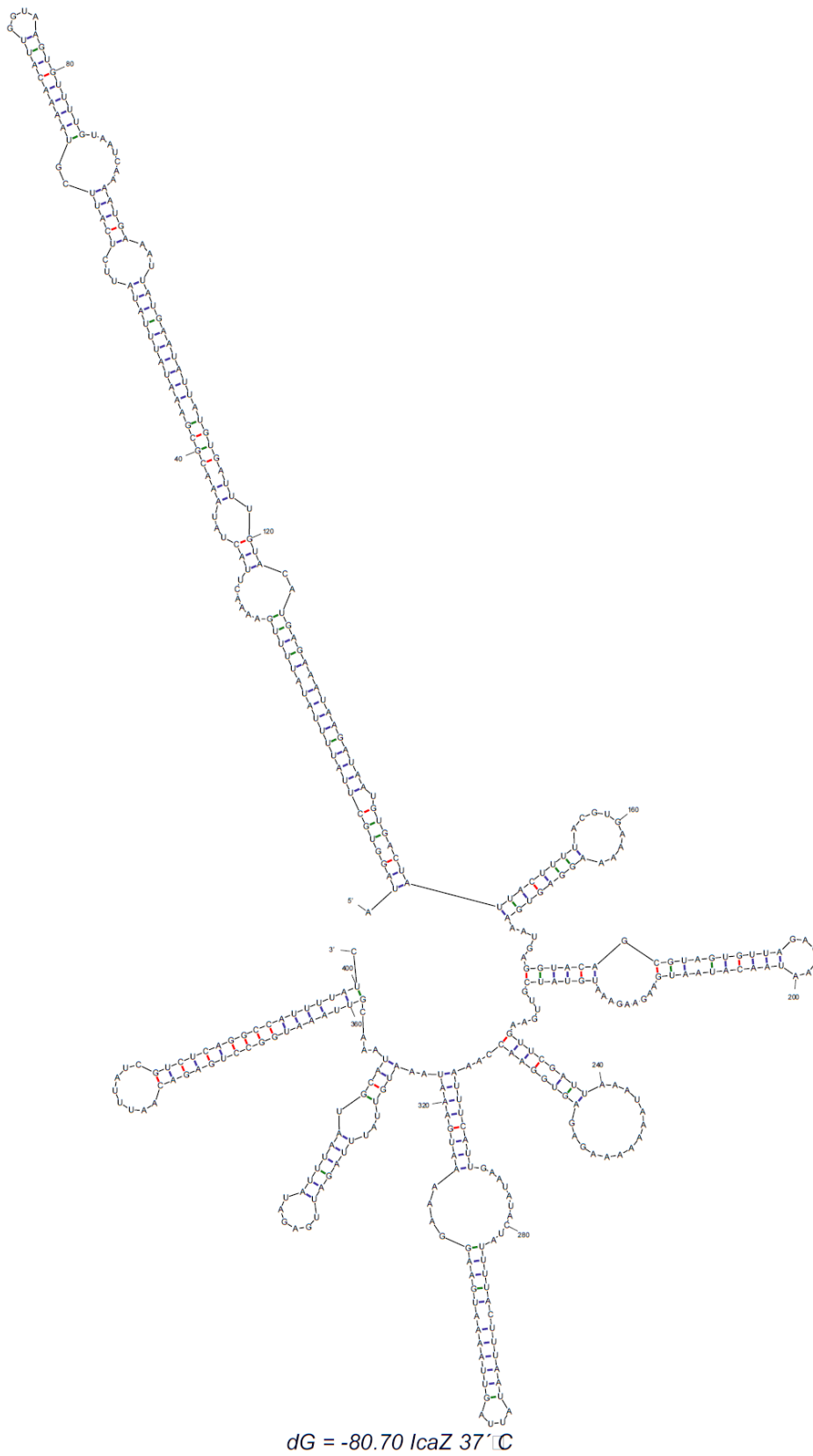
Fig. VIII-3: Predicted secondary structure of IcaZ by *Mfold* 4.7 at 37°C
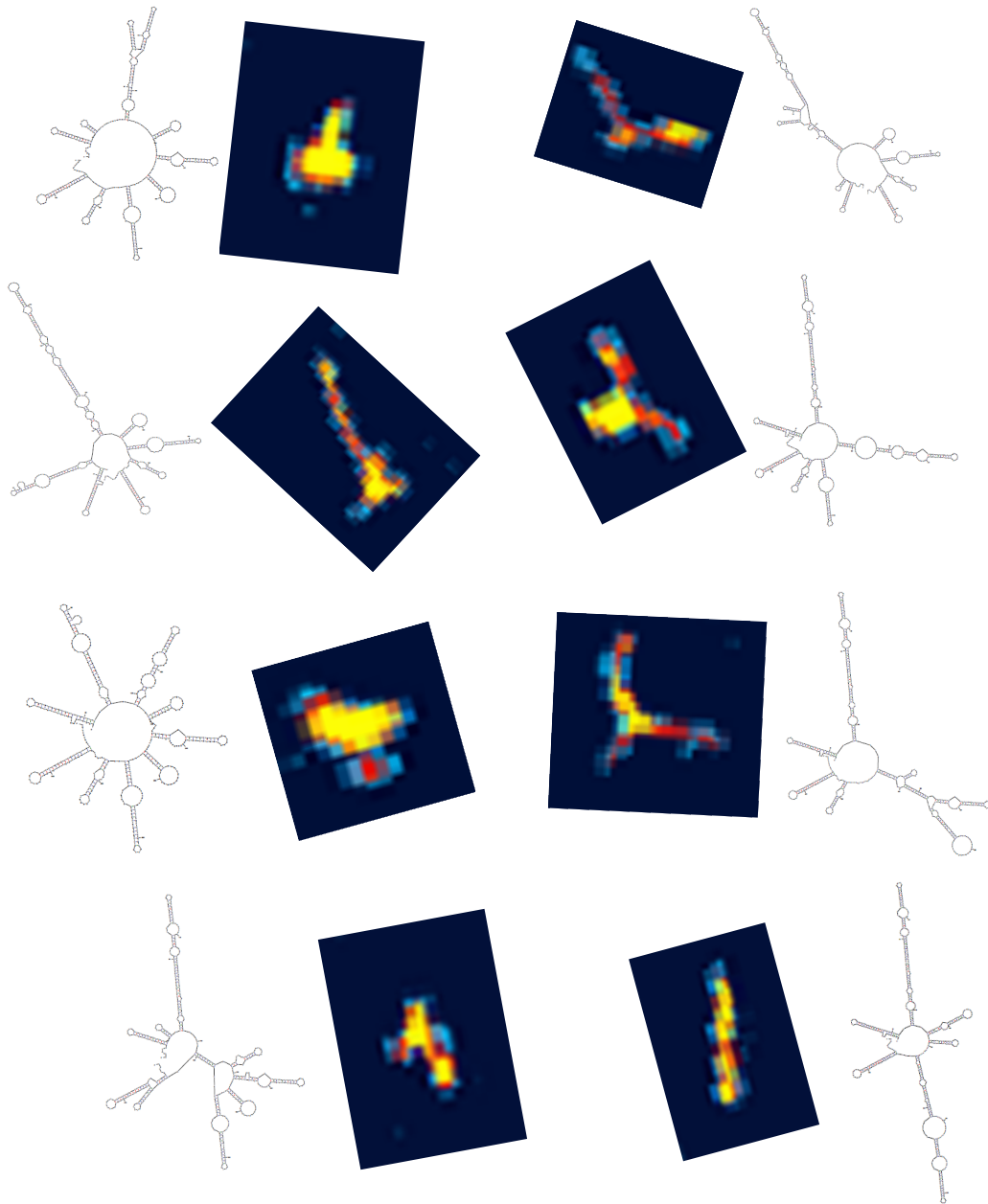
Fig. VIII-4: IcaZ secondary structure variants visualised by AFM

In collaboration with Dr Ingrid Tessmer (Rudolf Virchow Center, Würzburg), the secondary structures of IcaZ were visualised by atomic force microscopy (AFM). 10 µM aliquots of *in vitro* transcribed ncRNA IcaZ (IVT$_{17}$) were prepared and provided for AFM analysis, as well as the previously predicted secondary structures of IcaZ by *Mfold*.

Tab. VIII-3: Comparison C

Proteome analysis of *S. epidermidis* O-47 Wt and IcaZ mutant O-47Δ*tRNA*$^{Thr-4}$ Δ*icaZ*Δ*icaR*-3′ UTR (O-47ΔΔΔ). Proteins were sampled in exponential growth phase at 30°C. Summary of two biological replicates from the mutant and three biological replicates from the wildtype (upregulated genes of the wildtype are green, whereas upregulated genes of the IcaZ mutant are red).

No.	Ratio	Uniprot	Locustag	Labelname (gel)	Recommended name
1	0,204	Q5HRU7	SERP0095	SERP0095(1), SERP2316	Trans-sulfuration enzyme family protein
	0,204	Q5HKM8	SERP2316	SERP0095(1), SERP2316	UPF0176 protein SERP2316
2	0,244	Q5HS35	SERP0004	MnmG(2)	tRNA uridine 5-carboxymethylaminomethyl modification enzyme MnmG
3	0,286	Q5HS35	SERP0004	MnmG(1)	tRNA uridine 5-carboxymethylaminomethyl modification enzyme MnmG
4	0,302	Q5HM98	SERP1731	MurA2	UDP-N-acetylglucosamine 1-carboxyvinyltransferase 2
5	0,303	Q5HRI7	SERP0206	Azo1, SERP0335	FMN-dependent NADPH-azoreductase
	0,303	Q5HR58	SERP0335	Azo1, SERP0335	Decarboxylase family protein
6	0,305	Q5HMG7	SERP1661	Gcp	Probable tRNA threonylcarbamoyladenosine biosynthesis protein Gcp
7	0,306	Q5HQX6	SERP0420	SecA1	Protein translocase subunit SecA 1
8	0,348	Q5HQ06	SERP0751	FtsZ(1)	Cell division protein FtsZ
9	0,359	Q5HNK7	SERP1261	Pyk(5)	Pyruvate kinase
10	0,372	Q5HMF1	SERP1677	RpoF	RNA polymerase sigma factor
11	0,372	Q5HPR4	SERP0844	SERP0844	Transcriptional regulator, putative
12	0,383	Q5HRM0	SERP0173	SERP0173	Uncharacterized protein
13	0,392	Q5HPY1	SERP0776	Gmk(1), IsaA	Guanylate kinase
	0,392	Q5HL49	SERP2138	Gmk(1), IsaA	Probable transglycosylase IsaA
14	0,407	Q5HPT5	SERP0823	RpsB(3)	30S ribosomal protein S2
15	0,416	Q5HQ97	SERP0658	PurH(4)	Bifunctional purine biosynthesis protein PurH
16	0,420	Q5HNK7	SERP1261	Pyk(4)	Pyruvate kinase
17	0,425	Q5HLK9	SERP1978	SERP1978	Nitroreductase family protein
18	0,433	Q5HQH1	SERP0578	MecA	Adapter protein MecA
19	0,437	Q5HNK7	SERP1261	Pyk(2)	Pyruvate kinase
20	0,442	Q5HRT0	SERP0113	SERP0113	Acetyltransferase, GNAT family
21	0,448	Q5HQV5	SERP0441	GapR	Gap transcriptional regulator
22	0,451	Q5HRK5	SERP0188	FusA(1), PurL	Elongation factor G
	0,451	Q5HQA1	SERP0654	FusA(1), PurL	Phosphoribosylformylglycinamidine synthase 2
23	0,455	Q5HMC2	SERP1706	MurA1	UDP-N-acetylglucosamine 1-carboxyvinyltransferase 1
24	0,455	Q5HLD2	SERP2055	PgcA(2)	Phosphoglucomutase
25	0,457	Q5HRX4	SERP0067	Xpt	Xanthine phosphoribosyltransferase
26	0,460	Q5HQQ1	SERP0497	SufD(2)	FeS assembly protein SufD
27	0,461	Q5HQ60	SERP0696	SERP0696(1)	GTP-binding protein TypA
28	0,462	Q5HPT8	SERP0820	AsnS(3), HslU	ATP-dependent protease ATPase subunit HslU
	0,462	Q5HP89	SERP1024	AsnS(3), HslU	Asparagine--tRNA ligase
29	0,462	Q5HRZ4	SERP0045	Ssb	Single-stranded DNA-binding protein
30	0,469	Q5HMD9	SERP1689	MurF, Tuf(4)	UDP-N-acetylmuramoyl-tripeptide--D-alanyl-D-alanine ligase
	0,469	Q5HRK4	SERP0189	MurF, Tuf(4)	Elongation factor Tu
31	0,472	Q5HNL6	SERP1252	CoaE	Dephospho-CoA kinase
32	0,487	Q5HS33	SERP0006	SERP0006	Chromosome partioning protein, ParB family
33	0,489	Q5HPS8	SERP0830	ProS	Proline--tRNA ligase
34	0,489	Q5HNH4	SERP1295	Fhs(2)	Formate--tetrahydrofolate ligase
35	0,489	Q5HNM1	SERP1246	ThrS(3)	Threonine--tRNA ligase
36	0,489	Q5HQM1	SERP0527	SERP0527(5)	NADH dehydrogenase-like protein SERP0527
37	0,491	Q5HNK7	SERP1261	Pyk(1)	Pyruvate kinase
38	0,491	Q5HKJ3	SERP2352	ArcC	Carbamate kinase
39	0,492	Q5HNH4	SERP1295	Fhs(4)	Formate--tetrahydrofolate ligase
40	0,497	Q5HQC3	SERP0632	MenB(1)	1,4-Dihydroxy-2-naphthoyl-CoA synthase
41	0,497	Q5HNM6	SERP1241	SERP1241	MutT/nudix family protein
42	0,497	Q5HPW2	SERP0795	PlsX(2)	Phosphate acyltransferase

No.	Ratio	Uniprot	Locustag	Labelname (gel)	Recommended name
1	2,039	Q5HQ75	SERP0681	PdhB(4)	Pyruvate dehydrogenase E1 component subunit beta
2	2,069	Q5HQ60	SERP0696	SERP0696(2)	GTP-binding protein TypA
3	2,085	Q5HQ36	SERP0721	HemL2, PheS, SERP1072	Phenylalanine--tRNA ligase alpha subunit
	2,085	Q5HP41	SERP1072	HemL2, PheS, SERP1072	Peptidase T-like protein
	2,085	Q5HN71	SERP1401	HemL2, PheS, SERP1072	Glutamate-1-semialdehyde 2,1-aminomutase 2
4	2,102	Q5HPU1	SERP0817	SERP2327(1), TrmFO	Methylenetetrahydrofolate--tRNA-(uracil-5-)-methyltransferase TrmFO
	2,102	Q5HKL7	SERP2327	SERP2327(1), TrmFO	Dihydrolipoyl dehydrogenase
5	2,107	Q5HR46	SERP0347	Mdh	Malate dehydrogenase
6	2,111	Q5HNL0	SERP1258	GltA(1)	Citrate synthase
7	2,129	Q5HL01	SERP2186	Sat(3)	Sulfate adenylyltransferase
8	2,199	Q5HRX1	SERP0070	GuaA	GMP synthase [glutamine-hydrolyzing]
9	2,218	Q5HL01	SERP2186	Sat(2)	Sulfate adenylyltransferase
10	2,224	Q5HN85	SERP1387	FumC	Fumarate hydratase class II
11	2,249	Q5HQ97	SERP0658	PurH(2)	Bifunctional purine biosynthesis protein PurH
12	2,266	Q5HKZ7	SERP2190	CysI(5)	Sulfite reductase [NADPH] hemoprotein beta-component
13	2,275	Q5HKZ5	SERP2192	CysH	Phosphoadenosine phosphosulfate reductase
14	2,329	Q5HLU4	SERP1888	SERP1888(1)	Putative 2-hydroxyacid dehydrogenase SERP1888
15	2,373	Q5HPC6	SERP0986	OdhA(1)	2-oxoglutarate dehydrogenase E1 component
16	2,382	Q5HP48	SERP1065	ProC	Pyrroline-5-carboxylate reductase

#	Value	UniProt	SERP	Genes	Protein
	2,085	Q5HP41	SERP1072	HemL2, PheS, SERP1072	Peptidase T-like protein
	2,085	Q5HN71	SERP1401	HemL2, PheS, SERP1072	Glutamate-1-semialdehyde 2,1-aminomutase 2
4	2,102	Q5HPU1	SERP0817	SERP2327(1), TrmFO	Methylenetetrahydrofolate--tRNA-(uracil-5-)-methyltransferase TrmFO
	2,102	Q5HKL7	SERP2327	SERP2327(1), TrmFO	Dihydrolipoyl dehydrogenase
5	2,107	Q5HR46	SERP0347	Mdh	Malate dehydrogenase
6	2,111	Q5HNL0	SERP1258	GltA(1)	Citrate synthase
7	2,129	Q5HL01	SERP2186	Sat(3)	Sulfate adenylyltransferase
9	2,218	Q5HL01	SERP2186	Sat(2)	Sulfate adenylyltransferase
10	2,224	Q5HN85	SERP1387	FumC	Fumarate hydratase class II
11	2,249	Q5HQ97	SERP0658	PurH(2)	Bifunctional purine biosynthesis protein PurH
12	2,266	Q5HKZ7	SERP2190	CysI(5)	Sulfite reductase [NADPH] hemoprotein beta-component
13	2,275	Q5HKZ5	SERP2192	CysH	Phosphoadenosine phosphosulfate reductase
14	2,329	Q5HLU4	SERP1888	SERP1888(1)	Putative 2-hydroxyacid dehydrogenase SERP1888
15	2,373	Q5HPC6	SERP0986	OdhA(1)	2-oxoglutarate dehydrogenase E1 component
16	2,382	Q5HP48	SERP1065	ProC	Pyrroline-5-carboxylate reductase
17	2,507	Q5HKL7	SERP2327	SERP2327(2)	Dihydrolipoyl dehydrogenase
18	2,541	Q5HKT1	SERP2261	ManA-2	Mannose-6-phosphate isomerase, class I
19	2,606	Q5HP43	SERP1070	MalA	Alpha-glucosidase
20	2,643	Q5HPC6	SERP0986	OdhA(3)	2-oxoglutarate dehydrogenase E1 component
21	2,739	Q5HPU4	SERP0814	SucD(1)	Succinyl-CoA ligase [ADP-forming] subunit alpha
22	2,853	Q5HPP0	SERP0868	GlpD(1)	Aerobic glycerol-3-phosphate dehydrogenase
23	2,870	Q5HQ75	SERP0681	PdhB(1), SERP2325(2)	Pyruvate dehydrogenase E1 component subunit beta
	2,870	Q5HKL9	SERP2325	PdhB(1), SERP2325(2)	Acetoin dehydrogenase, E1 component, beta subunit
24	2,908	Q5HL18	SERP2169	SERP2169	Putative pyruvate, phosphate dikinase regulatory protein 2
25	2,944	Q5HQK4	SERP0545	RocD(1)	Ornithine aminotransferase
26	2,980	Q5HL01	SERP2186	Sat(4)	Sulfate adenylyltransferase
27	2,998	Q5HPJ0	SERP0921	AcnA(3)	Aconitate hydratase
28	3,001	Q5HPE8	SERP0964	Asd	Aspartate-semialdehyde dehydrogenase
29	3,101	Q5HQK4	SERP0545	RocD(5)	Ornithine aminotransferase
30	3,127	Q5HQX7	SERP0419	SERP0419(1)	Uncharacterized protein SERP0419
31	3,277	Q5HQK4	SERP0545	RocD(4)	Ornithine aminotransferase
32	3,295	Q5HNL0	SERP1258	GltA(6), RocD(3)	Citrate synthase
	3,295	Q5HQK4	SERP0545	GltA(6), RocD(3)	Ornithine aminotransferase
33	3,435	Q5HQ26	SERP0731	SERP0731(2)	Succinate dehydrogenase, flavoprotein subunit
34	3,467	Q5HKM0	SERP2324	SERP2324(1)	Acetoin dehydrogenase, E2 component, dihydrolipoamide acetyltransferase
35	3,636	Q5HM77	SERP1752	ManA-1	Mannose-6-phosphate isomerase, class I
36	3,640	Q5HRD6	SERP0257	Adh(2)	Alcohol dehydrogenase
37	3,665	Q5HNL0	SERP1258	GltA(5), RocD(2)	Citrate synthase
	3,665	Q5HQK4	SERP0545	GltA(5), RocD(2)	Ornithine aminotransferase
38	3,672	Q5HRD6	SERP0257	Adh(4)	Alcohol dehydrogenase
39	3,727	Q5HKL7	SERP2327	SERP2327(3)	Dihydrolipoyl dehydrogenase
40	3,836	Q5HL59	SERP2128	RocA(1)	1-pyrroline-5-carboxylate dehydrogenase
41	3,851	Q5HPJ0	SERP0921	AcnA(1)	Aconitate hydratase
42	3,863	Q5HPC6	SERP0986	OdhA(2)	2-oxoglutarate dehydrogenase E1 component
43	3,864	Q5HRD6	SERP0257	Adh(5)	Alcohol dehydrogenase
44	3,904	Q5HKL9	SERP2325	SERP2325(3)	Acetoin dehydrogenase, E1 component, beta subunit
45	3,948	Q5HNJ5	SERP1273	SERP1273(2)	Putative universal stress protein SERP1273
46	4,182	Q5HMZ1	SERP1484	GroL, SERP2324(6)	60 kDa chaperonin
	4,182	Q5HKM0	SERP2324	GroL, SERP2324(6)	Acetoin dehydrogenase, E2 component, dihydrolipoamide acetyltransferase
47	4,262	Q5HNL0	SERP1258	GltA(3)	Citrate synthase
48	4,334	Q5HNJ5	SERP1273	SERP1273(1)	Putative universal stress protein SERP1273
49	4,452	Q5HRD1	SERP0262	ArgS	Arginine--tRNA ligase
50	4,492	Q5HRD6	SERP0257	Adh(3)	Alcohol dehydrogenase
51	4,712	Q5HKJ8	SERP2346	GldA	Glycerol dehydrogenase
52	4,948	Q5HQM1	SERP0527	SERP0527(7)	NADH dehydrogenase-like protein SERP0527
53	5,124	Q5HPE7	SERP0965	DapA	4-hydroxy-tetrahydrodipicolinate synthase
54	5,197	Q5HQ85	SERP0670	PtsI(1)	Phosphoenolpyruvate-protein phosphotransferase
55	5,213	Q5HQ26	SERP0731	SERP0663(2), SERP0731(1	Succinate dehydrogenase, flavoprotein subunit
	5,213	Q5HQ92	SERP0663	SERP0663(2), SERP0731(1	67 kDa Myosin-crossreactive antigen
56	5,613	Q5HRL0	SERP0183	RpoB(1)	DNA-directed RNA polymerase subunit beta
57	5,875	Q5HPR7	SERP0841	Pnp(2), PpdK(3)	Polyribonucleotide nucleotidyltransferase
	5,875	Q5HL17	SERP2170	Pnp(2), PpdK(3)	Pyruvate phosphate dikinase
58	6,698	Q5HQ92	SERP0663	SERP0663(1)	67 kDa Myosin-crossreactive antigen
59	7,057	Q5HL17	SERP2170	AcnA(7), PpdK(5)	Pyruvate phosphate dikinase
	7,057	Q5HPJ0	SERP0921	AcnA(7), PpdK(5)	Aconitate hydratase
60	7,203	Q5HL59	SERP2128	RocA(4)	1-pyrroline-5-carboxylate dehydrogenase
61	7,514	Q5HKM0	SERP2324	SERP2324(5)	Acetoin dehydrogenase, E2 component, dihydrolipoamide acetyltransferase
62	7,910	Q5HQ06	SERP0751	FtsZ(5)	Cell division protein FtsZ
63	8,011	Q5HL31	SERP2156	Ldh(2)	L-lactate dehydrogenase
64	8,432	Q5HKM0	SERP2324	SERP2324(4)	Acetoin dehydrogenase, E2 component, dihydrolipoamide acetyltransferase
65	9,303	Q5HL19	SERP2168	Mqo4(1)	Probable malate:quinone oxidoreductase 4
66	9,355	Q5HK15	SERP2537	DnaB, SERP2324(2)	Replicative DNA helicase
	9,355	Q5HKM0	SERP2324	DnaB, SERP2324(2)	Acetoin dehydrogenase, E2 component, dihydrolipoamide acetyltransferase
67	9,559	Q5HKL8	SERP2326	SERP2326(2)	Acetoin dehydrogenase, E1 component, alpha subunit
68	10,931	Q5HKL8	SERP2326	SERP2326(1)	Acetoin dehydrogenase, E1 component, alpha subunit
69	11,539	Q5HKM0	SERP2324	SERP2324(3)	Acetoin dehydrogenase, E2 component, dihydrolipoamide acetyltransferase
70	11,611	Q5HL59	SERP2128	RocA(2)	1-pyrroline-5-carboxylate dehydrogenase
71	12,538	Q5HL17	SERP2170	AcnA(6), PpdK(2)	Pyruvate phosphate dikinase
	12,538	Q5HPJ0	SERP0921	AcnA(6), PpdK(2)	Aconitate hydratase
72	13,257	Q5HRK5	SERP0188	FusA(5)	Elongation factor G
73	13,868	Q5HL59	SERP2128	RocA(3)	1-pyrroline-5-carboxylate dehydrogenase
74	15,214	Q5HNL7	SERP1250	AroA, GapA2	Glyceraldehyde-3-phosphate dehydrogenase 2
	15,214	Q5HP79	SERP1034	AroA, GapA2	3-phosphoshikimate 1-carboxyvinyltransferase

63	8,011	Q5HL31	SERP2156	Ldh(2)	L-lactate dehydrogenase
64	8,432	Q5HKM0	SERP2324	SERP2324(4)	Acetoin dehydrogenase, E2 component, dihydrolipoamide acetyltransferase
65	9,303	Q5HL19	SERP2168	Mqo4(1)	Probable malate:quinone oxidoreductase 4
66	9,355	Q5HK15	SERP2537	DnaB, SERP2324(2)	Replicative DNA helicase
	9,355	Q5HKM0	SERP2324	DnaB, SERP2324(2)	Acetoin dehydrogenase, E2 component, dihydrolipoamide acetyltransferase
67	9,559	Q5HKL8	SERP2326	SERP2326(2)	Acetoin dehydrogenase, E1 component, alpha subunit
68	10,931	Q5HKL8	SERP2326	SERP2326(1)	Acetoin dehydrogenase, E1 component, alpha subunit
69	11,539	Q5HKM0	SERP2324	SERP2324(3)	Acetoin dehydrogenase, E2 component, dihydrolipoamide acetyltransferase
71	12,538	Q5HL17	SERP2170	AcnA(6), PpdK(2)	Pyruvate phosphate dikinase
	12,538	Q5HPJ0	SERP0921	AcnA(6), PpdK(2)	Aconitate hydratase
72	13,257	Q5HRK5	SERP0188	FusA(5)	Elongation factor G
73	13,868	Q5HL59	SERP2128	RocA(3)	1-pyrroline-5-carboxylate dehydrogenase
74	15,214	Q5HNL7	SERP1250	AroA, GapA2	Glyceraldehyde-3-phosphate dehydrogenase 2
	15,214	Q5HP79	SERP1034	AroA, GapA2	3-phosphoshikimate 1-carboxyvinyltransferase

----

A

B

Fig. VIII-5: Carbon flow in staphylococci in exp. and stat. growth phase

The figures summarise the carbon flow in the exponential growth phase (**A**) and stationary growth phase (**B**) in staphylococci. Figures were kindly provided by PD Dr Wilma Ziebuhr.

A

```
                    31                50
                    |                 |
        5'-GGG...AAACA          ACUUA...UCU-3'
Target               GUAAUAUUUGUAAUUUUA
                     :|||||||::|||||||:|
Query                UAUUAUAAGUAUUAAAGU
        3'-UAU...UAGUG          AAAAC...GGG-5'
                    |                 |
                   124               105
```

Energy	**-6.11564 kcal/mol**	Position - Target RNA	32 – 49
Hybridization Energy	-18.0	Position - Query RNA	106 – 123
Unfolding Energy - Target	4.27988	Position Seed - Target RNA	43 – 49
Unfolding Energy - Query	7.56424	Position Seed - Query RNA	106 – 112

B

```
                    187               206
                    |                 |
        5'-GGG...CUAAA          ACAUU...CGA-3'
Target               UAUUUUUUAUGUGCAAAU
                     |||||:|:|||||:|||||
Query                AUAAAGAGUACAUGUUUA
        3'-UAU...AUAGA          GUGUA...GGG-5'
                    |                 |
                   145               126
```

Energy	**-10.56620 kcal/mol**	Position - Target RNA	188 – 205
Hybridization Energy	-22.2	Position - Query RNA	127 – 144
Unfolding Energy - Target	5.14586	Position Seed - Target RNA	198 – 204
Unfolding Energy - Query	6.48832	Position Seed - Query RNA	128 – 134

C

```
                    258        268
                    |          |
        5'-UAU...UCAUU      AUUUU...CCA-3'
Target               GAAUAUACU
                     |||||||||
Query                CUUAUAUGA
        3'-UUU...UGUCA      ACCAG...AUG-5'
                    |          |
                   605        595
```

Energy	**-9.24494 kcal/mol**
Hybridization Energy	-12.2
Unfolding Energy - Target	1.28518
Unfolding Energy - Query	1.71678

D

```
                        490        501
                        |          |
        5'-GUA...AAUAA        ACUAA...UUU-3'
Target               AAGCAUCUAU
                     |||||:||||
Query                UUCGUGGAUA
        3'-ACU...UUUUA          -5'
                    |          |
                   11          1
```

Energy	-10.76940 kcal/mol
Hybridization Energy	-12.4
Unfolding Energy - Target	0.96481
Unfolding Energy - Query	0.68133

Fig. VIII-6: Predicted interaction sites of IcaZ and *icaR* mRNA by *IntaRNA*

Different length of IcaZ (O-47 or RP62A sequence) or *icaR*-mRNA were used for the predictions of interaction sites by *IntaRNA*. The software was freely available at http://rna.informatik.uni-freiburg.de/IntaRNA/Input.jsp (Busch *et al.*, 2008; Mann *et al.*, 2017; Wright *et al.*, 2014). The numbers on the nucleotide strands do not resemble genuine numbers from sequence length of either IcaZ or *icaR* mRNA. (A) target: *icaR* mRNA of O-47, query: IcaZ, 30°C; (B) target: *icaR* mRNA of RP62A, query: IcaZ (C) target: IcaZ, query: *icaR* mRNA of O-47, *IntaRNA* version 1.2.5. (D) target: *icaR*-5′ 3′ UTR of O-47, query: IcaZ, *IntaRNA* version 4.4.5.
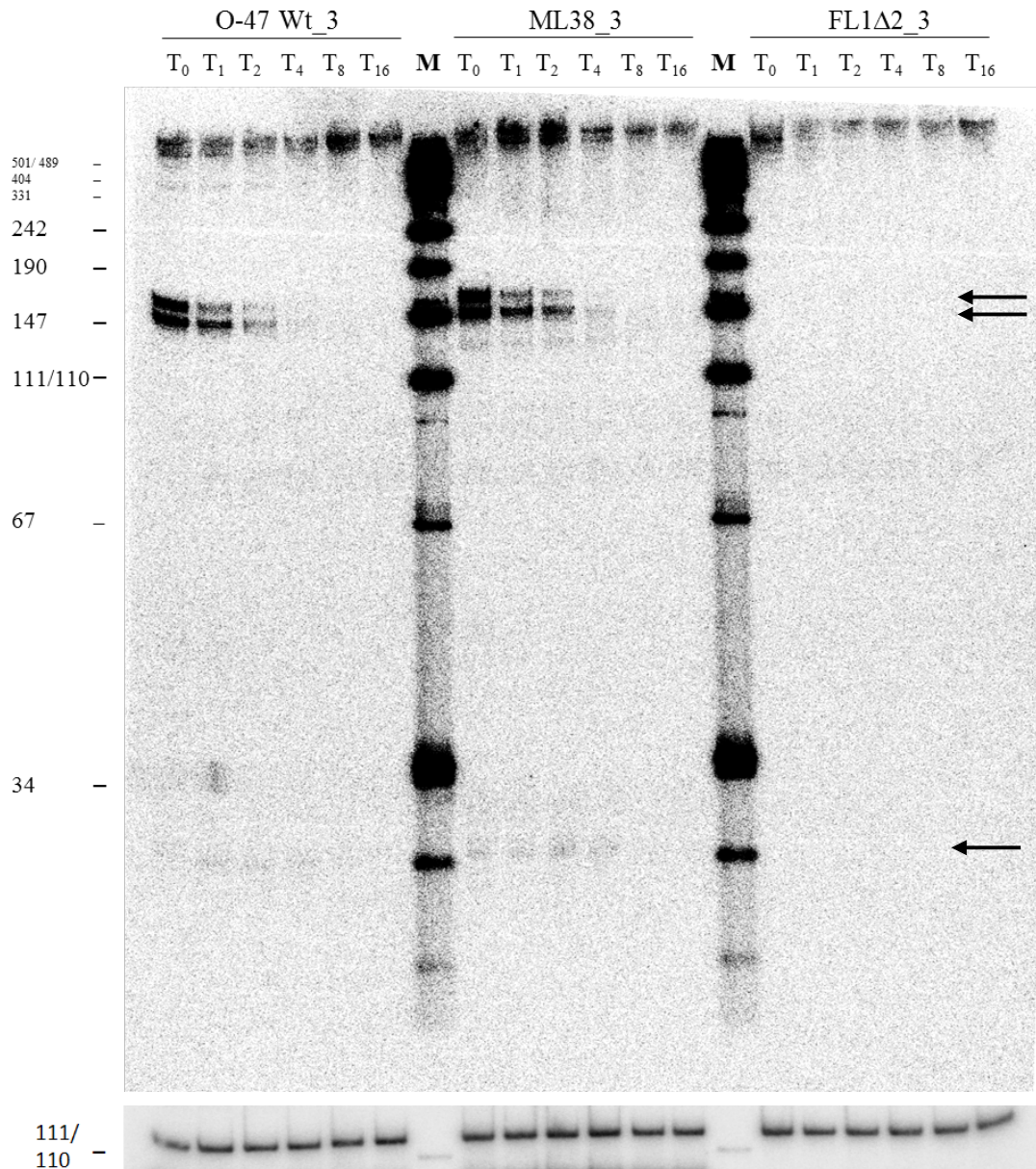
Fig. VIII-7: Rifampicin Northern blot assay of Wt and *icaZ* mutants

Total RNA was sampled at 30°C from O-47 Wt, *S. epidermidis* O-47Δ*icaZ* (ML38) and *S. epidermidis* O-47Δ*tRNA*$^{Thr-4}$Δ*icaZ*Δ*icaR*-3′ UTR (FL1Δ2) by rifampicin assay. T_0 = uninduced sample at OD_{600} ~ 1-2; T_1-T_{16} = time in min after addition of rifampicin (endconc. 100 µg/ml); M = radioactively labelled pUC Mix marker 8. Samples were loaded onto 6% PAA/7M urea gel and electrophoresis was done at 300V for 2h 10 min. (**Top**) Bands were detected by hybridisation of the nylon membrane with radioactively labelled oligonucleotide probe tRNA-3'UTR-as detecting the tRNA^{Thr-4}-3′ UTR. Black arrows indicate the detected bands. The residual signals around 400 nt result from former hybridisations. (**Bottom**) 5S rRNA was used as loading control.

Tab. VIII-4: List of transcripts used for atomic force microscopy

Transcripts, generated by *in vitro* transcription and corresponding T7 DNA template numbers, as well as the primer, the PCR conditions, the length of the PCR product and the length of the transcribed RNA are listed. PCR was done in 50 µl Phusion Green High-Fidelity DNA Polymerase standard reaction. Genomic DNA of *S. epidermidis* O-47 (for IVT$_2$, IVT$_3$, IVT$_{17}$, IVT$_{19}$, IVT$_{19\,lf}$ and IVT$_{19\,rf}$) and *S. aureus* 8325 (for IVT$_{23}$ and IVT$_{24}$) was used.

IVT No.	Forward primer	Reverse primer	PCR conditions	PCR product length [bp]	RNA length [nt]
IVT$_{17}$	T7-2_IGRica_MF	IGRica_rev3	$t_A = 62.3°C$, $t_E = 30s$, 34x	455	437
IVT$_2$	MF_icaR5'_T7-F2	MF_icaR5'_R	$t_A = 63°C$, $t_E = 20s$, 34x	136	118
IVT$_3$	MF_icaR3'_T7-F	MF_icaR3'_R	$t_A = 63°C$, $t_E = 20s$, 34x	343	186
IVT$_{19\,lf}$	ML_icaR3'_lf	ML_icaR3'_R2	$t_A = 59.9°C$, $t_E = 15s$, 5x $t_A = 64.3°C$, $t_E = 15s$, 28x	428	-
IVT$_{19\,rf}$	ML_icaR5'_T7-F3	ML_icaR5'_rf	$t_A = 57.6°C$, $t_E = 15s$, 5x $t_A = 67.1°C$, $t_E = 15s$, 28x	153	-
IVT$_{19}$	ML_icaR5'_T7-F3	ML_icaR3'_R2	$t_A = 64.3°C$, $t_E = 30s$, 34x	546	528
IVT$_{23}$	SA_IcaR-5'-T7-F	SA_IcaR-5'-R	$t_A = 65°C$, $t_E = 30s$, 34x	125	107
IVT$_{24}$	SA_IcaR-3'-T7-F	SA_IcaR-3'-R	$t_A = 65°C$, $t_E = 30s$, 34x	451	433
IVT$_9$	MF_icaA5'_T7-F	MF_icaA5'_R	$t_A = 63°C$, $t_E = 20s$, 34x	194	176
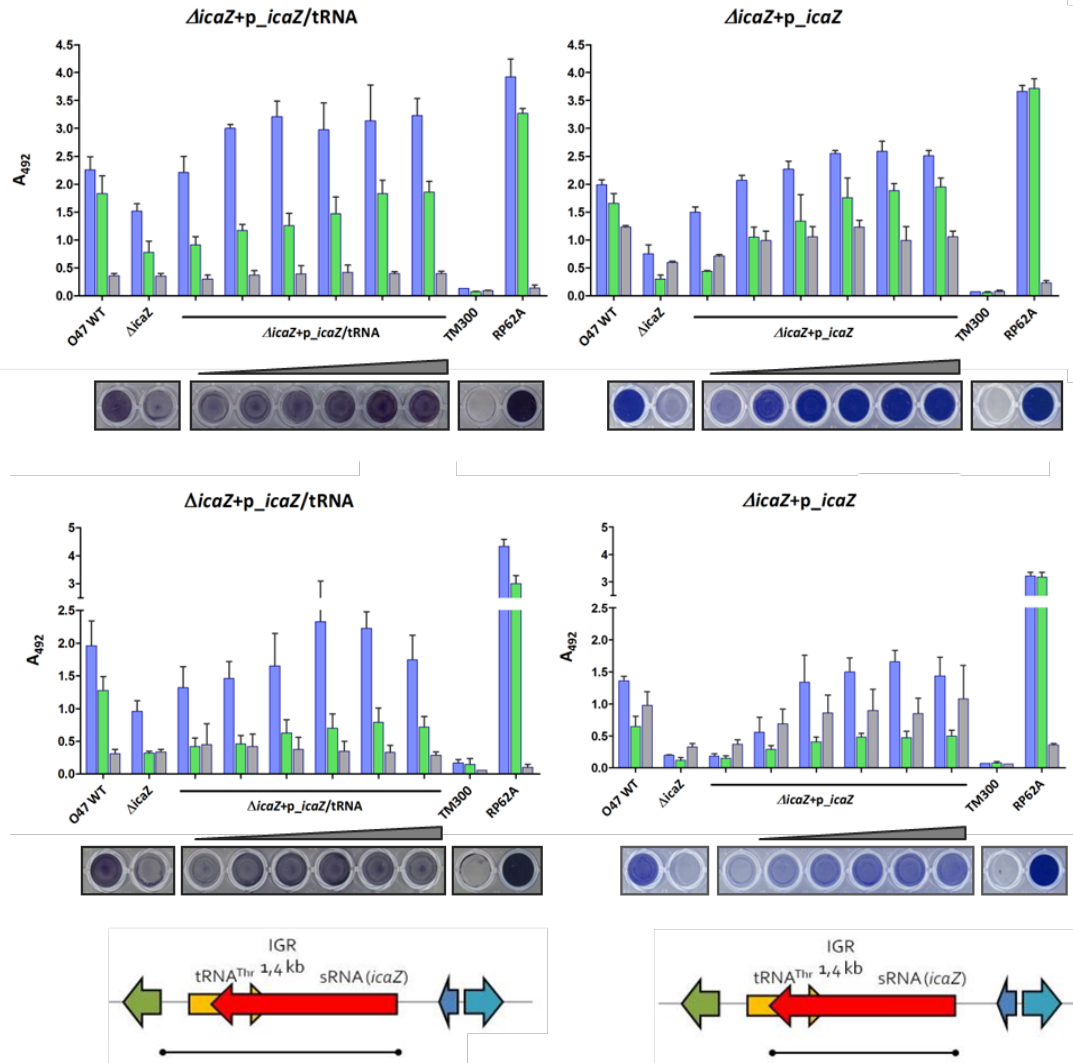
Fig. VIII-8: Biofilm formation of IcaZ overexpression strains MF52 and JE13

Strain 'ΔicaZ' actually is O-47ΔΔΔ (strain collection code FL1Δ2).
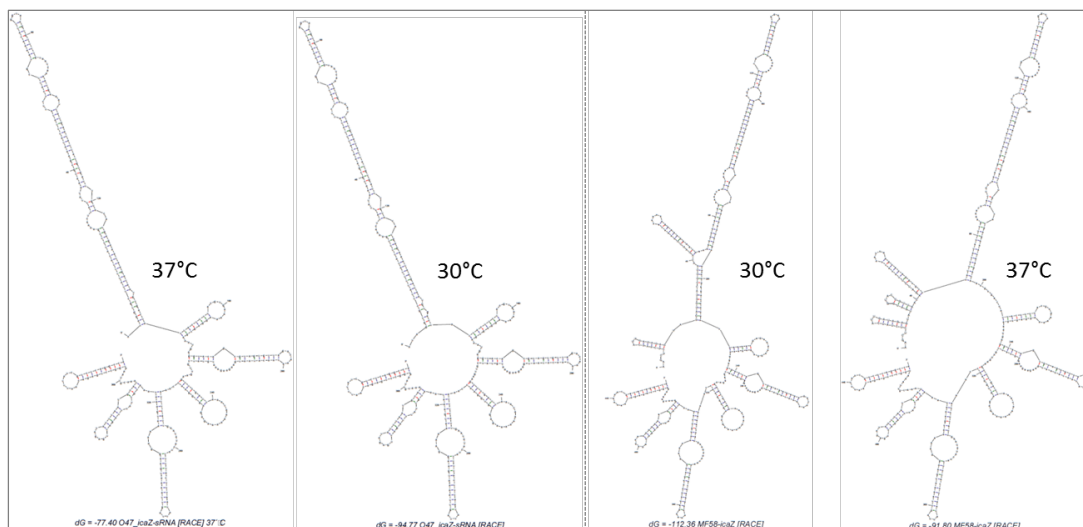
Fig. VIII-9: Secondary structure prediction of O-47-IcaZ and overexpressed IcaZ

Secondary structure predictions with natural IcaZ length from *S. epidermidis* O-47 (left) and *in trans* overexpressed IcaZ (right) from plasmid pCG248 backbone (strains MF58, MF52 and JE13) were carried out, because overexpressed IcaZ carried additional nucleotides at the 5'UTR, deriving from the plasmid (between TSS and cloned IcaZ sequence). The additional nucleotides did not change the overall secondary structure. The predictions were carried out by *Mfold* version 2.3.
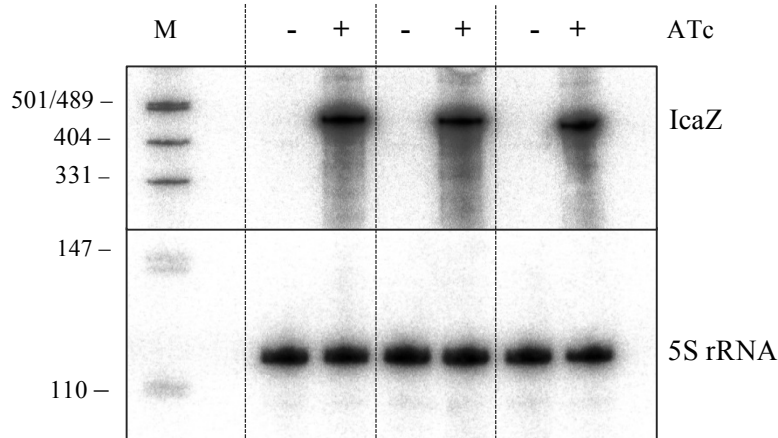
Fig. VIII-10: Northern blot detection of IcaZ pulse-expression transcripts

RNA samples were separated on denaturing 6% PAA/ 7M urea gel (300V/1.5-2h). Radioactively end-labelled pUC Mix Marker 8 was used as DNA ladder. The first lane was left empty, then sets 1-3 were loaded. Each set contained the total RNA of ATc-uninduced (-) and ATc-induced (+) bacterial culture of *S. epidermidis* O-47 Δ*tRNA*$^{Thr-4}$Δ*icaZ*Δ*icaR*-3′ UTR +pCG248_icaZ/tRNA (strain collection code JE13). IcaZ probe was an [α^{32}P]-dCTP labelled PCR product, amplified with primers tRNA_x_as and ica_rev294. 5S rRNA was used as loading control and detected with [γ^{32}P]-ATP end-labelled 5S rRNA oligonucleotide.
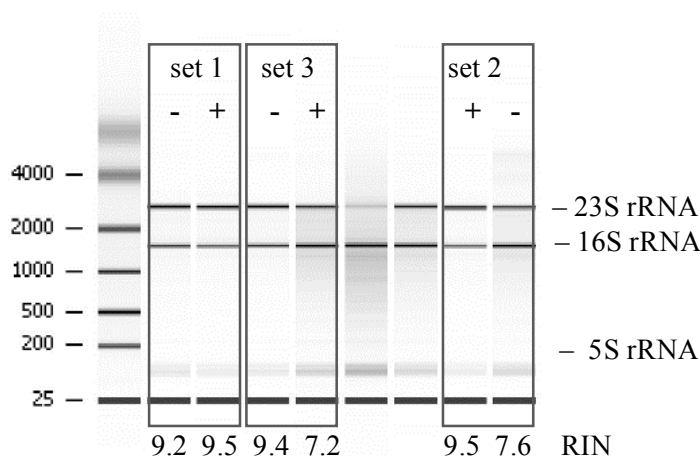
Fig. VIII-11: RNA quality measurement with Agilent 2100 Bioanalyzer

Depicted is the chromatogram of RNA set 1-3 by Agilent 2100 Bioanalyzer. Each set contained the total RNA of ATc-uninduced (-) and ATc-induced (+) bacterial culture of *S. epidermidis* O-47Δ*tRNA*$^{Thr-4}$Δ*icaZ*Δ*icaR*-3′ UTR+pCG248_icaZ/tRNA (strain collection code JE13).

A *icaR* 5′ UTR fragment for EMSA:

B
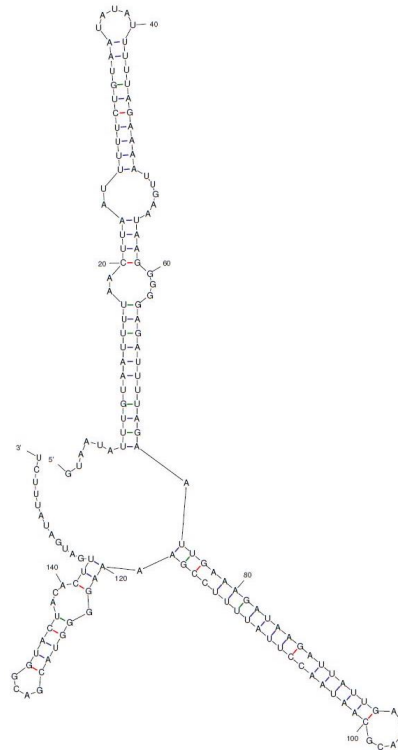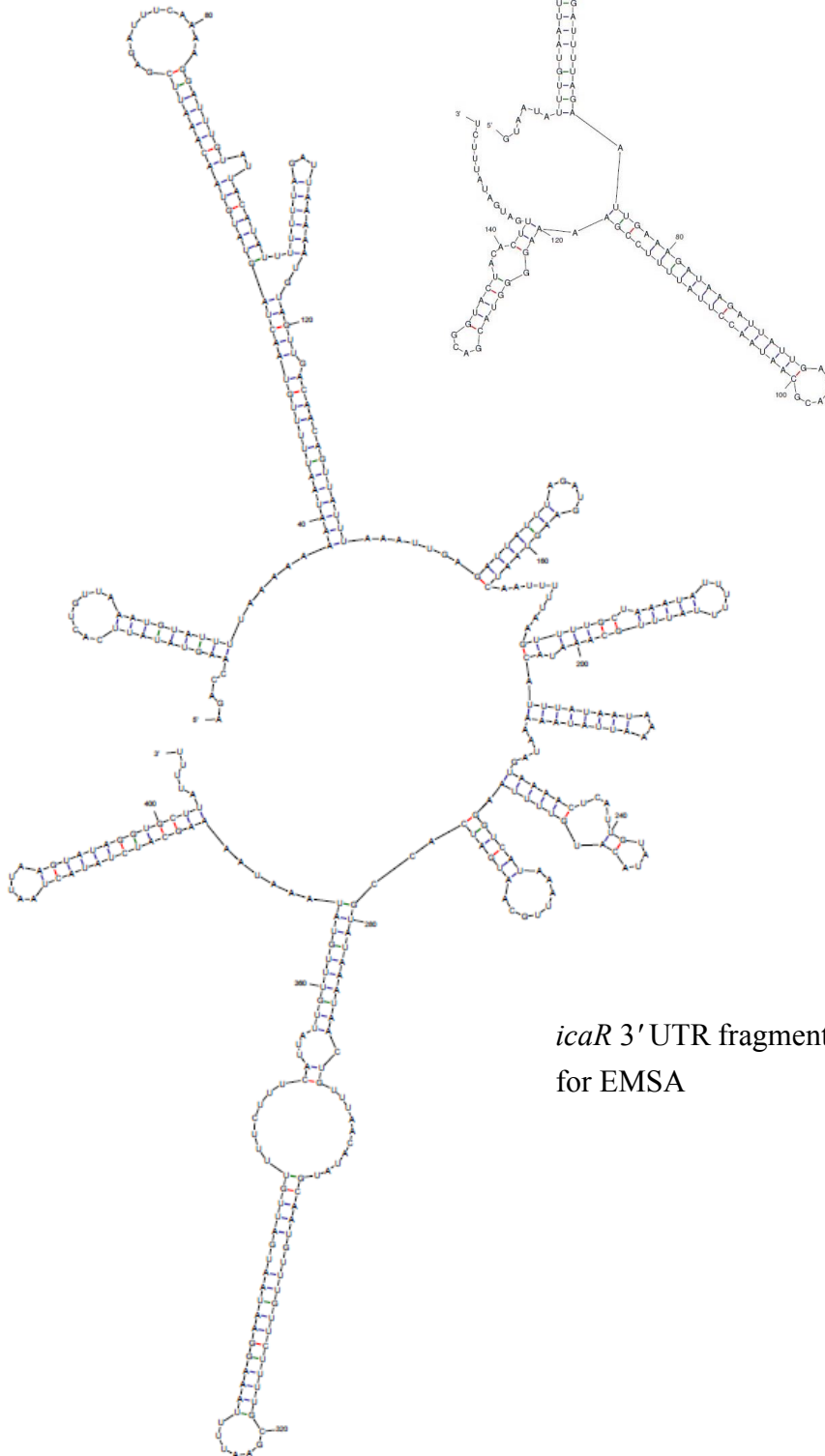
icaR 3′ UTR fragment
for EMSA

C *icaR* 5′ 3′ UTR fusion product for EMSA:
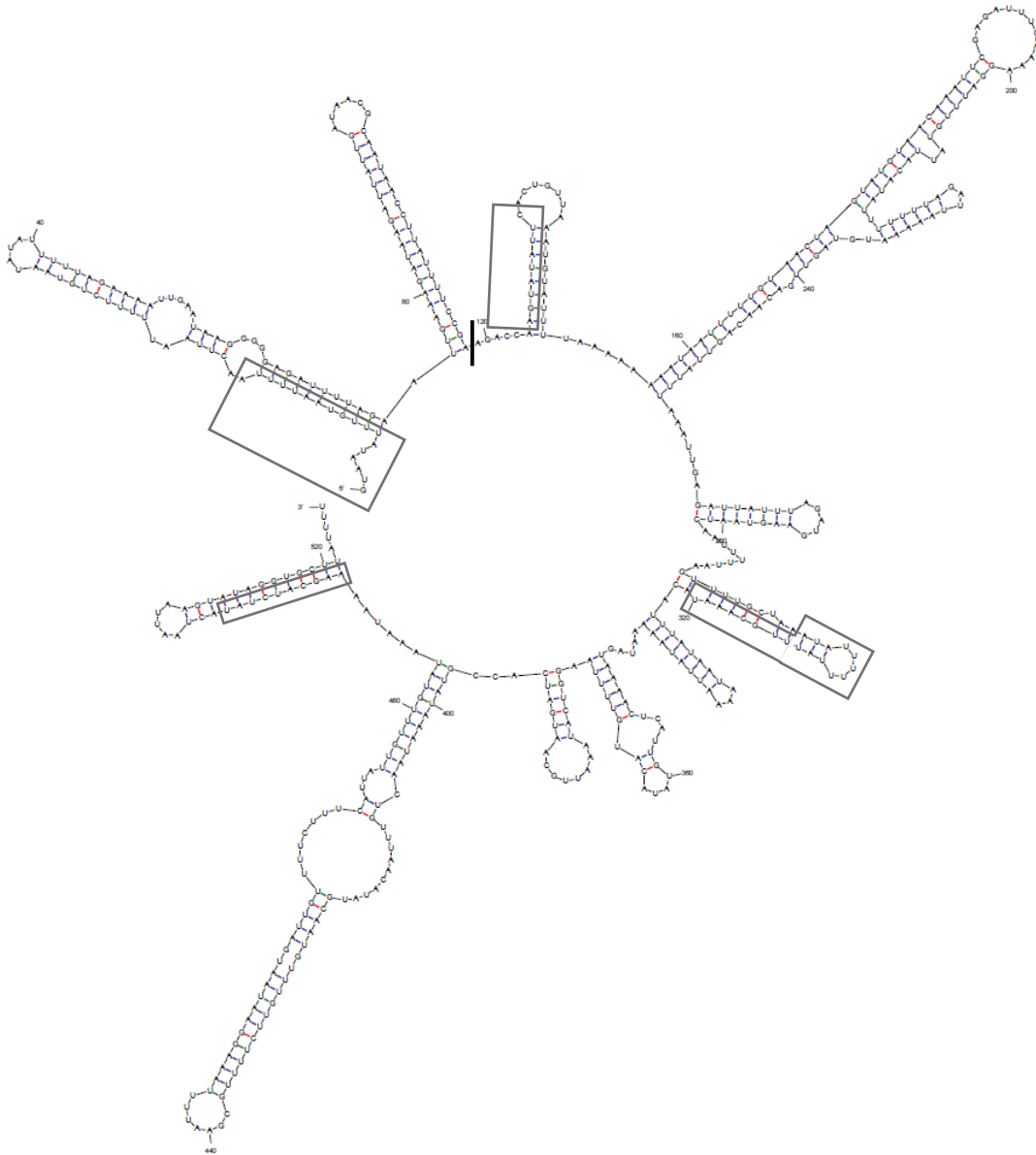
Fig. VIII-12: Secondary structures of *in vitro* transcribed RNAs

Depicted are the secondary structures of *in vitro* transcribed RNAs (folded by *Mfold*) that were used in electrophoretic mobility shift assays. (**A**) *icaR* 5′ UTR fragment (IVT$_{18}$) (**B**) *icaR* 3′ UTR fragment (IVT$_{20}$) (**C**) *icaR* 5′ 3′ UTR fusion product (IVT$_{21}$), which is generated by linkage of *icaR* 5′ UTR fragment with *icaR* 3′ UTR fragment. The bold, black line indicates the position, where the UTRs are linked. On the left side of the bold line, the *icaR* 5′ UTR fragment is positioned and on the right side, the *icaR* 3′ UTR fragment is positioned. Predicted binding sites with IcaZ are marked by grey rectangles.

A 30°C folding temperature

B
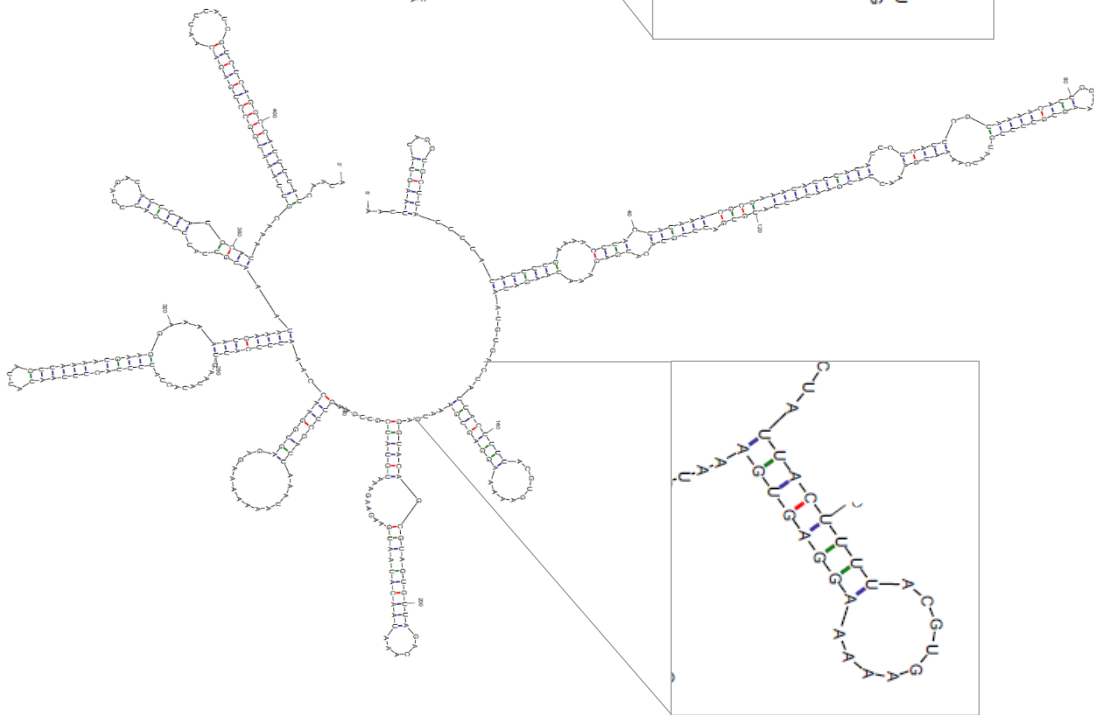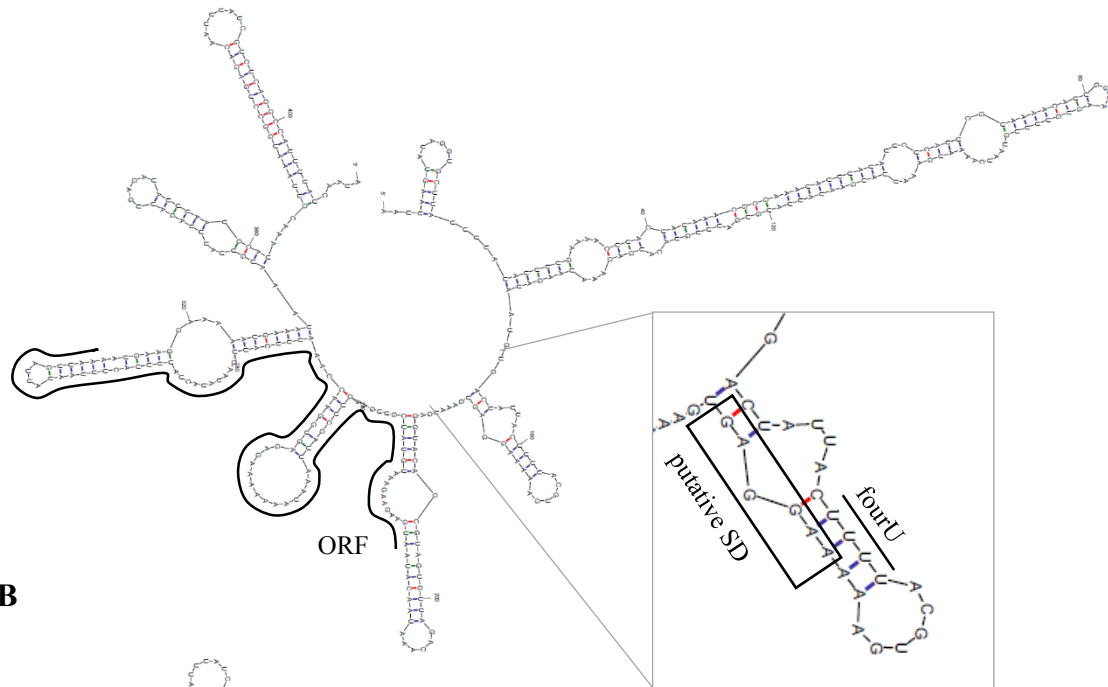
Fig. VIII-13: Secondary structure folding of truncated IGR*ica*-RNA

413 nt from the TSS of IGR*ica*-RNA were analysed for their secondary structure formation by *Mfold* prediction. It was noticed that the truncated IGR*ica*-RNA differs in stem loop 3 (equivalent to stem loop 2 of IcaZ), when different temperature conditions were applied (highlighted by magnification in A and B). **A)** 30°C folding temperature; putative peptide 2 is indicated with black line. **B)** 37°C folding temperature.
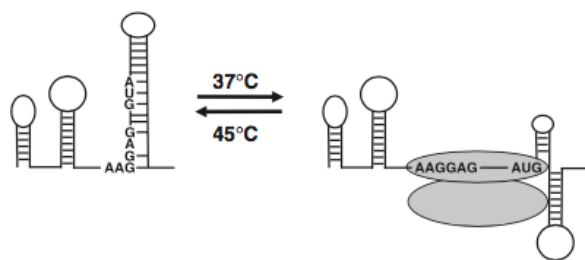
Fig. VIII-14: Schematic illustration of RNA thermosensors

Figure was taken from Narberhaus *et al.*, 2006 (Figure 2). Depicted is the temperature-dependent sequestration of the λ cIII ribosome-binding site. Grey ovals represent the ribosome. Shine-Dalgarno sequence is AAGGAG and AUG is the start codon.

Tab. VIII-5: List of primers used for cloning and sequencing of *S. epidermidis rnc* mutant and complementing strain

Listed are the primers with nucleotide sequence, PCR product sizes and its purpose. The list is divided into primers for cloning of *rnc* mutant (above bold line) and *rnc* complementing strain (below bold line). Restriction sites or overlapping sequences from left and right fragment are written in small letters.

Purpose	Primer	Sequence	T_A [°C]	Product size [bp]
Left fragment	O47rnc_L1_BglII	TGCagatctTCACGAGGTATTACAGTGAACG	66,8	828
	O47rnc_L2_5'R1	cggattcttTCTGGTTAGCCACAACCTAAC	66,8	
Right fragment	O47rnc_R1_5'L2	ggctaaccagaAAGAATCCGAACAAAAGGCA	66,8	831
	O47rnc_R2_EcoRI	AGTTgaattcTTAACGGTTCCACTCGTCCC	66,8	
Plasmid insert	O47rnc_L1_BglII	TGCagatctTCACGAGGTATTACAGTGAACG	66,8	1620
	O47rnc_R2_EcoRI	AGTTgaattcTTAACGGTTCCACTCGTCCC	66,8	
Plasmid control	pBASE6_MCS_F	GATGCCTCAAGCTAGAGAGTCATTACC	65	1869
	pBASE6_MCS_R	CCATGTATTCACTACTTCTTTCAAACTCTCTC	64,4	
Deletion control	O47rnc_R2_seq	AGCACCGCGTAGTGATTTGGCA	62,1	-
	O47rnc_seq_for	GGTGCAATGGGTAATCCTGGA	59,8	Wt: 2495
	O47rnc_seq_rev	ACGCTCATCTAATCGCTGATTATCT	59,7	Δ*rnc*: 1835
Plasmid insert	rnc_BglII_for	TACTTGagatctCTGAATTAGTAATGGAATTAGAAGACGA	66,4	1118
	rnc_EcoRI_rev	GATTGAgaattcTGTATTCTCCTTATCACAGTCGTG	67,2	

Plasmid control	pBASE6_MCS_F	GATGCCTCAAGCTAGAGAGTC ATTACC	65	1343
	pBASE6_MCS_R	CCATGTATTCACTACTTCTTTCAA ACTCTCTC	64,4	

Tab. VIII-6: List of *in vitro transcription* products

IVT nr.	Region	Primerpair		PCR products [bp]	RNA lengtl [nt]	M.W. approx.
1	*icaR*-5'UTR	MF_icaR5'_T7-F1	MF_icaR5'_R	204	186	59772
2	*icaR*-5'UTR	MF_icaR5'_T7-F2	MF_icaR5'_R	136	118	37978
3	*icaR*-3'UTR	MF_icaR3'_T7-F	MF_icaR3'_R	343	325	104322
4	*murAA*-5'UTR	T7-murA	murA-reverse	205	187	60093
5	*murAA*-5'UTR control	T7-murA-control	murA-reverse	155	137	44068
6	*ebh*-5'UTR	MF_ebh5'_T7-F	MF_ebh5'_R	186	168	54003
7	*hcrA*-5'UTR	MF_hrcA5'_T7-F	MF_hrcA5'_R	200	182	58490
8	*ctsR*-5'UTR	MF_ctsR5'_T7-F	MF_ctsR5'_R	224	206	66182
9	*icaA*-5'UTR	MF_icaA5'_T7-F	MF_icaA5'_R	194	176	56567
16	IcaZ	T7_IGRica_MF	IGRica_rev3	438	420	134769
17	IcaZ (AFM)	T7-2_IGRica_MF	IGRica_rev3	455	437	140218
18	*icaR*-5'UTR	ML_icaR5'_T7-F3	MF_icaR5'_R	176	157	50478
19	*icaR*-5'3'UTR	ML_icaR5'_T7-F3	ML_icaR3'_R2	577	528	169383
20	*icaR*-3'UTR	MF_icaR3'_T7-F	ML_icaR3'_R2	429	411	131885
21	IcaZ part 1	T7_IGRica_MF	IGRtr-1_RT_rev	190	172	55285
22	IcaZ part 2	T7-3_IGRica_MF	tRNA-3'UTR-s	280	262	84130
23	SA *icaR*-5'UTR	SA_IcaR-5'-T7-F	SA_IcaR-5'-R	125	107	34453
24	SA *icaR*-3'UTR	SA_IcaR-3'-T7-F	SA_IcaR-3'-R	451	433	138936

Tab. VIII-7: List of transcripts used for analysis of *icaR* mRNA autoregulation in *S. aureus* and *S. epidermidis*

Transcripts, generated by *in vitro* transcription and corresponding T7 DNA template numbers, as well as the primer, the PCR conditions, the length of the PCR product and the length of the transcribed RNA are listed. PCR was done in 50 µl Phusion High-Fidelity DNA Polymerase standard reaction. Genomic DNA of *S. epidermidis* O-47 (for IVT_{18} and IVT_{20}) and *S. aureus* 8325 (for IVT_{23} and IVT_{24}) was used.

IVT No.	Forward primer	Reverse primer	PCR conditions	PCR product length [bp]	RNA length [nt]
IVT_{18}	ML_icaR5'_T7-F3	MF_icaR5'_R	$t_A = 64°C$, $t_E = 20s$, 34x	176	157
IVT_{20}	MF_icaR3'_T7-F	ML_icaR3'_R2	$t_A = 59°C$, $t_E = 30s$, 5x $t_A = 64°C$, $t_E = 30s$, 28x	429	411
IVT_{23}	SA_IcaR-5'-T7-F	SA_IcaR-5'-R	$t_A = 65°C$, $t_E = 30s$, 34x	125	107
IVT_{24}	SA_IcaR-3'-T7-F	SA_IcaR-3'-R	$t_A = 65°C$, $t_E = 30s$, 34x	451	433

2. Supplementary experiment

Visualisation of RNA-RNA interactions by using atomic force microscopy

RNA-RNA interactions were attempted to be visualised with atomic force microscopy. For the construction of RNA transcripts, T7 DNA templates were amplified with Phusion Green High-Fidelity DNA Polymerase using the primer listed in Tab. VIII-4. The forward primers contained the T7 promoter sequence to allow transcription with T7 polymerase. As positive interaction control, the UTRs of *icaR* from *S. aureus* 8325 were used, because it was shown by own experiments and known from Ruiz de los Mozos *et. al.* that they interact with each other (chapter III-1.1.2.2). As negative control, the RNAs IcaZ and *lrgA*-5′ UTR (215 nt RNA), the latter was kindly provided by Dr Claudia Lange, were used. 2 µl RNA aliquots (~ 10 µM) were prepared and handed over to Dr Ingrid Tessmer.

Interactions of IcaZ (IVT$_{17}$) with *icaR*-5′ UTR (IVT$_2$), *icaR*-3′ UTR (IVT$_3$), *icaR*-5′ 3′ UTR (IVT$_{19}$) and *icaA*-5′ UTR (IVT$_9$) were analysed (see **Tab. VIII-4**). Romina Eisenhauer, who did her practical course in Dr Tessmer's laboratory at that time, could confirm secondary structures of IcaZ, that were previously predicted by *Mfold* (**Fig. VIII-4**). She also measured an interaction of IcaZ with *icaR*-3′ UTR. Unfortunately, the interaction between 5′ and 3′ UTR of *S. aureus icaR* could not be used as positive control, as repeated experiments done by Dr Tessmer revealed. The reason, why it was not possible, was probably the small size of the used fragments. Structures with more volume size were generally better to study with AFM (personal communication with Dr Tessmer). Also, binding would have led to a smaller volume of the binding complex than calculated previously by simple addition of single fragment volumes, so that in consequence no volume increase was measurable, as it was expected.

In consequence, atomic force microscopy could not be used for the visualisation of RNA-RNA interactions.

3. Supplementary materials

3.1 Lists of hardware equipment, glass and plastic ware

Tab. VIII-8: Hardware equipment list

Equipment	Manufacturer/ Distributor and Cat.-No.
Agilent 2100 Bioanalyzer	Agilent Technologies, G2938C
Agilent 2100 Bioanalyzer vortexter	IKA® Works
Biomolecular imager	GE Healthcare, Typhoon^{TM} FLA 7000 laser scanner
Centrifuge, benchtop	Heraeus, Biofuge Pico 17
Centrifuge, benchtop	Thermo Scientific, Heraeus Pico 21
Centrifuge rotor	Heraeus, Megafuge 1.0 R
Centrifuge	Heraeus, Multifuge X1R
Centrifuge rotor	Heraeus, Multifuge X3R
Centrifuge rotor	Sorvall 75002000
Centrifuge, cooling	Eppendorf, Centrifuge 5424R
Confocal laser scanning microscope (CLSM)	Leica Microsystems GmbH, Leica TCS SP5
Field Emission Scanning Electron Microscope (SEM)	JEOL Ltd., JSM-7500F
Gel dryer, radioactivity lab (EMSA)	Bio-Rad, Model 583
Electrophoresis chamber	Bio-Rad
Electrophoresis chamber, radioactivity lab (EMSA)	Peqlab Biotechnologie GmbH, model 45-2020-i
Electroporator	Bio-Rad, Gene Pulser Xcell^{TM}
Flow hood	Renggli Laboratory Systems GmbH, ENTA 120
Freezer, -80°C	Thermo Fisher Scientific, HERAfreeze HFU 686 Basic
Fridge-freezer combination	Privileg, Öko energy saver combi
Heatable magnetic stirrer	Heidolph, MR-3001
Heater	Liebisch
Heater, radioactivity laboratory	Stuart®, SBH 130
Homogeniser	FastPrep® Instrument MP Biomedicals, FastPrep®-24 Instrument
Hybridisation oven	Hybaid, Mini 10
Hybridisation oven	UVP, HB-1000
Ice machine	Ziegra Eismaschinen GmbH, S-No. 094829
Ice machine	Scotsman, Eisbereiter AF30
Image eraser	GE Healthcare Life Sciences, FLA Image Eraser

Incubator, circulatory 30°C	B. Braun, Certomat® BS-1
Incubator, static 30°C	Braun Biotech International Sartorius Group, Certomat®BS-1
Incubator, static 37°C	Kendro Laboratory Products, HERAcell
Micro centrifuge	STARLAB, MiniFuge
Micro wave	Clatronic, MWG 737
Micro wave	Privileg, 8017
Microbiological safety cabinet class II	Nuaire Biological Safety Cabinets, Class II Type A/B3
Microplate reader	VWR, Multiskan Ascent
Microplate reader	TECAN, infinite F200Pro
MilliQ system	TKA (Thermo Fisher Scientific), GenPure XCad Dispenser
Peristaltic pump	Watson-Marlow Fluid Technology Group, UK; 205S/CA
pH adjustment	WTW, Inolab pH 720
Pipette, multi (30-300 µl)	Brand, Transferpette® S -8
Pipette, electronic multi (20-200 µl)	Brand, Transferpette® -8
Pipettes (100-1000 µl, 10-100 µl, 0.5-10 µl, 0.1-2.5 µl)	Eppendorf, Eppendorf Research® plus
Pipettes controller	Brand, Accu-jetR Pro
Pipettes for radioactivity	STARLAB, MicroOne
Power supplies	Peqlab Biotechnologie GmbH, EV202, EV232, peqpower 300
Radioactivity counter	Berthold Technologies, LP 124
Scales	Kern & Sohn GmbH, Kern 470, Kern 572, Kern EW2200
SDS-Page System	Bio-Rad, Mini-PROTEAN Tetra Electrophoresis System
Shaker (benchtop, heating and cooling)	Serva, ThermoMix 500
Shakers (growth exp. and RNA assays)	GFL, GFL-1083, GFL-1092
Shaker, analogue orbital shaker with universal mount	GFL, GFL-3005
Shaker	Edmund Bühler GmbH, SM 30 A, SM 30 A control
Special accuracy weighing machine	Chyo Balance Corp. Japan, JL-180
Spectrophotometer	Amersham Biosciences, Ultrospec 3100 pro
Spectrophotometers	Thermo Fisher Scientific Inc., ND-1000, ND-2000
Steam steriliser	Münchner Medizin Mechanik GmbH, Vakulab PL 669
Steam steriliser	Rühl
Storage phosphor screen, 20 x 40 cm	VWR, BAS-IP SR 2040 E; 28-9564-77
Thermocycler	Biometra, T3 Thermocycler

UV chamber, Crosslinker	Bio-Rad, GS Gene Linker^{TM}
UV Crosslinker, radioactivity laboratory	Cleaver Scientific Ltd, CL-508.G
UV imaging system for gel documentation	INTAS, INTAS® GDS
UV-imaging system, flat	Benda, N90
Vortexer	Labinco, Vortex Power Mix L46
Vortexer, radioactivity laboratory	Scientific Industries, Inc., Vortex-Genie 2
Water bath, circulating	GFL, GFL-1092
X-ray film box	A. Hartenstein, RO13
X-ray film processor	CAWO solutions, CAWOMAT 2000 IR

Tab. VIII-9: Glass and plastic equipment

Glass and plastic equipment	Manufacturer/ Distributor and Cat.-No.
Aluminium foil	A. Hartenstein GmbH, AF30
Blotting paper	Albet Lab Science, BP 0025860
Cell culture flask	SPL Life Sciences, Cat.-No.:70075
Cell culture flask, 75cm^2	PAA Laboratories GmbH, AUT, PAA70075X
Cell culture flask	Greiner Bio-One, Cellstar®, Cat.-No.: 658175
Cover slip, 20x20 mm	A. Hartenstein, DK20
Cryogenic tubes	Thermo Fisher Scientific, Nalgene^{TM}
Screw cap micro tube, 2 ml	Sarstedt, REF 72.694.006
Cuvettes (one-time), 1.5 ml	Brand, 759150
ECL hyperfilm, 18x24 cm	GE Healthcare, Amersham Hyperfilm^{TM} ECL
Electroporation cuvettes (brown, 1 mm ø)	Bio-Rad, Gene Pulse®/Micro Pulser^{TM} Cuvettes, #165-2089
Electroporation cuvettes, long electrode (red, 1 mm ø)	Cell Projects Ltd, EP-201
Erlenmeyer flask, DURAN® 100 ml	A. Hartenstein GmbH, EK04
Erlenmeyer flask, DURAN® 250 ml	A. Hartenstein GmbH, EK06
Erlenmeyer flask, DURAN® 500 ml	A. Hartenstein GmbH, EK08
Erlenmeyer flask, DURAN® 1000 ml	A. Hartenstein GmbH, EK09
Filter membrane, 0.2 µm, non-pyrogenic	Pall Corporation, Acrodisc® 32mm Syringe Filters, REF 4652
Filter membrane, 0.45 µm, non-pyrogenic	Sarstedt, Filtropur S (REF 83.1826)
Filtertips, low binding (20 µl)	Biozym, SafeSeal SurPhob VT0220
Filtertips, low binding (200 µl)	Biozym, SafeSeal SurPhob VT0240
Filtertips, low binding (1000 µl)	Biozym, SafeSeal SurPhob VT0260
Gel electrophoresis chamber	Bio-Rad, Sub CellTM
Glass pipe	A. Hartenstein GmbH, RG06

Glass pipettes, reusable (10 ml, 25 ml)	Superior Marienfeld,
Hybridisation glass tubes	Biometra
Imaging plate and cassette	Fujifilm, BAS cassette2 2340
Inoculation loop	A. Hartenstein, IO01
Laboratory bottles DURAN® 100 ml-1l	A. Hartenstein GmbH, FL02-05
Lysing matrix E	MP Biomedicals, Lysing Matrix E
Micro spin columns, G-25	GE Healthcare, Illustra MicroSpin G-25
Micro spin columns, G-50	GE Healthcare, Illustra MicroSpin G-50
Microplate, 6-well, 24-well	Greiner Bio-One, Cellstar® (F-form)
Microplate, 96 well, sterile with lid	Greiner Bio-One, Cellstar® (F-form) Cat.-No. 655180
Microscope slides, SuperFrost®	A. Hartenstein GmbH, OSM
Needle, ø 0,90 x 40 mm	B. Braun Melsungen AG, Sterican® Gr. 1, G 20 x 1 1/2" REF4657519
Nitrocellulose membrane	GE Healthcare, Optitran BA-S 85, Cat.No. 10 439 196
Nylon membrane	GE Healthcare, VWR, Hybond-XL (20 cm ~ 3 m); RPN203S
Parafilm	Pechiney Plastic Packaging, PM996
PCR tubes and caps, strips of 8	BRAND GMBH + CO KG, Brand® #781327
Petri dishes	Nerbe Plus, #09-031-0000
Pipette tip 200 μl, neutral	Sarstedt, REF 70.760.002
Pipette tip 1000 μl, neutral	Sarstedt, REF 70.762
Pipette tip 20 μl, neutral	Sarstedt, REF 70.1116
Pipette, serological, sterile (10 ml)	Greiner Bio-One, Cellstar® #607 180
Pipette, serological, sterile (25 ml)	Greiner Bio-One, Cellstar® #760 180
PLG-tubes	5 Prime, #2302830
Reaction tubes, 1.5ml	Sarstedt, #72.690.001
Reaction tubes, 2.0ml safe lock	Sarstedt, #72.695.500
RNase-free tubes 1.5ml	Ambion-Life Technologies., AM12400
Scalpel, one-time	B. Braun Melsungen AG,
Shield	Thermo Fisher Scientific, Nalgene™ Cat.-No. 6802-0002
Steritop, 500 ml	Sarstedt, 83.1823.101
Syringe, one-time, 2 ml, 5 ml, 10 ml	B. Braun Melsungen AG, Injekt®
Tube, non-pyrogenic (15 ml)	Sarstedt, REF 62.554.502
Tube, non-pyrogenic (50 ml)	Sarstedt, REF 62.547.254

3.2 List of chemicals

Tab. VIII-10: List of chemicals

Chemicals in the table marked with an asterisk were used specifically for work with RNA.

Chemicals	Producer/ Distributor	Cat.-No.
Acetic acid (100 %)	Carl Roth GmbH + Co. KG	6755.1
Acetone, ROTIPURAN®	Carl Roth GmbH + Co. KG	9372.6
Agarose, peqGOLD universal agarose	VWR Peqlab	35-1020
Ammonium acetate	Carl Roth GmbH + Co. KG	7869
Ammonium persulfate (APS)	AppliChem GmbH	A1356
Aqua-Clean, water bath preservative	A. Hartenstein GmbH	CAC1
Boric acid	Carl Roth GmbH + Co. KG	6943.1
Bromophenol Blue	Carl Roth GmbH + Co. KG	A512.1
Calcium chloride dihydrate [$CaCl_2 \cdot 2\ H_2O$; MW: 147,02 g/mol]	Carl Roth GmbH + Co. KG	5239.1
Chlorine tablets	Carl Roth GmbH + Co. KG	C787.1
Chloroform	Carl Roth GmbH + Co. KG	Y015.2
Congo red	Merck Millipore	101340
Crystal violet	Merck Millipore	115940
Diethyl dicarbonate (DEPC)	Carl Roth GmbH + Co. KG	K028.1
Dimethyl sulphoxide (DMSO)	Carl Roth GmbH + Co. KG	4720.4
di-Sodium hydrogen phosphate 2-hydrate [$Na_2HPO_4 \cdot 2H_2O$; MW: 177.99 g/mol]	AppliChem GmbH	A3905.1000
dNTP set, 100 mM solutions	Thermo Fisher Scientific Inc.	R0182
D-Sucrose, D(+)-Saccharose [MW: 342.30 g/mol]	Carl Roth GmbH + Co. KG	4621.2
EDTA	Carl Roth GmbH + Co. KG	8043.4
EDTA 0.5 M, pH 8.0 *	Thermo Fisher Scientific Inc.	AM9260G
Ethanol	Carl Roth GmbH + Co. KG	K928.2
Ethanol, extra pure *	Carl Roth GmbH + Co. KG	5054.3
Ethidium bromide solution 1%	Carl Roth GmbH + Co. KG	2218.1
Formaldehyde solution 37%	Carl Roth GmbH + Co. KG	4979.1
Formamide (99.5%)	Carl Roth GmbH + Co. KG	6749.3
Gelatin solution 2% in H_20	Sigma-Aldrich Co. LLC	G1393
Glucose, D(+)-Glucose monohydrate [MW: 198.17 g/mol]	Carl Roth GmbH + Co. KG	6780.2
Glycerol	Sigma-Aldrich Co. LLC	G2025-1L
Glycine, PUFFERAN®	Carl Roth GmbH + Co. KG	3908.3
GlycoBlue™ Coprecipitant (15 mg/ml)	Thermo Fisher Scientific Inc.	AM9515

Hydrochloric acid 37% (HCl)	Carl Roth GmbH + Co. KG	4625.1
Hydrogen peroxide 30% (H_2O_2)	Carl Roth GmbH + Co. KG	CP26.4
Isoamyl alcohol, ROTIPURAN®	Carl Roth GmbH + Co. KG	T870.3
Isopropanol, 2-Propanol [C_3H_8O; MW: 60.10 g/mol]	Carl Roth GmbH + Co. KG	
KH_2PO_4	Carl Roth GmbH + Co. KG	P749.1
Luminol sodium salt [$C_8H_6N_3O_2Na$; MW: 199.14 g/mol]	Sigma-Aldrich Co. LLC	A4685-1G
Magnesium chloride hexahydrate [$MgCl_2 \cdot 6\ H_2O$; MW: 203.3 g/mol]	Carl Roth GmbH + Co. KG	HN03.3
$MgSO_4$	Sigma-Aldrich Co. LLC	63136
Midori green	Biozym Scientific GmbH	617004
NTP set, 100 mM solutions	Thermo Fisher Scientific Inc.	R0481
Para-hydroxycoumaric acid [MW: 164.16 g/mol]	Sigma-Aldrich Co. LLC	C9008-1G
Potassium acetate [MW: 98.15 g/mol]	Carl Roth GmbH + Co. KG	4986.1
Potassium chloride [KCl; MW: 74.56 g/mol]	Carl Roth GmbH + Co. KG	6781.3
RNase ZAP *	Thermo Fisher Scientific Inc.	AM9780
Roti Hybri Quick *	Carl Roth GmbH + Co. KG	A981.1
Roti®-Aqua-P/C/I *	Carl Roth GmbH + Co. KG	X985.1
Roti-Aqua Phenol *	Carl Roth GmbH + Co. KG	A980.3
Rotiphorese® Gel 40 (19:1) *	Carl Roth GmbH + Co. KG	3030.1
SDS ultra-pure	Carl Roth GmbH + Co. KG	2326.2
SDS, 20% solution *	Thermo Fisher Scientific Inc.	AM9820
Skimmed milk	Carl Roth GmbH + Co. KG	T145.3
Sodium acetate (3 M), pH 5.5 *	Thermo Fisher Scientific Inc.	AM9740
Sodium chloride [NaCl; MW: 58.44 g/mol]	Carl Roth GmbH + Co. KG	9265.3
Sodium hydroxide, in pellets [NaOH; MW: 40.0 g/mol]	Carl Roth GmbH + Co. KG	6771.1
Sodium perchlorate [$NaClO_4$]	Carl Roth GmbH + Co. KG	310514
Sodium periodate [$NaIO_4$; MW: 213.89 g/mol]	Carl Roth GmbH + Co. KG	2603.1
TEMED	Carl Roth GmbH + Co. KG	2367.3
Tris 1M, pH 8.0 *	Thermo Fisher Scientific Inc.	AM9855G
TRIS hydrochloride (Tris-HCl) [MW: 157.60 g/mol]	Carl Roth GmbH + Co. KG	9090.2
tri-Sodium citrate dihydrate [$C_6H_5Na_3O_7 \cdot 2\ H_2O$; MW: 294.1g/mol]	Carl Roth GmbH + Co. KG	4088.1

Tween-20 (Polyoxyethylene (20) sorbitan monolaurate)	Carl Roth GmbH + Co. KG	9127.2
Urea [MW: 60.06 g/mol]	Carl Roth GmbH + Co. KG	3941.1
Xylene cyanol	Carl Roth GmbH + Co. KG	A513.2

3.3 List of media ingredients

Tab. VIII-11: Media ingredients

Media ingredients	Manufacturer	Item no
Agar-Agar, Kobe I	Carl Roth GmbH + Co. KG, GER	5210
Brain Heart Infusion	Oxoid Ltd., UK	CM1135
Congo red dye	Merck Millipore	101340
D-Sucrose	Carl Roth GmbH + Co. KG, GER	4621
Glucose, D(+)-Glucose monohydrate [MW: 198.17 g/mol]	Carl Roth GmbH + Co. KG	6780.2
Mannitol Salt Agar	Carl Roth GmbH + Co. KG, GER	CL81
NaCl	Carl Roth GmbH + Co. KG, GER	9265
Skim milk powder	Carl Roth GmbH + Co. KG	T145.3
Trypticase™ Soy Broth	BD BBL™, USA	211768

3.4 List of primers

Primers used in this work are listed in **Tab. VIII-12**. They were either designed for this work (origin: MF or ML) or taken from the existing primer pool (see initials for origin).

Tab. VIII-12: List of primers

> Primers are numbered. Missing numbers are primer used for projects not directly related to this thesis. Nucleotides underlined indicate restriction sites or T7 promoter sequence. *Initials:* ME: Dr Martin Eckart; WZ: PD Dr Wilma Ziebuhr; FL: Franziska Herbst (née Lampmann); CL: Dr Claudia Lange; ZG: general primer; SoS: Dr Sonja Schoenfelder. *Abbreviations:* PCR: polymerase chain reaction, NB: Northern blot, OE: overexpression, cRACE: circularised rapid amplification of cDNA ends, IVT: *in vitro* transcription, SDM: site directed mutagenesis.

Nr.	Name	Sequence (5′->3′)	Tm	Main purpose	origin
001	Lf1	GGAGGATCCGTCTCAATGTGAAGAGTAAGTT	66,8	PCR	ME
002	Lf2	TATCCCTCCAAAATTTCAACcaatgtttgttcttttgcga	67,4	PCR	ME
003	Rf1	TCGCAAAAGAACAAACATTG	51,2	PCR	ME
004	Rf2	ggaggatccGCAAAGCATATGCTAATCGAAAGT	68,2	PCR	ME
005	ica-sRNA-1	ggaggatccgttgaaattttggagggata	65,3	PCR	WZ
006	ica-sRNA-2	ggaggatccGGTCATAAATTGCAATGATCACCG	69,5	PCR	WZ
007	ica-sRNA4_EcoRI	ggcGAATTCCTAGTATGTAACAAATTCGAGAT	64,4	PCR	MF
008	ica-sRNA-3	GGAGGATCCGATTGAATGATAATCACAGTCCAA	67,0	PCR	MF
009	5'IGR_BamHI_for	cgaaGGATCCcgtcttcttttccctgtttgatc	69,5	PCR	MF
010	3'IGR_BamHI_rev	cgaaGGATCCtgctccagaagcactgaattca	69,5	PCR	MF
011	icaX_NB	TATTTAGCAAAACTTAAAAATTGATTACTTC	56,3	NB	MF
012	icaZ_NB	CACTTACCAATGTTTTACGAATGAGAAT	59,3	NB	MF
013	icaZ_NB_2	CAAATCCTTCTCCCTCCGCT	59,4	NB	MF
014	t-RNA-thr-oligo	GAAGGATTTGAACCAACGCGAGCA	62,7	NB	FL
015	5SrRNA	CAG TCC GAC TAC CAT CGG CG	63,5	NB	FL

016	icaZ_BglII_forw	agttagatcttatactaattaagtataggtgc	60,5	OE	MF
017	icaZ_XmaI_rev1	aattcccgggaagaggctaatcattc	63,2	OE	MF
018	icaZ_XmaI_rev2	aattcccgggggtggcttaatgaaga	63	OE	MF
019	icaZ_XmaI_rev3	aattcccgggataatattgataaaatggc	61	OE	MF
020	icaZ_XmaI_rev4	aattcccgggatgtttgaaggtaatttg	62,2	OE	MF
021	ica-sRNA-5_for	ggagtgaaatgaggtacagcgtagtg	64,8	PCR	MF
022	PP4_C7T_out2	cgcgttAgttcaaatccttctccctc	64,8	PCR	MF
023	PP4_C7T_out1	tgaacTaacgcgagcaaaaagctcctac	65,1	PCR	MF
024	lf1_icaZd_BglII	agttagatctCGTCTCAATGTGAAGAGTAAGTT	64,5	Cloning of O47ΔicaZ_MF	MF
025	lf2_icaZd	CATTGGTAAGTGaaacgttaaatggcctgagacaatttat	67,4	O47ΔicaZ_MF	MF
026	rf1_icaZd	CGTTTcacttaccaatgttttacgaatgagaat	63,3	O47ΔicaZ_MF	MF
034	307-sRNAica	ctacgctgtacctcatttcactc	60,6	cRACE	FL
035	307-sRNAica_rev	agagagtggaaccaaatttcattgaatatac	61,6	cRACE	MF
036	IGRtr-1_RT	aaacgttaaatggcctgagac	55,9	cRACE	ME
037	IGRtr-1_RT_rev	tcacgtaaaagtaatagtcacattatc	57,4	cRACE	MF
038	IGRica1	cgctactaaaatcggtaacagacggtg	65	*ica* PCR	FL
039	IcaR-R	TCCAAAGCGATGTGCGTAGGA	59,8	*ica* PCR	CL
040	IGRica2	GTTCAATTATCTAGTGCTCCAGAAGCA	61.9	*ica* PCR	FL
041	icaC-for	TTATCGCTGTTTCCGGTAGTG	57,9	*ica* PCR	ZG
042	icaA_for2	CCTTTACGATGACCTTTATCAATATCATCC	62,7	*ica* PCR	MF
043	icaB-forw	ATGGCTTAAAGCACACGACGC	59,8	*ica* PCR	ZG
044	icaC_rev1	ATAGATAGGAGTGAGATACATGACAGGTG	63,9	*ica* PCR	MF
045	IcaC-F	ATAAACTTGAATTAGTGTATT	46,2	*ica* PCR	CL
046	IcaA-R	CCCAGTATAACGTTGGATACC	57,9	*ica* PCR	CL
047	IcaR-F	GGGGTACGATGGTACTACACTTG	62,4	*ica* PCR	CL
048	T7_IGRica_MF	CTAATACGACTCACTATAGGGaattaagtataggtgcttatttttatattttg	68,6	IVT	MF

049	IGRica_rev	aagaggctaatcattcgtgattagtagg	62,2	IVT	MF
050	IGRica_rev3	ataatattgataaaatggcctgagacga	59,3	IVT	MF
051	IGRica_rev294	aaaatagtatattcaatgaaatttggttccac	59,2	IVT	MF
052	MF_icaA5'_T7-F	CTAATACGACTCACTATAGGGC AAATATTACTGTTTCAGTATAA CAAC	69,4	Gel shift	MF
053	MF_icaA5'_R	AGTAAATCGATCCTACTATCCA GTAAATTG	61,3	Gel shift	MF
054	MF_icaR5'_T7-F2	CTAATACGACTCACTATAGGGT TTTAGAAAATTGAATAAGGGGG AGAT	70,3	Gel shift	MF
055	MF_icaR5'_R	AGAAATATCATCAAGTGTAGTA CCATCG	60,7	Gel shift	MF
056	MF_icaR5'_T7-F1	CTAATACGACTCACTATAGGGT GCAATAGAATGTTGTTATACTG	69,4	Gel shift	MF
057	T7-2_IGRica_MF	CTAATACGACTCACTATAGGGat aaaagcatctatactaattaagtatag	68,6	Gel shift	MF
058	MF_icaR3'_T7-F	CTAATACGACTCACTATAGGGA GACCAAGTATATTCACTGTTAA ATG	70,3	Gel shift	MF
059	MF_icaR3'_R	TCGCAAAAGAACAAACATTGC ATATGTTAAAC	61,8	Gel shift	MF
060	MF_ebh5'_T7-F	CTAATACGACTCACTATAGGGC TTCGTGAATTAATTTCACAAAG TT	69,4	Gel shift	MF
061	MF_ebh5'_R	TGACAATGAATAACTCATACAT TTGCTC	59,3	Gel shift	MF
062	MF_hrcA5'_T7-F	CTAATACGACTCACTATAGGGA GAAATTTTAGTGCTTTAACATT GACT	69,4	Gel shift	MF
063	MF_hrcA5'_R	AGAGTTTTAGATCCAATCGGTT GTCC	61,6	Gel shift	MF
064	MF_ctsR5'_T7-F	CTAATACGACTCACTATAGGGG AACACGCTAACATCATTAATTT GAA	70,3	Gel shift	MF
065	MF_ctsR5'_R	AGCAATATGAGCGCGTTGTATT TCTAC	61,9	Gel shift	MF

066	T7-murA	CTAATACGACTCACTATAGGGA GActgattagagtttttaagtggagg	57,1 - 72,0	Gel shift	SoS
067	T7-murA-control	CTAATACGACTCACTATAGGGA GATGGTGGAAATCGTTTAACAG GTGAAG	61,6 - 73,5	Gel shift	SoS
068	murA-reverse	catcgcttaactctgggacattaactag	63,7	Gel shift	SoS
069	Sa_IGRica_for	TCATTAACCCAACTCACAGTGA CGG	63	S.a. IGR NB	MF
070	Sa_IGRica_rev	ACGACCACAAAACATACACAA CTACATT	60,7	S.a. IGR NB	MF
071	cerul_BglII_sd	TGTAAGATCTACCAGATCCTAG GAAAGGAGG	66,8	Cloning	ZG
072	cerul_BamHI	ATAGGATCCGTGATGGTAACTT CACGGTAAC	66,8	Cloning	ZG
073	pCer_MCS_F	CGTTATACAAATTTTAACCCTG TTAGGAACT	61,6	PCR MCS	ZG
074	pCer_MCS_R	TGTTAATGTTGTTACTAATGTTG GCCAAG	61	PCR MCS	ZG
075	icaZprom _BamHI	ataGGATCCggtcataaattgcaatgatc	62,4	Cloning	ML
076	icaZprom_BglII	ggcAGATCTacttaattagtatagatgc	60,7	Cloning	ML
077	agr4	GAAGGTGTACTAACAACACAT ATCGATGTAGAC	65,8	*agr* PCR	ZG
078	S.e.agr3	TCATATCGTAAAGATGGGTGTT	54,7	*agr* PCR	ZG
079	Se_icaR_rev1	TGCTCCAGAAGCACTGAATTCA GA	61	cRACE	ML
080	Se_icaR_rev2	ACGCACATCGCTTTGAATAAAG AGG	61,3	cRACE	ML
081	Se_icaR_for1	AAGTCCGTCAATGGAATAATTA TCGTC	60,4	cRACE	ML
082	Se_icaR_for2	GTGTAGTACCGTCGTACCCT	61,8	cRACE	ML
085	O47icaZ_G167T_r	tgaaaaagTagtgaaatgaggtacagcg	62,2	SDM	ML
086	O47icaZ_G167T_f	ttcactActttttcacgtaaaagtaatagtcac	62	SDM	ML
087	O47icaZ_G195C_r	tgttaCacaaataacataatgaagaagaaatgt	59,5	SDM	ML
088	O47icaZ_G195C_f	atttgtGtaacactacgctgtacctc	61,6	SDM	ML
089	O47icaZ_A323G_r	atgaaatGaatgttatttagattgagatatttaatgc	60,6	SDM	ML
090	O47icaZ_A323G_f	ataacattCatttcattttttccttcattttaacta	58,9	SDM	ML

091	O47icaZ_d251_f	ccactctttttttttatttaatcgaacttcaacg	**62**	SDM	ML
092	O47icaZ_d251_r	gattaaataaaaaaaagagtggaaccaaatttcatt g	**61,7**	SDM	ML
093	MF57icaZ_out_5'p	ataggtgcttattttatattttgaaaacttactataaacg	**62,3**	Cloning	ML
094	pCG248_out_5'p	ATTTTAATTATACTCTATCAATG ATAGAGTGTCAA	**60,1**	Cloning	ZG
100	IGRica_for120	tgtgatttgtacatgagaaataagataatgt	**58,9**	NB	ML
101	IGRica_rev294	aaaatagtatattcaatgaaatttggttccac	**59,2**	NB	MF
102	Se_Eno_NB	AGGTATCGAACAAGGTATTGGT AACTCA	**62,2**	NB oligo	ML
103	For_RNAIII_T7	TAATACGACTCACTATAGGGAT ATCACAGAGATGTGATTGAAA G	**69,4**	IVT	CL
104	Rev_RNAIII	AGCCGTGAGCTTGGGAGAGAC TC	**66**	IVT	CL
111	icaZ_XmaI_rev3_p	CCCGGGataatattgataaaatggc	**59,7**	ΔTT-Cloning	ML
112	pCG248_dTT_5'p	TTTGCGGAAAGAGTTAATAAGT TAACAG	**59,3**	ΔTT-Cloning	ML
113	tRNA-3'UTR-as	gacaatttatcgtctcaggccattttatcaata	**63,3**	NB Oligos	ML
114	pCG248_TT-as	ATCAGTATTTATTATGCATTTA GAATAGGC	**58,6**	NB Oligos	ML
115	O47_rnc-as	GTGAAACCGTCAATTCTAATAC CGCATCA	**63,9**	NB Oligos	ML
118	ML_icaR5'_T7-F3	CTAATACGACTCACTATAGGGT AATATTTGTAATTTTAACTTAAT TTTTCTGTA	**67,1**	Gel shift	ML
119	ML_icaR5'_rf	GAATATACTTGGTCTtcggaaataag gttattgcgttatcaataatc	**68,6**	Gel shift	ML
120	ML_icaR3'_lf	gcaataaccttattttccgaAGACCAAGTA TATTCACTGTTAAATG	**68,5**	Gel shift	ML
121	ML_icaR3'_R2	AAAATAAGCACCTATACTTAAT TAGTATAGATGCT	**61,3**	Gel shift	ML
122	T7-3_IGRica_MF	CTAATACGACTCACTATAGGGat tactttttacgtgaaaaaggagtgaaatgagg	**72,4**	Gel shift	ML
123	T7-3_IGRicaRP	CTAATACGACTCACTATAGGGat tactttttacgtgaaaaagtagtgaaatgagg	**71,7**	Gelshift	ML

124	tRNA-3'UTR-s	tattgataaaatggcctgagacgataaattgtc	63,3	Gel shift NB oligo	ML
125	O47rnc_R2_seq	AGCACCGCGTAGTGATTTGGCA	62,1	PCR	ML
126	O47rnc_seq_for	GGTGCAATGGGTAATCCTGGA	59,8	PCR	ML
127	O47rnc_seq_rev	ACGCTCATCTAATCGCTGATTATCT	59,7	PCR	ML
128	IGR-ica3	GGACAATGTAGTAGTATGTGAT		PCR	FL
129	IGR-ica4	TCTCGAATTTGTTACATACTAG		PCR	FL
130	IcaC-R	atatataaaactctcttaaca		PCR	CL
131	IcaA-F	gacctcgaagtcaatagaggt		PCR	CL
134	SA_IcaR-3'-R	AAAAAAGCGCCTATGTCATGATTTACCATCA	62,9	IVT AFM	ML
135	SA_IcaR-3'-T7-F	CTAATACGACTCACTATAGGGTGAAGTGTATTCGCTACTAAATATAT	69,4	IVT AFM	ML
136	SA_IcaR-5'-T7-F	CTAATACGACTCACTATAGGGAAATATTTGTAATTGCAACTTAATTTTC	67,7	IVT AFM	ML
137	SA_IcaR-5'-R	GGTTATTGCGTTATCAATAATCTTATCCTTCAA	62	IVT AFM	ML
138	Se_IcaR-3'UTR-as	ACAATAATGAAAGAAAACAATCATTATTCCTT	58	NB-Oligo	ML
139	gfp_for_seq	AGTCCGCCATGCCCGAAG	60,5	PCR	ML
140	gfp_rev_seq	acggcaggaggaacttcagct	61,8	PCR	ML
141	Pami_seq_for	gaaaatttgtttgattttttaatggataatgtgatataatgg	62,4	PCR	ML
142	IcaR_prom_PstI	ttgCTGCAGCGAAAGTATTTCAATTTGCAATAGAATGTTG	67,4	Cloning	ML
143	IcaZ_KpnI_rev3	ttgGGTACCATAATATTGATAAAATGGCCTGAGACGATAAAT	67,5	Cloning	ML
144	IcaZ_KpnI_rev2	ttgGGTACCGTGGCTTAATGAAGACGATTTACATGT	68,3	Cloning	ML
145	5'IcaR_EcoRV_re	TGCTTCTAGAGATATCCAATTCTAAAATCTCCCCCTTATTC	68,4	Cloning	ML
146	gfp_EcoRV_for	AGATTTTAGAATTGGATATCTCTAGAAGCAAAGGAGAAGAACT	67,5	Cloning	ML

147	gfp_XmaI_rev	ATACTTGGTCTCCCGGGTTATT TGTAGAGCTCATCCATGCCATG T	**74**	Cloning	ML
148	3'IcaR_XmaI_for	TCTACAAATAACCCGGGAGACC AAGTATATTCACTGTTAAATG	**69,4**	Cloning	ML
149	gfp_rev2_seq	TGTGTCCGAGAATGTTTCCATC TTCT	**61,6**	Cloning	ML
150	PtufA_for_seq	catcattacgttcaaacactcaaggt	**60,1**	PCR	ML
151	IcaR_prom_PstI_2	tacttgCTGCAGCGAAAGTATTTCA ATT	**60,7**	Cloning	ML
152	IcaZ_KpnI_rev3_2	tacttgGGTACCATAATATTGATAA AATGG	**59,9**	Cloning	ML
153	IcaR_5'UTR_BglII	TAGTACagatctGTAATATTTGTAA TTTTAACTTAATTTTTCTGT	**63,1**	Cloning	ML
154	IcaR_5'UTR_EcoR V	TCTAGAGATATCCATTTCTAAA ATCTCCCCCTTATTC	**66,1**	Cloning	ML
155	pCN33_seq_for	CTGATTCTGTGGATAACCGTAT TACC	**61,6**	PCR MCS	ML
156	pCN33_seq_rev	CTCTTCGCTATTACGCCAGCTG	**62,1**	PCR MCS	ML
	Hfq_end_HindIII	CCAAGCTTTTATTCTTCACTATT CACTTC	**61**	PCR pME16 plasmid	ME
	Hfq_start_BamHI_ FXa	CGGGATCCATCGAGGGCAGGA TGATTGCAAACGAAAACATCCA A	**75**	PCR pME16 plasmid	ME
157	5'IcaR_BglII_for	TTGATTGAagatctTTACGATCCTA CTATCCAGTAAATTGA	66,4	Cloning_n ew	ML
158	SA2208TT_PstI	TACTTGctgcagAAGGATTATTTA ACAAGTTGCAGGTA	67,3	Cloning_n ew	ML
159	SA2208TT_BglII	GATAGTAGGATCGTAAagatctTC AATCAAAAATATCTTCTCTAGT T	67,7	Cloning_n ew	ML
160	MutGFP-2-5'P	ATCATTAGCTGCTGGACGTTTG TAGAGCTCATC	68,2	Cloning mutGFP	ZG
161	MutGFP-3-5'P	GAAAACTATGCATTAGTTGCAT AACCCGGGAGACCA	69,5	Cloning mutGFP	ZG
162	rnc_BglII_for	TACTTGagatctCTGAATTAGTAAT GGAATTAGAAGACGA	66,4	Cloning JH	ML

163	rnc_EcoRI_rev	GATTGAgaattcTGTATTCTCCTTATCACAGTCGTG	67,2	Cloning JH	ML
164	SeO-47_tcaR_for	GATGTTAATACATTAACGGCAAAGTTACT	59,6	NB	ML
165	SeO-47_tcaR_rev	GTCACTCGTCATATCACTAGCAATA	59,7	NB	ML
166	SeO-47_sarA_for	GCTATGGTCACTTATGCTGACAGA	61	NB	ML
167	SeO-47_sarA_rev	GCTTCTGTGATACGGTTGTTTACTC	61,3	NB	ML
168	LVA-repair-1	CCAGCAGCTAATGATGAAAACTATGCATTAGTTGCATAA	67,4	Cloning	SoS
169	LVA-repair-2	CATAGTTTTCATCATTAGCTGCTGGACGTTTGTAGA	67,2	Cloning	SoS
-	M13-for	GTAAAACGACGGCCAG	51.7	Cloning	ZG
-	M13-rev	CAGGAAACAGCTATGAC	50.4	Cloning	ZG
-	RsaE_Oligo new	GAGAAATTTTTCACTTCAAACA	50.9	NB	ZG

4. CLC vector maps of the plasmids

CLC vector map files are stored on the server of the Institute for Molecular Infection Biology (Group Ziebuhr) in Würzburg and are included in the digital version of this thesis that was given, in addition to the hardcopy, to the committee members and the *Graduate School of Life Sciences* (GSLS). Files can be opened with the software *CLC Main Workbench*.

5. Strain collection

Each genetically manipulated organism was registered in the strain collection and stored in glycerol stocks at -80°C in the Institute for Molecular Infection Biology (Group Ziebuhr) in Würzburg.

6. Publications and meeting contributions

6.1 Publications

Lerch M.F., Schoenfelder S.M.K., Eckart M., Förstner K.U., Sharma C.M., Thormann K.M., Ziebuhr W. (2017). A non-coding RNA from the intercellular adhesin (*ica*) locus of *Staphylococcus epidermidis* controls polysaccharide intercellular adhesin (PIA)-mediated biofilm formation. *In preparation.*

Schoenfelder S.M.K., Lange C., Lerch M.F., Wencker F.D.R., Förstner K., Sharma C.M., Thormann K.M., Ziebuhr W. (2017). RsaE, a riboregulator of staphylococcal carbon metabolism, facilitates eDNA release and polysaccharide intercellular adhesin (PIA)-mediated biofilm formation in *Staphylococcus epidermidis*. *In preparation.*

6.2 Presentations (selection)

Oral presentations were held at internal meetings of SFB-TRR34 and on retreats of the graduate programme 'Infectious Diseases Research' of the Institute for Molecular Infection Biology (IMIB) in Würzburg.

Lerch M.F., Ziebuhr W. (2014). A novel regulator of *Staphylococcus epidermidis* biofilm formation. *Poster presentation* at the 16th International Symposium on Staphylococci and Staphylococcal Infections (ISSSI) in Chicago, USA.

Lerch M.F., Ziebuhr W. (2014). A non-coding RNA, specific for *S. epidermidis*, is a novel regulator of biofilm formation. *Poster presentation* at the Deutsche Gesellschaft für Hygiene und Mikrobiologie (DGHM; 7. Tagung der Fachgruppe Mikrobielle Pathogenität) in Bad Urach, Germany.

Lerch M.F., Ziebuhr W. (2014). Riboregulation of biofilm formation in *Staphylococcus epidermidis*. *Poster presentation with poster award* at the 3rd Molecular Microbiology Meeting Würzburg (MMMW) in Würzburg, Germany.

Lerch M.F., Ziebuhr W. (2013). Riboregulation of biofilm formation in *Staphylococcus epidermidis*. *Poster presentation* at the 3rd international conference of the priority program SPP1258 'Regulating with RNA in bacteria – sensory and regulatory RNA in prokaryotes' in Würzburg, Germany.

Lerch M.F., Ziebuhr W. (2012). Involvement of a sRNA in *Staphylococcus epidermidis* biofilm regulation. *Poster presentation* at the 2nd international conference on the Pathophysiology of Staphylococci in the post-genomic era (SFB-TRR34) in Banz, Germany.

7. Curriculum Vitae

Full name: Maike Franziska Lerch (née Feldhahn)